An examination of ischaemic penumbra in the spontaneously hypertensive stroke-prone rat (SHRSP) using the MRI perfusion-diffusion mismatch model.

Emma Reid

BSc, BSc (Hons)

A Thesis submitted in fulfilment of the requirements for the degree of Doctor of Philosophy to the Institute of Neuroscience and Psychology,
College of Medical, Veterinary and Life Sciences,
University of Glasgow, Nov 2011

Wellcome Surgical Institute, University of Glasgow,
Garscube Estate, Bearsden Road,
Glasgow, UK, G61 1QH

Acknowledgements

Firstly, I would like to thank my principal supervisor, Dr Chris McCabe for his continual support and encouragement over the past three years and for helping me to see the light at the end of the tunnel. I'd also like to thank Professor Mhairi Macrae for her continuing support and wisdom and also my third supervisor, Professor Anna Dominiczak.

I'd like to say a big thank you to all the technical staff at the Wellcome Surgical Institute, Lindsay, Linda, Margaret and George, for all their help and support over the years. In particular I'd like to thank Lindsay for passing on her extensive knowledge of surgical technique and general animal handling skills and thanks to Linda for all those long hours spent with me performing the tail cuff method on grumpy rats!

I'd also like to thank Dr Delyth Graham from the BHF Glasgow Cardiovascular Research Centre for showing me how to perform the tail cuff method and for supplying me with SHRSP and WKY rats throughout the duration of my PhD.

Finally, I'd to thank all my fellow students at the Wellcome Surgical Institute for their support and endless discussions on experimental stroke and beyond: Dave, Craig, Adrianna and Ashleigh. I'll miss our chats in the student room, especially on a Friday afternoon when we weren't feeling very productive!

Declaration

I declare that this thesis comprises my own work, unless otherwise acknowledged, and has not been previously submitted for any other degree at the University of Glasgow or any other institution.

Emma Reid,
November 2011

Contents

List of Figures

Chapter 1

Chapter 2

Chapter 3

Chapter 4

Chapter 5

Chapter 6

List of Tables

Chapter 2

Chapter 3

Chapter 5

Publications

Manuscripts

Reid E, Gallagher L, Mullin JM, Holmes WM, Lopez-Gonzalez MR, Graham D, Dominiczak AF, Macrae IM, McCabe C (2011). Detection of penumbra using PWI/DWI mismatch MRI in rodent stroke models: comparison of methods. **Paper in preparation for Journal of Cerebral Blood Flow & Metabolism.**

Abstracts

Reid E, Gallagher L, Mullin JM, Holmes WM, Lopez-Gonzalez MR, Graham D, Dominiczak AF, Macrae IM, McCabe C (2011). Studying potentially salvageable penumbra and its lifespan in the stroke-prone spontaneously hypertensive rat (SHRSP): a MRI perfusion-diffusion mismatch study. *J. Cereb Blood Flow & Metab*. (abstract published at the XXVth International Symposium for Cerebral Blood Flow, Metabolism and Function conference).

Abbreviations

4-HNE	4-hydroxy-2-nonenal
8-OHdG	8-hydroxy-2'-deoxyguanosine
7T	7 tesla
20-HETE	20-hydroxyeicosatetraenoic acid
ACA	anterior cerebral artery
ADC	apparent diffusion coefficient
AIF	apoptosis inducing factor
AMPA	alpha-amino-3-hydroxy-5-methyl-4-isoxazolepropionate
ANF	atrial natriuretic factor
ANOVA	analysis of variance
AP1	activator protein 1
Apaf-1	apoptosis activating factor 1
ASL	arterial spin labelling
ATLANTIS	Alteplase Thrombolysis for Acute Noninterventional Therapy in Ischemic Stroke
ATP	adenosine triphosphate
BBB	blood-brain barrier
bFGF	basic fibroblast growth factor
BNF	brain natriuretic factor
BP	blood pressure
Ca^{2+}	calcium ion
cASL	continuous arterial spin labelling
CBF	cerebral blood flow
CBV	cerebral blood volume
Cl^-	chlorine ion
$CMRO_2$	cerebral metabolic rate of oxygen
COX	cyclo-oxygenase
CNS	central nervous system
CSD	cortical spreading depolarisations
CSF	cerebrospinal fluid
CT	computed tomography
DAG	diacylglycerol
DEFUSE	Diffusion and perfusion imaging Evaluation For Understanding Stroke Evolution trial

DIAS	Desmoteplase in Acute Ischemic Stroke trial
DMSO	dimethylsulphoxide
DNA	deoxyribonucleic acid
DWI	diffusion-weighted imaging
ECASS	European Cooperative Acute Stroke Study
ECG	electrocardiogram
eNOS	endothelial nitric oxide synthase
EPI	echo planar imaging
EPITHET	Echoplanar Imaging Thrombolytic Evaluation Trial
ER	endoplasmic reticulum
FMISO	fluromisonidazole
FMZ	flumazenil
FOV	field of view
GFAP	glial fibrillary acidic protein
H^+	hydrogen ion
H_2O_2	hydrogen peroxide
H & E	haematoxylin and eosin
HET0016	*N*-hydroxy-*N'*-(4-butyl-2-methylphenyl)-formamidine
HIF1	hypoxia inducible factor 1
Hsp70	heat shock protein 70
ICAM-1	intracellular adhesion molecule 1
IGF-1	insulin-like growth factor 1
IL-1β	interleukin 1 beta
IMAGES	Intravenous Magnesium Efficacy in Stroke trial
IP_3	inositol 1,4,5-trisphosphate
IQ	interquartile range
IV	intravenous
K^+	potassium ion
MABP	mean arterial blood pressure
MCA	middle cerebral artery
MCAO	middle cerebral artery occlusion
MCP-1	monocyte chemoattractant protein 1
mGluR	metabotropic glutamate receptor
MR	magnetic resonance
MRI	magnetic resonance imaging
MRS	magnetic resonance spectroscopy

MTT	mean transit time
Na^+	sodium ion
NCX	sodium-calcium exchanger
NFκB	nuclear factor kappa B
NINDS	National Institute of Neurological Disorders and Stroke
NMDA	N-methyl-D-aspartate
nNOS	neuronal nitric oxide synthase
NO	nitric oxide
NOS	nitric oxide synthase
O_2^-	superoxide anion
OEF	oxygen extraction fraction
OH^-	hydroxyl anion
$OONO^-$	peroxynitrite anion
$PaCO_2$	arterial partial pressure of carbon dioxide
PAF	platelet activating factor
PAM	paraformaldehyde in phosphate buffered saline
PaO_2	arterial partial pressure of oxygen
PARP	poly (ADP-ribose) polymerase
PET	positron emission tomography
PIP_2	phosphatidylinositol 4,5-bisphosphate
PWI	perfusion-weighted imaging
QTL	quantitative trait loci
RARE	rapid acquisition with refocused echoes
rCBF	regional cerebral blood flow
rCMRglc	regional cerebral metabolic rate of glucose
RF	radio frequency
RH-WKY	renovascular hypertensive Wistar Kyoto rat
RNA	ribonucleic acid
ROI	region of interest
ROS	reactive oxygen species
rtPA	recombinant tissue plasminogen activator
SD	standard deviation
S-D	Sprague-Dawley rat
SHR	spontaneously hypertensive rat
SHRSP	spontaneously hypertensive stroke-prone rat
SOD	superoxide dismutase

SPECT	single photon emission computed tomography
STAIR	Stroke Therapy Academic Industry Roundtable
T_1	longitudinal relaxation time
T_2	transverse relaxation time
T_2^*OC	T_2^* oxygen challenge
TE	echo time
TGFb1	tumour growth factor b1
TNFα	tumour necrosis factor alpha
TOF	time of flight
tPA	tissue plasminogen activator
TR	repetition time
TTC	2,3,5-triphenyltetrazolium chloride
TTP	time to peak
VCAM-1	vascular cell adhesion molecule 1
WKY	Wistar Kyoto rat

Abstract

Stroke accounts for 9% of all deaths worldwide and is a major cause of severe disability (Donnan et al, 2008). Following ischaemic stroke, the penumbra represents tissue which is hypoperfused and functionally impaired but is not yet irreversibly damaged. However, the penumbra has a finite lifespan and will proceed to infarction in the absence of swift reperfusion. Therefore, the identification and potential salvage of penumbral tissue in acute ischaemic stroke is the ultimate goal for both clinicians and experimental stroke researchers. Positron emission tomography (PET) is the 'gold standard' imaging modality for identifying the penumbra, but the complex logistics of PET limit its widespread use.

Magnetic Resonance Imaging (MRI) is widely used for penumbra imaging in both clinical and pre-clinical research. The MRI perfusion-diffusion mismatch model provides an approximation of the penumbra, where diffusion weighted imaging (DWI) identifies the core of ischaemic injury and perfusion weighted imaging (PWI) reveals the perfusion deficit. The mismatch between the DWI and PWI provides a measure of penumbral tissue. However, there is no consensus on the perfusion and diffusion thresholds used to identify mismatch tissue in clinical and preclinical stroke research. Furthermore, in rodent stroke models differences in the evolution of ischaemic injury between strains may limit the use of a single set of threshold values. Therefore, the first aim of this thesis was to establish strain specific perfusion and diffusion thresholds to compare penumbra volume in the clinically relevant spontaneously hypertensive stroke-prone rat (SHRSP) and the normotensive control strain, Wistar-Kyoto (WKY) using 3 different methods. The SHRSP strain is characterised by the progressive development of severe hypertension which is followed by a tendency to spontaneous stroke and an increased sensitivity to experimental stroke.

Experimental stroke was induced by permanent middle cerebral artery occlusion (MCAO) by the intraluminal filament method. DWI and PWI were obtained every hour from 1-4 hours post-MCAO. Strain-specific diffusion and perfusion thresholds were established from final infarct at 24 hours post-MCAO, as defined by T_2 weighted imaging. The calculated ADC thresholds were comparable between the strains but the absolute perfusion threshold was significantly higher in SHRSP compared to WKY. This may be indicative of an increased sensitivity to ischaemia in the hypertensive strain. Furthermore, application of these thresholds to the acute MRI data revealed that the volume of ischaemic injury and the perfusion deficit were significantly larger in SHRSP compared to WKY and this was also reflected in the significantly larger infarct volume observed in SHRSP at 24 hours post-MCAO. Interestingly, there was evidence of a temporal increase in the volume of the

perfusion deficit in SHRSP and WKY. This may indicate that there is a progressive failure of collateral blood supply in both strains following stroke.

Penumbra volume was then assessed in SHRSP and WKY rats using the mismatch method and also indirectly by examining the growth of the volume of ADC derived ischaemic injury. Mismatch volume was determined by arithmetic subtraction of the volume of ischaemic injury from the volume of perfusion deficit (volumetric method) and also by manual delineation of mismatch on each of 6 coronal slices (spatial method). There was a limited volume of mismatch tissue in either strain from as early as 1 hour post-MCAO and the volumetric method generated smaller mismatch volumes than the spatial mismatch method. Mismatch volume was comparable in SHRSP and WKY from 1-4 hours post-MCAO. Penumbra was also determined retrospectively by subtracting the volume of ischaemic injury at each time point from final infarct volume. Using this method, penumbra volume was significantly larger in WKY compared to SHRSP at 30 minutes post-MCAO but penumbra volume was comparable at all later time points. This suggests that there is reduced potential for tissue salvage in SHRSP compared to WKY within the first hour following MCAO but from 1 hour onwards, there is limited potential for penumbra salvage in both strains.

In addition, there was evidence of 'negative' mismatch tissue in SHRSP and WKY rats, where the ADC derived lesion expanded beyond the boundary of the perfusion deficit. The volume of negative mismatch tissue was comparable between the strains and was persistent over the 4 hour time course. This phenomenon may arise from the spread of toxic mediators from the ischaemic core.

Oxidative stress is a major mediator of cellular injury following ischaemic stroke and reactive oxygen species, like superoxide, have multiple deleterious effects on the components of the neurovascular unit. It is well established that NADPH oxidase is the principal source of superoxide in acute ischaemic stroke and is therefore a target for potential neuroprotective strategies (Moskowitz et al, 2010). Consequently, the second aim of this thesis was to evaluate the potential neuroprotective effect of NADPH oxidase inhibition with low and high dose apocynin following permanent or transient ischaemia. Rats were administered apocynin at a dose of 5mg/kg or 30mg/kg or vehicle, at 5 minutes post-MCAO. Apocynin treatment had no significant effect on infarct volume or functional outcome at 24 hours following permanent MCAO in WKY rats. However, both low and high dose apocynin treatment significantly reduced infarct volume at 72 hours post-MCAO by 60% following 1 hour of ischaemia in Sprague-Dawley rats. Furthermore, functional outcome was improved in the low dose apocynin treated group, although this did not reach the level of statistical significance. On the basis of these results, low dose apocynin

treatment was evaluated in SHRSP rats following 1 hour of ischaemia. However, apocynin treatment had no effect on the acute evolution of ischaemic injury and failed to improve stroke outcome, where the mortality rate was high in both the apocynin treated and the vehicle treated group. The conflicting effects of apocynin may be attributable to a differential expression of NADPH oxidase subunits in normotensive and hypertensive rat strains. These findings may also explain the failure of neuroprotective drugs to translate from bench to bedside, as therapies which are neuroprotective in young healthy animals may not demonstrate the same efficacy in animal models with stroke co-morbidities. Therefore, potential therapeutic strategies should be extensively evaluated in animal models with stroke risk factors before proceeding to clinical trial.

Chapter 1.
Introduction

1.1 Stroke

1.1.1 Types of Stroke and Major Risk Factors

Stroke is a common multifactorial neurological disorder, which arises as a result of a severe reduction in cerebral blood flow. The brain accounts for around 2-3% of body weight yet receives approximately 15% of the total cardiac output. Furthermore, it has high metabolic requirements; accounting for around 20% of total body oxygen consumption and 25% of total body glucose consumption. The brain has a very limited capacity to store energy and therefore requires a constant supply of substrates for normal metabolic function. This great demand for substrates helps to illustrate how damaging even a transient reduction in blood flow could potentially be to brain tissue.

Stroke is the third leading cause of death in the Western hemisphere, after heart disease and cancer. Every year in the UK approximately 150,000 people have a stroke, which equates to a stroke occurring in the population every 5 minutes (Office of National Statistics). In Scotland, there are 13,000 new strokes every year with 3,000 of these new cases occurring in people who are under 65 years of age (Chest, Heart & Stroke Scotland,www.chss.org.uk/stroke/index.php). Increasing age is a major stroke risk factor as most strokes occur in the elderly population, with 75% of first strokes occurring in the over 75 age group (Sudlow & Warlow, 1997). In addition to increasing age, hypertension is also a powerful determinant of risk for stroke, where the lifetime risk of stroke is doubled in hypertensive patients (Lloyd-Jones et al, 2010). Other factors which contribute to the incidence of stroke are diabetes mellitus and dyslipidemia, in addition to lifestyle factors including being overweight, cigarette smoking and excessive alcohol consumption.

It has been proposed that the incidence of stroke will rise in future years due to the world's ageing population, thereby further increasing the healthcare burden on the economy. Stroke patients occupy around 20% of all acute hospital beds and 25% of long term beds (Department of Health, 2005). The direct cost to the National Health Service is estimated to be £2.8 billion per year. This burden is increased further since 50% of stroke patients are rendered severely disabled and require day to day care, while 30% of patients die within a year of the first stroke onset (Warlow et al, 2003).

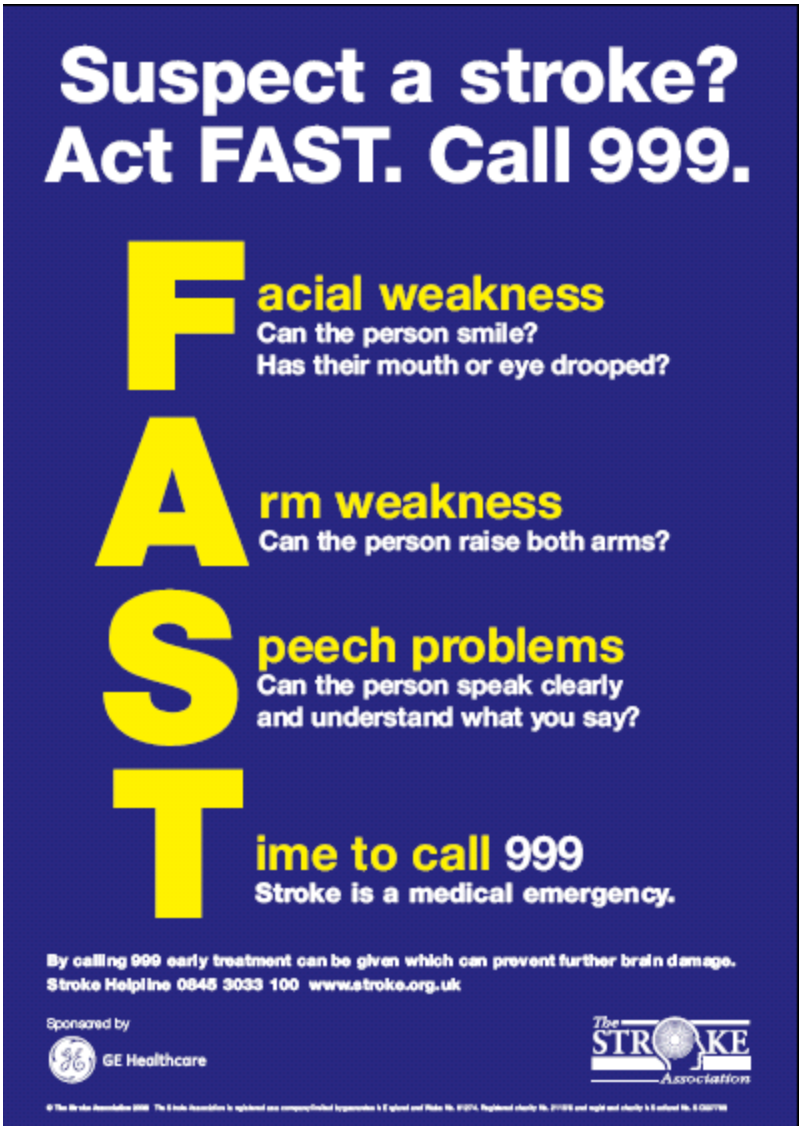

Figure 1-1. An example of a poster produced by The Stroke Association to promote the FAST campaign which aims to raise public awareness of the common visible symptoms of stroke and highlights the need for early diagnosis and treatment to limit brain injury.

A recent campaign by The Stroke Association in the UK has sought to raise public awareness of the symptoms of stroke and highlights the importance of getting the stroke patient to hospital as quickly as possible in order to limit brain damage and functional impairment. This highly successful campaign is called FAST and focuses on recognising the common stroke symptoms of Facial weakness, Arm weakness, Speech problems and Time to call 999 (Figure 1-1). The FAST campaign has been supported by UK wide television commercials, billboard posters and leaflets in hospitals, GPs surgeries and health centres.

The reduction in cerebral blood flow observed in stroke can arise from haemorrhage or from occlusion of a cerebral blood vessel. These are termed haemorrhagic and ischaemic, or occlusive strokes, respectively. Haemorrhagic strokes are less common than ischaemic strokes (Figure 1-2), accounting for approximately 20% of all strokes (Warlow et al, 2003).

Haemorrhagic Stroke

Hypertension is a major stroke risk factor and is closely correlated with the incidence of haemorrhagic stroke. Excessive alcohol consumption and cigarette smoking have also been identified as risk factors for haemorrhagic stroke (Feigin et al, 2005). This type of stroke can arise from a subarachnoid haemorrhage or primary intracerebral haemorrhage, where the latter is more common, accounting for 75% of all haemorrhagic strokes (Warlow et al, 2003).

Subarachnoid haemorrhage results from the rupture of an intracranial aneurysm, leading to a build up of blood in the subarachnoid space, which is situated between the arachnoid and pia mater meningeal layers. The mortality rate is high and most deaths occur as a result of the period of initial bleeding, with over 40% of patients dying within one month following aneurysmal rupture (Kissela et al, 2002). In approximately one third of aneurysmal subarachnoid haemorrhage patients the haemorrhage extends into the parenchyma. These patients have a higher mortality rate and a reduced functional recovery (van Gijn et al, 2007). Recently, it has been reported that patients with aneurysms located in the middle cerebral artery are at greater risk of intraparenchymal extension (Liu & Rinkel, 2011).

Primary intracerebral haemorrhage may result from rupture of microaneurysms of 1-2mm in diameter, which are most often located deep within the cerebral hemispheres (Standgaard & Paulson, 1990) and are predominantly found in hypertensive patients. Other risk factors include long-term alcohol abuse, male sex and increasing age (Ariesen et al,

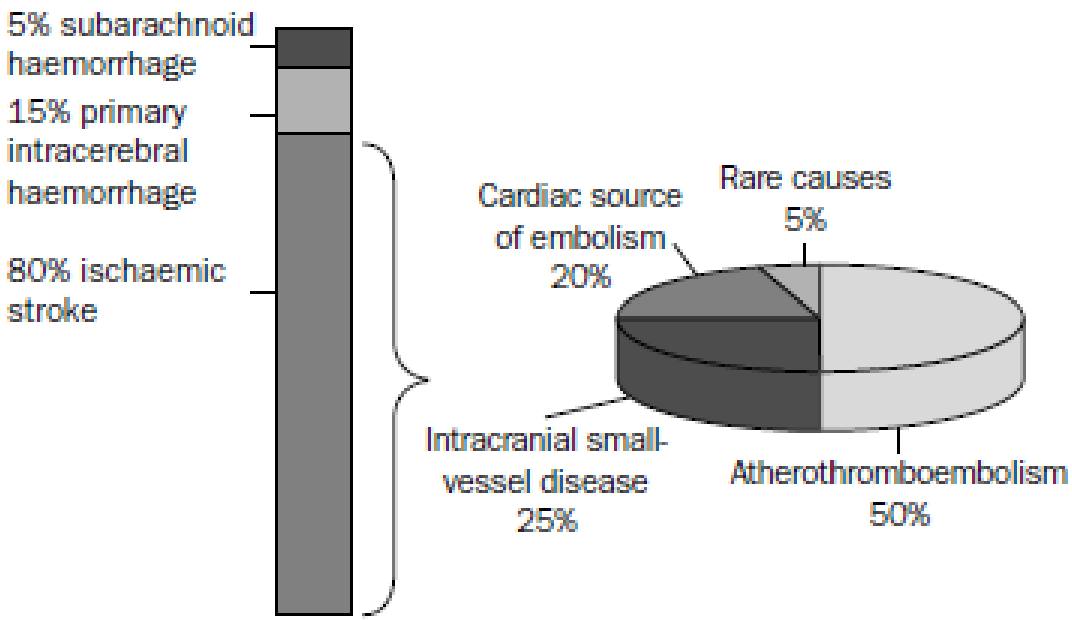

Figure 1-2. Approximate frequency of the three main causes of stroke in Caucasian populations and of the main subtypes of ischaemic stroke. Reproduced from Warlow et al (2003).

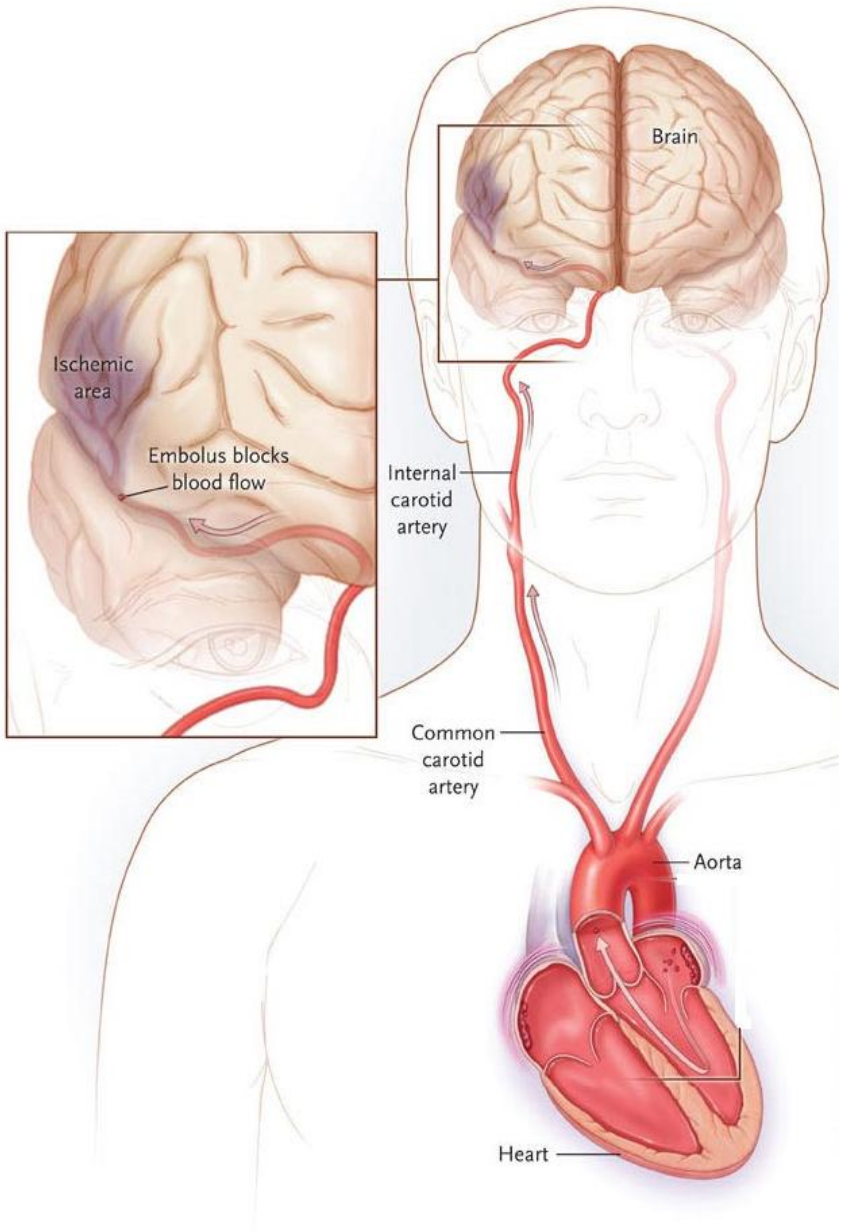

Figure 1-3. Ischaemic stroke arising from a cardiac embolus. The embolus ascends from the heart to the cerebral circulation via the aorta and the common carotid artery. It can travel through the cerebrovasculature to occlude a cerebral artery. Adapted from Go (2009).

2003; Zia et al, 2007). Mortality rates following intracerebral or subarachnoid haemorrhage are high, with 50% of patients dying within 1 month of stroke onset (Donnan et al, 2008).

Ischaemic Stroke

Occlusive or ischaemic stroke is the most common type and accounts for 80% of all strokes (Figure 1-2). In Western countries, stroke causes 10-12% of all deaths (Brouns & De Deyn, 2009). In the Developing World these statistics are likely to be much higher but there are difficulties obtaining accurate figures in countries where death certificates are not routinely available or where death certificates feature unreliable details (Warlow et al, 2003).

Cerebral artery occlusion most often arises from the production of an atherosclerotic plaque, or thrombus, or from an embolism, which has travelled through the circulation from its origin in the heart (Figure 1-3). The reduction in blood flow can be transient or permanent and the territory of the occluded cerebral artery determines the brain area affected by the stroke and the symptoms exhibited by the patient. Fifty percent of ischaemic strokes are as a direct result of atherothrombotic disease of the extra or intracranial vessels, although the large intracranial vessels are less commonly the source of the thrombus (Warlow et al, 2003). The site of the occlusion is often at bifurcation points of the arterial system due to a combination of turbulent flow and weakened vessel walls at these regions.

Emboli which arise from the heart account for 20% of occlusive strokes. There are various sources of cardiac embolism, the most common being atrial fibrillation and this link has been well established (Warlow et al, 2003). Other sources include cardiac valve disease and patent foramen ovale, although there has been some difficulty in establishing a causal relationship between recurrent ischaemic events and the latter condition (Almekhlafi et al, 2009).

A quarter of all ischaemic strokes arise from occlusion of small intracranial vessels and lacunar stroke, which affects small arterioles, which become tortuous, often as a result of chronic hypertension. These vessels are small ($\leq$ 400μm) and are deeply penetrating and the resulting tortuosity makes the vessel susceptible to occlusion from micro-thrombi and fibrin deposition which can result in lipohyalinosis (Ogata et al, 2011).

1.1.2 Clinical Treatments for Stroke

On admission to hospital following stroke, patients are assessed in order to establish if the clinical diagnosis of stroke is correct and to establish if the stroke is haemorrhagic or ischaemic in origin. This is achieved by the use of the brain imaging techniques, such as computed tomography (CT) and magnetic resonance imaging (MRI). If the stroke is ischaemic in origin, then recanalisation of the occluded vessel will allow restoration of blood supply to the affected brain region and potential salvage of penumbral tissue. Rapid reperfusion of the occluded artery with thrombolysis has been shown to result in favourable clinical outcomes (NINDS, 1995). The only licensed therapy currently available for acute ischaemic stroke is the administration of recombinant tissue plasminogen activator (rtPA). Endogenous tPA is a serine protease which is found in vascular endothelial cells and it catalyzes the activation of plasmin from plasminogen by cleavage of the peptide bond between Arg-560 and Val-561. Activated plasmin has a fibrinolytic function and dissolves fibrin rich blood clots, leading to recanalisation of the occluded blood vessel.

In 1995, the National Institute of Neurological Disorders and Stroke (NINDS) study group evaluated the use of thrombolytic therapy with rtPA in ischaemic stroke patients. Intravenous rtPA (0.9mg/kg) was administered up to 3 hours following stroke onset and the authors reported that patients who received rtPA were at least 30% more likely to have minimal or no disability at 3 months following stroke, compared to those patients who received placebo (NINDS, 1995). However, these authors also reported that there was an increased incidence of intracerebral haemorrhage following thrombolysis.

The European Cooperative Acute Stroke Study (ECASS) examined the effects on neurological outcome when rtPA was administered within 6 hours of stroke onset. This study group reported that thrombolytic therapy effectively improved functional outcome in patients who demonstrated moderate to severe neurological impairment. However, the mortality rate at 30 days following stroke onset was higher than that observed in the placebo treated group and there was also an increased incidence of parenchymal haemorrhage. These findings led the ECASS group to conclude that rtPA should not be administered to an unselected population of acute ischaemic stroke patients due to the increased risk of mortality and haemorrhage asscociated with administration up to 6 hours following stroke onset (Hacke et al, 1995). The second ECASS trial (Hacke et al, 1998) failed to show a significant improvement in patient outcome following administration of

rtPA up to 6 hours following stroke onset. Similarly to the original ECASS trial, the authors reported an increased risk of haemorrhage following thrombolysis.
Thrombolytic therapy with rtPA was therefore recommend for acute ischaemic stroke patients up to 3 hours following stroke onset as it was believed that the risk of haemorrhage following administration at later time points outweighed the clinical benefits. Despite this recommendation, thrombolytic therapy with rtPA is relatively underused with less than 5% of stroke patients receiving treatment to restore cerebral blood flow (Weinberger, 2006). As a consequence, clinical trials continued to explore the effects of administering rtPA outwith the narrow 3 hour time window to increase the number of patients who can potentially benefit from thrombolysis.

The Desmoteplase in Acute Ischemic Stroke Trial (DIAS) evaluated the potential benefit of extending the therapeutic time window to 9 hours following stroke onset. The DIAS trials differed from those discussed previously in that it used desmoteplase as a thrombolytic, not alteplase, which was evaluated in the other thrombolysis trials. The DIAS authors reported that patients who received intravenous desmoteplase within 9 hours of stroke onset demonstrated a higher rate of reperfusion and improved clinical outcome compared to placebo treated patients (DIAS, 2005). The potential benefits of extending the thrombolysis treatment window were also examined in the third ECASS trial. ECASS III reported that intravenous rtPA administered between 3 to 4.5 hours following stroke onset, significantly improved clinical outcome in ischaemic stroke patients (Hacke et al, 2008).
As a result of these findings, the Stroke Therapy Academic Industry Roundtable (Saver et al, 2009) recommended that the therapeutic time window should be extended to 4.5 hours following stroke onset and this has recently been put into place. This will allow greater numbers of stroke patients to benefit from thrombolytic therapy. Despite this extension to the thrombolytic time window, the development of new stroke therapies is still urgently required, to ensure that a greater proportion of patients can obtain treatment and experience an improved outcome following stroke.

It is estimated that up to 30% of first stroke patients are likely to experience another stroke within 1 month of stroke onset (Donnan et al, 2008). Therefore, patients may be prescribed a daily dose of aspirin to reduce the likelihood of secondary stroke. Aspirin can lower the risk of stroke by around 20% due to its antiplatelet actions, which are mediated via inhibition of the cyclo-oxygenase (COX) pathway (Deb et al, 2010). Furthermore, if the patient is hypertensive, their anti-hypertensive medication may be reassessed to reduce the risk of stroke reoccurrence.

Following diagnosis and administration of thrombolytic therapy, if appropriate, stroke patients may be referred to a specialised stroke unit, if the facilities are available. Stroke patients who are admitted to a specialist stroke unit have a better outcome than those patients who are admitted to a general hospital ward (Donnan et al, 2008). Stroke patient mortality is 14-25% higher in general wards compared to stroke units (Clinical Audit Report, Royal College of Physicians, 2001).

1.1.3 Stroke Pathophysiology and the Ischaemic Cascade

The ischaemic cascade describes the complex series of events which contribute to cellular injury following ischaemic stroke (Figure 1-4). Occlusion of a cerebral vessel results in the initiation of multiple deleterious pathways which converge to mediate irreversible ischaemic injury.

Anoxic Depolarisation

Reduced blood flow results in complete absence or a severe reduction in oxygen and glucose delivery to all cell types which comprise the neurovascular unit in the territory served by the occluded vessel. The neurovascular unit consists of neuronal, glial and vascular cell types which contribute to normal brain function. Lack of nutritive delivery renders cells of the neurovascular unit unable to meet their required energy demands via oxidative phosphorylation. This in turn reduces ATP levels and decreases cell pH as lactic acid accumulates as a result of anaerobic glycolysis. Lack of ATP results in neurons being unable to maintain their normal resting membrane potential (-65 to -90mV), since ATP is required to power the Na^+/K^+ ATPase. Under normal conditions, this pump acts to maintain the resting membrane potential by extruding $3Na^+$ ions out of the cell and allows entry of $2K^+$ ions for every molecule of ATP utilised. This preserves a high intracellular concentration of potassium and a low intracellular concentration of sodium ions.

Inactivity of the pump due to ATP depletion allows intracellular sodium levels to rise leading to depolarisation of the membrane potential. Membrane depolarisation triggers opening of voltage-gated calcium channels with subsequent influx of calcium down the electrochemical gradient. Further calcium entry may occur due to reversal of the sodium-calcium exchanger, NCX, which is widely expressed in the brain. This transmembrane protein uses the sodium gradient generated by the Na^+/K^+ ATPase to catalyze the extrusion of one calcium ion and influx of three sodium ions in each reaction cycle, under normal

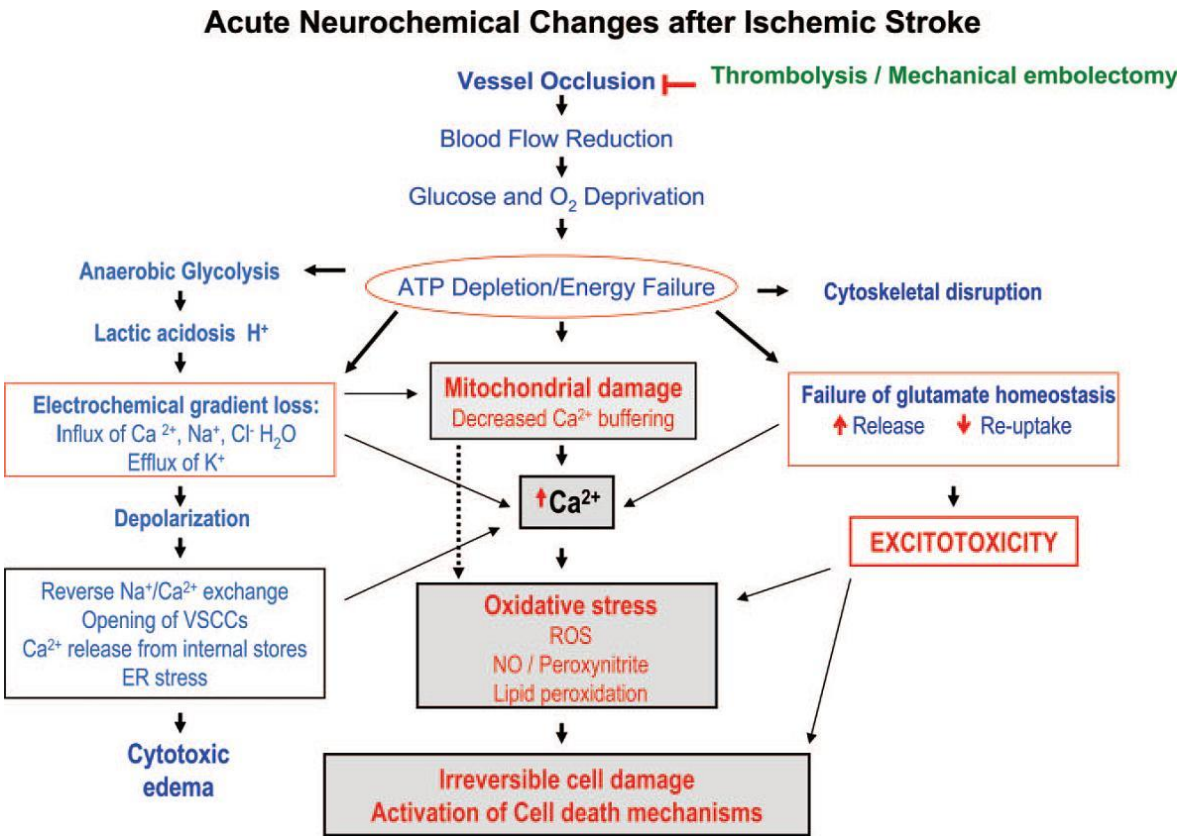

Figure 1-4. The Ischaemic Cascade. A wide spectrum of neurochemical alterations are triggered following occlusion of a cerebral blood vessel. Multiple pathways converge to contribute to irreversible cellular injury and cytotoxic oedema. The ischaemic cascade presents multiple targets for neuroprotection following ischaemia. Reproduced from Chavez et al. (2009).

resting conditions (Besancon et al, 2008). In severe ischaemia, where ATP levels are low and Na^+/K^+ pump activity is compromised, intracellular overloading of sodium causes NCX to operate in the reverse mode, leading to entry of 3 calcium ions per cycle. The combined influx of calcium via NCX reversal and through voltage gated calcium channels can trigger spontaneous release of neurotransmitters from the active zone of the presynaptic neuronal element via calcium-mediated exocytosis. Glutamate is the major excitatory neurotransmitter of the central nervous system and when its release and re-uptake are not under physiological control, is largely responsible for initiating a cascade of excitotoxic events.

Glutamate Excitotoxicity

The mechanism of presynaptic glutamate release may occur via spontaneous exocytosis, by reverse operation of the sodium dependent glutamate uptake system, or by standard calcium-mediated exocytosis. However, the excessive extracellular glutamate levels observed in ischaemia are likely to be attributable to all three modes of release.
The excess glutamate release into the extracellular space allows for an increased activation of postsynaptic glutamate receptors, of which there are four classes: Ionotropic kainate, AMPA and NMDA receptors and metabotropic glutamate receptors (mGluR). Kainate receptors are found in specific brain regions only, and along with AMPA receptors, they mediate basal synaptic transmission. Ligand binding triggers channel opening, allowing entry of sodium and chloride ions and extrusion of potassium ions along their electrochemical gradients. Water enters the cell passively as a result of high Na^+ and Cl^- entry, leading to cytotoxic oedema. This may have an effect on the perfusion of regions of brain tissue surrounding the infarct and may also cause a slight rise in intracranial pressure, vascular compression and herniation. These are major determinants of whether a patient survives beyond the first few hours following a stroke (Dirnagl et al, 1999).

Excessive and prolonged membrane depolarization occurs as a result of AMPA receptor stimulation and this in turn results in activation of the NMDA receptor. The NMDA receptor is unique in that it requires both ligand binding and a voltage change to induce channel opening. Local depolarisation displaces the voltage-dependent magnesium block from the channel to allow entry of sodium and calcium and extrusion of potassium ions.

Additionally, glutamate activation of mGluRs leads to activation of Phospholipase C. This enzyme catalyzes the hydrolysis of the membrane protein, phosphatidylinositol 4,5-

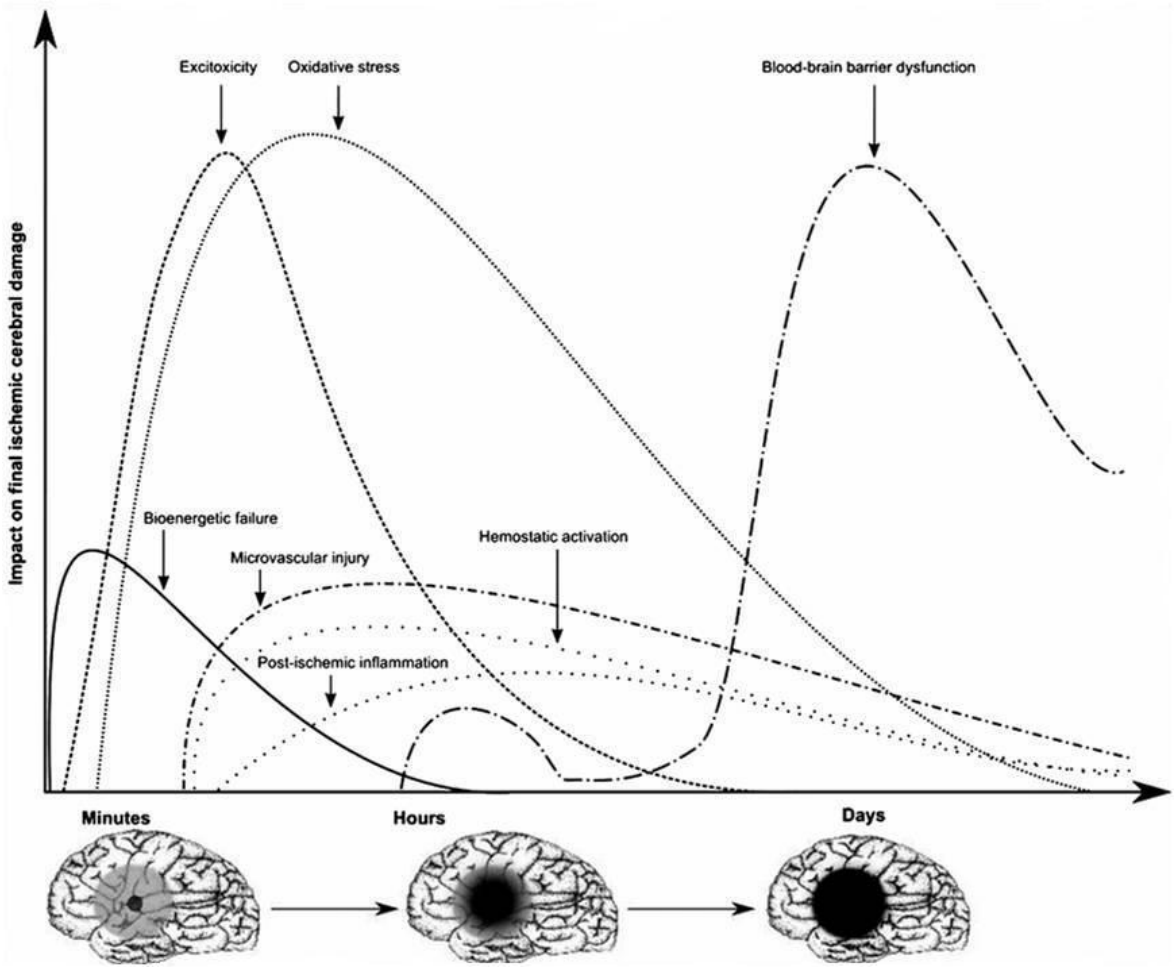

Figure 1-5. A representation of the temporal profile of the pathophysiological mechanisms underlying acute focal ischaemia and their contribution to cerebral ischaemic injury. In the absence of reperfusion, the ischaemic penumbra (shown in grey) will proceed to infarction as the ischaemic core expands to encompass the perfusion deficit (shown in black). Reproduced from Brouns & De Deyn (2009).

bisphosphate (PIP_2) to release the 2nd messengers diacylglycerol (DAG) and inositol 1,4,5-trisphosphate (IP_3). DAG activates protein kinase C, which further stimulates voltage-gated calcium channels. IP_3 mediates the release of calcium from intracellular stores by binding to an IP_3 sensitive channel located in the membrane of the endoplasmic reticulum (ER). The ER is a major source of calcium since under normal conditions, 99% of total cell calcium (1000µmol/l) is bound or stored, with only 0.1µmol/l free in the cytosol. Furthermore, resequestration of calcium into the ER is mediated via a calcium ATPase, so re-uptake of calcium into the ER lumen is reduced as a result of decreased ATP levels. This further contributes to the increase in intracellular calcium and it is evident that the rise in cytosolic calcium associated with ischaemia is derived from multiple pathways (Kristian & Siesjo, 1998).

Calcium Activation of the Ischaemic Cascade

Calcium is the major mediator of ischaemic cell damage and death, by triggering a cascade of reactions within the cell. It activates a variety of enzymes including endonucleases, which result in DNA and RNA damage, as well as proteases and lipases, along with other factors, which mediate further cell dysfunction and damage. The calcium-mediated cascade also involves the production of free radicals including nitric oxide, which have numerous effects on cell function and viability. The temporal profiles of the components of the ischaemic cascade are illustrated by Figure 1-5.

Free Radical Generation

Calcium mediated activation of the enzyme phospholipase A_2 triggers the breakdown of membrane phospholipids to form arachidonic acid, which then undergoes oxidative metabolism via the COX or lipoxygenase pathways, resulting in the synthesis of eicosanoids. Superoxide or hydroxyl free radicals are also released during this process. This pathway involves a positive feedback cycle, as free radical production further stimulates phospholipase A_2 activity and consequently enhances the generation of free radicals. Free radicals may also be generated as a result of hypoxanthine oxidation. Hypoxanthine accumulates under hypoxic conditions due to the breakdown of adenine nucleotides. Superoxide radicals are released as xanthine dehydrogenase is converted to xanthine oxidase during the metabolism of hypoxanthine.

Nitric oxide (NO) production increases in ischaemia as a result of increased intracellular calcium levels. Calcium activates calcineurin, which in turn activates neuronal nitric oxide synthase (nNOS). This enzyme catalyzes the synthesis of NO from its precursor, L-arginine. Under normal physiological conditions, NO functions as a neurotransmitter and has a role in synaptic plasticity (Pacher et al, 2007) as well as in the control of cerebral blood flow, where it acts as a vasodilator. Under ischaemic conditions, NO combines with superoxide to form peroxynitrite, which is a highly reactive oxidant. In ischaemia, where L-arginine levels may become rate limiting, nNOS may generate peroxynitrite directly by producing both NO and superoxide. Peroxynitrite is extremely potent and causes extensive tissue damage via inhibition of DNA synthesis and nucleic acid damage, lipid peroxidation, leading to membrane breakdown. This oxidant also mediates mitochondrial dysfunction and activation of poly (ADP-ribose) polymerase (PARP). PARP is a nuclear enzyme, which is strongly activated by single stranded breaks in DNA caused by the actions of peroxynitrite and free radicals (as reviewed by Lipton, 1999). PARP upregulates the transcription factors activator protein 1 (AP1) and nuclear factor kappa B (NFκB), which enhance post-ischaemic brain inflammation. PARP toxicity also involves depletion of ATP and stimulates release of apoptosis inducing factor (AIF) from mitochondria which activates caspase independent apoptosis (as reviewed by Beckman & Koppenol, 1996). Therefore PARP neurotoxicity is multifactorial and influences multiple pathways.
NO may also have an indirect neuroprotective effect by inducing vasodilatation to increase local blood flow and enhance collateral circulation. NO also inhibits platelet aggregation and leukocyte adhesion, thereby preventing microvascular plugging and occlusion. Furthermore, vascular NO may inhibit the ischaemic cascade by preventing inflammation, oxidative injury and neuronal apoptosis (as reviewed by Pacher et al, 2007).

Free radicals have extremely destructive effects on cells and under ischaemic conditions their high production levels completely overwhelm endogenous free radical scavengers, like uric acid and glutathione. The brain is particularly susceptible to free radical mediated cellular injury due to its limited antioxidant responses (Adibhatla & Hatcher, 2010). Free radicals have a range of detrimental cellular effects including enzyme inactivation, release of calcium ions from intracellular stores, protein denaturation, lipid peroxidation and damage to DNA and RNA, in addition to cytoskeletal component breakdown (Brouns & De Deyn, 2009). Free radicals also act as signalling molecules to induce an inflammatory response and trigger apoptosis (Brouns & De Deyn, 2009). Free radicals have detrimental effects on mitochondria, where they disrupt the inner mitochondrial membrane via lipid peroxidation. In addition, free radicals impair mitochondrial function further by oxidising

the proteins, which are involved in the electron transport chain to mediate ATP production and H^+ extrusion (Dugan & Choi, 1994). Overall, free radicals result in severe mitochondrial dysfunction and mediate cellular damage via various actions within the cell.

Peri-infarct Spreading Depolarisations

In the ischaemic core, cells undergo anoxic depolarisation and are unable to repolarise. However, in less severely hypoperfused penumbral tissue located at the boundary of the ischaemic core, cells retain the ability to repolarise but they do so at the expense of further energy consumption and oxygen extraction levels are increased to compensate for the reduced cerebral blood flow. Once repolarised, these cells can then again depolarize in response to high glutamate and potassium ion levels, which accumulate in the extracellular space. This cycle can continue and repetitive depolarisations are called peri-infarct depolarisations. Peri-infarct depolarisations occur spontaneously over several days following stroke onset and this has been demonstrated both in pre-clinical (Hartings et al, 2003) and clinical stroke research (Dohmen et al, 2008). This phenomenon has been particularly well documented in rodent models of stroke and as the frequency of these events increases, greater numbers of cells in the penumbra become incorporated into the ischaemic core (Mies et al, 1993). This has also been demonstrated in human stroke patients, where delayed ischaemic brain damage was associated with spreading depolarisations (Drier et al, 2006).

Inflammatory Responses to Ischaemia

An inflammatory response is triggered by various factors in ischaemic conditions, including increasing free radical levels, calcium activated second messenger systems and by the state of hypoxia itself. This results in the synthesis of transcription factors, like NFκB and hypoxia inducible factor 1 (HIF1), which promote expression of pro-inflammatory genes to produce inflammatory mediators like tumour necrosis factor α (TNFα), interleukin1β (IL-1β) and platelet activating factor (PAF), to name but a few. Production of these mediators induces surface expression of adhesion molecules like intercellular adhesion molecule 1 (ICAM-1), vascular cell adhesion molecule 1 (VCAM-1) and E-selectin. These molecules interact with complementary receptors located on the surface of neutrophils, allowing their passage across the blood-brain barrier (BBB). Macrophages and monocytes follow suit, migrating into the ischaemic brain, guided by

chemokine signals produced by cells at the site of the lesion (as reviewed by Dirnagl et al, 1999).

Four to six hours following cerebral ischaemia, microglia become activated and attracted to the site of injury by monocyte chemoattractant protein 1 (MCP-1) (Brouns & De Deyn, 2009). MCP-1 is activated by plasmin following opening of the BBB due to death of endothelial cells in response to ischaemia. Once activated, microglia assume an ambeoid appearance and retract their processes (Dirnagl et al, 1999), allowing proliferation to occur. They then secrete a variety of neurotoxic and neuroprotective compounds. The neuroprotective factors include plasminogen, thrombospondin and tumour growth factor b1 (TGFb1), which has a role in angiogenesis and extracellular matrix formation. However, there is increasing evidence that post-ischaemic inflammation actually contributes to brain injury via microvascular obstruction by neutrophils (Del Zoppo, 1991). Activated microglia secrete neurotoxins, such as TNFα, which may exacerbate ischaemic neuronal damage. Furthermore, TNFα is also released by ischaemic neurons (Barone et al, 1997). In addition, the ischaemic inflammatory response may also be linked to the initiation of apoptotic pathways, since it has been described that the use of antibodies against cell surface adhesion molecules, reduced ischaemic cell damage and apoptotic cell death (Chopp et al, 1996). Therefore, the inflammatory response observed following ischaemia appears to have a dual role in both neuroprotection and neurotoxicity, although its principal role is not yet clear.

Astrocyte Response to Ischaemia

Within the neurovascular unit, astrocytes provide trophic, metabolic and antioxidant support to neurons and also react to ischaemic conditions in the brain (Pastor et al, 2009). Within minutes of reduced cerebral blood flow, astrocytes swell and the cytoplasm becomes lucent. This particularly occurs in perivascular foot processes surrounding capillaries. In irreversible ischaemic injury, swelling leads to a doubling of cell volume with a reduction in cell organelle content and complete loss of glial fibrillary acidic protein (GFAP). Reactive astrocytes are stimulated by the release of TGFb1 by activated microglia and they can be distinguished morphologically by the large quantity of GFAP and vimentin intermediate filaments in the cytosol (Li et al, 2008). These astrocytes produce a variety of neurotrophic factors, including basic fibroblast growth factor (bFGF) and insulin-like growth factor 1 (IGF-1), to potentiate recovery of damaged neurons (Ridet et al, 1997). However, the precise molecular mechanisms involved in the astrocyte response to ischaemia are not yet clear.

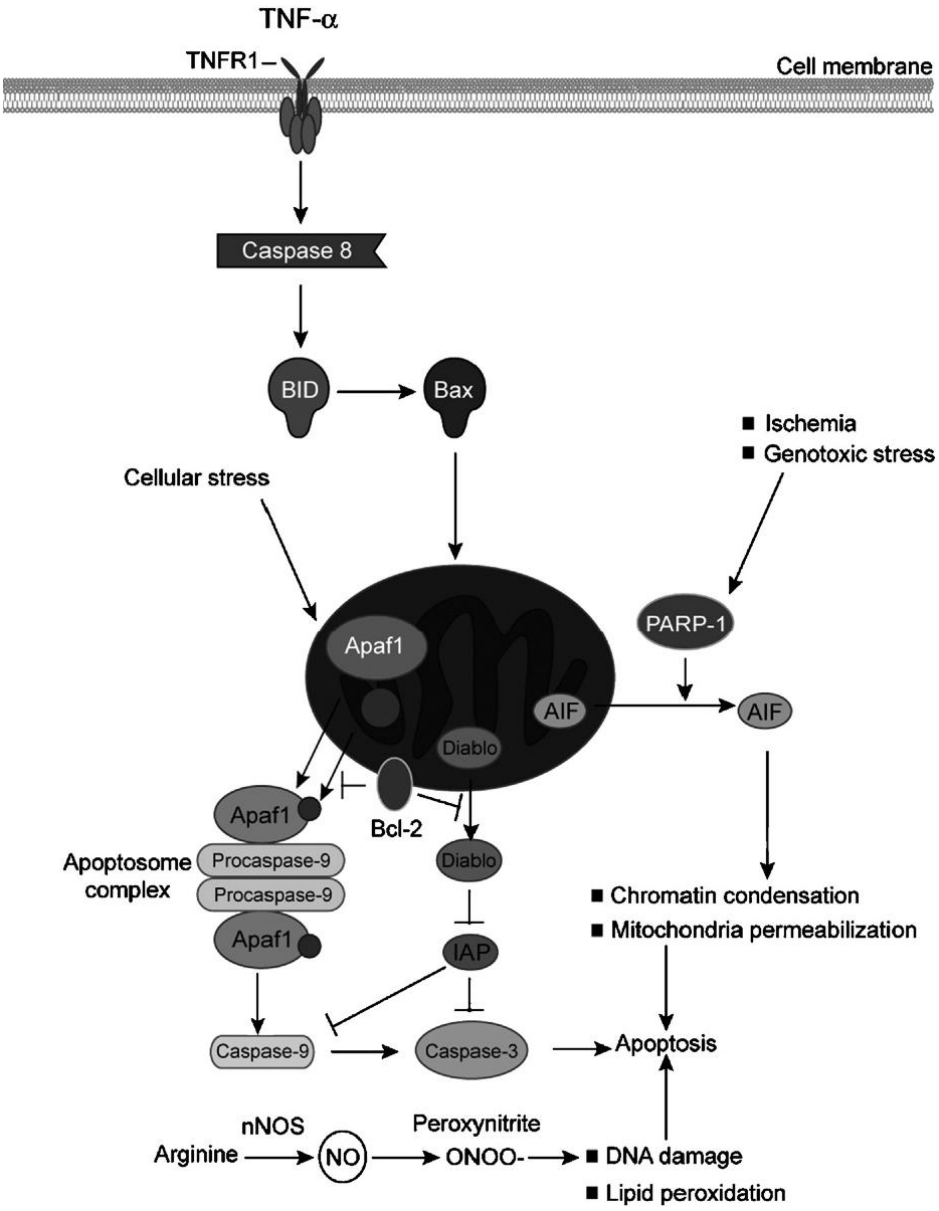

Figure 1-6. Apoptosis cascades mediated by TNFα and mitochondrial pathways. The activation of TNF receptors can induce apoptosis directly by activating caspase cascades and indirectly by stimulating mitochondrial mediated apoptosis. Cytochrome c released from the mitochondrion mediates formation of the apotosome complex and subsequent activation of caspases 9 and 3, leading to induction of apoptosis. Ischaemia induced release of AIF from the mitochondrion promotes apoptosis independently of caspase activation. Reproduced from Weinberger (2006).

Mechanisms of Cell Death

Under ischaemic conditions, cells of the neurovascular unit may die either by necrosis or by apoptotic pathways which are highly conserved biochemical pathways which signal and execute cell death. The mechanism of cell death employed depends on the nature of the excitotoxic stimulus, cell type and the stage in development or life cycle (Leist & Nicotera, 1998).

Necrosis appears to be the predominant mechanism of neuronal cell death following acute, permanent vascular occlusion (Dirnagl et al, 1999). Therefore, necrotic cell death occurs in the ischaemic core, where perfusion is most severely reduced and cells are irreversibly damaged, since necrosis only occurs following an exogenous insult and is not involved in normal physiological processes. If a cell dies through the necrotic pathway, it releases more glutamate and toxic mediators into the environment, affecting surrounding cells (Brouns & De Deyn, 2009).

Apoptosis

Apoptosis is a programmed cell death mechanism, which appears to occur in cells that are affected by milder injury and particularly occurs in the ischaemic penumbra (Dirnagl et al, 1999). Characterization of programmed cell death processes in *Caenorhabditis elegans* lead to much greater understanding of the mechanisms involved in apoptosis in mammalian systems.

Apoptotic pathways can either be caspase dependent or independent (Figure 1-6), although neurons are particularly susceptible to caspase mediated cell death programmes following focal cerebral ischaemia. Caspase dependent apoptosis involves the release of cytochrome c from the mitochondrial intermembrane space as a result of free radical induced mitochondrial dysfunction. Cytochrome c enters the cytosol and activates apoptosis activating factor 1 (Apaf-1) and procaspase 9, which combine to form an apoptosome complex. This complex then activates an apoptosis effector system, which involves a cascade of endonucleases and caspases. Caspases are cysteine proteases, which cleave proteins of the nuclear lamina and cytoskeleton, including PARP and gelsolin,

Caspase 3 activation has been shown to be one of the most critical steps in apoptosis induction and occurs hours before cell death occurs. Following transient middle cerebral artery occlusion in the mouse, cytochrome c release was detected after 6 hours, caspase

processing occurred at 9 hours and prominent cell death was not evident until 24 hours following occlusion (Endres et al, 1998).

Caspase independent apoptosis is mainly driven by apoptosis inducing factor (AIF). AIF is a mitochondrial inner membrane flavoprotein oxioreductase, which acts as a pro-survival factor. It is essential for long time mitochondrial function and is important in maintaining complex 1 integrity and H_2O_2 scavenging capability. However, when AIF is released from the mitochondrion into the cytosol, it reaches the nucleus, where it has an anti-survival role by triggering DNA degradation and cell death.

1.2 Animal Models of Cerebral Ischaemia

1.2.1 Rodent Stroke Models

The main features of human ischaemic stroke can be modelled in animal models of focal cerebral ischaemia. Primate and higher mammal models of stroke are of greatest relevance to the human condition but such models present a variety of problems. Primate models in particular are most relevant when examining the behavioural effects of stroke, especially with regards to manual dexterity, which is lacking in lower mammals. However, there are many disadvantages to using such models, namely cost of maintenance and the need for specialist animal facilities. There are also many ethical considerations as there are lower levels of social acceptance with the use of these models (Carmichael, 2005).
However, there are many advantages in the use of rodent stroke models. Mice are the most suitable species when examining the molecular pathophysiology of stroke, since genetic modifications can be easily introduced (Fujimura et al, 1999). Rat models are the most appropriate to model focal cerebral ischaemia due to their size, which allows physiological parameters to be easily monitored and brain tissue can also be easily examined by neuroimaging techniques or histological staining methods. Furthermore, reproducible studies can be conducted with ease due to the relative homogeneity within strains of rat (Durukan & Tatlismak, 2007). However, by far the most convincing argument for the relevance of rat models of stroke, is the similarity between the cerebrovascular systems of humans and rats, both on an anatomical and functional level (Macrae, 1992), with both species possessing a circle of Willis (Figure 1-7).

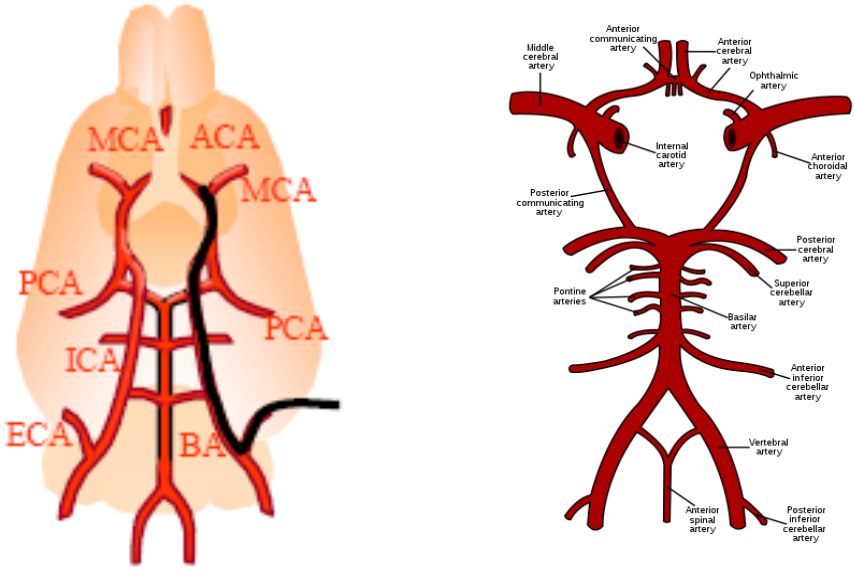

Figure 1-7. The cerebrovascular systems of rat (left) and man (right). Both species possess a circle of Willis which makes the rat a suitable species for modelling human stroke. In humans the middle cerebral artery is commonly occluded and therefore most rat models of focal cerebral ischaemia involve occlusion of this artery. This procedure is most often performed using the intraluminal thread model where a nylon suture (shown in black) is introduced into the internal carotid artery and progressed until it blocks the origin of the middle cerebral artery.

The middle cerebral artery is the vessel which is most commonly occluded in human stroke (Mohr et al, 1986) and therefore, rat models involving middle cerebral artery occlusion (MCAO) are of particular relevance to the clinical situation. The intraluminal filament model of MCAO was first described by Koizumi et al (1986) and this technique has since been refined by various study groups (Belayev et al, 1996; Schmid-Elsaesser et al, 1998). This technique involves introducing and passing a filament of a specified diameter along the internal carotid artery until the filament reaches the bifurcation point and is lodged at the junction of the anterior and middle cerebral arteries, blocking off the proximal origin of the middle cerebral artery. This model can induce either transient or permanent ischaemia, since the filament can be retracted after a defined time period. There are various factors which can influence the reproducibility of this model, including filament diameter, insertion length and filament coating. Filaments coated with silicon have been shown to reduce the risk of haemorrhage and premature reperfusion (Belayev et al, 1996; Schmid-Elsesser et al, 1998) and the size of the filament correlates well with infarct volume (Durukan & Tatlisumak, 2007). However, intraluminal thread MCAO models present their own problems, primarily from the risk of blood vessel rupture and haemorrhage. Furthermore, artery occlusion may be incomplete, allowing some perfusion of the territory served by the middle cerebral artery (MCA). Additionally, blood vessels outside of the territory of the MCA may also be occluded by the filament.

Although the intraluminal filament model is the most commonly used stroke model, the middle cerebral artery can be occluded by other means. For example, the MCA can be permanently occluded by electrocoagulating the proximal region of the artery (Tamura et al, 1981). This model requires a craniectomy, which reduces the mortality associated with ischaemia induced acute brain swelling and produces a highly reproducible infarct, which is smaller than that produced by the intraluminal filament model (Macrae, 1992). Experimental stroke can also be induced by stereotaxic injection of the potent vasoconstrictor, endothelin-1 which can produce selective grey or white matter ischaemia depending on the location of the injection. This allows small white matter infarcts to be produced (Frost et al, 2006) and can also be used to occlude the middle cerebral artery by injecting endothelin-1 into the adjacent grey matter (Sharkey et al, 1993). Embolic stroke can also be induced experimentally where an embolus is introduced into the cerebrovasculature to occlude a cerebral artery. The embolic model is of particular relevance when examining the effect of thrombolytic therapy (Henninger et al, 2009; Zhu et al, 2010). However, infarcts produced by embolic models are generally less reproducible than those produced by the intraluminal filament and electrocoagulation models of MCAO.

This is likely to arise from variations in clot stability and the final lodgement of the embolus within the cerebrovasculature (DiNapoli et al, 2006).

There are many who question the validity of rat stroke models and their relevance to the human condition due to the lack of research using aged animals with stroke risk factors and poor study design. In addition, experimental strokes are highly reproducible in rodent models but in the human stroke patients the size and location of the stroke is highly variable. The intraluminal filament model of MCAO in particular, produces very large infarcts which may not model the most treatable and common human strokes (Carmichael, 2005). In addition, many of the anaesthetics commonly used during stroke surgery, have been demonstrated to have neuroprotective effects, which will influence stroke outcome. Therefore, the choice of anaesthetic used during the experiment, must be carefully considered.

1.2.2 Neuroprotection in Animal Models of Stroke

In animal models of stroke, pharmacological targeting of the pathways involved in the ischaemic cascade have been successful in reducing infarct size and the extent of neuronal damage as well as improving functional outcome. However, when these treatments were introduced into human clinical trials, their efficacy was lost and in some cases, even led to exacerbation of ischaemic damage (Internet Stroke Centre:www.strokecenter.org/trials/). There are many hundreds of published pre-clinical articles reporting the neuroprotective effects of drugs which target the mechanisms involved in stroke pathophysiology but to date, none of these therapeutic strategies have translated to human stroke patients. There are many reasons why this may occur, including the increased age of clinical trial patients compared to the use of young adult animals, as well as anatomical and physiological differences between the brains of humans and animals, poor study design and lack of penumbral imaging for patient recruitment in clinical trials (Dirnagl et al, 1999; Röther, 2008; Chavez et al, 2009). Despite these disappointing results, the pathophysiological pathways involved in stroke remain a prime target for the development of future stroke therapies. Therefore understanding the pathophysiological mechanisms underlying stroke can identify targets for possible pharmacological intervention to allow development of stroke therapies, which will reduce the high mortality rates and the degree of disability associated with this disorder.

1.2.3 The Spontaneously Hypertensive Stroke-Prone Rat (SHRSP)

The spontaneously hypertensive stroke-prone rat (SHRSP) is commonly utilised in models of malignant hypertension and cerebrovascular disease, including stroke. This strain develops progressive hypertension at a young age and is prone to spontaneous stroke, which is similar to the human condition. Hypertension is well established as a major risk factor for human stroke and contributes to the development of stroke in the SHRSP.

The SHRSP was developed in 1974 by Okamoto and colleagues, by selective inbreeding of spontaneously hypertensive rats (SHR). The offspring produced, where at least one of the breeding pair experienced spontaneous stroke, were maintained over successive generations. The SHR strain had been previously developed from selective inbreeding of normotensive Wistar-Kyoto (WKY) rats which exhibited elevated blood pressure (Okamoto & Aoki, 1963).

Both SHR and SHRSP show increased sensitivity to experimental stroke compared to normotensive rat strains (Duverger & MacKenzie, 1988). However, the SHRSP strain demonstrates more severe hypertension and an increased susceptibility to spontaneous stroke. There are many factors implicated in the increased stroke sensitivity observed in the SHRSP, including an enhanced inflammatory response, impaired collateral flow and a variety of other anatomical and physiological abnormalities, in addition to genetic hypertension.

Furthermore, the SHRSP can also be used as a model of metabolic syndrome, which is a complex multifactorial disease linked to insulin resistance. Hypertension is a known risk factor for metabolic syndrome and feeding SHRSPs a 60% fructose diet induces impaired glucose tolerance, dyslipidaemia and increased adiposity compared to WKY rats (Strahorn et al, 2005).

1.2.4 Genetic Background of SHRSP

The structural and physiological differences that are demonstrated by the SHRSP, compared to SHR and WKY, are determined by their genetic background. At least three major genes are known to influence the development of severe hypertension and the gene

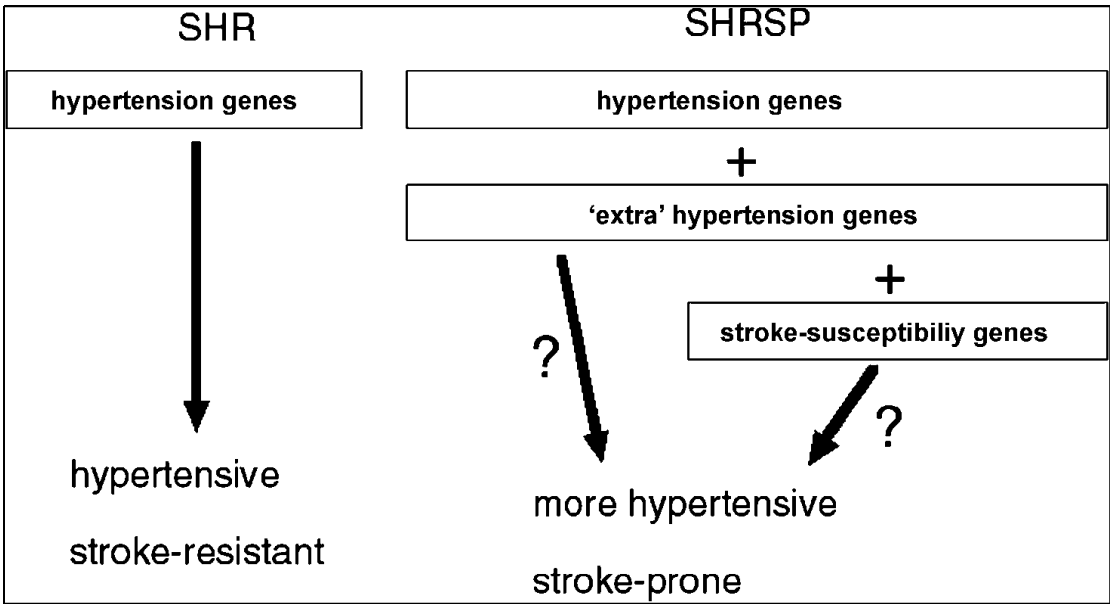

Figure 1-8. Hypothetical genetic make-up of SHR and SHRSP. SHRSP possess additional genes which contribute to increased sensitivity to experimental stroke which are independent of blood pressure since larger infarcts are observed in SHRSP before the development of hypertension. Reproduced from Nabika et al (2004).

loci which contribute to the development and maintenance of hypertension are different depending on the age of the animal (Mashimo et al, 1999). In young animals, quantitative trait loci (QTLs) on chromosomes 1, 3 and 4 contribute to the elevated basal blood pressure observed in the stroke-prone strain. However, the rise in blood pressure observed following salt-loading can be linked to a QTL on chromosome 10. In addition, there are other genes which are involved in stroke which are independent of blood pressure since SHRSP show increased stroke sensitivity before the onset of hypertension, indicating other genetic factors (Figure 1-8).

The increased stroke sensitivity demonstrated by the stroke-prone strain has been shown to be inherited as a dominant trait. Gratton et al (1998) reported that the offspring of a SHRSP/WKY cross (WKY father) exhibited infarcts following experimental stroke which were directly comparable with that observed in the SHRSP strain, indicating a dominant mode of inheritance for increased stroke sensitivity. Furthermore, Carswell et al (1999) reported that male offspring from a WKY/SHRSP cross, where the father was of the stroke-prone strain, demonstrated reduced sensitivity to experimental stroke than those with a WKY father. The authors proposed that this effect may be attributed to the increased blood pressure exhibited by males with a Y chromosome inherited from SHRSP, since they demonstrated that there was a significant negative correlation between high blood pressure and small infarct volume following permanent MCA occlusion.

Jeffs et al (1997) proposed that increased sensitivity to experimental stroke in the SHRSP was linked to a QTL on chromosome 5, which co-localises with the genes which encode atrial natriuretic factor (ANF) and brain natriuretic factor (BNF). Both of these proteins are vasoactive and may play a role in the control of vasoreactivity, growth and remodelling of cerebral blood vessels (Jeffs et al, 1997). However, in a later study by the same group, the genes encoding ANF and BNF were excluded as candidates for the increased stroke sensitivity demonstrated by SHRSP as they were unable to identify any differences in the coding regions of these genes between the stroke-prone and the normotensive reference strain. In addition, there was no difference in the expression of ANF and BNF between strains, even following MCA occlusion (Brosnan et al, 1999).

Rubbatu and colleagues (1999) examined the genes involved in stroke proneness and these authors did identify strain differences in the sequence coding atrial natriuretic peptide, resulting in altered structure of the gene product in the stroke-prone strain. The conflicting findings of these studies show that the genes involved in the risk of spontaneous stroke

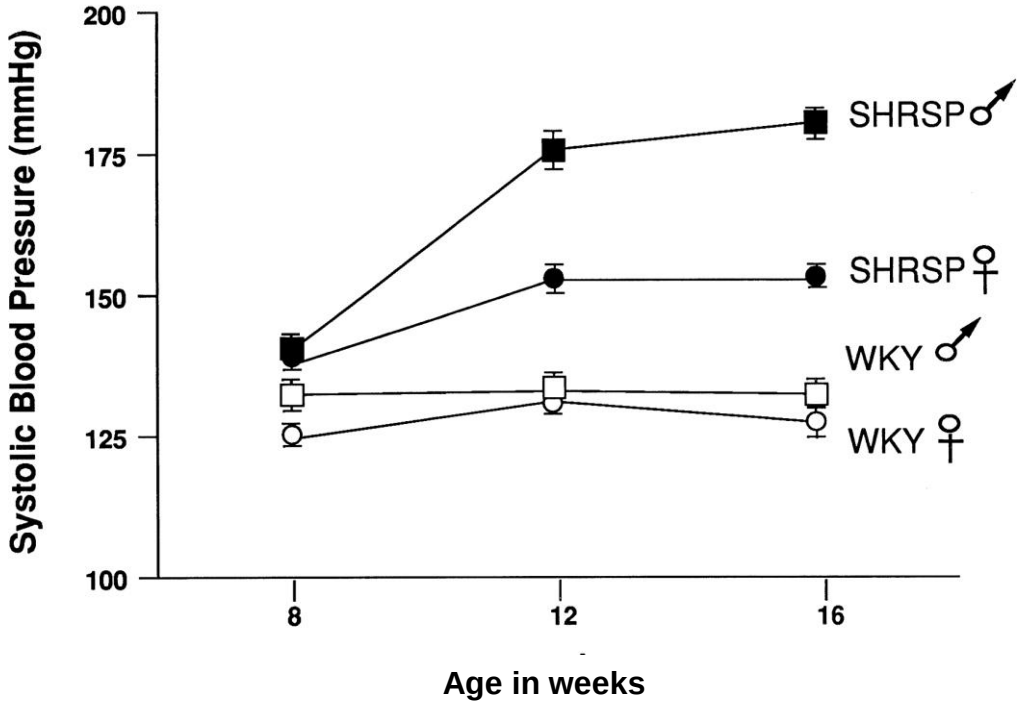

Figure 1-9. The range of systolic pressures of the SHRSP and normotensive WKY strain, measured using the tail cuff method at weeks 8, 12 and 16. Both sexes of the stroke-prone strain display higher pressures than the normotensive reference strain WKY. However, female SHRSP develop hypertension which is not as severe as that observed in male SHRSP. Adapted from Davidson et al (1995).

differ from those genes which predispose SHRSP to increased sensitivity to experimental stroke although both QTLs are localised on chromosome 5.

1.2.5 Development of Hypertension in SHRSP

Immature SHRSP are normotensive, with blood pressure values which are comparable to that of the reference strain WKY (Davidson et al, 1995). When the animals reach around 8 weeks of age, systolic blood pressure begins to rise progressively from approximately 140mmHg to 175mmHg by 16 weeks. Blood pressure of the normotensive WKY remains at around 135mmHg. However, Okamoto et al (1974) reported frequent severe hypertension in the SHRSP of up to 250mmHg by 20 weeks of age, while maximal blood pressure observed in the stroke-resistant SHR strain did not rise above 200mmHg.
Therefore, the increased susceptibility to stroke demonstrated by the SHRSP may be attributed to the increased blood pressure observed in this strain since induction of severe hypertension (>225mmHg) in normotensive rats using a kidney clip procedure, resulted in spontaneous stroke and infarct sizes comparable to that observed in SHRSP (Zeng et al, 1998). Despite this, other genetic factors must contribute to stroke susceptibility in the SHRSP, since experimental stroke produces significantly larger infarcts in this strain compared to WKY, even before hypertension develops (Coyle & Jokelainen, 1983).

Interestingly, females develop hypertension much more slowly and to a much lesser degree than their male counterparts (Figure 1-9). In immature SHRSP females, systolic blood pressure is comparable with that of the male and also begins to rise at around 8 weeks. By week 12, female systolic blood pressure has reached a peak of around 150mmHg (Ibrahim et al, 2005). Chronic hypertension is associated with growth and remodelling of the cerebral vasculature, where the lumen diameter of vessels is reduced and the vascular wall is thickened in response to increased pressure. This results in an increased wall to lumen ratio and increased vascular resistance. Thickening of the vascular wall is an adaptation to the increased intraluminal pressure and serves to counteract the increased wall tension and protect the vessel against high pressure changes (Izzard et al, 2003). The autoregulation curve is shifted to the right as the resistance vessels act to regulate diameter at a higher pressure range and the vasodilatory response to lower pressures is impaired as a consequence of reduced lumen diameter (Izzard et al, 2003). This means that cerebral blood flow will be compromised at blood pressure values which are capable of maintaining cerebral blood flow (CBF) in normotensive rats.

1.2.6 Spontaneous Stroke

Okamoto and colleagues (1974) reported a high incidence of spontaneous stroke in both sexes of adult SHRSP, although the likelihood of stroke in males was markedly greater than that observed in females, where incidence of spontaneous stroke was 80% in males aged over 100 days and 60% in females over 150 days old.

Common symptoms of spontaneous stroke in the SHRSP include hyperirritability, aggression, and motion disturbances, comprising of episodes of repetitive paw lifting, ataxia and paralysis (Okamoto et al, 1974). Following the appearance of these symptoms, the rats typically survived from a couple of days to 24 weeks. Just prior to death, many animals displayed additional symptoms of apathy and urinary incontinence and a small group of animals also demonstrated self-biting behaviours.

Examination of brains following death revealed cerebral lesions resulting from fresh intracerebral haemorrhage or infarction. In some cases, infarcts were accompanied by evidence of previous haemorrhage (Okamoto et al, 1974). Most lesions were located in the cortex or subcortical region of the left occipital area but around 15% of animals which had experienced spontaneous stroke demonstrated lesions in the basal ganglia. Occasionally, lesions were observed in the frontal cortex. Okamoto et al (1974) recognised that cerebral lesions correspond to the boundary areas between the three major cerebral arteries and that anastomoses between these vessels were scarcely observed. This suggests a vascular abnormality in this strain of rat and it has been widely reported that spontaneous stroke in the SHRSP occurs as a result of pathological changes in small perforating arteries, leading to fibrinoid necrosis and brain oedema. This mirrors the clinical situation of malignant hypertension in humans (Ogata et al, 1980). In addition, the onset of spontaneous stroke can be accelerated by feeding the animals a salt-loaded diet or by administration of 1% sodium chloride in their drinking water (Okamoto et al, 1974).

Furthermore, the incidence of stroke is highly correlated with a rapid increase in blood pressure and also with the severity of hypertension. This may give some explanation why the incidence of stroke in higher in male SHRSP than females, as hypertension progresses more quickly in males and increases to a greater level, as previously discussed. This means that females may die of another condition, like pneumonia, before spontaneous stroke occurs (Okamoto et al, 1974), since this strain is particularly susceptible to respiratory

infections, as a result of an impaired immune system and may die before there is evidence of hypertensive vascular changes (Ogata et al, 1982).

1.2.7 Increased Sensitivity to Experimental Stroke

It is well established that SHRSP are more sensitive to experimental stroke than the normotensive control strain, WKY (Coyle & Jokelainen, 1983; Carswell et al, 1999; Marks et al, 2001). Following permanent middle cerebral artery occlusion via electrocoagulation of the distal portion of the artery, infarct volume was significantly greater in the ipsilateral hemisphere of the SHRSP compared to that observed in the WKY (36.6% of the hemisphere vs. 14.0% respectively – see Figure 1-10), as reported by Carswell et al (1999). Similarly, Marks and colleagues also reported significant differences in infarct volume following permanent distal MCAO, between the two strains. Twenty four hours post occlusion, infarct volume in the SHRSP was recorded as 135mm^3. In comparison, infarct volume in the ipsilateral hemisphere of the WKY was measured as 102mm^3 (Marks et al, 2001). However, a more accurate representation of infarct volume is given by the percentage of the hemisphere, rather than actual volume, since there are differences in overall brain volume between the two strains and this method does not take brain oedema into account and therefore may overestimate infarct size.

There are many factors which may account for the increased sensitivity to stroke exhibited by the SHRSP. It has been demonstrated that the stroke-prone strain display increased release of glutamate during cerebral ischaemia, compared to normotensive WKY and stroke-resistant SHR (Gemba et al, 1992). This may contribute to increased excitotoxicity and neuronal damage contributing to the increased infarct volume observed in SHRSP. There are many additional anatomical and physiological factors which may contribute to the increased sensitivity to experimental stroke in this strain and these shall now be discussed.

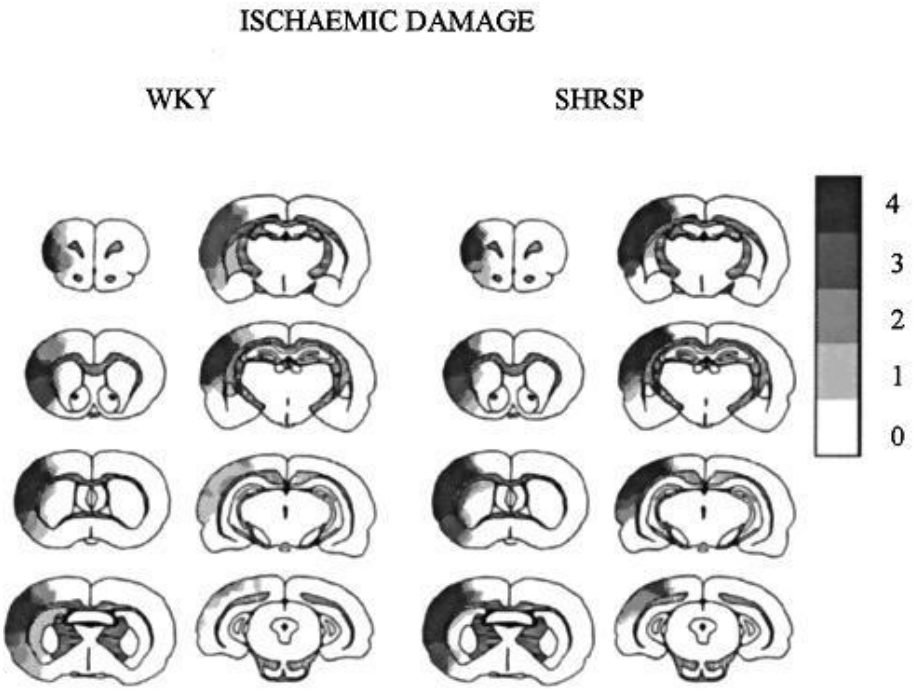

Figure 1-10. The topography of the infarct observed in WKY and SHRSP across 8 coronal levels following distal middle cerebral artery occlusion. The shaded bar (scale 0 to 4) indicates the infarct areas observed, where 4 represents areas which were infarcted in 100% of animals; 3- areas infarcted in 75% of animals; 2- areas infarcted in 50% of animals and 1- areas infarcted in 25% of animals. Note the greater infarct density in SHRSP compared to WKY. Reproduced from Marks et al (2001).

1.2.8 Anatomical and Physiological Characteristics of SHRSP

Vascular Abnormalities

Many studies have reported impaired collateral flow and other anatomical vascular abnormalities in the SHRSP. Coyle and Jokelainen (1983) observed that the collateral circulation of the SHRSP was inadequate compared to that of the WKY and proposed that this may contribute to the increased infarct size following experimental stroke. A later study examined collateral flow a month after MCA occlusion and reported that the number of collateral vessels to the territory of the middle cerebral artery was the same in both the SHRSP and the normotensive WKY strain. However, the internal diameter of anastomoses was reduced in the SHRSP, 33μm compared to 50μm in the WKY (Coyle & Heistad, 1987). These authors also reported that some collateral vessels had an internal diameter which was often less than half the diameter of the upstream arteriole, creating a "bottleneck effect" leading to increased resistance to flow. The reverse was observed in WKY rats, where the collateral vessels were larger in diameter than the cortical penetrating arterioles (Figure 1-11). In addition, large diameter branches of the anterior and middle cerebral arteries were significantly smaller in aged SHRSP (40-69 weeks old) compared to age matched WKY. However, there was no difference between the strains in the young animal groups (5-10 weeks old). This illustrates the vascular effects of progressive hypertension in the aged SHRSP. Since the internal diameter of ACA-MCA anastomoses was smaller in SHRSP in both age groups, this study suggests that the vascular resistance in fully relaxed collaterals is greater in the SHRSP, which compromises dorsal collateral flow even before the onset of hypertension (Coyle, 1987). This may partly explain why SHRSP demonstrate larger infarcts, compared to WKY, even before hypertension develops.

Vascular function also appears to be impaired in the SHRSP strain. Volpe and colleagues (1996) demonstrated that in the thoracic aorta and the basilar artery of the SHRSP, endothelium-dependent vasodilatation was strikingly reduced compared to the vessels of the SHR. This is particularly interesting since the SHRSP and SHR strains show similar development of hypertension and therefore this observation must be independent of blood pressure. This may contribute to the reduced regional cerebral blood flow and increased infarct size observed in the SHRSP following experimental stroke, relative to that of the

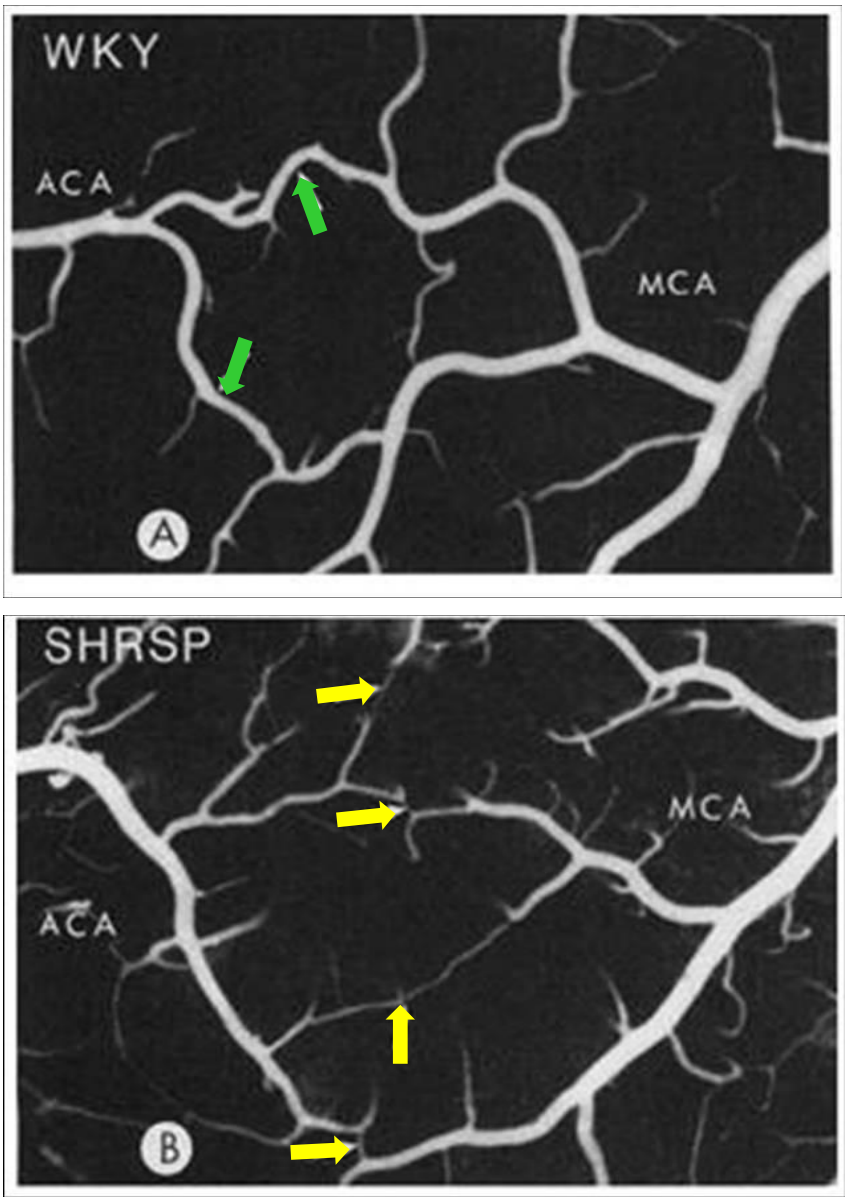

Figure 1-11. End-to-end anastomosing branches of the anterior and middle cerebral artery in young WKY and SHRSP. (A) In 8 week old WKY, the anastomoses are larger in internal diameter than cortical penetrating branches (green arrows) (B) in 5 week old SHRSP, the anastomoses (denoted by yellow arrows) are often less than 50% of the internal diameter of the supply vessels and the collaterals are smaller in diameter than cortical penetrating arterioles. Adapted from Coyle (1987).

SHR (Volpe et al, 1996). Therefore, impaired endothelium dependent vasodilation may account for part of the increased stroke sensitivity demonstrated by the stroke-prone strain.
With greater relevance to experimental stroke, Izzard et al (2003) examined the vasoreactivity of the middle cerebral arteries of both hypertensive strains and discovered that the ability to autoregulate was reduced in the vessels of the SHRSP. Furthermore, they reported that the diameter of these arteries progressively increased as a linear function with increasing hypertension, presumably as a result of increased growth in response to increased wall stress. Therefore the impaired autoregulatory ability of SHRSP vessels compared to that of SHR may play a role in the increased stroke susceptibility observed in the stroke-prone strain (Izzard et al, 2003).

Dysfunction of the Blood-Brain Barrier

Dysfunction of the BBB has also been reported in SHRSP. The BBB is characterized by the presence of tight-junctions between endothelial cells and decreased levels of vesicular transport, which serves to limit passage of materials between the cerebral circulation and the brain parenchyma (Yamagata et al, 1997). There are many reports of an increased permeability of the BBB in SHRSP, although the underlying mechanisms involved are not clear. The functions of the BBB are supported by astrocytes and it has been demonstrated by Yamagata and colleagues (1997) that in vitro, the astrocytes of SHRSP show a reduced ability to support the BBB, compared to WKY astrocytes.
There is also evidence of differences in the structure of tight junctions of SHRSP, in addition to an alteration in the polarity of endothelial cells of the BBB prior to stroke onset. This may predispose the SHRSP to stroke-induced BBB breakdown rather than contribute to stroke onset *per se* (Lippoldt et al, 2000).
Although there are reports of structural differences and increased BBB permeability in the SHRSP, the contribution to stroke pathogenesis is not yet clear, however BBB dysfunction is likely to enhance cerebral oedema formation following stroke.

Oxidative Stress

Increased levels of oxidative stress are also thought to contribute to increased sensitivity to experimental stroke in SHRSP. In both SHR and SHRSP, production levels of superoxide anions have been shown to be higher than that observed in normotensive rats in the vasculature and the brain (Suzuki et al, 1995; Kerr et al, 1999; Kishi et al, 2004) Furthermore, reactive oxygen species (ROS), such as superoxide anions and hydroxyl

radicals have been implicated in the pathogenesis of hypertension (Kerr et al, 1999). In addition, superoxide dismutase (SOD) activity is reduced in SHRSP in comparison to WKY (Kishi et al, 2004). This enzyme is an endogenous antioxidant and catalyzes the formation of oxygen and hydrogen peroxide from superoxide anions. Therefore, reduced SOD activity will result in increased superoxide levels, contributing to increased oxidative stress.

Increased superoxide levels may result in increased damage following stroke by disrupting the blood-brain barrier, leading to brain oedema and also by lipid peroxidation of cell membranes, increasing cellular damage. Kim-Mitsuyama and colleagues (2005) demonstrated that superoxide production in the cortex and hippocampus was increased in SHRSP. Furthermore, they identified that NADPH oxidase was the source of the increase in superoxide anions, since inhibition of NADPH oxidase significantly reduced the elevation in superoxide levels.

It has also been reported that levels of the eicosanoid 20-hydroxyeicosatetraenoic acid (20-HETE) are twice as high in SHRSP as that observed in WKY. 20-HETE is a potent vasoconstrictor and has been reported to contribute to the enhanced stroke sensitivity of SHRSP. It mediates endothelial dysfunction and increased oxidative stress by stimulating superoxide production via interactions with NADPH oxidase and uncoupling of NOS (Cheng et al, 2008). Inhibition of 20-HETE with *N*-hydroxy-*N*' –(4-butyl-2-methylphenyl)-formamidine (HET0016) significantly reduced infarct volume in SHRSP following transient MCA occlusion but had no effect on the WKY infarct size (Dunn et al, 2008).

Heightened Inflammatory Response

In addition to increased levels of oxidative stress, it has been reported that SHRSP demonstrate an increased inflammatory response to focal cerebral ischaemia compared to the reference strain WKY. Following permanent MCA occlusion, SHRSP showed significantly greater numbers of activated microglia. In the ischaemic core region, 183 activated microglia were identified per mm^2, compared to 156/mm^2 in WKY rats (Marks et al, 2001). It has been proposed that the increased level of microglial activation may contribute to the increased infarct volume observed in SHRSP, since activated microglia release neurotoxins including oxygen radicals, nitric oxide and glutamate, leading to lipid peroxidation, oedema and necrosis. Rather interestingly, this team of investigators also

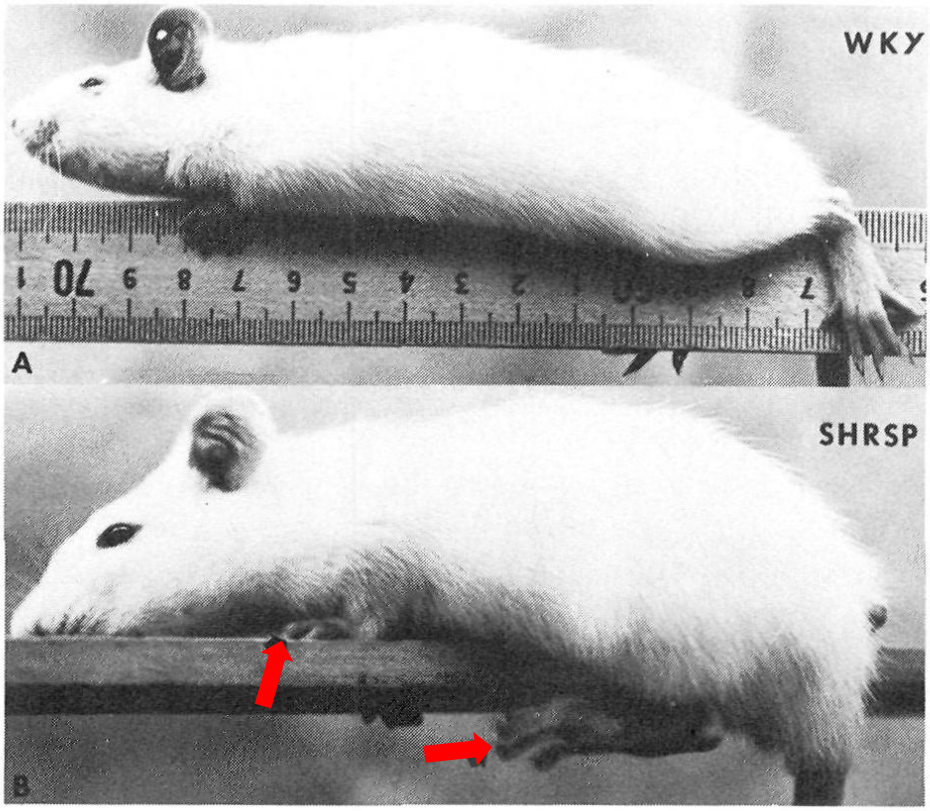

Figure 1-12. Reduced functional recovery in the SHRSP 2 days following experimental stroke. Note the asymmetrical placement of the forepaw and the hindpaw location for the SHRSP (red arrows). Adapted from Coyle & Jokelainen (1983).

observed that levels of resting and activated microglia in control SHRSP were increased relative to control WKY rats. This may account for the increased inflammatory response in the stroke-prone strain.

1.2.9 Reduced Functional Recovery in SHRSP

SHRSP display a poorer functional recovery following experimental stroke when compared to their normotensive control, the WKY (Figure 1-12), even when the focal ischaemic insult has been manipulated to produce comparable infarct volumes (McGill et al, 2005). Despite similar neurological deficits in both strains 2 hours post occlusion, SHRSP rats scored significantly lower on the 33 point neurological test at days 3, 7 and 28 post surgery. Long-term impairment of contralateral limb use in the SHRSP was also accompanied by a decline in general health, with a reduction in body weight and dishevelled coat appearance. A similar study examined functional deficits in SHRSP in comparison to SHR following permanent MCAO (Maguire et al, 2004). This team reported prolonged behavioural deficits in SHRSP despite almost identical infarct size to that observed in SHR. This suggests that there is a genetic basis for the reduced recovery shown by the stroke-prone strain, since the degree of brain damage was comparable in both strains. The authors of both behavioural studies have suggested that this phenomenon may be indicative of impaired brain plasticity but the possible mechanisms involved have yet to be examined.

1.3 Imaging the Ischaemic Penumbra

1.3.1 Ischaemic Core and Penumbra

The observed haemodynamic, metabolic and ionic changes observed following stroke do not occur in a homogenous manner across the ischaemic territory. In the severely hypoperfused core, cells are irreversibly damaged as permanent anoxic depolarization begins to develop within minutes of the onset of ischaemia. Cell damage occurs as a result of ionic homeostatic breakdown, and activation of multiple cellular pathways which converge to initiate the irreversible degradation of cellular components, as previously described in this chapter.

The concept of the ischaemic penumbra arose from a series of seminal experiments performed in the 1970s which measured the effects of progressive reductions in cerebral

blood flow on the baboon cortex (Branston et al, 1974; Branston et al, 1977; Astrup et al, 1977). These studies examined cortical-evoked responses to determine the reduction in CBF required to abolish electrical activity and established the principle that there are two ischaemic thresholds which exist in the pathogenesis for cerebral infarction; one threshold for morphological damage and a less severe threshold for functional impairment. The concept of two separate blood flow thresholds for the disruption of functional and structural integrity was refined by Symon and colleagues (1977). This team of investigators used a primate model to identify that cerebral blood flow below 12ml/100g/min rendered neurons non-functional. In brain areas where cerebral flow was above 20ml/100g/min, neurons were fully functional and evoked somatosensory responses. At a flow rate of 15ml/100g/min the evoked somatosensory response sharply declined and therefore marks the threshold for disruption of function (Symon et al, 1977).

These experiments led to the definition of the ischaemic penumbra as a region of brain tissue which is functionally impaired but structurally intact surrounding a severely hypoperfused central core where both functional and structural damage is evident (Astrup et al, 1981, Figure 1-13). Over the past 30 years, the definition of the ischaemic penumbra has evolved as a result of advances in neuroimaging and in light of both clinical and pre-clinical studies which have examined the characteristics and lifespan of the penumbra. A revised definition of the penumbra defines it as

"ischaemic tissue which is functionally impaired and is at risk of infarction and has the potential to be salvaged by reperfusion and/or other strategies. If it is not salvaged this tissue is progressively recruited into the infarct core which will expand with time into the maximal volume originally at risk" (Donnan et al, 2007).

Furthermore, a set of criteria have been established to define the ischaemic penumbra (Donnan et al, 2007):

(1) The penumbra is a region of hypoperfused, abnormal tissue with physiological and biochemical characteristics consistent with cellular dysfunction but not cellular death.
(2) The tissue is located within the same ischaemic territory as the infarct core.
(3) The tissue can either survive or progress to necrosis.
(4) Salvage of the tissue is associated with better clinical outcome.

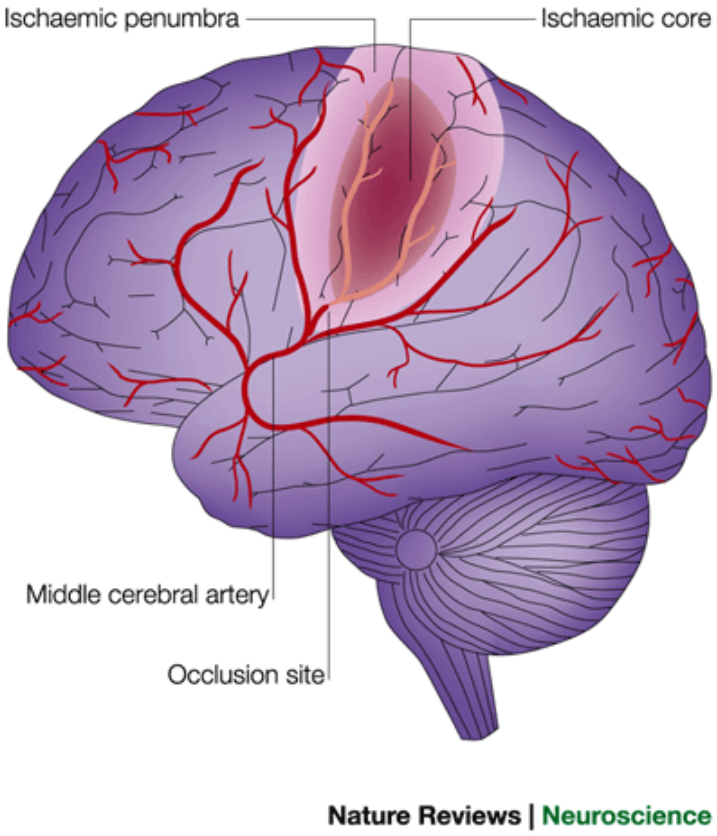

Figure 1-13. The Ischaemic Core and Penumbra. Following occusion of a cerebral vessel, most commonly the middle cerebral artery, a core of severely hypoperfused injured tissue is found within the territory of the occluded vessel. Outwith the ischaemic core, there is a region of less severely hypoperfused tissue which is still metabolically active. This is the ischaemic penumbra and represents tissue which may be salvaged following stroke but has a finite lifespan and will proceed to infarction in the absence of reperfusion. Reproduced from Allan & Rothwell (2001).

Characteristics of the Ischaemic Penumbra

Advances in neuroimaging have allowed the biochemical and metabolic characteristics of the ischaemic penumbra to be defined. Positron emission tomography (PET) has allowed measurement of regional CBF (rCBF), cerebral metabolic rate of oxygen ($CMRO_2$), regional cerebral metabolic rate of glucose ($rCMR_{glc}$) and oxygen extraction fraction (OEF). In humans, regional CBF below 12ml/100g/min and $rCMRO_2$ below 65µmol/100g/min corresponds to the infarct core (Ackerman et al, 1981). The penumbra has been defined as rCBF decreased to 12-22ml/100g/min with the $rCMRO_2$ above 65µmol/100g/min. This relative preservation of $CMRO_2$ is an indicator of maintained neuronal metabolism. Hypoperfused tissue where rCBF is greater than 22mL/100g/min represents benign oligaemic tissue which will not proceed to infarction (as reviewed by del Zoppo et al, 2011). In addition, the penumbra displays an increased OEF compared to normal brain tissue in an attempt to compensate for the reduction in blood flow. In the penumbra OEF is increased to 50-90% (Heiss, 2000) compared to an OEF of approximately 40% in normal tissue (del Zoppo et al, 2011).

In addition to biochemical and metabolic alterations, the ischaemic penumbra has also been characterised at the molecular level. As regional CBF decreases to approximately 30% to 50% of baseline CBF, a reduction in protein synthesis is observed. In the severely hypoperfused infarct core, the ability to synthesise proteins is lost relatively early following ischaemia and is associated with ATP depletion. However, in the penumbra, ATP levels are maintained and protein synthesis is initially depressed but recovers over time (Hossman, 1994). It has been suggested that the loss of protein synthesis in the ischaemic core is a protective function to prevent the formation of partially denatured or incorrectly processed proteins. It is not yet understood why protein synthesis resumes in penumbral tissue but this area is currently under study (del Zoppo et al, 2011).

There is also compelling evidence that heat shock protein 70 (Hsp70) is upregulated in penumbral tissue. Under normal conditions, Hsp70 is expressed in brain cells at levels which are almost undetectable. However, in ischaemic conditions, Hsp70 is massively induced and it can promote cell survival by refolding denatured proteins or alternatively, it can allow protein degradation and progression to cell death (Hohfeld et al, 2001). Following MCA occlusion, Hsp70 mRNA has been shown to be expressed throughout the MCA territory. However, in the ischaemic core, Hsp70 mRNA is not translated into the Hsp70 protein (Kinouchi et al, 1993). Conversely, in the ischaemic penumbra both

transcription and translation of Hsp70 occur, allowing refolding of proteins to occur and promoting cell survival.

The ischaemic penumbra is of great interest to both clinicians and stroke researchers as it represents tissue which may be potentially salvaged following stroke. However, the penumbra has a finite lifespan and as time passes without reperfusion, the penumbra can progress to become part of the ischaemic core as a result of ongoing excitotoxicity, spreading depolarization, post ischaemic inflammation and apoptosis. This illustrates that the penumbra is not a fixed structure; it is highly dynamic and changes its boundaries over time. The existence of the penumbra is well established in rat models of focal cerebral ischaemia but in human stroke patients the extent, location and the lifespan of the penumbra is highly variable.

1.3.2 Multi-Modal Identification of the Penumbra

Identification of potentially salvageable penumbra, a region of hypoperfused but viable tissue which is at risk of infarction, is of the utmost importance to clinicians and experimental stroke researchers. Clinically, the presence of a significant volume of penumbral tissue can be used to identify those patients who are most likely to benefit from thrombolytic therapy. Furthermore, penumbra imaging can be potentially utilised to group stroke patients together in clinical trials, where the extent and location of the penumbra is similar. This will allow potential therapeutic strategies to be assessed in comparable groups of patients. In experimental stroke, identification of the penumbra can allow the efficacy of neuroprotective agents to be assessed. In this setting, the use of magnetic resonance imaging (MRI) is favoured. Although, positron emission tomography (PET) is considered to be the ‘gold standard’ imaging modality for penumbra imaging and is still used as a clinical research tool, MRI is now becoming the modality of choice for identifying potentially salvageable tissue in clinical research. In addition, the use of computed tomography (CT perfusion) to identify the penumbra is being increasingly used in the clinical setting due to its cost effectiveness and availability (Heiss & Sorensen, 2009).

1.3.3 Positron Emission Tomography

PET is widely regarded as the ‘gold-standard’ imaging modality for clinical identification of the ischaemic penumbra as it provides quantitative assessment of cerebral blood flow and oxygen metabolism. This technique involves intravenous administration of a positron

emitting radioisotope bound to a ligand. The radioactivity emitted is then reconstructed to produce a tomographic image. Multi-tracer PET, using the ligands $H_2{}^{15}O$ and ^{15}O, has been used to quantitatively measure cerebral blood flow (CBF), cerebral metabolism of oxygen ($CMRO_2$) and oxygen extraction fraction (OEF) (Ebinger et al, 2009, Figure 1-14). The penumbra can therefore be identified as a hypoperfused region, where oxygen metabolism is preserved and oxygen extraction is increased, to compensate for the reduction in cerebral blood flow. This phenomenon was described as 'misery-perfusion' by Baron et al (1981). Clinical studies have defined irreversibly damaged tissue using thresholds of oxygen metabolism and cerebral blood flow of 65µmol/100g/min and 12ml/100g/min respectively and defined penumbra as tissue where regional CBF decreased to 12-22ml/100g/min, with a $CMRO_2$ above 65µmol/100g/min and OEF increased to 50-90% (Heiss, 2000).

Modern PET tracers like ^{18}F-fluromisonidazole (FMISO) and ^{11}C-flumazenil (FMZ) can also be used to identify potentially salvageable tissue post-stroke. FMZ is a central benzodiazepine receptor ligand, a marker of neuronal integrity and has been used to detect neuronal damage within the first few hours of the onset of cerebral ischaemia. FMISO is a tracer of hypoxic viable tissue and can therefore be used to identify the ischaemic penumbra in the acute phase of stroke, where increased areas of tracer uptake are detected (Heiss, 2003).

In experimental stroke, serial multi-tracer PET studies in the baboon (Touzani et al, 1995) and the cat (Heiss et al, 1994) have demonstrated the spatial and temporal evolution of the ischaemic penumbra following occlusion of the middle cerebral artery. Both studies have demonstrated the progressive incorporation of the penumbra into infarct core and that this process is complete at 24 hours or later post-MCAO. This aids to reinforce the dynamic nature of the penumbra and that the life-span of this tissue is finite.

Despite the ability of PET to provide quantitative measurements of cerebral blood flow and oxygen metabolism, there are a variety of factors which limit its use, both clinically and experimentally. Primarily, the availability of PET has been hampered by its expense and the fact that it requires experienced chemists to synthesise short half-life radioisotopes, in addition to physicists and radiographers who run the scans. Furthermore, it is limited in the clinical setting due to the necessity to cannulate arteries for arterial blood sampling to allow quantitative measurements of cerebral blood flow. This invasive procedure and the need for exposure to radioisotopes therefore limits the clinical use of this imaging

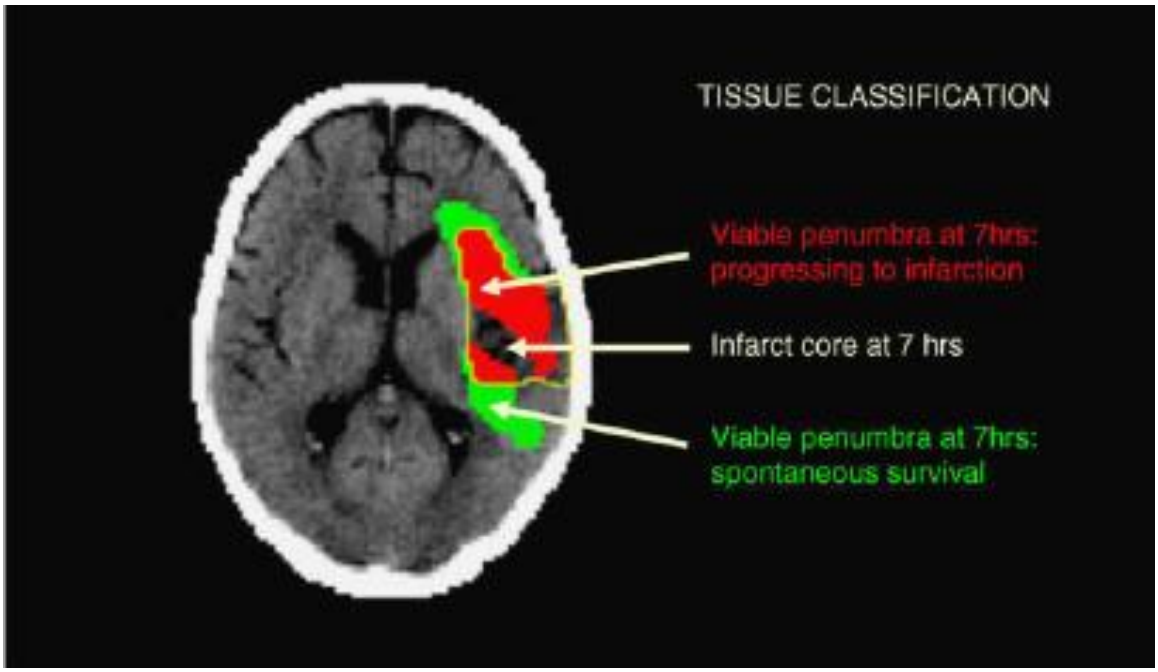

Figure 1-14. Identification of the ischaemic penumbra using positron emission tomography. [18] F-fluromisonidazole (FMISO) PET scan was performed 7 hours after stroke onset, where a significant volume of penumbral tissue surrounds the infarct core. The yellow outline denotes the final infarct as defined by CT 7 days post stroke onset, indicating penumbral tissue which has been incorporated into the infarct. Adapted from Ebinger et al (2009).

modality. The cost of PET is also a major limiting factor in experimental stroke research in addition to the poor resolution in small rodent brains and as a consequence, MRI is more widely utilised to image the penumbra in this setting.

1.3.4 Perfusion Computed Tomography

Computed tomography (CT) is one of the most readily available imaging modalities and is becoming increasingly utilised in the clinical identification of the penumbra in acute stroke patients. Perfusion CT in particular can help to predict the fate of ischaemic tissue (Ebinger et al, 2009). This technique involves the intravenous injection of an iodinated contrast agent and the bolus is tracked through the cerebral circulation. Parametric maps of cerebral blood volume (CBV), cerebral blood flow (CBF) and mean transit time (MTT) can be generated and quantified using post-processing software (Figure 1-15). However, there can be qualitative differences in the software used and currently there is a lack of agreement with regards to quantification of the perfusion CT parameters (Ebinger et al, 2009).
In the ischaemic penumbra, tissue perfusion is reduced leading to vasodilatation and recruitment of collaterals in an attempt to restore cerebral blood flow. This results in an increased cerebral blood volume in the penumbra, compared to the infarct core, where severe hypoperfusion induces loss of the ability to autoregulate and as a consequence, cerebral blood volume falls. Following a systematic evaluation of 130 acute stroke patients, Wintermark et al (2006) reported that the infarct core is most accurately described by absolute CBV, with an optimal threshold of $\leq$2ml/100g. The parameter which optimally defines the penumbra is the relative MTT, where the threshold for this parameter is $\geq$145% of the contralateral tissue MTT (Wintermark et al, 2006).

Earlier clinical perfusion CT studies used absolute CBF thresholds or combined CBF and CBV thresholds to identify the ischaemic penumbra. However, as discussed by Wintermark et al (2006), these were small pilot studies, each with less than 23 acute stroke patients. Furthermore, these studies defined the penumbra using parameters where the thresholds were arbitrarily selected.

In addition, the ability of this technique to define the ischaemic penumbra has been assessed against MR measurements of perfusion-diffusion mismatch, with a significant correlation (r^2 =0.81, P<0.001) between the two imaging modalities (Schaefer et al, 2008). Despite these results, perfusion CT has yet to be sufficiently validated for the identification

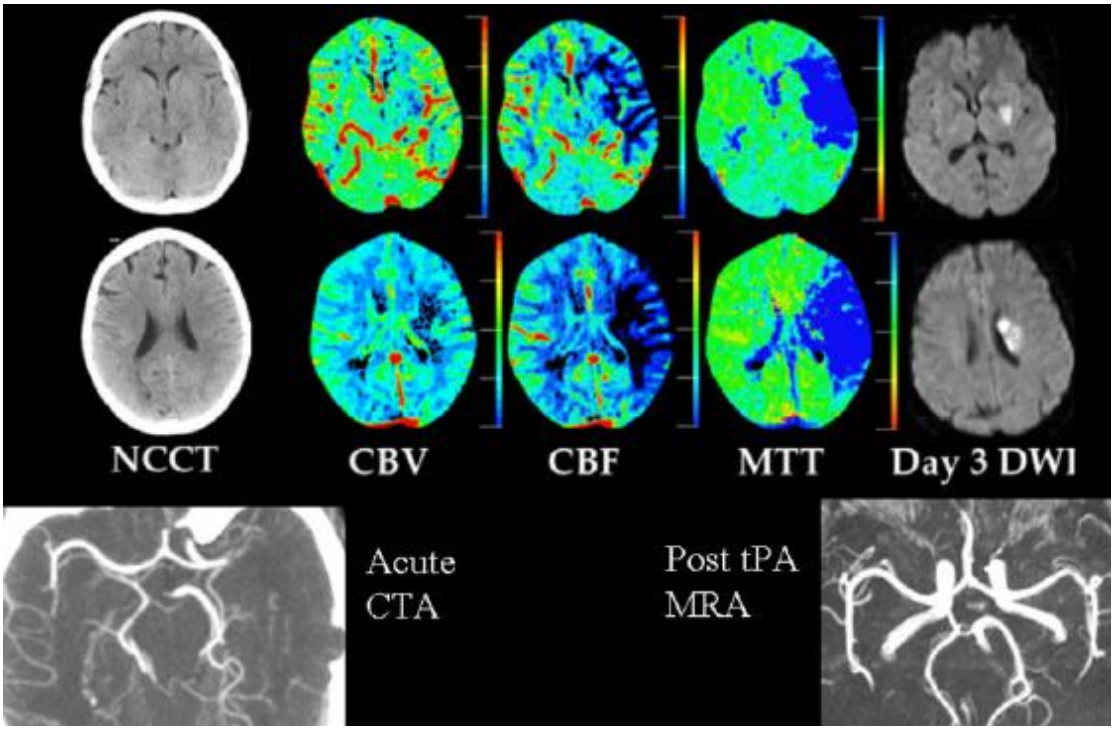

Figure 1-15. Identification of the penumbra by perfusion CT. The patient was imaged with multimodal CT at 3.5 hours after stroke onset with National Institute of Health Stroke Scale (NIHSS) of 14. Vessel occlusion was demonstrated by CT angiography (CTA, bottom left). A small area of reduced cerebral blood volume (CBV) was apparent in the lentiform nucleus and deep white matter but surrounded by much larger areas of reduced cerebral blood flow (CBF)/prolonged mean transit time (MTT) consistent with the ischaemic penumbra. Minimal change was detected by non-contrast CT (NCCT). The patient was treated with intravenous thrombolysis and had major early improvement of neurological symptoms. Magnetic resonance angiography (MRA) indicated complete recanalization (lower right) and only a small volume of tissue infarction on the follow-up diffusion weighted images (DWI). Reproduced from Ebinger et al (2009).

of the ischaemic penumbra and standardisation of the perfusion CT definitions for core and penumbral tissue has not yet been performed. However, when this technique has been extensively validated it is likely to become one of the most widely used imaging modalities to approximate the ischaemic penumbra and identify those acute stroke patients who are most likely to benefit from tissue salvage therapies. At present, some stroke centres are using a multi-modal CT approach to identify patients who are potentially eligible for thrombolytic therapy, using perfusion CT in combination with CT angiography and non-contrast CT, which detects isolated focal swelling associated with tissue at risk of infarction (Wintermark et al, 2006).

1.3.5 Magnetic Resonance Imaging

Nuclear magnetic resonance analysis is used to determine the presence and concentration of certain atomic nuclei within a sample. In MRI, hydrogen atoms are the nuclei of choice in medical imaging since they are the most abundant nuclei in the body. Each hydrogen nucleus consists of a single positively charged proton. The proton behaves like a small magnet since it continually spins and has an electrical charge. This also means that protons can be influenced by external magnetic fields. Under normal conditions, these protons spin with their axes pointing in random directions. However, in the presence of an external magnetic field, a proportion of hydrogen nuclei will align in parallel to the external magnetic field. In order to record the magnetic resonance signal, protons are excited from a low to a high energy state, by exposure to electromagnetic radiation of radio frequency (RF). Excitation of protons causes them to spin with their axes pointing in the opposite direction. This alters their magnetic effect and the resulting deflection in the angle of the magnetization vector can be recorded. In MRI, the magnetization vector is deflected by 90^o or 180^o by exposure to precise radio frequencies, called the 90^o RF pulse and 180^o RF pulse, respectively.

Following excitation of protons and subsequent deflection of the magnetization vector, the time taken for the magnetic resonance (MR) signal to fade is measured, as the protons return to a low energy state and magnetic equilibrium is regained. This parameter is termed the relaxation time. The return to equilibrium results from two independent processes called spin-lattice interaction and spin-spin interaction. Spin-lattice relaxation, or T_1 relaxation as it is otherwise known, involves the dissipation of energy from the excited nuclei to their surroundings in order to return to steady state. This time constant, T_1, is dependent on the strength of the external magnetic field, where the greater the magnetic

field strength, the longer it takes for excited nuclei to return to steady state. Spin-spin interaction results in transverse relaxation. This process involves the interaction of adjacent nuclear spins. The MR signal fades as the magnetic fields of adjacent nuclei interfere with each other. The time constant for transverse relaxation is known as T_2. Unlike T_1 relaxation, T_2 relaxation time is independent of magnetic field strength. Furthermore, despite T_1 and T_2 relaxation being completely independent processes, they occur almost simultaneously.

The MR image is constructed from the MR signal and there are three factors which influence the contrast of the image by determining how bright the image appears. Firstly, the proton density of the biological tissue determines the maximum signal which can be obtained. MR images in which contrast is determined mainly by proton density are called proton density-weighted images. The T_1 relaxation time of the tissue also has an affect on image contrast and those images where contrast is determined mainly by T_1 are called T_1-weighted images. Similarly, T_2-weighted images are produced when T_2 relaxation time is used to determine image contrast.

Magnetic resonance imaging techniques have also allowed the penumbra to be identified, by the use of diffusion and perfusion weighted imaging. The logistics of magnetic resonance imaging are less complex than PET and are therefore more widely available in both the clinic and the laboratory.

Diffusion Weighted Imaging (DWI)

The production of diffusion-weighted images display signal changes which are dependent on the diffusion of water protons in biological tissues. The diffusion of water protons is quantified by the diffusion constant, which varies with the direction of movement. In an isotropic medium, water molecules move randomly in all directions, according to Brownian motion. However, in biological tissues, diffusion may be impeded by natural barriers like cell membranes and protein structures, resulting in anisotropic diffusion. For example, in axons, protons will tend to travel along the axis of the fibre due to the barrier presented by the myelin sheath. This results in a greater diffusion constant along the longitudinal axis of the axon, compared to that of the perpendicular axis, across the myelin sheath. The degree of signal loss on the diffusion-weighted image increases with the diffusion constant. Therefore tissue areas with restricted diffusion will have greater signal

intensity than those tissues where diffusion is normal and signal loss is greater. DWI can therefore be used to obtain a quantitative measure relating to diffusion within a voxel.
In biological tissues, the diffusion constants can be measured and are represented by the apparent diffusion coefficient (ADC), which can then be used to construct ADC maps. Tissue areas where diffusion is restricted will appear dark on an ADC map due to the reduced value of the diffusion constant. Compare this to the diffusion-weighted image, where the same area of tissue will appear bright due to increased signal intensity, resulting from reduced mobility of water protons.
In acute stroke, diffusion of water molecules becomes restricted as a result of cytotoxic oedema following ischaemic injury (Moseley et al, 1990a). Diffusion of water molecules is reduced by the redistribution of water from the extracellular to the intracellular space and increased tortuosity or viscosity as failure of the Na^+/K^+ pump ensues (Abe et al, 2003). The reduction in ADC produces a hyperintense signal on diffusion-weighted images, identifying the bright region of ischaemic tissue damage within the first 6 hours of stroke onset (Moseley at al, 1990a). This timescale gives DWI a great advantage over conventional MRI techniques.

In animal models of stroke, DWI can be used to identify ischaemic damage within minutes of MCA occlusion (Moseley et al, 1990b; Hoehn-Berlage et al, 1995). Similarly, in human stroke patients, this imaging technique has been used to detect ischaemic lesions less than 40min following stroke onset (Yoneda et al, 1999). If the stroke patient is untreated, the diffusion lesion will expand over time and follows a relatively consistent pattern of growth during the first 3 days after stroke onset and will then decrease in size up to day 7 (Baird et al, 1997; Beaulieu et al, 1999; Lansberg et al, 2001). This is reflected in the changes in ADC which occur following stroke. As the ischaemic lesion evolves over the first 24h post-stroke, the ADC will decrease further and the lesion will appear brighter on diffusion weighted images. In the subacute and chronic phases of stroke, the ADC will start to return to normal. However, since the tissue is infarcted and can never recover, this process is termed ‘pseudonormalization’. Later in the chronic phase (>7 days from stroke onset), ADC will further increase (Warach et al, 1995). This allows acute and chronic stroke to be confidently distinguished using DWI. This is in contrast to T_2 weighted imaging, where similar signal intensity is displayed by the infarct in both the subacute and chronic stages of stroke.

However, areas of hyperintense signalling on DWI are not always associated with low ADC values, since T_2 also has an effect on signal intensity and in some cases the effect of

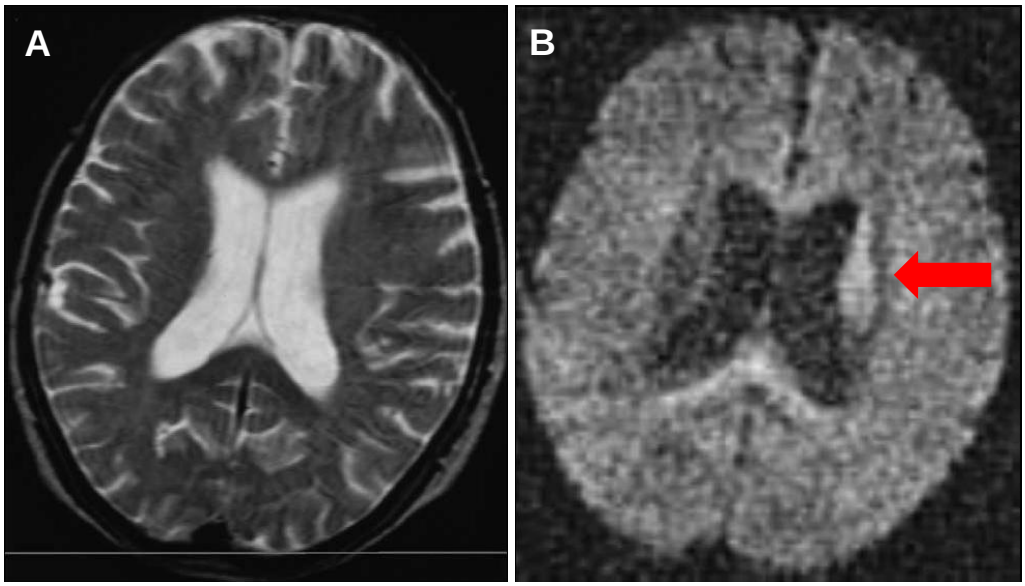

Figure 1-16. MR images produced 3 hours following stroke onset in a 75 year old female patient. In the acute phase of stroke, there is no evidence of abnormal signal intensity in the T_2-weighted image (A). However, examination of the diffusion weighted image (B) reveals a hyperintense lesion in the left caudate body and corona radiata (red arrow). Adapted from Abe et al (2003).

an elongated T_2 can result in hyperintense signalling, even when diffusion is normal or increased. This effect is called T_2 shine-through and can be reduced by increasing the amount of diffusion-weighting. Furthermore, hyperintense signalling on diffusion-weighted images may also be attributable to a previous stroke or susceptibility artefacts (Baird & Warach, 1998). Therefore, DWI should always be examined alongside the appropriate T_2 image and/or the calculated ADC map to assess the extent and severity of ischaemic injury and identify brain tissue which is likely to proceed to infarction (Figure 1-16).

Perfusion Imaging

Brain blood flow can be evaluated by MR perfusion imaging techniques. These techniques can provide quantitative assessment of tissue perfusion regardless of whether the blood is delivered by the main artery supplying the brain territory, or by collaterals. This type of imaging is dependent on signal changes that are induced by an exogenous or endogenous tracer and there are two techniques which are commonly utilised in clinical and preclinical research: contrast agent bolus tracking and arterial spin labelling.

Contrast Agent Bolus Tracking

Contrast agent bolus tracking is the most commonly utilised perfusion imaging technique and it involves the intravenous introduction of gadolinium-based contrast agents into the circulation. These contrast agents are paramagnetic and therefore result in magnetic inhomogeneity when administered into the bloodstream. This increases magnetic susceptibility and reduces T_2 relaxation time, resulting in decreased signal intensity as the agent passes through blood vessels. Homogeneity of the magnetic field is restored as the contrast disappears from the detection plane and the intensity of the signal returns to normal. This allows the contrast agent to be tracked throughout the cerebral circulation.
This type of imaging is commonly performed using T_2^*-weighted 2D or 3D echo planar sequences, which allow fast image acquisition, where a new image can be produced every second (Weishaupt et al, 2006).

A time-intensity curve can be constructed from the changes in signal intensity as the contrast agent passes through the circulation. The amount of signal loss is proportional to the concentration of the contrast agent and in healthy brain tissue, is directly proportional to cerebral blood volume (CBV) (Belliveau et al, 1990). From the curve, the time to peak

(TTP) is the time from the start of the scan to the point where signal intensity is maximal. The mean transit time (MTT) is the time taken for the contrast bolus to pass from the arterial cerebral circulation to the venous side.

In healthy humans, to calculate CBF and MTT, an estimate of arterial input function is required. Where the blood-brain barrier is disrupted, both cerebral blood volume and blood flow are represented by changes in signal intensity (Edelman et al, 1990) and the latter part of the time-intensity curve can be examined to estimate the permeability of the blood-brain barrier. However, in acute stroke patients, blood-brain barrier permeability is likely to be small, since disruption of the BBB does not predominantly occur until 24 hours following stroke onset (Baird & Warach, 1998). Following acute ischaemic stroke, this technique reveals well demarcated reductions in cerebral blood flow (Fisher et al, 1995).

Arterial Spin Labelling

Cerebral blood flow can also be assessed using perfusion imaging techniques which use blood itself as a tracer, rather than gadolinium based contrast agents, as previously described. This technique allows MR imaging of blood flow by spin labelling of water protons in an artery supplying the anatomical area of interest. It involves inversion of the longitudinal magnetization of the arterial blood and a decrease in signal is produced as the labelled blood reaches its target anatomy before relaxation of its magnetization. However, the decrease in signal is too small to be viewed directly and therefore in order to view the contrast, two image sets are used to highlight the contrast by image subtraction, where one image set shows inversion of inflowing water protons in the blood and the other does not (Weishaupt et al, 2006).

Arterial spin labelling has been widely used in animal models to quantify the perfusion deficit following experimental stroke in rodent models (Shen et al, 2003; McCabe et al, 2009; Foley et al, 2010) and is advantageous over other perfusion imaging techniques in that it is non-invasive, can be repeated to assess temporal changes in CBF and does not require administration of an exogenous tracer into the circulation. It also provides a more direct assessment of cerebral blood flow and can generate absolute blood flow quantification (Baird & Warach, 1998). However, this technique is less widely used than contrast agent bolus tracking because it is relatively more difficult to perform (Duong & Fisher, 2007)

1.3.6 MRI Perfusion-Diffusion Mismatch

The use of DWI and PWI in stroke neuroimaging led to the emergence of a new concept for defining the ischaemic penumbra using MRI. The perfusion-diffusion mismatch model was constructed to identify potentially salvageable penumbral tissue following stroke. The mismatch model arose from observations that diffusion lesions expand over time to encompass the region of PWI defined perfusion deficit in the absence of early reperfusion (Baird et al, 1997). According to the model, the DWI lesion represents the ischaemic core, where severely hypoperfused brain tissue is experiencing bioenergetic failure and becomes irreversibly damaged. PWI reveals hypoperfused tissue and the mismatch between the PWI and the DWI lesions provides an approximation of the ischaemic penumbra, which represents tissue which is hypoperfused but is not yet experiencing bioenergetic failure (Schlaug et al, 1999, Figure 1-17). As time progresses, mismatch tissue will reduce as the diffusion lesion expands and penumbral tissue becomes incorporated into the ischaemic core.

Clinical Use of Perfusion-Diffusion Mismatch

The perfusion-diffusion mismatch model has been widely used in clinical research to define the ischaemic penumbra (Figure 1-18). Darby and colleagues demonstrated that despite the presence and volume of mismatch decreasing over time, up to 70% of patients will display substantial regions of mismatch up to 24 hours following stroke onset (Darby et al, 1999).

The mismatch model has been used in clinical trials to assess the efficacy of thrombolytic therapy. The Desmoteplase in Acute Ischemic Stroke Trial (DIAS) was the first phase II clinical trial which employed the perfusion-diffusion mismatch model as a criterion for selecting patients suitable for thrombolytic therapy. All stroke patients recruited into the trial showed evidence of a perfusion-diffusion mismatch of ≥20% of perfusion deficit and those patients who received intravenous desmoteplase within 9 hours of stroke onset demonstrated a higher rate of reperfusion and improved clinical outcome compared to placebo treated patients (Hacke et al, 2005). A phase III trial was then undertaken to confirm the findings of DIAS but unfortunately the results were negative (Hacke et al, 2009). The DIAS-2 study reported no improvement in clinical outcome with administration of desmoteplase 3-9 hours following stroke onset. In this trial however, patients were

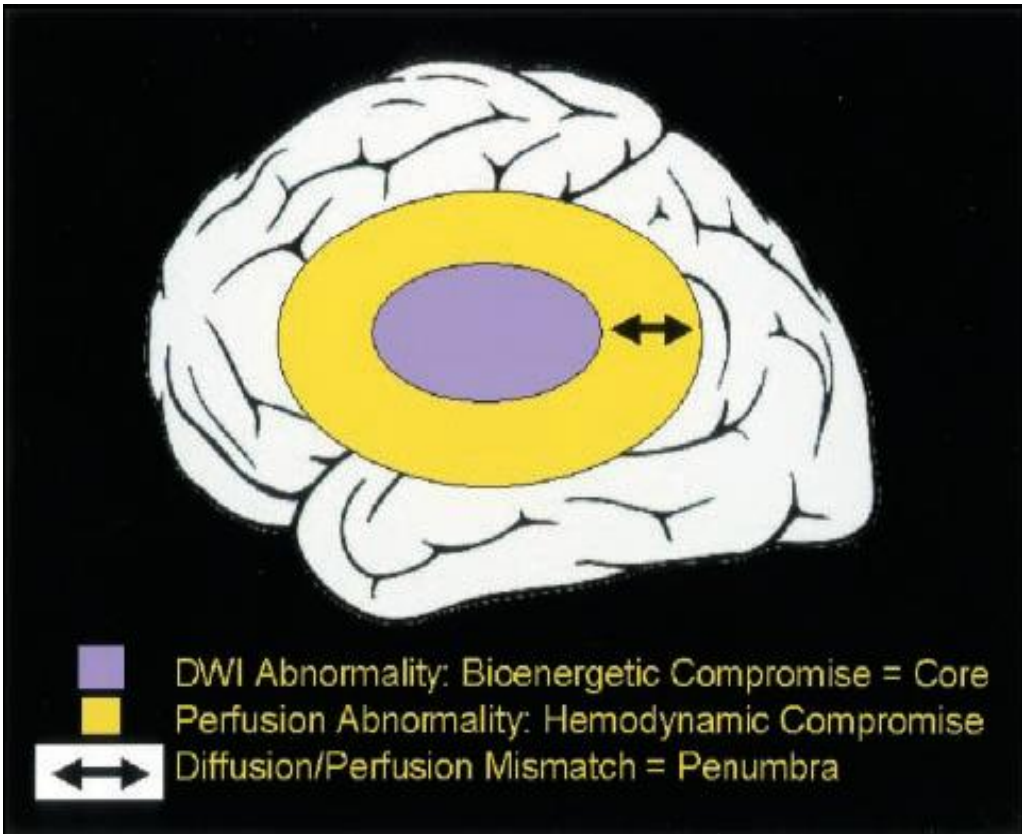

Figure 1-17. The Perfusion-Diffusion Mismatch Model. The diffusion abnormality represents the irreversibly damaged ischaemic core and the perfusion abnormality represents hypoperfused tissue. The mismatch between the diffusion and perfusion abnormalities provides an approximation of the ischaemic penumbra. Reproduced from Kidwell et al (2003).

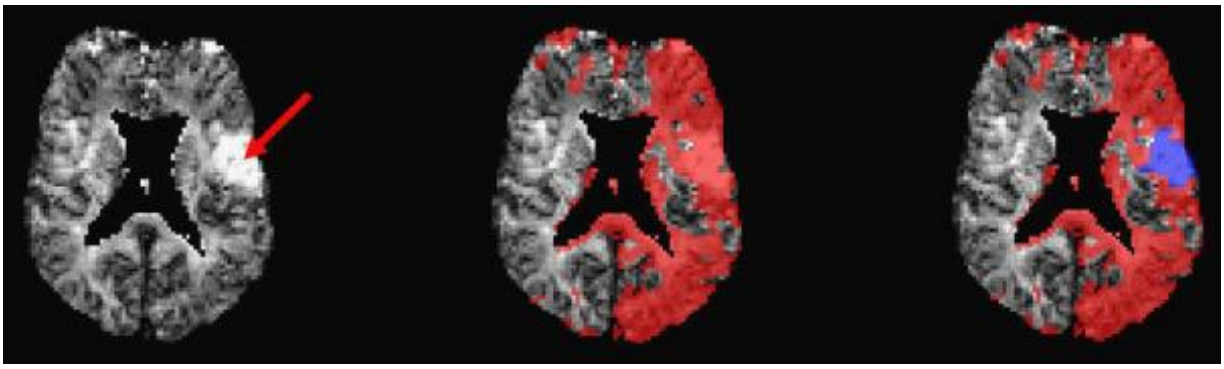

Figure 1-18. Identification of the penumbra in a stroke patient by magnetic resonance imaging. The arrow denotes the acute diffusion weighted imaging (DWI) lesion (left image). The area in red signifies the perfusion deficit (centre) and the penumbra as defined by diffusion-perfusion mismatch (right). Reproduced from Ebinger et al (2009).

selected by the presence of penumbra as determined by perfusion-diffusion mismatch or by perfusion CT and the pooling of these data may not be appropriate since the authors reported inconsistencies between MRI and CT.

The DIAS trial was followed by the Diffusion and Perfusion Imaging Evaluation for Understanding Stroke Evolution (DEFUSE) Study, which sought to validate the use of perfusion-diffusion mismatch to identify those patients who were likely to benefit from thrombolytic therapy administered 3-6 hours following stroke onset (Albers et al, 2006). Patients were categorised into 'mismatch' and 'no mismatch' groups, where the mismatch profile was defined as a PWI lesion which was greater than 10ml and at least 120% of the DWI lesion. In cases where the PWI lesion was less than 120% of the DWI lesion patients were assigned to the 'no mismatch' group. Patients with the 'no mismatch' profile did not appear to benefit from early reperfusion with rtPA. However, patients who were identified as having the target mismatch profile demonstrated a significantly improved clinical outcome following early reperfusion. This study indicates that the perfusion-diffusion mismatch model is a useful tool for identifying potentially salvageable tissue in acute stroke.

Similar observations were reported from the Echoplanar Imaging Thrombolytic Evaluation Trial (EPITHET), where patients who received thrombolytic therapy within 3-6 hours of stroke onset demonstrated reduced infarct growth and increased reperfusion when there was evidence of mismatch tissue. Increased reperfusion was also associated with an improved functional outcome (Davis et al, 2008). However, this study differs from the earlier DEFUSE study as the presence of mismatch was not used for patient selection as the sample size was small and the authors were keen to include patients who did not show evidence of mismatch tissue for the purpose of exploratory analysis.

The DIAS, DEFUSE, and EPITHET trials have demonstrated that the perfusion-diffusion mismatch model can be successfully used to identify patients who are likely to benefit from thrombolytic therapy and demonstrate an improved clinical outcome following stroke. The mismatch model can be used to identify groups of stroke patients with similar lesion size and location to improve the characterization of therapeutic efficacy (or inefficacy) in clinical trials (Baird & Warach, 1998).

Perfusion-Diffusion Mismatch in Experimental Stroke Models

The perfusion-diffusion mismatch model has been used in animal stroke models to assess the temporal evolution of the ischaemic penumbra but the use of the mismatch model to assess potential neuroprotective strategies in experimental stroke models is notably lacking. In animal models, the mismatch model could be used to evaluate the potential therapeutic window of interventions to salvage penumbra following stroke.

Meng and colleagues (2004) defined the temporal evolution of the penumbra in Sprague-Dawley rats following permanent or transient MCAO using perfusion-diffusion mismatch. These authors reported that following permanent MCAO, the diffusion lesion expands to encompass the larger perfusion deficit and as a consequence, the volume of penumbra, as defined by the mismatch model, decreases over time. By 2-3 hours post-MCAO the diffusion lesion has fully evolved and no penumbral tissue remains. This suggests that in Sprague-Dawley rats, there may be a narrow time window for penumbra salvage.

In a transient stroke model, perfusion-diffusion mismatch was used to evaluate the effect of reperfusion following 60 minutes of ischaemia in Sprague-Dawley rats (Meng et al, 2004). The authors observed that the diffusion lesion at 3 hours post-MCAO and 2,3,5-triphenyltetrazolium chloride (TTC) infarct volume at 24 hours post-MCAO were significantly smaller than those observed following permanent MCAO, indicating that early reperfusion had successfully salvaged penumbral tissue.
The same study group also used perfusion-diffusion mismatch to assess the temporal evolution of ischaemic injury in Wistar rats following permanent MCAO (Bardutzky et al, 2005a). It was reported that 90 minutes post-MCAO, Wistar rats demonstrated a mismatch volume which was significantly larger than that observed in Sprague-Dawley rats at the same time point. Recently, Foley and colleagues (2010) defined quantitative temporal profiles of penumbra in Sprague-Dawley rats using dual parameter voxel analysis. All voxels which had normal ADC values but an abnormal CBF value were defined as penumbra. This method revealed that penumbra persisted even after 4 hours following MCAO, which conflicts with previous reports in the Sprague-Dawley strain (Shen et al, 2003; Meng et al, 2004).

The perfusion-diffusion mismatch model has also been used to assess penumbral tissue in rat models with genetic stroke risk factors. McCabe and colleagues reported that mismatch area was reduced in the spontaneously hypertensive stroke-prone rat (SHRSP) compared to

the normotensive control, Wistar-Kyoto (WKY) (McCabe et al, 2009). Similarly, Letourneur and colleagues reported a reduced perfusion-diffusion mismatch in spontaneously hypertensive rats (SHR) compared to WKY rats following permanent focal ischaemia (Letourneur et al, 2011). These studies illustrate how the mismatch model can be used to assess differences in the temporal evolution of perfusion-diffusion mismatch between rat strains.

The potential use of the mismatch model to assess neuroprotective strategies has not been widely investigated in experimental stroke. Bardutzky and colleagues (2005b) evaluated the neuroprotective effects of dimethylsulphoxide (DMSO) in a rodent permanent stroke model and reported that administration of 33% DMSO at 60 minutes post-MCAO preserved the mismatch region and therefore salvaged penumbra and prevented it from proceeding to infarction. The efficacy of normobaric hyperoxia has also been evaluated in rat stroke models using perfusion-diffusion mismatch as an outcome measure. Kim and colleagues (2005) reported that normobaric hyperoxia initiated at 30 minutes following permanent MCAO, reduced the growth of the diffusion lesion and therefore preserved the lifespan of the penumbra. However, the treatment effect was only observed during treatment and the neuroprotective effect is lost when treatment stops.

Preservation of the perfusion-diffusion mismatch has also been examined in rodent models with genetic risk factors. It has been reported that Sprague-Dawley rats display a significant mismatch which is maintained until 150 minutes post-MCAO and administration of a selective endothelin receptor antagonist successfully reduced progression to infarction (Legos et al, 2008). However, the authors reported that there was little evidence of mismatch in SHR rats from as early as 60 minutes post-MCAO and consequently, administration of endothelin receptor antagonist had no protective effect and did not reduce infarct volume. These studies illustrate how perfusion-diffusion mismatch can be used in animal models of stroke to evaluate potential neuroprotective strategies but at present, there is a notable lack of such investigations in the pre-clinical literature.

1.3.7 Challenges to the Mismatch Model

Despite the widespread use of the diffusion-perfusion mismatch model in both experimental and clinical stroke studies, its definition of the penumbra has been widely challenged by various study groups. The first challenge to the model is the inability of perfusion imaging to distinguish between the penumbra and tissue which is experiencing

benign oligaemia. Although this region of tissue displays a perfusion deficit, it functions normally and is not at risk of infarction. Therefore perfusion weighted images are likely to overestimate the outer boundary of the penumbra. This problem has been addressed by several groups by studying the evolution of the diffusion and perfusion abnormalities in untreated patients. This allows identification of the penumbra, as tissue which proceeds to infarction and areas of benign oligaemia, which does not become part of the infarct. These studies allowed a range of ADC and perfusion thresholds to be identified, designed to differentiate between penumbra and benign oligaemia (Kidwell et al, 2003).

In addition, the mismatch model has been challenged for the apparently clear distinction between the penumbra and ischaemic core tissue. The model assumes that the initial diffusion abnormality represents tissue which is irreversibly damaged and cannot be salvaged even if reperfused. However, animal models have shown that the diffusion lesion can be partially or fully reversed if reperfused within 3 hours (Kidwell et al, 2003). This has also been demonstrated to occur in human stroke patients following intra-arterial thrombolytic therapy, although some tissue redevelops diffusion abnormalities as late secondary injury (Kidwell et al, 2002). These findings are significant as they demonstrate that patients who do not show evidence of diffusion-perfusion mismatch may still benefit from thrombolytic therapy. These findings have led to the construction of a modified perfusion-diffusion mismatch model (Figure 1-19).

Furthermore, it has recently been reported that penumbra as defined by perfusion-diffusion mismatch does not reliably reflect the PET defined penumbra (Zaro-Weber et al, 2009). Areas of mismatch were compared with areas of increased OEF. All of the 13 stroke patients examined in the study demonstrated areas of mismatch but only 8 of those patients showed evidence of penumbra as defined by OEF elevation using PET. However, the mismatch model could potentially be improved by refining the perfusion and diffusion thresholds which are used to define tissue at risk of infarction by distinguishing the penumbra from the ischaemic core and benign oligaemic tissue.

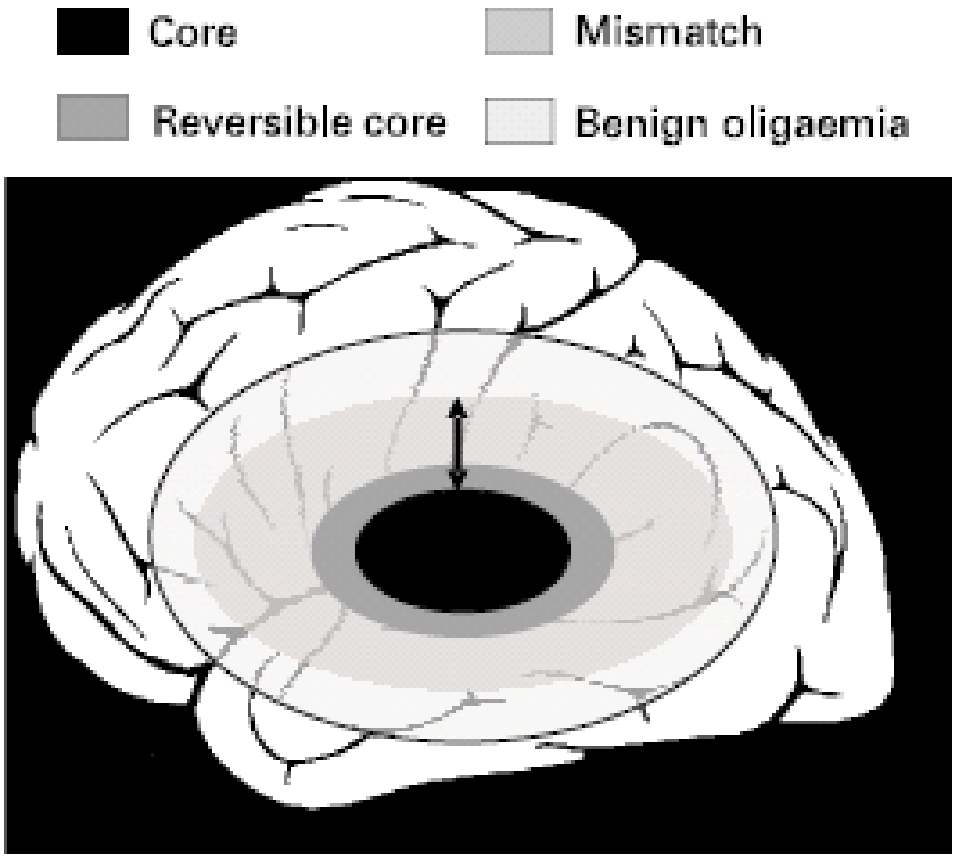

Figure 1-19. The current concept of the ischaemic penumbra. This model recognises that tissue within the diffusion abnormality is not necessarily irreversibly damaged and may recover with early reperfusion. It also recognises the perfusion abnormality may include benign oligaemic tissue which is not at risk of infarction. The arrow shows penumbral tissue which is at risk of infarction but is potentially salvageable with adequate reperfusion. In this model the penumbra includes a component of the diffusion abnormality in addition to the perfusion abnormality, with the exclusion of benign oligaemic tissue. Reproduced from Davis & Donnan (2004).

1.4 Aims of the Thesis

The aims of the first study were to define strain-specific MRI perfusion and diffusion thresholds in the SHRSP and WKY rat. These thresholds would then be applied to quantitative perfusion and diffusion MRI data acquired in the acute phase following experimental stroke to allow the temporal evolution of ischaemic injury and perfusion deficit to be assessed and compared between the strains. The acute MRI data would then be used to assess and compare three different methods of calculating penumbra volume to evaluate the strengths and limitations of each method. Each calculation method would be used to compare the extent and lifespan of the ischaemic penumbra following permanent MCAO in SHRSP and WKY rats.

The aim of the second study was to evaluate the neuroprotective efficacy of the NADPH oxidase inhibitor, apocynin, in rodent stroke models. First, the effects of apocynin treatment on stroke outcome following permanent MCAO would be assessed. Apocynin treatment would then be evaluated in a model of transient ischaemia. Finally, the effect of apocynin treatment on the acute evolution of the ischaemic penumbra would be assessed in a rat model with stroke co-morbidities (SHRSP) using the MRI perfusion-diffusion mismatch model.

Chapter 2.
Methods

2.1 Animal and Surgical Procedures

2.1.1 Animal Preparation

All animal procedures were performed under licence from the UK Home Office (Personal Licence number 60/11949, working under Project Licence numbers 60/3759 and 60/3618) and in accordance with the Animals (Scientific Procedures) Act, 1986. Prior to surgery, all animals were housed in groups with water and food freely available and were kept on a 12 hour light/dark cycle. All surgical procedures were performed by Emma Reid.

On the day of surgery, rats were weighed following transfer from the animal housing unit to the operating theatre. Anaesthesia was initially induced in an anaesthestic gas chamber, where 5% isofluorane (Baxter Healthcare Ltd, UK) was administered in a 30%/70% mixture of oxygen and nitrous oxide, respectively. Depth of anaesthesia was assessed by means of the withdrawal reflex, where the footpad of the hindlimb is tightly squeezed to evoke a reflex withdrawal of the foot. If this reflex absent then the animal is deep enough to proceed with surgery. This reflex was assessed at regular intervals during surgical procedures to establish if the anaesthetic dose needed to be adjusted.

Once deeply anaesthetised the rat was removed from the chamber and was artificially ventilated following tracheal intubation or tracheotomy. In experiments where animals were not allowed to recover following surgery, a surgical tracheotomy was performed. Following removal from the anaesthetic chamber, the rat was transferred to a face mask where the dose of isofluorane was reduced to between 2% and 3% in the same gas mixture stated previously, to maintain surgical anaesthesia. The animal was positioned on its back and hair was shaved from the neck using an electrical shaver (Wahl, UK). A tracheotomy was then performed to allow artificial ventilation of the animal and removal of the face mask. An incision was made in the neck using large scissors and the underlying musculature was split by blunt dissection to expose the trachea. Two ligatures of 2-0 thread (Davis & Geck, UK) were loosely tied around the proximal and distal ends of the trachea, approximately 1-1.5cm apart. A small incision was then made in a ring of tracheal muscle equidistant between the ties using microscissors. The ventilation tube (Linton Instruments, UK) was then quickly inserted into the incision and advanced down the trachea towards the bronchi. Particular care was taken not to advance the tube more than 2cm distal to the incision site to prevent the tube from blocking off one of the bronchi. The ventilation tube was then connected to the ventilator (Ugo Basile, Linton Instuments, UK) where the stroke

volume was set to ~3ml at a frequency of 45 strokes per minute to maintain surgical anaesthesia and was secured by tightening the ligatures and tying them around the tube. The neck of the rat was stitched using 4-0 silk suture (Covidien, UK).

In experiments where the animal was allowed to recover following surgery, artificial ventilation was maintained by intubation, where the tube can be removed without trauma to the trachea. Following removal from the anaesthetic chamber, the rat was placed in an upright position against a cork board by hooking a loop of 2-0 thread, which was pinned to the top of the cork board, around the upper incisors to secure the position of the rat. The mouth was opened and the tongue was pulled to the side of the mouth using small forceps to allow the trachea to be observed. A fibre optic light (Meiji Techno) was shone onto the neck to gain a clear view of the vocal cords and trachea and a 16 gauge catheter (MillPledge Veterinary, UK) was then swiftly inserted. The intubation tube was then connected to the ventilator and anaesthetic dose was adjusted until breathing was steady and in time with the ventilator, where the stroke volume was set to 2.5-3ml with a stroke frequency of 60 strokes per minute. The anaesthetic dose was maintained via this method and the intubation tube was secured by stitching it to the side of the mouth using 4-0 silk suture to prevent it being pulled out during transfer of the rat to the MRI scanner.

In all experiments, with the exception of the permanent stroke model in Chapter 5, cannulation of the right femoral artery was performed to allow continual monitoring of blood pressure. The right hindlimb and groin were shaved and an incision was made using large scissors. Blunt dissection of the underlying musculature was performed to expose the right femoral artery. The artery was then isolated from the femoral vein by blunt dissection using small curved and straight-edged forceps. Two ligatures (4-0 silk suture) were loosely tied at the proximal and distal ends of the artery, approximately 2cm apart. The ligatures were pulled tightly by using sticky tape to secure the ends of the ties to the cork board and a small incision was made into the artery using microscissors, equidistant between the two ligatures. The artery was then cannulated using a length (25cm) of PE-50 tubing (Portex, UK) which was advanced approximately 2-3cm along the vessel. The cannula was secured in place by tying 4-0 silk suture around the tubing and the artery. The cannula was then connected to a transducer which was linked to a computer, where physiological parameters including heart rate and mean arterial blood pressure were recorded (Biopac, Acqknowledge). Mean arterial blood pressure was maintained within the range of 85-95mmHg in normotensive rats and was maintained within the range of 105-115mmHg in hypertensive rats. Body temperature was monitored with a rectal themal probe (Physitemp,

New Jersey, USA) and was maintained at 37±0.5^{o} C using an angle poise heat lamp. Care was taken to avoid burning the skin of the animal by placing a layer of gauze (Vernon-Carus Ltd, UK) over the body.

2.1.2 Focal Cerebral Ischaemia

Permanent MCAO

Occlusion of the middle cerebral artery was then performed according to the model first described by Koizumi et al (1986) with subsequent modifications (Longa et al, 1989). All surgery was performed under a light microscope (Zeiss, Germany). First, blunt dissection of the shaved tissue of the neck revealed the tracheal strap musculature, which was retracted to expose the common carotid artery. The surrounding connective tissue was dissected and the vessel was tied off using 4-0 silk thread. The external carotid artery was then identified and securely tied at an intermediate position between the ascending pharyngeal artery and the lingual and maxillary branches. The three branches of the external carotid where then subjected to cauterisation using diathermy forceps (Eschmann Equipment, UK). The external carotid artery itself was then cauterised above the tie and the three branches of this vessel were cut when it had been established that the vessels had been sealed off to prevent any bleeding. At this point the occipital artery, which runs alongside the internal carotid, was identified, cauterised and cut in the same manner as described previously. Any excess connective tissue was removed from the internal carotid artery and the vessel was subsequently tied loosely with 4-0 thread. Following this, the pterygopalatine artery was securely tied off to prevent the intraluminal thread from entering this vessel instead of following the course of the internal carotid artery (Figure 2-1).

In the stroke reproducibility study, described later in this chapter, the intraluminal thread was constructed from a length of 3-0 nylon monofilament (Covidien, UK) where a small diameter bulb was created using a cauterising pen (Aaron Medical, FL, USA). In all other experiments, a nylon filament with a silicon tip of length 5-6mm and of diameter 0.31-0.35mm (Doccol Corporation, CA, USA) was used. The length of filament was then

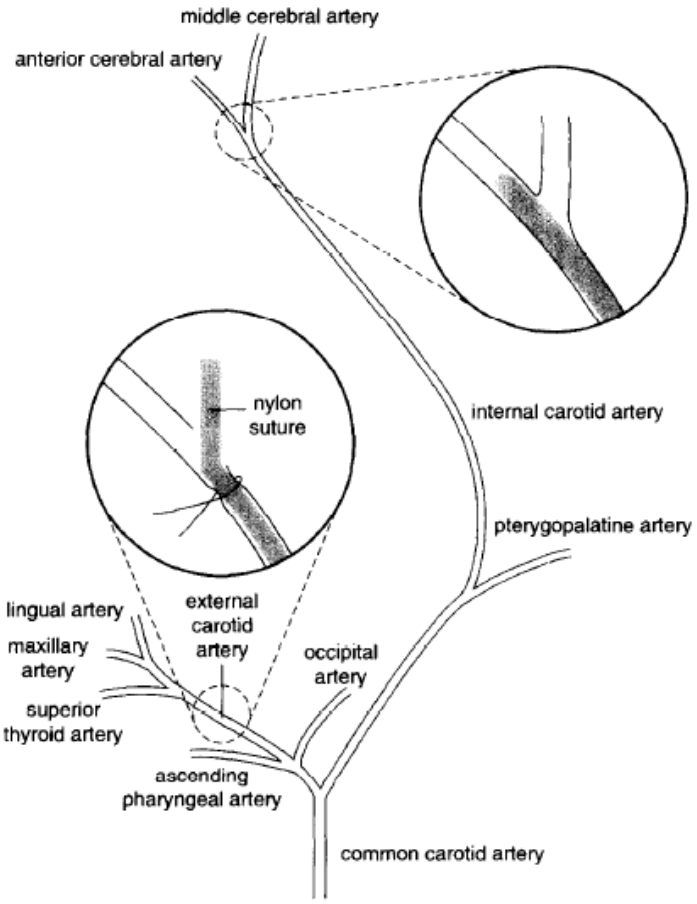

Figure 2-1. A schematic diagram of the intraluminal thread model of middle cerebral artery occlusion. The external carotid artery is ligated and all branches are transected to allow the artery to be manipulated for ease of passage of the nylon monofilament. The pterygopalatine artery is ligated and the monofilament is introduced into the internal carotid artery by arteriotomy. The filament is advanced along the internal carotid until it lodges in the narrow proximal anterior cerebral artery, where it blocks the origin of the middle cerebral artery. This method of middle cerebral artery occlusion can be transient or permanent. Image reproduced from Hunter et al (1995).

measured and at the point of 22mm, a bend was introduced. This ensured that the filament would block the vessel at the proximal origin of the middle cerebral artery.

The external carotid artery was then cut using microscissors resulting in an arterial stump which can be then be manipulated to aid the passage of the filament. The internal carotid tie can then be pulled tightly to limit blood loss as a small incision is made at the bifurcation point of the common carotid artery. The filament was then carefully advanced along the internal carotid artery until some resistance is felt, which should correspond to the point where only the bend of the filament is visible outwith the vessel. The internal carotid tie was then be tightened to secure the filament firmly in place. Furthermore, in permanent occlusion models the entry point of the filament was sealed using the diathermy forceps to further secure its position. The tissue of the animal was then sutured using 4-0 thread to prevent infection and dehydration.

Transient MCAO

In the transient MCAO models, a modified version of the occlusion method was used instead of the technique described in detail previously. Animal recovery following surgery may be impinged as a result of difficultly in eating and drinking, as transection of the external carotid artery renders the muscles of mastication and swallowing ischaemic. This may lead to weight loss and increased mortality following surgery. In the transient stroke experiments, animals were allowed to recover for 72 hours following stroke and it was decided that to aid eating and improve recovery, a modified filament model would be used. This model preserves the integrity of the external carotid artery and its branches. Two 4-0 thread ligatures were tied round the common carotid artery, one tied loosely at the carotid bifurcation and the other tied tightly approximately 1mm below the bifurcation. Loose ligatures were also tied around the external carotid, internal carotid and the pterygopalatine artery. A small incision was made between the two ligatures on the common carotid artery to allow insertion of the filament. All ligatures were pulled tightly at this point to limit blood loss. Once the filament had been advanced to block the origin of the middle cerebral artery, the pterygopalatine artery tie was removed and the other ties were secured to prevent blood loss and to secure the filament in place until it is removed after a fixed time period. In all transient MCAO experiments the filament was removed after 1 hour of ischemia. This was achieved by releasing the ligature around the internal carotid artery and the ligature at the common carotid artery bifurcation was also loosened. This allowed the filament to be retracted and subsequently removed. The incision point was then cauterised

using diathermy forceps and the external carotid ligature was removed, leaving only the common carotid tie in place. The wound was then flushed with sterile saline and stitched using 4-0 silk suture.

2.1.3 Perfusion Fixation

Animals were transcardially perfused with fixative to allow histological examination of the brain following stroke. Firstly, animals were deeply anaesthetised using 4-5% isofluorane delivered in a 30%/70% mixture of oxygen and nitrous oxide administered via a face mask to ensure the animal was deeply anaesthetised prior to opening up the chest cavity. An incision was made below the sternum and the skin overlying the chest was cut to expose the underlying musculature and the diaphragm, which were also incised. The ribcage was cut on both sides to allow the tissue of the chest to be retracted and clipped securely to expose the viscera of the chest cavity. The beating heart was then gently pulled down to allow detection of the aorta. A large needle which is connected to a flask of 0.9% saline containing heparin (10ml/Litre) and a flask containing 4% paraformaldehyde (PAM) was inserted into the left ventricle and advanced into the aorta. The heart was then clamped to secure the position of the needle and the right atrium was cut to allow blood to drain out of the heart. At this point, around 200-250 ml of heparinised saline was pumped through the circulation at a pressure of around 100mmHg to flush all of the blood out from the animal. Once the perfusate ran clear, indicating that all of the animal's blood had been flushed out, 200ml of 4% PAM was then pumped through the circulatory system at the same pressure to fix the animal. Spontaneous limb movement was observed as the fixative travelled through the circulation, indicating successful fixation.

2.2 Assessment of Final Infarct and Stroke Reproducibility

2.2.1 Haematoxylin and Eosin Staining

Following successful fixation, the animal was immediately decapitated and the entire head was stored in 4% PAM for 24 hours. The brain was then removed and post-fixed in 4% PAM for a further 24 hours before being embedded in paraffin wax. The embedding procedure was carried out in a paraffin processor (Miles Scientific) which undergoes many cycles of tissue dehydration and clearance, using alcohols and xylene respectively, before the brain is embedded in paraffin wax (Table 2-1). The entire procedure takes a total of 59 hours to complete. The embedded brain was then cut into 6 micron thick sections of the 8

Stage	Process	Time Period (Hours)
1	70% Alcohol	2
2	80% Alcohol	3
3	95% Alcohol	4
4	Absolute Alcohol 1	4
5	Absolute Alcohol 2	5
6	Absolute Alcohol 3	5
7	Absolute Alcohol 4	6
8	50% Alcohol/50% Xylene	4
9	Xylene 1	5
10	Xylene 2	5
11	Paraffin Wax 1	5
12	Paraffin Wax 2	5
13	Paraffin Wax 3	6

Table 2-1. Paraffin wax processing schedule for rat brains. Following an extensive period of dehydration by alcohol immersion and tissue clearance using xylene, the brains are immersed in paraffin wax at 60^{o} C for a period of 16 hours.

Stage	Process	Time Period (minutes)
1	Histoclear 1	4-5
2	Histoclear 2	4-5
3	Histoclear 3	4-5
4	Absolute Alcohol 1	3
5	Absolute Alcohol 2	3
6	90% Alcohol	3
7	70% Alcohol	3
8	Wash in running water	4
9	Haematoxylin Staining	4-5
10	Wash in running water	1-2
11	Differentiate in Acid Alcohol	A few dips only
12	Wash in running water	3
13	Scott's Tap Water Substitute	2
14	Wash in running water	2
15	70% Alcohol	2
16	90% Alcohol	2
17	Alcoholic Eosin (95%) Staining	4
18	Absolute Alcohol 1	4
19	Absolute Alcohol 2	4
20	Absolute Alcohol 3	4
21	Histoclear 1	4
22	Histoclear 2	4
23	Histoclear 3	4

Table 2-2. Haematoxylin and eosin staining procedure for paraffin embedded sections.

coronal levels (Osborne et al, 1987) using a microtome (Leica, UK) to allow determination of infarct volume following haematoxylin and eosin (H & E) staining. The sections were placed on poly-L- lysine coated slides and were left to dry overnight.

The paraffin wax was removed from the sections by immersing them in histoclear (National Diagnostics, UK) and the sections were then immersed in a series of graded alcohols before haematoxylin (Surgipath, UK) staining was performed. Following a period of washing and differentiation in acid alcohol, the sections were again dehydrated before eosin (Surgipath, UK) staining took place (Table 2-2). Further dehydration was followed by immersion in histoclear prior to mounting the slides using DPX mounting medium (Raymond Lamb Laboratory Supplies). H & E staining can be used to detect histopathological changes following focal cerebral ischaemia. Haematoxylin stains basophilic structures blue and eosin stains eosinophilic structures bright pink. Thus, under the light microscope, the neuronal nuclei are stained blue and the surrounding cytoplasm and extracellular components appear pink. However ischaemic damage can be readily detected as ischaemic neuronal cell bodies become dark and shrunken and can be easily distinguished from healthy neurons. There are other clear signs of ischaemic damage including pallor of eosin staining and vacuolation of the neuropil.

In order to assess infarct volume, 8 coronal levels spanning the territory of the middle cerebral artery (Osborne et al, 1987) were examined under a light microscope (Leica, UK) at a range of magnifications (x5, x10, and x20) to identify ischaemic neuronal damage. The cell soma of normal healthy neurons appears rounded with a clearly visible nucleus. However, ischaemic neurons become pyknotic in appearance, where they appear dark and shrunken into a triangular shape. The surrounding neuropil also becomes sponge-like in appearance and demonstrates pallor of eosin staining (Figure 2-2). These attributes can be identified under the microscope and the areas of ischaemic damage can then be transcribed by hand onto line diagrams at pre-determined coronal levels (Osborne et al, 1987) (Figures 2-3 & 2-4). This process is repeated 3 times for each animal on separate occasions to ensure reproducibility. The line diagrams are then scanned onto a computer and analysed using image analysis software, ImageJ (http://rsb.info.nih.gov/ij/). The area of ischaemic damage is directly measured on each coronal level. The total volume of damage is calculated by the integration of the areas and the distance between each level using the stereotaxic co-ordinates (Paxinos & Watson, 1998).

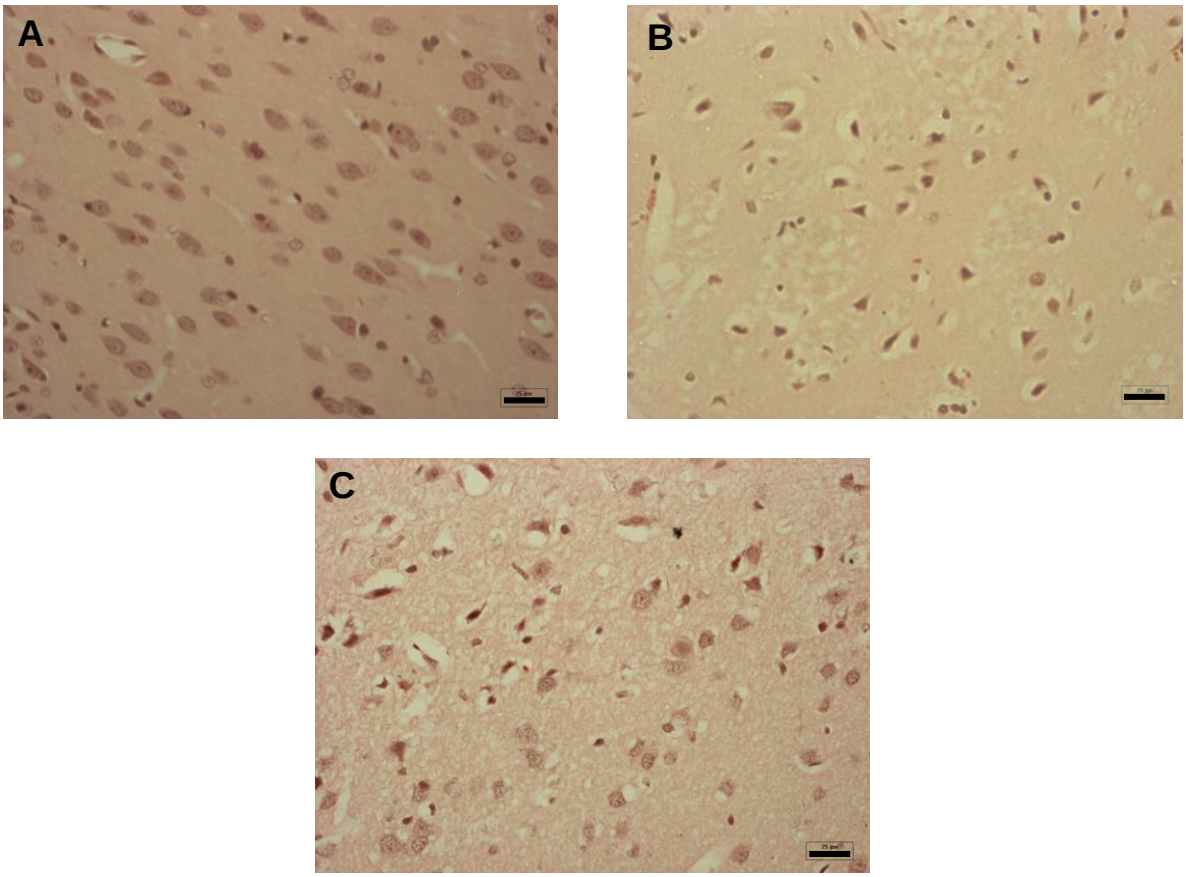

Figure 2-2. Light microscopic images (x20) depicting representative H & E staining of the ipsilateral hemisphere of a rat following 4 hours permanent MCAO. Image A shows normal, unaffected cortical tissue, where healthy neurons appear round and uniform. Image B depicts ischaemic tissue. Note the pallor of eosin staining of the neuropil and pyknotic neurons. Image C shows the border zone, where normal neurons appear alongside ischaemic neurons. Scale bars=25µm.

Level 1: Bregma = 3.20mm

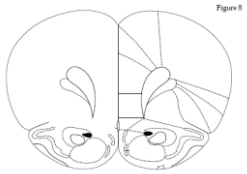

Level 2: Bregma = 1.20mm

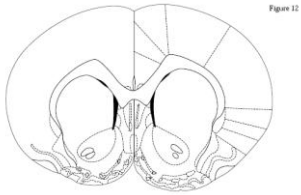

Level 3: Bregma = -0.26mm

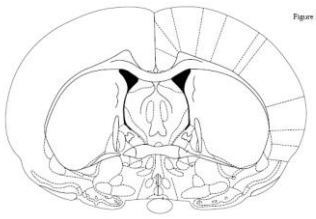

Level 4: Bregma = -0.80mm

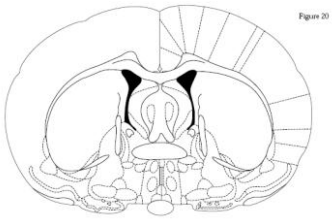

Level 5: Bregma = -1.80mm

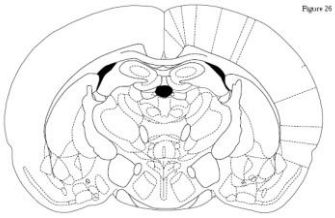

Level 6: Bregma = -3.14mm

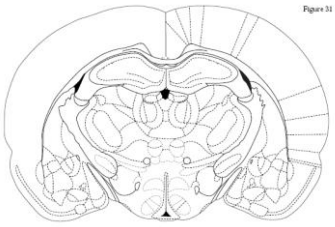

Level 7: Bregma = -4.80mm

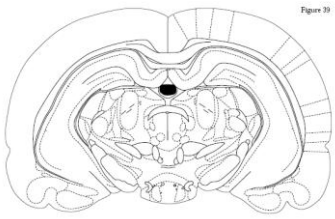

Level 8: Bregma = -6.30mm

Figure 2-3. The eight coronal levels defined by Osborne et al (1987). The figures are reproduced from the stereotaxic atlas of Paxinos & Watson (1998) with the distance from bregma defined at each level, where levels 1 and 2 are anterior to bregma and the remaining levels are found posteriorly.

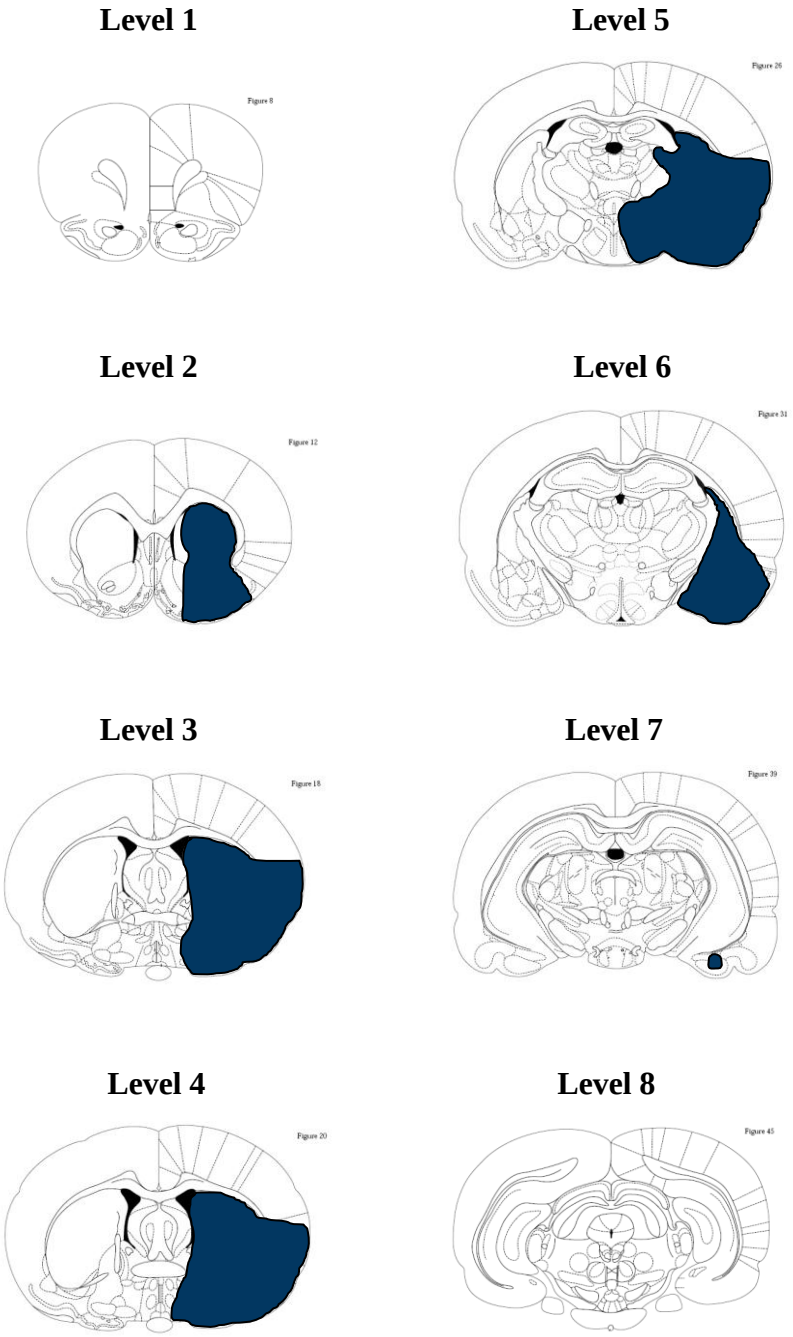

Figure 2-4. Line diagrams of the 8 coronal levels defined by Osborne et al (1987) with the area of ischaemic damage, as observed by light microscopic examination of H & E stained sections, manually traced onto the images (Paxinos & Watson, 1998). The images represent the ischaemic damage observed in the median animal of the H & E staining group in the stroke reproducibility study.

2.2.2 2,3,5-triphenyltetrazolium chloride (TTC) Staining

TTC has been utilised for over 50 years to identify areas of ischaemic tissue damage. It is a water-soluble salt which in normal brain tissue is reduced by mitochondrial dehydrogenase enzymes to form a deep red, fat soluble compound called formazan. However, in ischaemic tissue, these mitochondrial enzyme systems are incapacitated and consequently, these tissue areas remain unstained (Figure 2-5). It is therefore, a rather crude yet reliable method used to delineate areas of ischaemic damage following middle cerebral artery occlusion.

For TTC processing of the brain, the animal was deeply anaesthetised by using 5% isofluorane delivered in a 30%/70% mixture of oxygen and nitrous oxide before decapitation. The brain was then immediately removed from the skull and bathed in ice-cold 0.9% saline. The brain was then placed in a rat brain matrix (World Precision Instruments, UK) and microtome blades (Feather, Japan) were positioned 2mm apart to cut 6 coronal brain slices simultaneously. The slices were then incubated in a pre-warmed 40ml solution of 1% TTC (Sigma, Switzerland) in phosphate buffered saline, for 15 minutes at 37^{o} C. The brain sections were then removed from the TTC solution and allowed to incubate in PAM overnight. Following fixation, both faces of each brain slice were photographed using a digital video camera (Canon, UK) which was secured onto a stand (Kaiser, Germany) to keep the camera at the same height for all photographs. A graticule (Imaging Research Inc.) was used to determine scale for subsequent calibration. This allowed the infarct area of each slice to be determined by manually tracing the area of ischaemic damage using ImageJ software. The infarct area on both faces of each slice were added together and divided by 2 to give the mean infarct area for each slice. The total infarct volume was calculated by multiplying the sum of the infarct areas of each slice by the slice thickness (2mm).

A stroke reproducibility study was undertaken to assess surgical ability to induce MCAO and also to compare final infarct volume at 4 hours post-MCAO using both haematoxylin & eosin and TTC staining methods. Permanent stroke was induced in 12 Sprague-Dawley rats (300-350g, Harlan, UK) by the intraluminal filament model, as described earlier in this chapter. Following 4 hours of MCAO, 6 animals were sacrificed by perfusion fixation to allow H & E staining of brain tissue and 6 animals were sacrificed for TTC staining. Infarct volumes were determined for both techniques and compared between the groups.

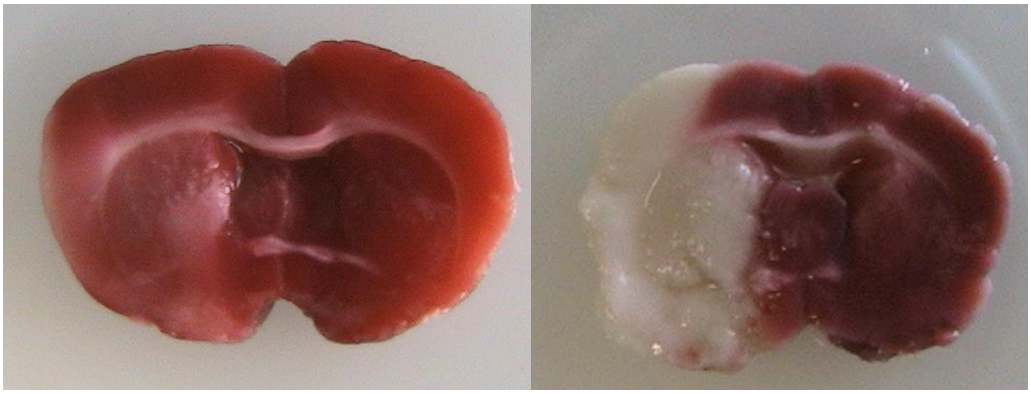

Figure 2-5. TTC staining of coronal brain slices following middle cerebral artery occlusion identifies area of ischaemic injury. The image on the left depicts the level of contrast observed when the staining is performed 4 hours post occlusion. Note that the delineation of the infarcted tissue is not as great as that observed when TTC staining is performed 24 hours following middle cerebral artery occlusion (right image). Both images depict coronal level three as defined by Osborne et al (1987).

Infarct volume as derived by TTC staining was significantly greater than infarct volume defined by histopathological examination of brain sections stained with H & E (Figure 2-6). Despite this, within each staining group the calculated infarct volumes were consistent, indicating stroke reproducibility. However, one rat was excluded from the H & E staining group as microscopic examination revealed no evidence of ischaemic damage. The median infarct volume in the TTC staining group was 268mm^3 compared to a median infarct volume of 121mm^3 in the H & E group. The data were analysed using non-parametric statistical tests due to the skewed data in the TTC group, where two rats displayed particularly large infarcts. Statistical analysis using the non-parametric Mann-Whitney test, revealed that the two groups were significantly different at the 95% level of significance (P=0.0043).

The ability of TTC staining to accurately identify cerebral infarction was examined by Bederson and colleagues (1986a). These authors reported that when the infarct was allowed to develop for 24 hours, there was no significant difference between the infarct volume determined by TTC staining or by H & E staining. However, when animals were sacrificed less than 6 hours post occlusion, it became more difficult to assess infarct volume via the TTC method, as the lesions are stained pink and it can be extremely difficult to delineate the borders of the lesion, since the contrast with the surrounding normal brain tissue is often very poor (Figure 2-5). By contrast, at the 24 hour time point, the infarct can be very clearly distinguished from brightly stained normal tissue. This was clearly evident in the stroke reproducibilty study, as there was no clear differentiation between normal and infarcted tissue after four hours of MCAO, thereby making it extremely difficult to demarcate the borders of ischaemic damage.

The difficulty in distinguishing ischaemic from normal tissue in TTC stained brain slices may account for the significant overestimation of infarct volume demonstrated by this method, since the process of delineation is extremely subjective. However, the same can be said when transcribing areas of ischaemic damage onto line diagrams from H & E stained sections. It can be difficult to determine the boundaries of ischaemic tissue damage when there is evidence of a substantial border zone, where both ischaemic and normal neurons are identified. Since transcribing areas of ischaemic damage onto line diagrams corrects for brain swelling and prevents overestimation of infarct volume, it was considered that this may explain the larger infarct volumes demonstrated with the TTC staining method. However, when the hemispheric areas of TTC stained brain slices were examined, there

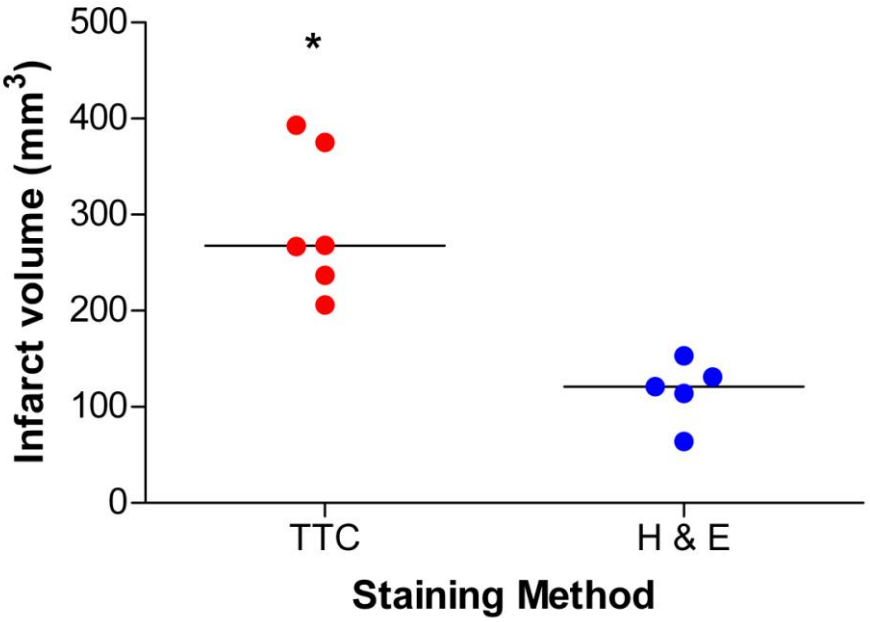

Figure 2-6. Comparison of the TTC and H & E staining methods for determination of infarct volume following 4 hours permanent MCAO in the Sprague-Dawley rat. Infarct volume as determined by TTC staining (n=6) is significantly greater than infarct volume calculated by examination of H & E stained brain sections (n=5) *p=0.0043.

was no significant difference between the ipsilateral and contralateral hemispheres, indicating that there was no evidence of cerebral oedema. This result was as expected since brain oedema is not usually evident until at least 4 hours post ischaemia in permanent rodent stroke models (Tyson et al, 1982).

Therefore, the results of the stroke reproducibility study indicate that in order to determine infarct volume following permanent MCAO of 4 hours duration, H & E staining of brain tissue should be the preferred method. Despite TTC determination of infarct volume being comparable to that observed by the H & E staining method following 24 hours of MCAO, at earlier time points there is no clear delineation between ischaemic and unaffected brain tissue.

2.2.3 MRI RARE T_2 Weighted Imaging

In chapters 3, 4 and 5, infarct volume was determined using MRI RARE T_2 weighted imaging. T_2 weighted imaging can be reliably used to identify ischaemic brain tissue 12 to 24 hours following stroke but during the critical period of 6-12 hours, this method does not adequately assess the severity and extent of ischaemia (Baird & Warach, 1998). In acute stroke, the changes in blood flow and tissue swelling which occur are associated with very subtle signal changes in T_2 images. Areas of injured tissue produce higher signal intensity than normal brain tissue allowing the infarct to be clearly distinguished.

All MRI data were acquired using a Bruker Biospec 7T/30cm system with a gradient coil (internal diameter=121mm, 400mT/m) and a 72mm birdcage resonator. MRI RARE T_2 weighted imaging was used to calculate infarct volume at 24 hours following permanent MCAO or at 72 hours following transient MCAO. Rats were anaesthetised in an anaesthetic chamber, as described previously, and were then immediately transferred to the MRI scanner, secured within the cradle by tooth and ear bars, to restrict head movement, and a 4-channel phased array surface receiver coil was placed on the head. Body temperature was maintained within physiological range ($37\pm0.5^{o}C$) during the MRI scanning procedure by a closed circuit thermal jacket.

Once a pilot sequence had been obtained to ensure correct geometry, a RARE T_2 weighted sequence was acquired (TE=72.7ms, TR=5086.1ms, matrix=256x256, 16 coronal slices; 0.75mm thick) to allow calculation of final infarct volume.

Final infarct was defined as the hyperintense area on T_2 weighted images. The hyperintense area was manually delineated on each of the 16 T_2 slices spanning the territory of the middle cerebral artery using Image J software (Figure 2-7). The area of the contralateral and ipsilateral hemisphere on each slice was also measured. The volumes of the contralateral and ipsilateral hemispheres and infarct volume were calculated by multiplying the total area across the 16 slices by the slice thickness (0.75mm). Total infarct volume was corrected for oedema using published equations which take compression of the contralateral hemisphere into account (Gerriets et al, 2004), in addition to swelling of the ipsilateral hemisphere (Swanson et al, 1990).

For the calculation of infarct volume corrected for swelling of the ipsilateral hemisphere the following equation was used:

Corrected lesion volume = volume of contralateral hemisphere - (volume of ipsilateral hemisphere – lesion volume)

A correction factor which accounts for compression of the contralateral hemisphere is calculated by the following equation:

Compression Factor=(ipsilateral volume + contralateral volume)/(2 x contralateral volume)

To calculate infarct volume which is corrected for both ipsilateral swelling and contralateral compression, the following equation was used:

Infarct volume = corrected lesion volume x compression factor

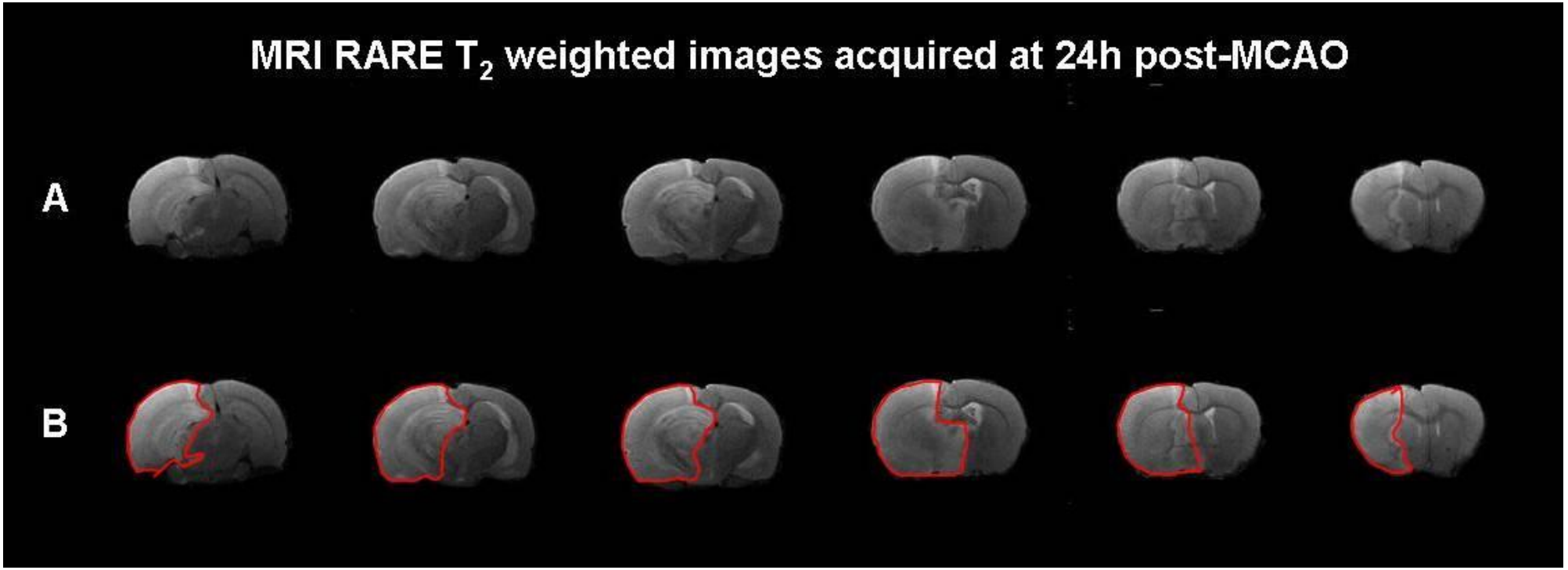

Figure 2-7. MRI RARE T_2 images from a representative SHRSP rat acquired at 24h following permanent occlusion of the middle cerebral artery. Row A shows 6 coronal slices spanning the territory of the MCA. Infarcted tissue is clearly visible as the hyperintense area within the ipsilateral hemisphere. Note also the extensive swelling of the ipsilateral hemisphere and compression of the contralateral hemisphere. Image J software was used to delineate the infarcted tissue, as shown in red in row B. Infarct volume was calculated by multiplying the summation of infarct area across 16 coronal slices and multiplying by slice thickness. Infarct volume was corrected for both ipsilateral swelling and contralateral compression using published equations (Swanson et al, 1990; Gerriets et al, 2004).

2.3 Behavioural Assessment

2.3.1 Modified Bederson Scale

In chapter 5, neurological function following stroke was assessed using a modified Bederson Scale. The original 4 point scale was developed by Bederson et al. (1986b) (Table 2-3a) and was used to grade stroke severity in rats following occlusion of the middle cerebral artery. The original Bederson scale has been modified and expanded by various study groups (Suzuki et al, 2004; Braeuninger et al, 2010 and others). The modified scale used in chapter 5 to assess functional outcome was a 6 point scale, where animals were assigned a grade of 0 to 5 (Table 2-3b). Animals were assessed by gently holding the base of the tail to suspend the rat in the air and the normal response is to extend both forelimbs. However, rats with infarction will consistently flex the forelimb contralateral to the ischaemic hemisphere. Rats which displayed no observable deficit and extended both forelimbs were scored a grade 0 and rats which exhibited flexion of the contralateral forelimb but no other deficits were scored a grade 1. Rats were then suspended by the base of the tail and allowed to grip the bars of their cage while being gently pulled away from the cage to assess grip strength. If any weakness of the contralateral forelimb was observed by the loss of grip, then the rat was scored a grade of 2. Rats were then allowed to move freely on the floor to assess circling behaviour. Rats that consistently circled to the paretic side, in addition to forelimb flexion and reduced grip strength, were assigned a grade of 3. In more severe cases, animals which exhibited no spontaneous movement were given a grade of 4 and rats which died prior to functional testing were assigned a grade of 5.

2.3.2 Vibrissae-evoked Forelimb Placement

In addition to the modified Bederson Scale, functional outcome was also assessed by the vibrissae-evoked forelimb placement test. This test assesses sensorimotor function and proprioceptive capacity and is sensitive to damage to the striatum and sensorimotor cortex in addition to the spinal cord and other sensorimotor structures (Schallert et al, 2000). It assesses placement of the forelimb in response to detection of a table top by the vibrissae. When the vibrissae of either side are brushed against a table top, the normal response is the placement of both forelimbs on to the table top. In functionally impaired animals, there is a reduced capacity to place the affected forelimb.

A

Neurologic Examination Grading System

Normal	grade 0:	no observable deficit
Moderate	grade 1:	forelimb flexion
Severe	grade 2:	decreased resistance to lateral push (and forelimb flexion) without circling
	grade 3:	same behavior as grade 2, with circling

B

Neurological Assessment Scale	***Observed Functional Deficits***
Grade 0	No observable deficit
Grade 1	Flexion of the contralateral forelimb
Grade 2	As grade 1 and with reduced grip strength of the contralateral forelimb
Grade 3	As grade 2 and with consistent circling
Grade 4	No spontaneous activity
Grade 5	Dead

Table 2-3. Neurological tests developed to assess function in rats following middle cerebral artery occlusion. Table A illustrates the original grading system devised by Bederson and colleagues. Reproduced from Bederson et al, (1986b). Table B shows the modified and extended neurological grading scale used to assess functional outcome in chapter 5.

In chapter 5, the vibrissae-evoked forelimb test was performed as described by Schallert et al (2000). All rats were handled frequently in the week prior to performing this test to ensure that they would not be stressed during the procedure. The test involved holding the rat loosely in the palm of the hand so that all four limbs were hanging freely. The rat is then moved laterally towards the table top and the vibrissae ipsilateral to the damaged hemisphere are gently brushed against the table top, whilst the contralateral forelimb is restrained by the forefinger so that only placement of the ipsilateral forelimb is assessed. This is repeated to assess the placement of the contralateral forelimb by restraining the ipsilateral forelimb and brushing the ipsilateral vibrissae against the table top. A successful placement is given a score of one. This is repeated ten times on each side to obtain a score out of ten for the number of successful placements achieved by the ipsilateral and contralateral forelimbs. Animals with unilateral brain damage will display varying degrees of impaired contralateral limb placing ability while the unaffected ipsilateral forelimb will typically show no evidence of impairment. The severity of brain injury can then be graded by calculating the percentage of unsuccessful contralateral placements (number of incorrect placements x 10).

This test was performed prior to surgery to ensure that there was no evidence of functional impairment or limb preference before experimental stroke was induced. There was no evidence of limb preference or functional impairment in any of the rats tested prior to stroke surgery.

2.3.3 18 point Neurological Score

In addition to the modified Bederson Scale and the vibrissae-evoked forelimb placement test, an 18 point composite neurological score (Garcia et al, 1995) was used to assess functional outcome in rats where transient ischaemia was induced (Chapter 5). This score comprises 6 neurological tests which assess spontaneous activity, symmetry in limb movement, forepaw outstretching, climbing ability, body proprioception and response to vibrissae touch, with each test scored with a maximum of 3 points. The maximum score which can be achieved is 18, which indicates that there is no neurological deficit and the lowest score which can be achieved is 3, for animals with the most severe impairment (Table 2-4).

Test	Neurological Score			
	0	1	2	3
Spontaneous activity (in cage for 5 min)	No movement	Barely moves	Moves but does not approach at least three sides of cage	Moves and approaches at least three sides of cage
Symmetry of movements (four limbs)	Contralateral side: no movement	Contralateral side: slight movement	Contralateral side: moves slowly	Both sides: move symmetrically
Symmetry of forelimbs (outstretching while held by tail)	Contralateral side: no movement, no outreaching	Contralateral side: slight movement to outreach	Contralateral side: moves and outreaches less than right side	Symmetrical outreach
Climbing wall of wire cage	...	Fails to climb	Contralateral side is weak	Normal climbing
Reaction to touch on either side of trunk	...	No response on contralateral side	Weak response on contralateral side	Symmetrical response
Response to vibrissae touch	...	No response on contralateral side	Weak response on contralateral side	Symmetrical response

Table 2-4. The 18 point composite neurological score to test functional outcome in rats following middle cerebral artery occlusion. This neurological evaluation comprises 6 tests which are each given a score up to 3. The scores for each test are added to given an overall score of functional outcome, where the maximum score of 18 indicates no observable deficit and the minimum score of 3 indicates severe neurological impairment. Adapted from Garcia et al (1995).

1. Spontaneous Activity

The rat was observed for a period of 5 minutes in its home cage with the cage top removed. The spontaneous activity of the rat was assessed by its ability to approach all four walls of the cage and was scored from 0 to 3. A score of 3 indicates that the rat moved around the cage, explored the environment and approached at least three walls of the cage. A score of 2 was given if the rat moved around in the cage but didn't approach all four walls, although it eventually reached at least one upper rim of the cage. A score of 1 indicates that the rat barely moved in the cage and didn't rise up on its hindlimbs to approach any of the cage walls and a score of 0 was given if the rat did not move at all during the observation period.

2. Symmetry in the Movement of Four Limbs

Symmetry in the movement of the four limbs was assessed by suspending the rat in the air by holding the base of the tail. Scores were assigned as follows: a score of 3 was given if all four limbs extended symmetrically and scored 2 if the limbs on the contralateral side extended less or more slowly than those on the unaffected side. A score of 1 was assigned if limbs on the contralateral side showed minimal movement and 0, if the contralateral forelimb did not move at all.

3. Forepaw Outstretching

The rat was held by the base of the tail so that it had to walk along the surface of the table using its forelimbs only. The hindlimbs were kept in the air and symmetry in the outreaching of both forelimbs was observed. Scores indicate the following: 3, both forelimbs were outstretched, and the rat walked symmetrically on forepaws; 2, the contralateral forepaw outstretched less than the ipsilateral forepaw, and forepaw walking was impaired; 1, the contralateral forelimb exhibited minimal movement; and 0, the contralateral forelimb did not move at all.

4. Climbing

The rat was placed on wire grid and was then pulled off the wire by gripping the base of the tail and the strength of attachment was noted. A score of 3 was given if the rat climbed easily and gripped tightly to the wire. The rat scored 2 if the contralateral side was impaired while climbing or did not grip as hard as the ipsilateral side and a score of 1 indicates that the rat failed to climb or tended to circle instead of climbing.

5. Body Proprioception

The rat was sharply prodded with a blunt wooden pencil on each side of the body, and the reaction to the stimulus was observed. A score of 3 indicates that the rat reacted by turning head and was equally startled by the stimulus on both sides. A score of 2 was given if the rat reacted slowly to stimulus on the contralateral side and a score of 1 if the rat did not respond to the stimulus at all on the contralateral side.

6. Response to Vibrissae Touch

A wooden pencil was brushed against the vibrissae on each side; the stick was moved toward the whiskers from the rear of the animal to avoid entering the visual fields. A score of 3 was assigned if the rat reacted by turning head or was equally startled by the stimulus on both sides. A score of 2 indicates that the rat reacted slowly to stimulus on the contralateral side and a score of 1 was given if there was no response to the stimulus on the contralateral side.

The scores from each test are added to give an overall neurological score, where the maximum score of 18 is achieved where there is no observable deficit and the minimum score of 3 indicates the most severely impaired animals.

2.4 Blood Pressure Determination

2.4.1 The Tail Cuff Method

It is necessary to regularly monitor systolic blood pressure in both the SHRSP and the WKY to ensure that the stroke-prone strain is indeed hypertensive compared to the normotensive control strain. The American Heart Association recommends indirect measurement of blood pressure to detect substantial group differences in systolic blood pressure (Kurtz et al, 2005). The tail cuff method of systolic blood pressure (BP) measurement is a non-invasive technique which was developed by the West of Scotland's Department of Clinical Physics and Bioengineering, based at the Southern General Hospital in Glasgow (Evans et al, 1994). This technique involves the placement of a cuff around the proximal end of the rat's tail which is then inflated with air until the point at which the pressure in the cuff matches that of the tail artery, resulting in a transient occlusion of the vessel. This leads to an absence of a pulse which is detected by a signal transducer, which is also located on the tail of the rat, at a more distal position than the tail

cuff. The signal is relayed to a central monitoring system which is connected to a laptop (Dell, UK) which then displays the systolic blood pressure reading in mmHg and the cuff is then deflated. This technique is advantageous as it does not require catheterisation of an artery as required for direct methods of blood pressure measurement and has been validated against direct measures of blood pressure measurement (Feng et al, 2008). Furthermore, it allows BP measurements to be obtained in conscious animals without the influence of anaesthesia on BP, as is the case with invasive methods. However, there may be an element of stress associated with the mild restraint involved which will be reflected in the measurements obtained but this can be minimised by incorporating an extensive acclimatisation and training period into the regime.

2.4.2 Tail Cuff Apparatus

Prior to BP measurement, the animals must be pre-warmed to induce maximal vasodilatation of the tail artery. This is achieved by placing the animals in an insulated heat box (dimensions 37cm x 35cm x 40cm) (Figure 2-8). The upper surface of the box has a circular opening (diameter 7cm) to allow the box to be warmed to a temperature of 34^{o}C using a hairdryer (Boots, UK) with temperature maintained by positioning an angle poise lamp over the opening of the box. A thermometer situated on the inner wall of the chamber is used to monitor the temperature within the box. The front panel of the heat box has a door to allow ease of removing animals from the chamber and an insulating tile can be removed from the door to observe the animals through a perspex screen. The screen also promotes heat loss if the temperature rises above 35^{o}C.

The tail cuff is constructed by cutting the medial portion of a 5ml syringe (Plastipak, UK) to a length of 2cm and a length of latex tubing (length 6cm, width 1.5cm) is inserted into the syringe. A 10 gauge catheter, cut to 4cm in length was inserted into the latex tubing and secured in place by tying 5-0 thread around the tubing. The opposite end of the latex tubing was turned over to the outer face of the syringe and was secured using a plastic o-ring (1.7cm diameter) (Figure 2-9). The catheter was then connected to the central BP measurement system. The central monitoring system was also connected to a cylinder of medical air (BOC Gases, UK) via a hose, a laptop (Dell, UK) and a piezoceramic transducer (Figure 2-8).

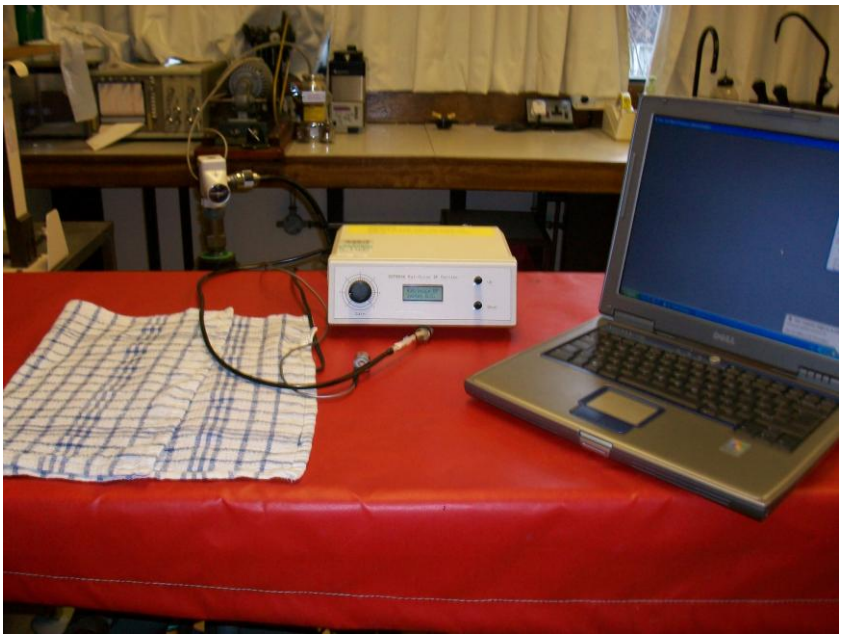

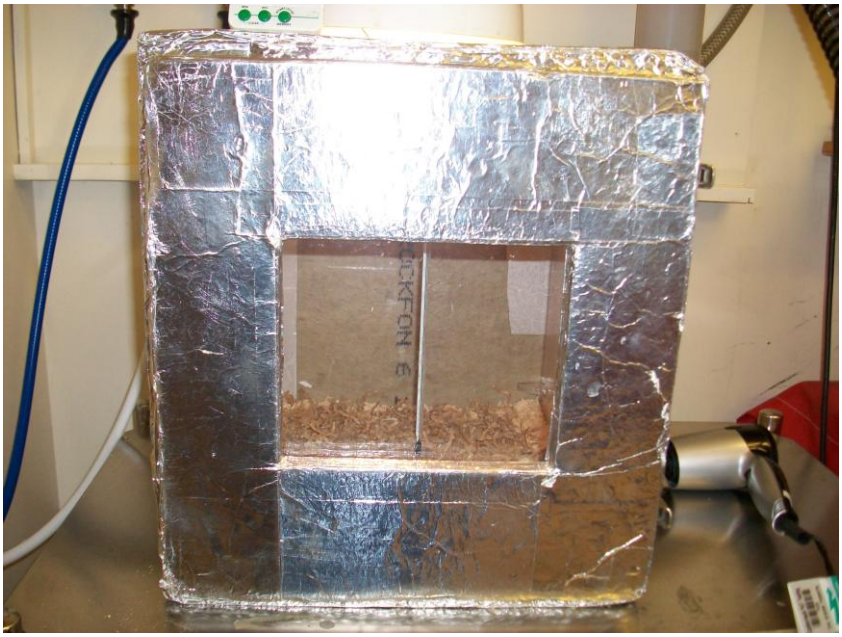

Figure 2-8. The tail cuff apparatus. The top image shows the central blood pressure monitoring system which is connected to a laptop, where the systolic blood pressure measurements are displayed and recorded. A heat mat and a towel are used to keep the rat warm and lightly restrain movement. The bottom image shows the heat box, which is pre-warmed to 34^{o}C. The rat is placed in the box for 10-15 minutes to induce maximal vasodilation of the tail artery prior to blood pressure measurement.

Figure 2-9. The tail cuff and transducer. The top image shows the tail cuff which is placed on the base of the tail and inflates and deflates in cycles. The bottom image shows the piezoceramic transducer which relays the blood pressure signal to the central blood pressure monitoring system.

2.4.3 Animal Training Procedure

All rats were subjected to an intensive 5 day training period to acclimatise them to handling and the tail cuff apparatus. On day one of training rats were taken to the room where the tail cuff apparatus was set up in their home cage. The animals were then handled for a period of 20-30 minutes and were allowed to explore the table where the tail cuff apparatus was set up. They were also wrapped in a towel to accustom them to mild restraint. On day two, rats were subjected to the same handling procedure as the previous day, with the addition of being placed in the heat box for 10 minutes, which had not been pre- warmed. The training on day 3 was the same as day two, except that the heat box was pre-warmed to 34^{o}C prior to the animals entering it. On day 4, the training procedure was as described for day 3 and then the tail cuff and transducer were positioned on the rats tail (Figure 2-10) whilst the rat was being mildly restrained within a towel. On the final day of training, the tail cuff apparatus was again positioned on the rat's tail following 10 minutes in the heat box and the cuff was inflated and deflated to allow the rat to acclimatise to the pressure of the tail cuff. At the end of each training day, rats were rewarded with a treat of 10 pumpkin seeds each.

2.4.4 Systolic BP Measurement Protocol

The tail cuff method was used to measure systolic blood pressure in WKY and SHRSP rats, three times a week for at least 2-3 weeks prior to the induction of experimental stroke. All BP measurement was performed in the afternoon between the hours of 2-3pm. BP measurement was not performed on a Monday afternoon, as the rats tended to be more stressed on this day and I discovered that their cages were cleaned out every Monday and this was likely to be the cause of their increased stress levels.

Rats were placed in the pre-warmed heat box with their cage-mates for 10-15 minutes and no longer than 20 minutes. Care was taken to regularly assess the temperature in the box by looking at the thermometer attached to the inner wall of the box. If the temperature was above 36^{o}C, then the front panel of the box was removed to aid heat loss. The front panel of the heat box also allowed the animals to be observed. The rats were deemed to be warm enough when there was very little spontaneous movement and the ears looked very pink.

At this stage the rat was removed from the box and swiftly wrapped in a towel with only the tail exposed. The rat was placed onto the heat mat to keep it warm and the tail cuff and the signal transducer were positioned on the tail (Figure 2-10). Once the rat was settled and was sitting on the heat mat, wrapped in the towel, with no need for restraint, then BP

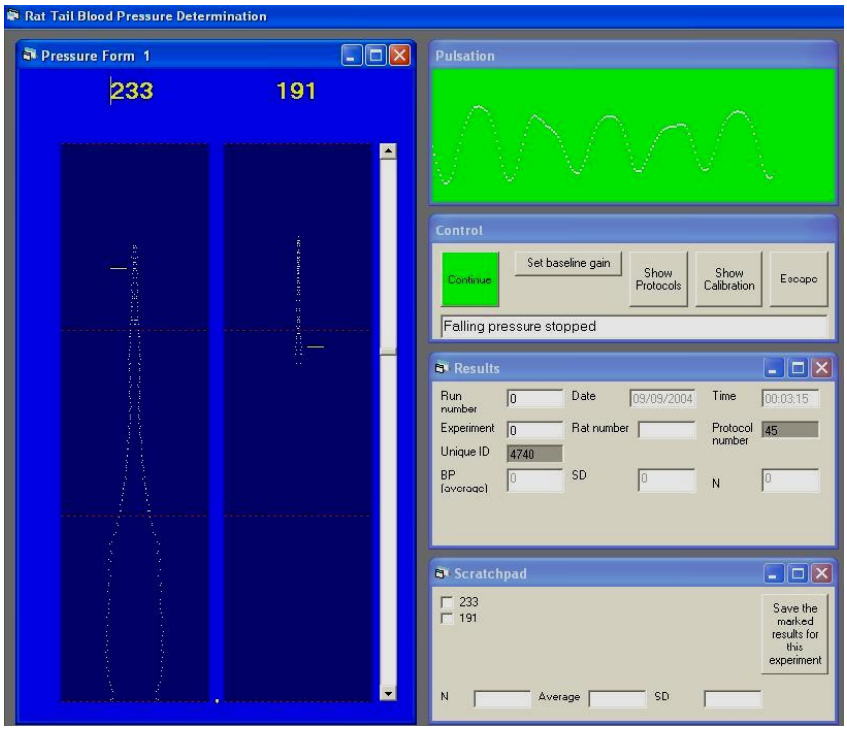

Figure 2-10. The tail cuff method of non-invasive blood pressure measurement. The top image illustrates the positioning of the tail cuff and the signal transducer on the tail of the rat, where the cuff is positioned at the base and the transducer is placed distal to the cuff. The bottom image shows the computer screen as displayed when blood pressure measurements are being recorded. The strength of the signal is shown in the green box in the top right hand corner of the display and the measurements are recorded in the box on the bottom right corner.

measurements were taken. The laptop was used to inflate and deflate the cuff in cycles to obtain measurements of systolic blood pressure. This was repeated until 8-10 consistent measurements of systolic blood pressure were acquired and the mean and standard deviation were then calculated. Only the most consistent measurements were used to calculate the mean systolic blood pressure for each animal. Measurements which were acquired when an animal was visibly stressed were excluded. After the tail cuff procedure, the rats were returned to their home cage and were rewarded with pumpkin seeds.

Chapter 3.

Establishing strain-specific MRI perfusion and diffusion thresholds in SHRSP and WKY rats

3.1 Introduction

MRI perfusion-diffusion mismatch is widely used to identify potentially salvageable penumbra in both clinical and pre-clinical research. Perfusion weighted imaging identifies tissue at risk of infarction, while diffusion weighted imaging identifies the core of ischaemic injury. The mismatch between the perfusion deficit on PWI and the region of abnormality on DWI provides an approximation of the ischaemic penumbra. Despite this technique being used for well over a decade, there is still no consensus on where to set perfusion and diffusion thresholds to accurately define the penumbra in both clinical and pre-clinical stroke research. This is particularly important where the presence of penumbra is used as a criterion for recruiting stroke patients into clinical trials. If the diffusion threshold is set too low then irreversibly injured tissue could be identified as being potentially salvageable and the penumbra will be overestimated. Conversely, if the diffusion threshold is set too high, then the ischaemic core will include a component of the penumbra, where tissue is hypoperfused but not yet experiencing bioenergetic failure. If the perfusion threshold is set too high, then the outer boundary of the penumbra will include benign oligaemic tissue which is not at risk of infarction, thereby overestimating the penumbra and if the threshold is set too low, then penumbra will be underestimated. This highlights the importance of defining perfusion and diffusion thresholds to accurately identify potentially salvageable tissue following stroke.

To date, there are no consistent thresholds in use in clinical (Bandera et al, 2006) or pre-clinical stroke research. In clinical research, thresholds of perfusion and diffusion abnormality have been calculated to identify the ischaemic penumbra and predict stroke outcome. In a retrospective study of 37 stroke patients, where DWI, PWI and MR angiography had been performed within 6 hours of stroke onset, an ADC threshold of 80% of contralateral hemispheric ADC was applied to identify the region of ischaemic injury (Thomalla et al, 2003). This group also performed perfusion imaging using contrast agent bolus tracking, where a gadolinium based contrast agent was administered into the patient's circulation intravenously. A time-intensity curve was constructed from the changes in signal intensity as the contrast agent passed through the circulation. The perfusion deficit was defined using the time to peak (TTP) of the contrast agent with a TTP delay of greater than 4 seconds compared to the contralateral hemisphere used to define hypoperfused tissue. These results are in agreement with earlier studies which reported that a TTP delay of between 4 and 6 seconds was the best predictor of hypoperfused tissue which would progress to infarction without reperfusion (Neumann-Haefelin et al, 1999).

However, this TTP delay threshold was later challenged by Sobesky et al (2005), who compared the ability of perfusion MR to identify the penumbra with PET and reported that a TTP delay threshold of 4-6 seconds grossly overestimated the PET defined penumbra. The greatest challenge when establishing perfusion deficit thresholds is to define the penumbra with the exclusion of benign oligaemic tissue to prevent overestimation of potentially salvageable tissue.

The perfusion deficit can also be defined by parameters other than TTP delay but there is no consensus on which perfusion parameter to use clinically to define the perfusion deficit. It has been reported that the volume of penumbra quantified by the mismatch technique can vary considerably depending on the perfusion parameter used to define hypoperfused tissue (Kane et al, 2007). In a study of 32 patients, these authors demonstrated that the proportion of those patients presenting with perfusion-diffusion mismatch varied from 9% to 72% using 10 different MRI methods to detect the perfusion deficit in each patient. The lack of a validated method to define the perfusion deficit will impact on patient management where the volume of potentially salvageable tissue is used to determine suitability for therapy. T_{max} is the measured TTP of the residual function and many groups use this parameter rather than TTP since it allows comparisons to be made across individual stroke patients. Shih and colleagues defined a T_{max} delay threshold of between 6 and 8 seconds as the most effective for the identification of tissue which would proceed to infarction without reperfusion by day 7 post stroke onset (Shih et al, 2003). However, Olivot et al (2009) defined the penumbra as hypoperfused tissue with a T_{max} delay of 4-6 seconds, in agreement with an earlier clinical study (Tawasaka et al, 2008). Therefore there still appears to be some uncertainty with regards to the perfusion thresholds used for the clinical identification of the ischaemic penumbra and regarding which parameter is the most appropriate measure of hypoperfused tissue. MRI based quantitative measures of perfusion are available, like arterial spin labelling, however, many clinical centres do not yet have the facilities available to use this technique.

In rodent stroke models, some groups have defined MRI perfusion and diffusion thresholds to define penumbra. Mancuso and colleagues (1995) assessed the relationship between the ADC derived lesion and cerebral blood flow, as measured by autoradiography. This group defined the ADC lesion as a 15% reduction when compared to the mean ADC value in the contralateral hemisphere. This threshold was selected by examining pre-ischaemic ADC maps and diffusion weighted images. Thirty minutes post-MCAO, the ADC-derived lesion correlated with a reduced CBF of $\leq$25ml/100g/min. In another group, where rats were

subjected to permanent MCAO, the ADC-derived lesion at 90 minutes correlated with CBF of 30-35ml/100g/min, demonstrating the temporal evolution of the ADC derived lesion to incorporate less severely hypoperfused tissue into the lesion as the ADC value of ischaemic tissue reduces further over time (Mancuso et al, 1995).

One study group in particular have worked extensively to establish thresholds of tissue viability in rat models of middle cerebral artery occlusion. Early studies by this group identified an absolute ADC threshold value of 0.55 x 10^{-3} mm^2/sec, when the ADC lesion at 2 hours post-MCAO most closely matched the TTC defined final infarct at 24 hours post-occlusion (Dardzinski et al, 1993). In later studies by this group (Shen et al, 2003; Meng et al, 2004) ADC and CBF thresholds were established by adjusting the respective thresholds until the ADC-derived and PWI-defined perfusion deficit at 3 hours post-MCAO were closely matched to the final infarct, defined at 24 hours post-MCAO by TTC processing of the brain. The absolute ADC threshold defined by this group was 0.53 ± 0.03 x 10^{-3} mm^2 /sec, which equates to a 30 ± 2% reduction in ADC compared to the mean ADC value of the contralateral hemisphere. The abnormal perfusion threshold was defined as 0.30 ± 0.09ml/g/min, which is a 57 ± 11% reduction in CBF, as compared with the mean contralateral hemisphere values. Therefore, pixels on ADC and CBF maps which fall below these thresholds defined the regions of ischaemic injury and hypoperfusion, respectively. These maps were then co-registered to define areas of perfusion-diffusion mismatch and therefore to identify the potentially salvageable penumbra. Later in the same year this group published another paper, using the same methods, to establish an absolute ADC threshold and a percent reduction ADC threshold relative to the mean ADC of the contralateral hemisphere (Kazemi et al, 2004). Optimum ADC thresholds were established as those which provided the best correlation between ADC- and TTC-derived lesion volume estimates. They defined the absolute ADC threshold value as 0.47 x 10^{-3} mm^2 /sec and the percent ADC reduction threshold at 33%, which is in agreement with their previous reports.

Li et al (2000) used a different approach to define ADC thresholds for the prediction of final infarct volume following permanent MCAO in the rat. They defined an ADC threshold specific to each time point post-MCAO. The threshold derived ADC lesions were correlated with the final infarct volume which was derived by TTC staining 24 hours post MCA occlusion. By 210 minutes following onset of ischaemia, the ADC lesion had fully evolved and at later time points the thresholds were unchanged. The authors state that defining a range of thresholds at various time points will allow prediction of the final

infarct volume as little as 25 minutes post-ischaemia and enables early prediction of stroke outcome. At early time points, the ADC derived lesion will include both injured tissue and penumbra. As the ADC values further decrease, the penumbra will become incorporated into the final infarct.

Other methods used to define perfusion and diffusion thresholds in rat models of focal cerebral ischaemia include using the empirical rule of mean ± 2SD from baseline ADC and CBF values of the ipsilateral hemisphere (Foley et al, 2010). In addition, ADC lesion area has been defined as the area in which ADC values decreased below a threshold value of 2 standard deviations from mean contralateral ADC values (Hoehn-Berlage et al, 1995). Hoehn-Berlage and colleagues reported that when reductions in ADC were matched to the corresponding areas of ATP depletion determined by bioluminescence imaging, the area of energetic failure corresponded to a 23% reduction in ADC. Both Hoehn-Berlage et al (1995) and Kohno et al (1995) reported a 70% reduction in CBF was associated with ATP depletion and progression to infarction. Foley et al (2010) also defined the perfusion deficit using a CBF threshold of 70% reduction from baseline ipsilateral CBF using voxel analysis.

To date, perfusion and diffusion thresholds have only been established in normotensive rat strains. Differences in lesion evolution between strains following experimental stroke may mean that thresholds defined in one rat strain may not be applicable to other rat strains, particularly those with genetic stroke risk factors, like the spontaneously hypertensive stroke-prone rat (SHRSP). Bardutzky et al (2005) demonstrated differences in the evolution of the ADC-derived lesion in Sprague-Dawley and Wistar Kyoto rats (WKY), the normotensive control strain from which SHR and SHRSP were derived. Following permanent MCAO induced by intraluminal filament, the ADC-derived lesion rapidly evolves over the first 3 hours and has fully evolved by the 3 hour time point in Sprague-Dawley rats. However, at 3 hours post-MCAO in Wistar Kyoto rats, the ADC lesion is still evolving. It may therefore be inappropriate to use the same ADC and CBF thresholds for both strains if the ADC lesion is continuing to evolve beyond the 3 hour time point in Wistar Kyoto rats. Therefore it is of utmost importance that thresholds of perfusion and diffusion abnormality are established for each strain used in experimental stroke, particularly since the evolution of the ischaemic lesion can vary between strains. Furthermore, each laboratory should aim to establish their own in-house thresholds for each strain of rat and each model used to induce focal cerebral ischaemia. This will serve to reduce the influence of additional variables, such as strain and stroke model differences,

and surgical technique, on the results obtained by using thresholds defined by other study groups. Inter-strain thresholds would allow accurate identification of the penumbra and prediction of final infarct regardless of the rat strain used. Furthermore, when assessing the efficacy of potential stroke therapies, one must be confident that the thresholds of abnormality are accurate to allow cross strain tissue salvage to be evaluated. This is becoming increasingly important since in order to demonstrate therapeutic efficacy, potential treatments should be assessed using a range of experimental stroke models with and without stroke co-morbidities before being translated to clinical trial. Unfortunately this has not been commonplace and may have contributed to the poor outcomes of neuroprotective drugs in clinical trials (O'Collins et al, 2006; Crossley et al, 2008; Howells et al, 2010).

Study Aims

The aims of this study were to define strain-specific MRI perfusion and diffusion thresholds in the SHRSP and WKY rat. These thresholds would then be applied to quantitative perfusion and diffusion data acquired in the acute phase following experimental stroke to allow the temporal evolution of ischaemic injury and perfusion deficit to be assessed and compared between the strains.

3.2 Methods

3.2.1 Animal Preparation and Surgical Procedures

SHRSP and WKY rats aged 8-10 weeks of age, were obtained from inbred colonies within the Institute of Cardiovascular and Medical Sciences within the University of Glasgow. From 11 weeks of age until surgery, systolic blood pressure was measured and recorded 3 times weekly as previously described (Chapter 2.4.4). The mean systolic blood pressure for each rat was calculated and the data were compiled to compare the mean systolic blood pressure of each strain.

From this group of animals, age-matched (16-20 weeks) male WKY (n=13) and SHRSP (n=16) weighing 250-350g, were anaesthetised, intubated and artificially ventilated (Chapter 2.1.1). The ventral surface of the right and left hindlimbs, the chest and the neck were shaved using an electric shaver. All rats were then given an intraperitoneal injection of 0.4ml of atropine sulphate (600µg/ml, Martindale Pharmaceuticals, UK) which is an anti-muscarinic drug used to prevent bronchial secretions building up in the airways for the

duration of the experiment. The right femoral artery was cannulated to allow continuous monitoring of heart rate and MABP (Biopac) with regular blood sampling every hour to ensure blood pH, $PaCO_2$ and PaO_2 (Bayer, Rapidlab 248) were maintained within the physiological range. Body temperature was assessed by a rectal thermocouple and maintained at 37±0.5ºC.

Permanent focal cerebral ischaemia was then induced as previously described (Chapter 2.1.2), where a silicon tipped filament was advanced along the internal carotid artery to block the origin of the middle cerebral artery. The filament was secured in place by electrocoagulation of the incision site located within the external carotid artery stump, using diathermy forceps. The neck was stitched using a 4-0 silk suture. Electrode gel (Sigma) was applied onto the shaved area of the left hindlimb and the right and left sides of the chest to allow placement of ECG leads. The rat was then disconnected from the ventilator and was immediately transferred to the MRI cradle where the intubation tube was reconnected to a ventilator to maintain anaesthesia.

3.2.2 MRI Scanning Protocol

The rat was secured within the cradle by tooth and ear bars, to restrict head movement, and was then transferred to the MRI scanner where a 4-channel phased array surface receiver coil was placed on the head. Body temperature was maintained during the MRI scanning procedure by a closed circuit thermal jacket and was monitored by a rectal thermocouple.

Once a pilot sequence had been obtained to ensure correct geometry, a 4-shot spin-echo echo planar imaging (EPI) DWI scan (TE=22.5ms, TR=4000.3ms, matrix=96x96, FOV=25x25mm, 3 directions=x, y, z, B-values=0 and 1000s/mm^2, 8 coronal slices; 1.5mm thick) was performed at 30 minutes post-MCAO to allow generation of quantitative ADC maps for assessment of ischaemically injured tissue. DWI scans were then repeated on the hour from 1 to 4 hours post-MCAO.

Non-invasive quantitative cerebral blood flow (CBF) measurements were carried out on 6 coronal slices within the MCA territory (slices 2-7 of the DWI scan) using a form of continuous arterial spin labelling (cASL) based on a train of adiabatic inversion pulses (Moffatt et al, 2005). The sequence employs a spin-echo EPI imaging module (TE=20ms, TR=7000ms, matrix=96x96, FOV=25x25mm, slice thickness 1.5mm, 16 averages, 4 shots)

preceded by 50 hyperbolic secant inversion pulses in a 3 second train. Inversion pulse frequency offset and gradient strength were set to provide 10mm wide label/control bands centred at ±30mm from the centre of the imaging slice. For quantification of CBF maps, T_1 maps were also acquired, using an EPI inversion recovery sequence (TE=20ms, TR=10000ms, matrix=96x96, FOV=25x25mm, slice thickness 1.5mm, 16 averages, 4 shots, using 16 inversion times from 200ms to 7700ms). CBF maps and T_1 maps were acquired every hour for 4 hours post-MCAO.

DWI scans across 8 coronal slices were acquired within 2 minutes. The ASL scans for each coronal slice took 7 minutes to acquire. Therefore, within each hour, ASL scans could only be acquired to match slices 2-7 of the DWI scan.

3.2.3 Animal Recovery

At the end of the 4 hour data acquisition session, the rat was removed from the MRI scanner within the cradle. When the rectal thermocouple, the thermal jacket, ECG leads and the ear bars were removed, the rat was disconnected from the ventilator and immediately transferred back into the operating theatre where it was reconnected to the ventilator to maintain anaesthesia. The dose of isoflurane was reduced to 1% to aid the speed of recovery when anaesthesia was withdrawn. The suture of the right hindlimb was cut and the tissue was pulled back to reveal the femoral artery. The ligatures were cut and the cannula was removed. The vessel was sealed by electrocoagulation using diathermy probes. The hindlimb wound was then re-sutured. At this point, the isoflurane and nitrous oxide were turned off and the rat was allowed to breathe 100% oxygen for a period of 15-20 minutes to aid recovery from anaesthesia. When the rat had been breathing against the ventilator for around 5 minutes, the intubation tube was disconnected from the ventilator. If the rat continued to breathe unassisted for another 5 minutes then the intubation tube was carefully removed. However, if the animal's breathing was inconsistent, then the intubation tube was reconnected to the ventilator until it could breathe unaided. Once the rat was recovering from the effects of anaesthesia and was attempting to move, it was transferred to a recovery cage. The cage was lined with absorbent pads instead of sawdust, which may irritate the wounds of the rat. Bedding and a cardboard tube were also placed in the cage to enrich the rat's environment with free access to water and soft diet. The soft diet consisted of rat chow pellets with had been softened with warm water and mixed with egg custard and rice baby food (Heinz). All animals were individually housed following surgery and their general condition was assessed at least 4 times throughout the working day and was recorded.

At 24 hours following surgery, animals were re-anaesthetised and transferred to the MRI scanner where anaesthesia was maintained via a face mask (2% isoflurane in 70/30 $N_20/0_2$ mixture) and a RARE T_2 weighted sequence was acquired to allow calculation of final infarct volume (Chapter 2.2.3). Animals were then sacrificed by perfusion-fixation (Chapter 2.1.3).

3.2.4 MRI Data Analysis

Quantitative ADC maps, in units of square millimetres per second, were generated in Paravision 5 software and subsequently processed using Image J software to produce an ADC map for each of the 8 coronal slices. Quantitative CBF maps (ml/100g/min) for each of 6 coronal slices were generated at each time point using the following equation (Williams et al, 1992):

$$CBF = \frac{\lambda}{T_1} \frac{(S^{control} - S^{label})}{2\alpha S^{control}}$$

where α is the inversion pulse efficiency (0.8), λ is the blood tissue partition function (assumed to be 0.9). $S^{control}$ and S^{label} are the signal intensity from the control and labelled images, acquired with inversion pulses applied above the head and in the neck, respectively.

The labelled ASL image was subtracted from the control image and the resulting image was then divided by the control image to produce a relative CBF map. The relative CBF map was then divided by the T_1 map of the same coronal slice to produce a quantitative CBF map in units of millilitres per 100g of tissue per min (ml/100g/min).

Final infarct at 24 hours post-stroke was defined and calculated as previously described (Chapter 2.2.3).The hyperintense area was manually delineated on the T_2 slices which anatomically corresponded to the 6 ADC (slices 2-7) and CBF slice maps and multiplied by the slice thickness. The final infarct volume was then corrected for brain swelling and compression of the contralateral hemisphere. Final infarct was also expressed as a percentage of the ipsilateral hemisphere (%HLV) to correct for any differences in brain

volume between the strains (Gerriets et al 2004). The following equation was used to define the %HLV and correct for oedema (Gerriets et al, 2004):

$$\%HLV = \frac{\text{contralateral hemisphere} - \text{ipsilateral hemisphere} + \text{lesion volume}}{\text{contralateral hemisphere}} \times 100$$

The absolute ADC threshold for each rat was determined by applying a range of increasing threshold values to the quantitative ADC maps acquired at 4 hours post-MCAO to generate ADC-derived lesion volume across the 6 coronal slices. This was achieved by manually delineating the ipsilateral and contralateral hemispheres on each coronal slice and using the histogram function within Image J to count the number of pixels within a given range for both hemispheres on each slice (0-2 x 10^{-3} mm^2/sec for ADC). These data were exported to Excel where the ADC threshold was adjusted to count the number of pixels below each threshold. The total number of pixels across the 6 slices was converted to an area by multiplying the number of pixels by the area of a pixel (0.0678mm^2) and lesion volume was calculated by multiplying the total area by slice thickness (1.5mm). The threshold value which generated a lesion volume which was equal to the oedema-corrected T_2 derived final infarct volume across the same anatomically matched coronal slices was identified as the specific ADC threshold for each rat. The same technique was used to define the absolute CBF threshold for each rat, where Image J was used to count the number of pixels within the range of -100-400ml/100g/min. Negative perfusion values were generated in some pixels with low or zero flow as a consequence of subtracting the magnitude images ($S^{control}$, S^{Label}), where the signal difference was comparable to image noise (Karlsen et al, 1999). These negative ASL-derived CBF values were assumed to represent zero flow.

In Excel, the CBF threshold was adjusted until the volume of the threshold defined perfusion deficit on the 4 hour quantitative CBF maps across 6 coronal slices, matched the volume of the corrected final infarct (Figure 3-1). The 4 hour post-MCAO time point was used to match the ADC and CBF lesion volumes with the 24 hour final infarct volume as previous studies have shown that the DWI defined ischaemic core has

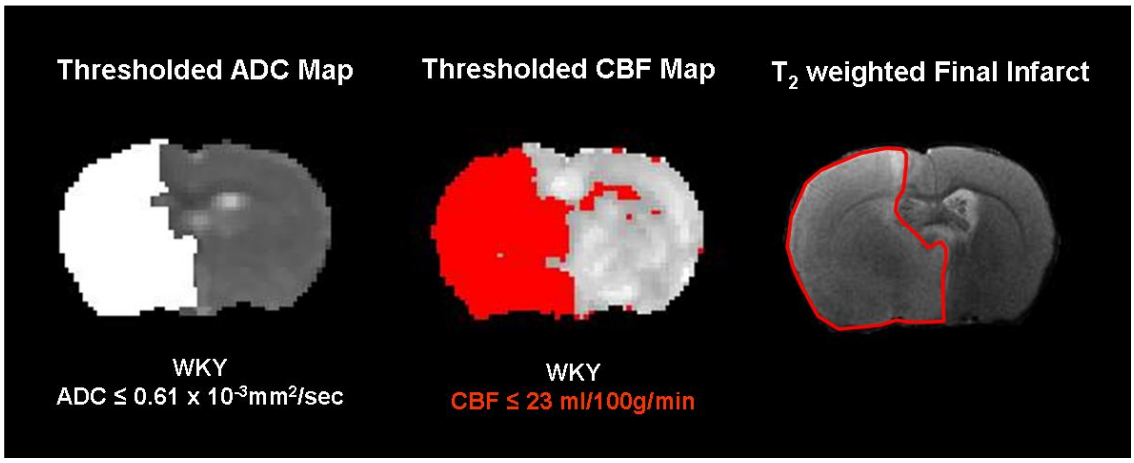

Figure 3-1. ADC and CBF thresholds adjusted to match the volume of ischaemic injury and perfusion deficit with the T_2 defined final infarct at 24 hours post-MCAO. The data presented are from a representative WKY rat and show the ADC and CBF thresholds applied to quantitative ADC and CBF maps of a coronal slice acquired at 4 hours post-MCAO. The ADC threshold defines ischaemic injury (shown in white) and the CBF threshold defines the perfusion deficit (shown in red). The T_2 defined infarct is delineated in red outline.

fully evolved by 3 hours post-MCAO and correlates well with final infarct at 24 hours post-MCAO (Reith et al, 1995; Li et al, 2000). Therefore, in the present study, we assumed that by 4 hours post-MCAO there is no further lesion expansion. The individual ADC and CBF thresholds for each rat were compiled to generate mean thresholds for WKY and SHRSP. The mean ADC and CBF thresholds for each strain were then applied retrospectively to the quantitative ADC and CBF maps acquired at each time point to calculate ADC-derived lesion and PWI perfusion deficit volumes at each time point over the first 4 hours following stroke.

Quantitative ADC and CBF values of the contralateral hemisphere were also determined in each rat from 1-4 hours post-MCAO using Image J. Using quantitative ADC and CBF maps at each time point, the ADC and CBF values of each pixel across the contralateral hemisphere of the 6 coronal slices were summed and divided by the total number of pixels. This generated a mean ADC or CBF value for the contralateral hemisphere for each rat from 1-4 hours post-MCAO. Pixels located in the ventricles of the contralateral hemisphere were excluded from the calculation to prevent their influence on mean ADC and CBF values, since the slow flow of CSF throughout the ventricular system results in high ADC and low CBF values which are not representative of the parenchyma. The ADC and CBF thresholds for each rat were then expressed as the percentage reduction from

contralateral ADC and CBF respectively, at 4 hours post-MCAO. The relative ADC and CBF thresholds for each rat were then compiled to generate mean relative ADC and CBF thresholds for each strain.

In addition, total brain volume was determined in each rat from 1-4 hours post-MCAO using Image J software. The area of the ipsilateral and contralateral hemisphere on each of the 6 coronal slices was manually delineated to determine the volume of the ipsilateral and contralateral hemispheres. These volumes were added together to calculate total brain volume across the 6 slices.

3.2.5 Statistical Analysis

All statistical analyses were undertaken using GraphPad Prism software and all data are presented as mean ± SD. An unpaired t-test was used to assess potential strain differences in mean systolic blood pressure, final infarct volume, % HLV and threshold values. The temporal evolution of ischaemic injury, perfusion deficit, physiological parameters, hemispheric volume and contralateral CBF for each strain were assessed by Repeated Measures ANOVA, with Bonferroni's multiple comparisons post-test. Temporal comparisons between strains were assessed by 2-way ANOVA with Bonferroni's post-test. Level of statistical significance was set at $p<0.05$. All analyses were undertaken blind to rat strain. Each rat was given a numbered code which was only broken on the completion of all data analysis.

3.3 Results

3.3.1 Mortality and Excluded Animals

Two out of twelve WKY rats and five out of fifteen SHRSP rats died overnight before final infarct could be determined by T_2 weighted imaging at 24 hours post-MCAO. Examination of the brains of the rats which died revealed large infarcts with extensive brain swelling. Another SHRSP rat was sacrificed during the acute phase following stroke when DWI revealed that the animal had suffered a spontaneous stroke prior to middle cerebral artery occlusion. A WKY rat was also excluded as DWI showed a small subcortical lesion, indicating incomplete occlusion of the middle cerebral artery. This animal was then euthanased. Therefore, the ADC and CBF thresholds were generated from the animals

which successfully recovered until 24 hours post-MCAO and demonstrated complete occlusion of the middle cerebral artery, where both cortical and subcortical injury was evident (WKY: n=10, SHRSP: n=10). However, the calculated thresholds were applied retrospectively to all rats to determine the acute evolution of ischaemic injury and perfusion deficit (WKY: n=12, SHRSP: n=15).

3.3.2 Systolic BP and Physiological Parameters

All SHRSP rats were severely hypertensive compared to the normotensive control strain WKY in the weeks prior to the induction of experimental stroke. Mean systolic blood pressure was significantly higher in SHRSP (183±12mmHg, n=15) than WKY (133±9mmHg, n=12, $P<0.0001$) (Figure 3-2). All of the WKY rats used in the present study were normotensive and mean systolic pressure recorded for each rat ranged from 117mmHg to 147mmHg. All of the SHRSP rats in the present study demonstrated severe hypertension, with mean systolic blood pressure ranging from 165mmHg to 202mmHg.

Throughout the duration of surgical procedures and the 4 hour MRI scanning period, all physiological parameters were maintained within physiological range in both WKY and SHRSP ($P>0.05$, Table 3-1). All parameters were comparable between the strains during the entire experimental procedure ($P>0.05$), with the exception of mean arterial blood pressure and arterial PO_2, which were significantly higher in the hypertensive strain at all time points ($P<0.05$). It is unknown why arterial PO_2 was higher in SHRSP as the same anaesthetic regime and ventilation parameters were used for all rats in the study and were adjusted as necessary. In WKY rats, MABP ranged from 85±5mmHg to 93±7mmHg and in SHRSP rats MABP ranged from 105±10mmHg to 109±10mmHg, illustrating that arterial blood pressure was kept within a narrow range throughout the experimental procedure.

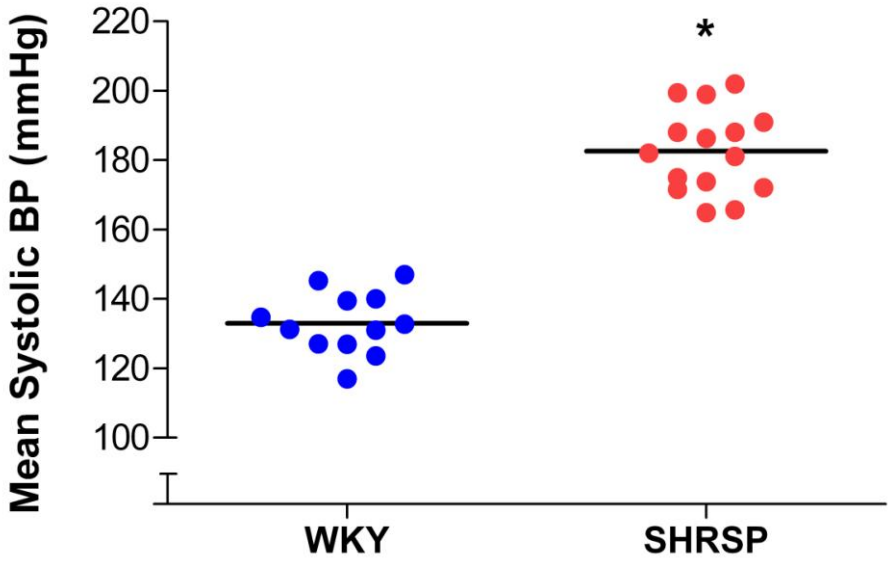

Figure 3-2. Mean systolic blood pressure of WKY and SHRSP rats. Mean systolic blood pressure was measured in WKY (n=12) and SHRSP (n=15) rats using the non-invasive tail cuff method. Mean systolic blood pressure was measured at least 3 times weekly prior to experimental stroke. The data presented show the mean systolic blood pressure of each rat as measured over the 3 weeks prior to stroke surgery. *p<0.0001, unpaired t test.

Physiological Parameter	*Baseline*	*1 hour*	*4 hours*
WKY			
Body Temp (^{o}C)	36.9±0.4	37.0±0.5	37.0±0.3
MABP (mmHg)	85±5	92±7	89±7
Heart Rate (bpm)	342±23	351±25	358±19
Blood pH	7.42±0.04	7.35±0.04	7.37±0.03
PaO_2 (mmHg)	119±18	119±23	124±19
$PaCO_2$ (mmHg)	39±6	44±5	41±6
SHRSP			
Body Temp (^{o}C)	36.8±0.4	37.1±0.3	37.0±0.4
MABP (mmHg)	109±10	106±9	107±10
Heart Rate (bpm)	348±28	358±33	359±20
Blood pH	7.43±0.06	7.40±0.04	7.41±0.03
PaO_2 (mmHg)	147±27	158±31	148±24
$PaCO_2$ (mmHg)	39±4	41±7	38±3

Table 3-1. Physiological parameters of anaesthetised WKY (n=12) and SHRSP (n=15) measured prior to permanent middle cerebral artery occlusion (baseline) and 1 and 4 hours following surgery.

3.3.3 Brain and Final Infarct Volume

Brain volume, across the 6 coronal slices, was smaller in SHRSP compared to WKY but the difference in brain volume between strains was not statistically significant at any time point from 30 minutes to 4 hours post-MCAO (P>0.05). There was also no evidence of brain swelling in the acute phase in either strain, as brain volume did not change significantly over the 4 hour time course. In WKY, brain volume was stable from 30 minutes (1115±55mm^3) to 4 hours post-MCAO (1115±54mm^3, P=0.56). Similarly in SHRSP, brain volume was also unchanged from 30 minutes (1063±30mm^3) to 4 hours post-MCAO (1060±33mm^3, P=0.17). The volume of the ipsilateral hemisphere was unchanged from 30 minutes to 4 hours post-MCAO in both WKY and SHRSP (P>0.05). In WKY, the volume of the ipsilateral hemisphere was relatively stable from 30 minutes (560±28mm^3) to 4 hours post-MCAO (564±29mm^3, P>0.05). Similarly, in SHRSP, the volume of the ipsilateral hemisphere was maintained from 30 minutes (543±16mm^3) to 4 hours post-MCAO (547±15mm^3, P>0.05).

SHRSP demonstrated a significantly larger infarct volume at 24 hours post-MCAO than WKY (387±55mm^3 vs 303±59mm^3, P=0.004, infarct volume of SHRSP and WKY, respectively, Figure 3-3A). Expressed as a percentage of the ipsilateral hemisphere, in SHRSP, 72±9% of the ipsilateral hemisphere was infarcted, compared to 53±10% in WKY rats (P=0.0002, Figure 3-3B). Difference in infarct volume between strains was particularly evident in the more caudal brain slices, where the infarct area was substantially larger in SHRSP compared to WKY (Figure 3-4). In SHRSP, the infarct extended further in the rostral and caudal planes than demonstrated in WKY. Substantial swelling of the ipsilateral hemisphere was evident in both strains by 24 hours post-MCAO in addition to compression of the contralateral hemisphere. Ipsilateral swelling and contralateral compression were observed to a greater degree in the hypertensive strain (Figure 3-4).

3.3.4 Strain Specific Perfusion and Diffusion Thresholds

The mean ADC value of the whole contralateral hemisphere across the 6 coronal slices was not significantly different between the strains and did not change significantly over the 4 hour time course. In WKY, mean contralateral ADC was 0.76±0.02 x 10^{-3} mm^2/sec at 1 hour post-MCAO and was not significantly different at 4 hours (0.77±0.01 x 10^{-3} mm^2/sec, P>0.05). Similarly, in SHRSP, mean contralateral ADC was maintained at 0.76±0.01 x 10^{-3} mm^2/sec from 1-4 hours post-MCAO.

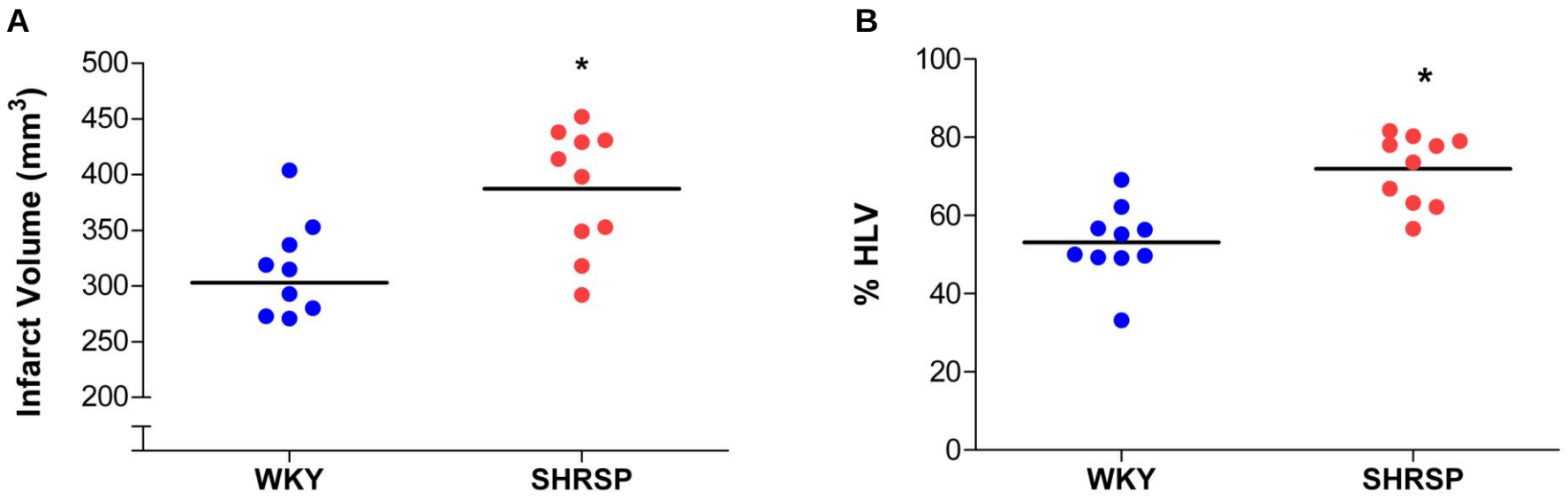

Figure 3-3. Final infarct in SHRSP and WKY rats at 24h following permanent occlusion of the middle cerebral artery. Final infarct was expressed as a volume (A) and as a percentage of the ipsilateral hemisphere (B). Both methods were corrected for swelling of the ipsilateral hemisphere and compression of the contralateral hemisphere. Horizontal line denotes the mean. *P<0.01, unpaired t tests. WKY; n=10, SHRSP; n=10.

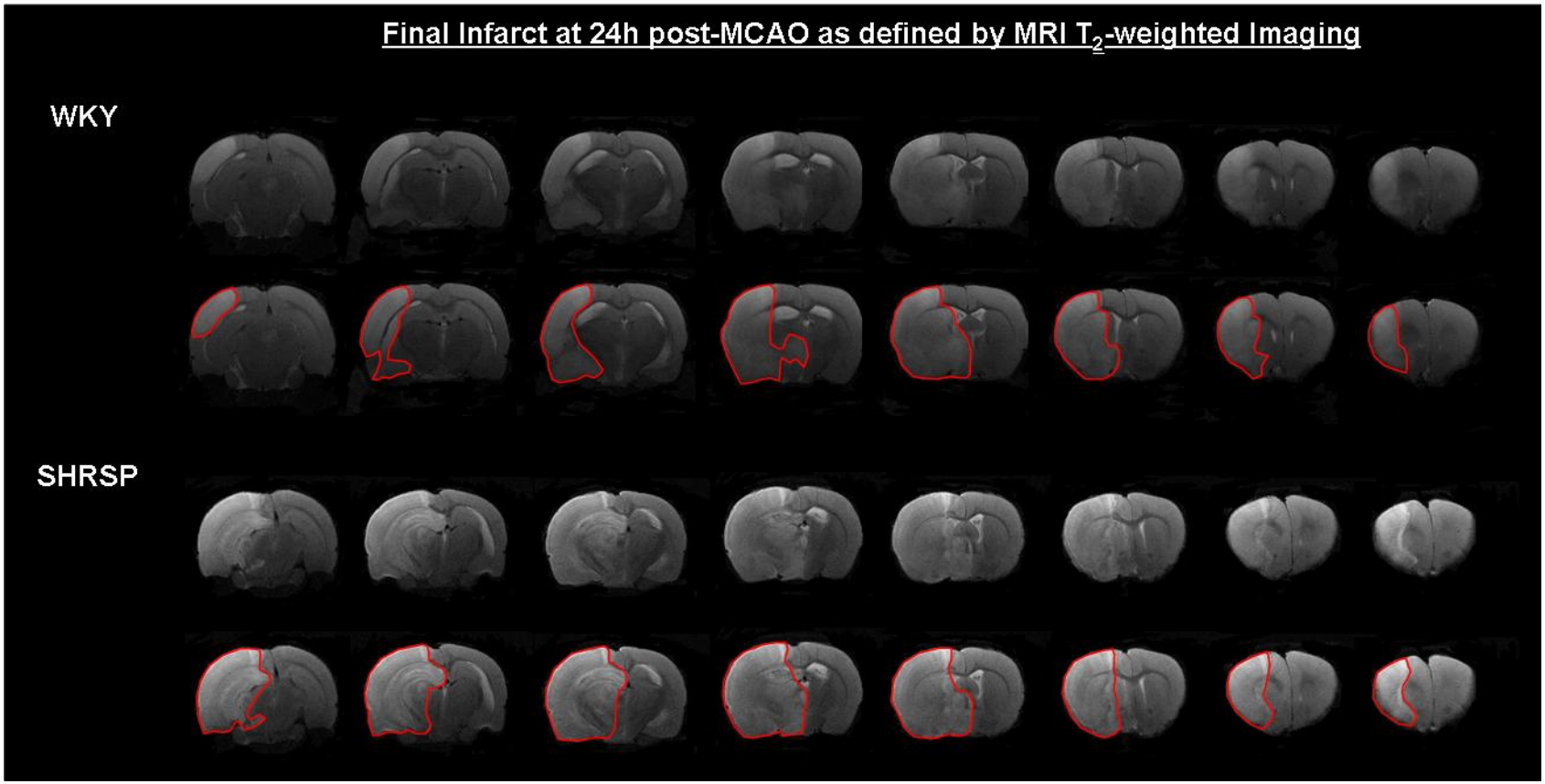

Figure 3-4. The spatial distribution of infarct area at 24h post-stroke in SHRSP and WKY rats following permanent MCAO. Representative MRI T_2-weighted images are shown for each strain to illustrate the spatial distribution of the infarct at 24h post-MCAO. The 8 coronal slices shown are representative of the rostro-caudal extent of the territory supplied by the MCA which was examined using T_2-weighted imaging. The infarct area was determined by manually delineating the hyperintense area on each of 16 coronal T_2 slices. Infarct volume was determined across the T_2 slices which anatomically matched the 6 coronal slices used to calculate the ADC-derived lesion and the CBF-defined perfusion deficit. Eight of the sixteen slices are shown, with and without the infarct outlined in red.

The absolute ADC threshold for WKY, determined from final infarct volume, was 0.61±0.03 x 10^{-3} mm^2/sec, representing a 21±4% reduction from mean contralateral ADC at 4 hours post-MCAO. The calculated ADC threshold for the hypertensive strain was 0.59±0.03 x 10^{-3} mm^2/sec, which represents a 23±4% reduction from the mean contralateral ADC value. Both the absolute and the % reduction ADC thresholds were comparable between the strains (P>0.05, Figure 3-5A).

Mean contralateral CBF was not significantly different between WKY and SHRSP and did not change significantly over the 4 hour time course in either strain. In WKY, mean contralateral CBF remained relatively stable from 135±23ml/100g/min at 1 hour post-MCAO to 124±21ml/100g/min at 4 hours (P=0.1). In SHRSP, mean contralateral CBF was unchanged from 1-4 hours post-MCAO (113±22ml/100g/min and 116±13ml/100g/min at 1 hour and 4 hours post-MCAO, respectively, P=0.6).
The mean CBF threshold determined from final infarct volume in WKY rats was 23±8 ml/100g/min, which was an 81±7% reduction in flow from the 4 hour contralateral CBF value. The calculated CBF threshold for SHRSP was 36±13 ml/100g/min, representing a 70±9% reduction from 4 hour contralateral CBF. Both the absolute and % reduction CBF thresholds were significantly higher for SHRSP than WKY (P<0.05, Figure 3-5B).

3.3.5 Acute Evolution of Ischaemic Injury

The mean absolute ADC thresholds were applied to the 30 minutes-4 hour ADC maps to assess the acute evolution of ischaemic injury in WKY and SHRSP. The thresholded ADC maps at 4 hours post-MCAO matched well spatially with the 24 hours T_2 infarct in both strains. The area of ischaemic injury identified by application of the strain specific ADC threshold was comparable to the hypointense areas on ADC maps across the 6 coronal brain slices being examined. Similarly, the threshold defined areas of injured tissue matched well with the hyperintense infarct area on T_2 slices (Figure 3-6).

At all time points following MCAO, ADC-derived lesion volume was significantly larger in SHRSP than WKY and this was evident from as early as 30 minutes post-MCAO (WKY; 203±70mm^3, SHRSP; 336±63mm^3, P<0.001). The ADC-derived lesion volume increased significantly over the 4 hour time course in both strains (P<0.001, Figure 3-7). In SHRSP, ADC-derived ischaemic injury increased from 336±63mm^3 at 30 minutes, to 410±56mm^3 at 4 hours post-MCAO. In WKY, the ADC-derived lesion evolved from 203±70mm^3 at 30 minutes following stroke, to 311±57mm^3 at 3 hours, at which point the lesion volume reaches a plateau. This suggests that using this model of stroke, the

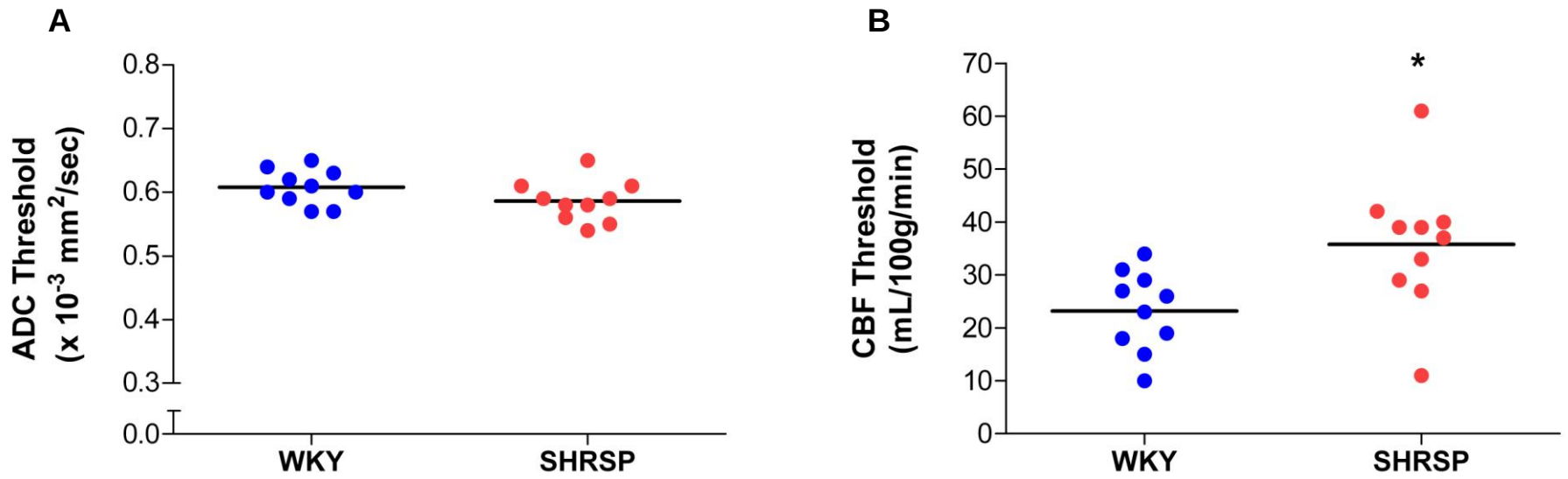

Figure 3-5. Strain-specific MRI diffusion (A) and perfusion thresholds (B) calculated in WKY and SHRSP rats following permanent MCAO. Thresholds were calculated by adjusting the diffusion and perfusion thresholds on quantitative ADC and CBF maps until the volume of the ADC-derived lesion and the perfusion deficit at 4h post-MCAO matched the volume of the T_2 defined final infarct at 24h. *$p<0.05$, unpaired t test.

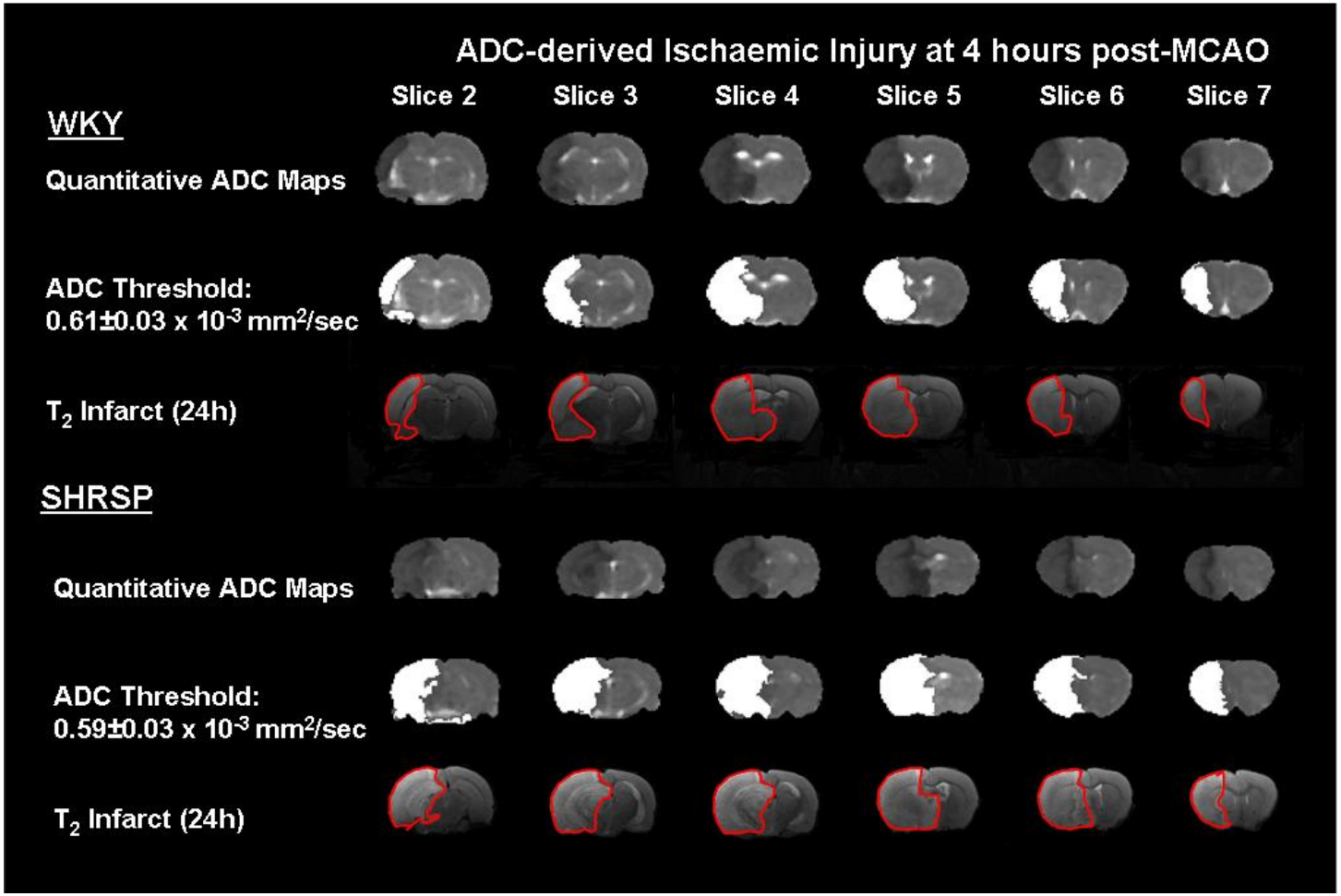

Figure 3-6. Ischaemic injured tissue at 4 hours post-MCAO as determined by strain-specific diffusion thresholds. ADC thresholds were adjusted until the ADC-derived lesion matched the volume of the corrected final infarct, defined by manually delineating the hyperintense areas on T_2 weighted images at 24h post-MCAO (shown in red). The data shown are from a representative SHRSP and WKY rat.

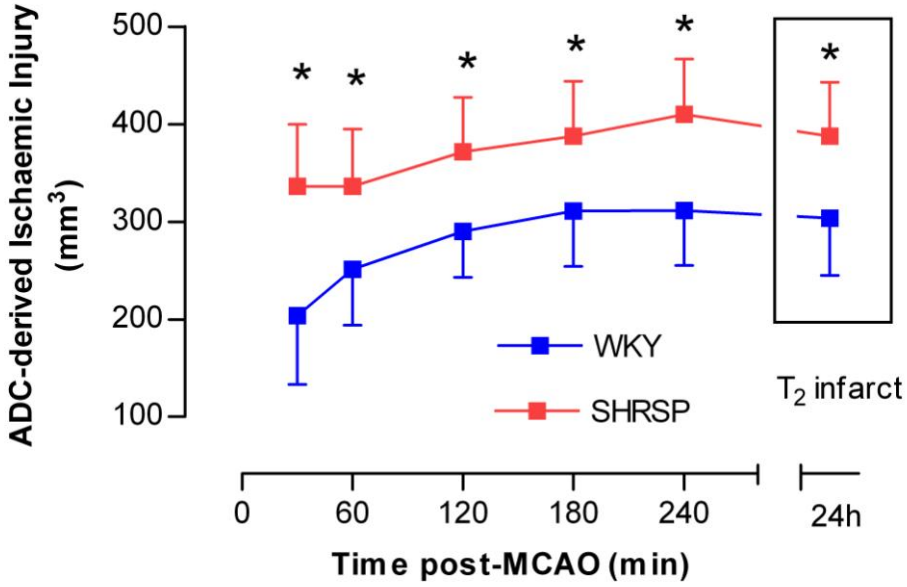

Figure 3-7. The acute evolution of ischaemic injury in SHRSP (n=15) and WKY (n=12) following permanent MCAO. Strain-specific ADC thresholds were applied to quantitative ADC maps acquired from 30min to 4h post-MCAO to determine the temporal evolution of ischaemic injury. *p<0.01, 2-way ANOVA with Bonferroni's post-test.

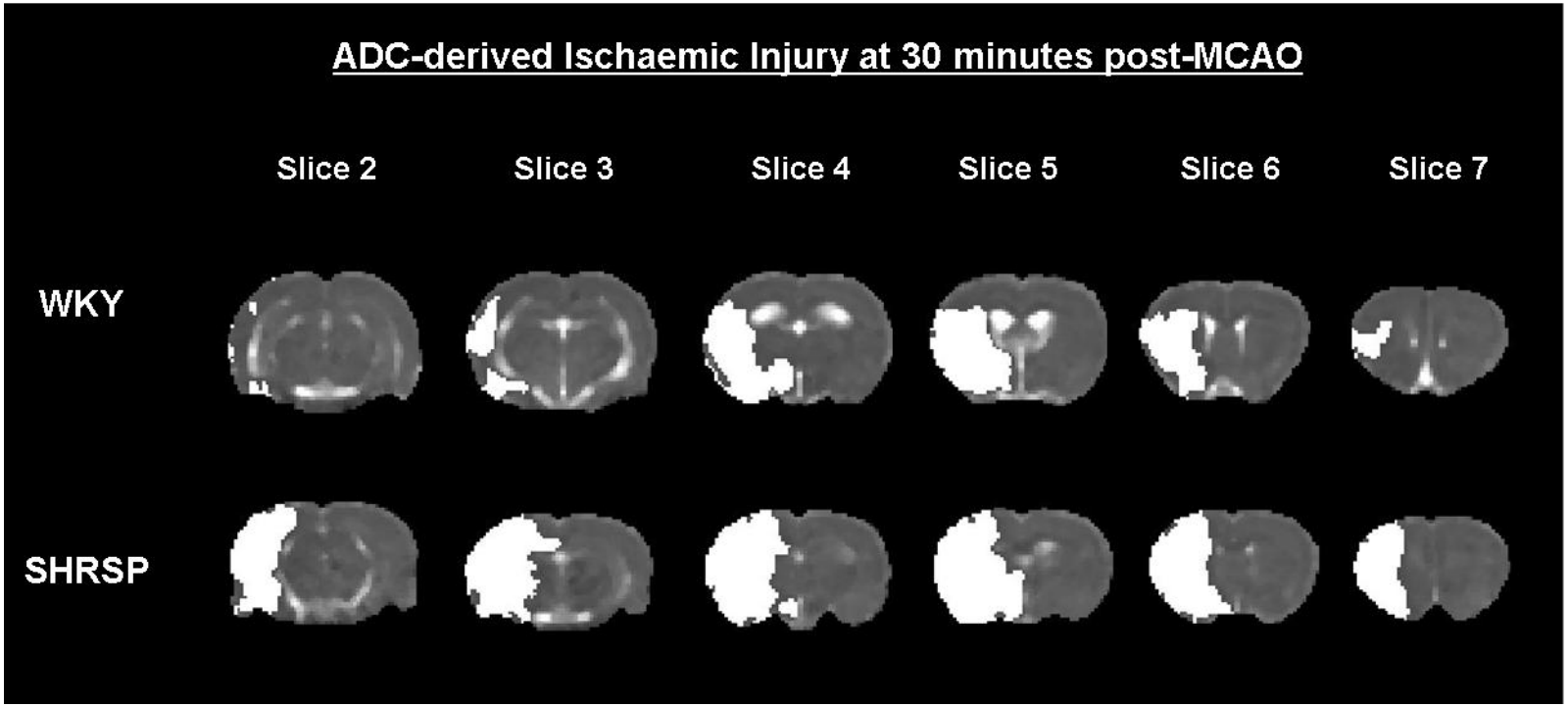

Figure 3-8. ADC-derived ischaemic injury in SHRSP and WKY rats at 30 minutes following permanent MCAO. Strain-specific ADC thresholds were applied to quantitative ADC maps acquired at 30 minutes post-MCAO to assess the spatial distribution of ischaemic injury between strains. The area of ischaemic injury is depicted by white shading on 6 coronal brain slices within the territory of the middle cerebral artery. The data presented are from a representative SHRSP and WKY rat.

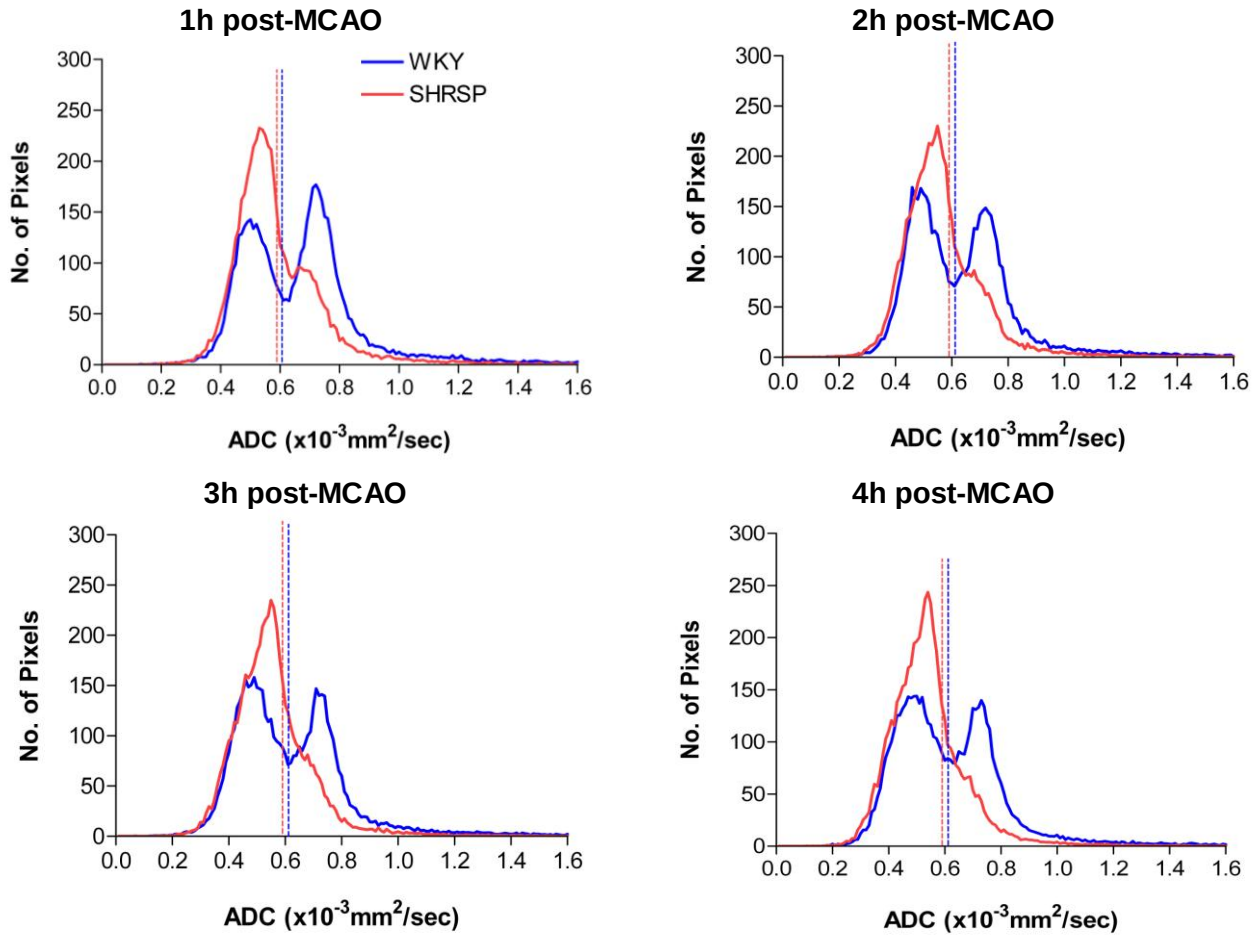

Figure 3-9. ADC profiles of the ipsilateral hemisphere in SHRSP and WKY rats from 1-4h post-MCAO. The graphs show the mean number of pixels with a particular ADC value from 0-1.6 x 10^{-3} mm^2/sec. The calculated ADC threshold for each strain is shown by the dotted line, where the SHRSP ADC threshold is shown in red (0.59 x 10^{-3} mm^2/sec) and the WKY ADC threshold is shown by the blue dotted line (0.61 x 10^{-3} mm^2/sec). The data presented show the mean data for each strain.

evolution of ischaemic injury is complete by 3 hours following MCAO in the WKY. The observed greater area of ischaemic injury in SHRSP is particularly evident in the most caudal coronal brain slices, especially in slices 2 and 3 (Figure 3-8).

These results are also illustrated by the pixel analysis of ADC maps of the entire ipsilateral hemisphere of WKY and SHRSP, where the hypertensive strain had a greater proportion of pixels with low ADC values. In both strains, the number of pixels which fall below the strain-specific ADC threshold increases over time as the ischaemic core expands. The ipsilateral ADC profile of WKY has a biphasic shape which allows clear distinction between injured and normal tissue. However, this biphasic profile is only evident in the SHRSP at 1 h post-MCAO and at later time points the biphasic shape is lost as most of the hemisphere becomes incorporated into the core of ischaemic injury (Figure 3-9). These ADC profiles demonstrate that ischaemic injury is greater in SHRSP compared to WKY, irrespective of the application of a ADC threshold to quantify the ADC-derived lesion volume.

3.3.6 Acute Evolution of Perfusion Deficit

The mean absolute CBF thresholds were applied to the quantitative CBF maps acquired from 1-4 hours post-MCAO to determine the acute evolution of the perfusion deficit for each strain. There was also good spatial matching between the thresholded 4 hour CBF maps and the 24 hour T_2 final infarct, where the threshold defined hypoperfused area on 6 coronal slices matched well with the hyperintense area on corresponding T_2 slices (Figure 3-10).

At all time points following stroke, the perfusion deficit was significantly greater in SHRSP than WKY ($P<0.001$, Figure 3-11). At 1 hour following stroke, a perfusion deficit of $368\pm45mm^3$ was observed in SHRSP, compared to $273\pm69mm^3$ in WKY rats (Figure 3-12). The greater perfusion deficit observed in the SHRSP was particularly evident on the caudal slices 2 and 3, where the hypoperfused area was substantially larger (Figure 3-12).

A significant increase in the volume of perfusion deficit over the 4 hour time course was observed in both strains. In WKY, the perfusion deficit increased from $273\pm69mm^3$ at 1 hour post-MCAO to $318\pm65mm^3$ by 4 hours ($P<0.001$; Figure 3-11). In SHRSP, the volume of perfusion deficit increased from $368\pm45mm^3$ at 1 hour to $411\pm48mm^3$ at 4 hours post-stroke ($P<0.001$). There was no significant difference in the growth of the perfusion

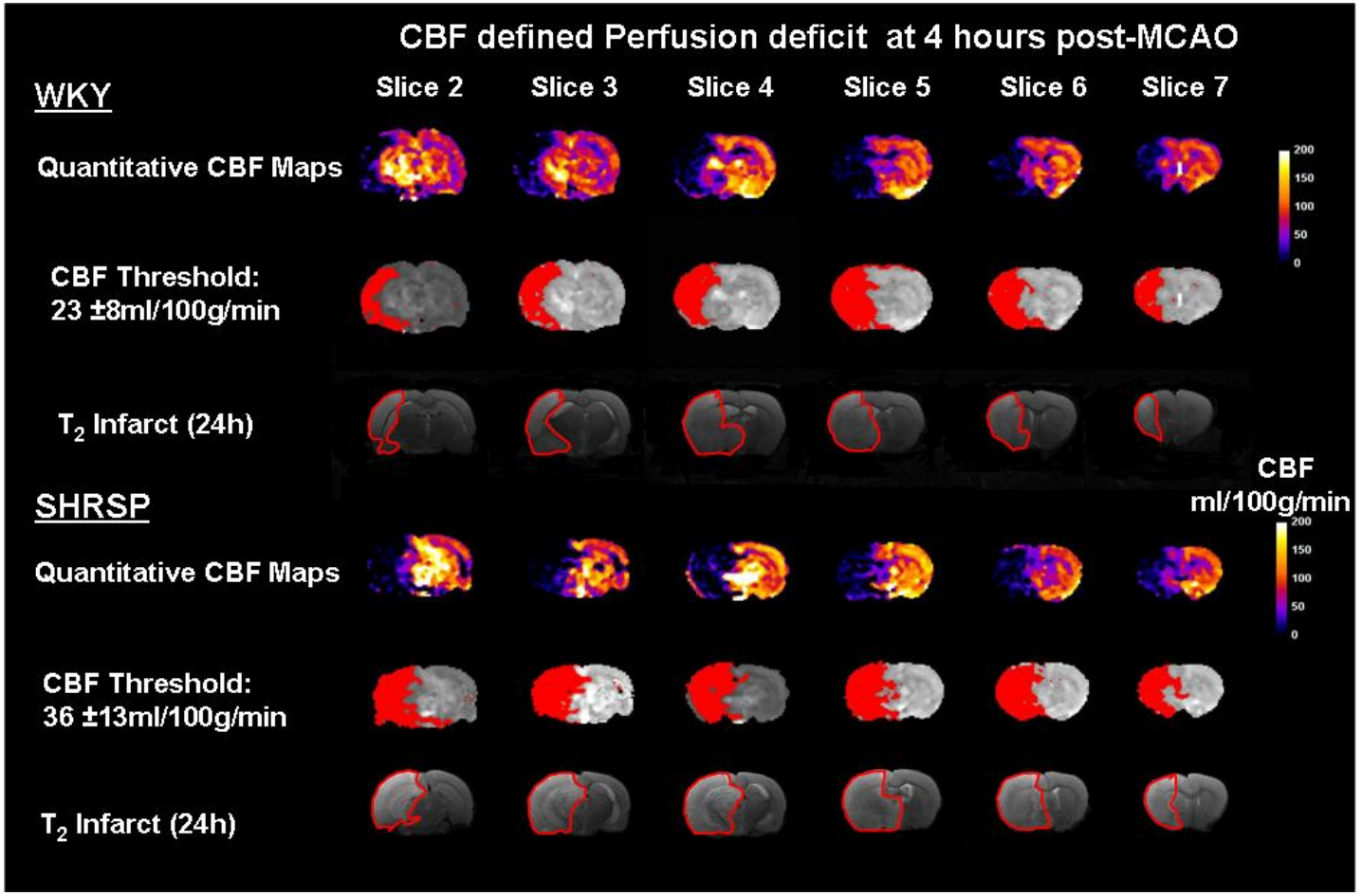

Figure 3-10. Quantitative CBF maps displaying hypoperfused tissue at 4 hours post-MCAO. CBF thresholds were adjusted until the volume of CBF defined perfusion deficit matched the volume of the oedema-corrected final infarct, defined by manually delineating the hyperintense areas on T_2 weighted images at 24 hours post-MCAO (shown in red). The data shown are from a representative SHRSP and WKY rat.

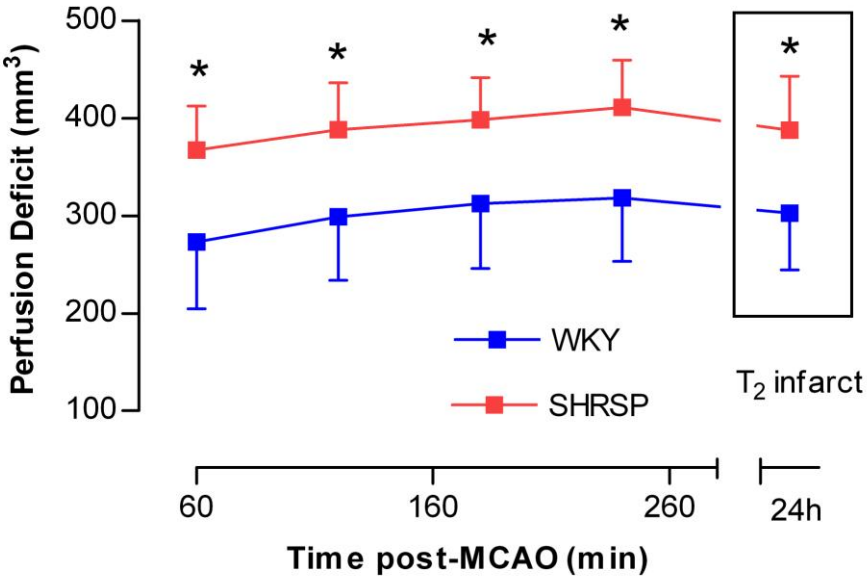

Figure 3-11. Temporal evolution of the perfusion deficit following permanent MCAO in SHRSP (n=15) and WKY (n=12) rats. Strain-specific perfusion thresholds were applied to quantitative CBF maps to compare the volume of hypoperfused tissue between strains and to assess the acute evolution of the perfusion deficit from 1-4h post-MCAO. *p<0.01, 2-way ANOVA with Bonferroni's post-test.

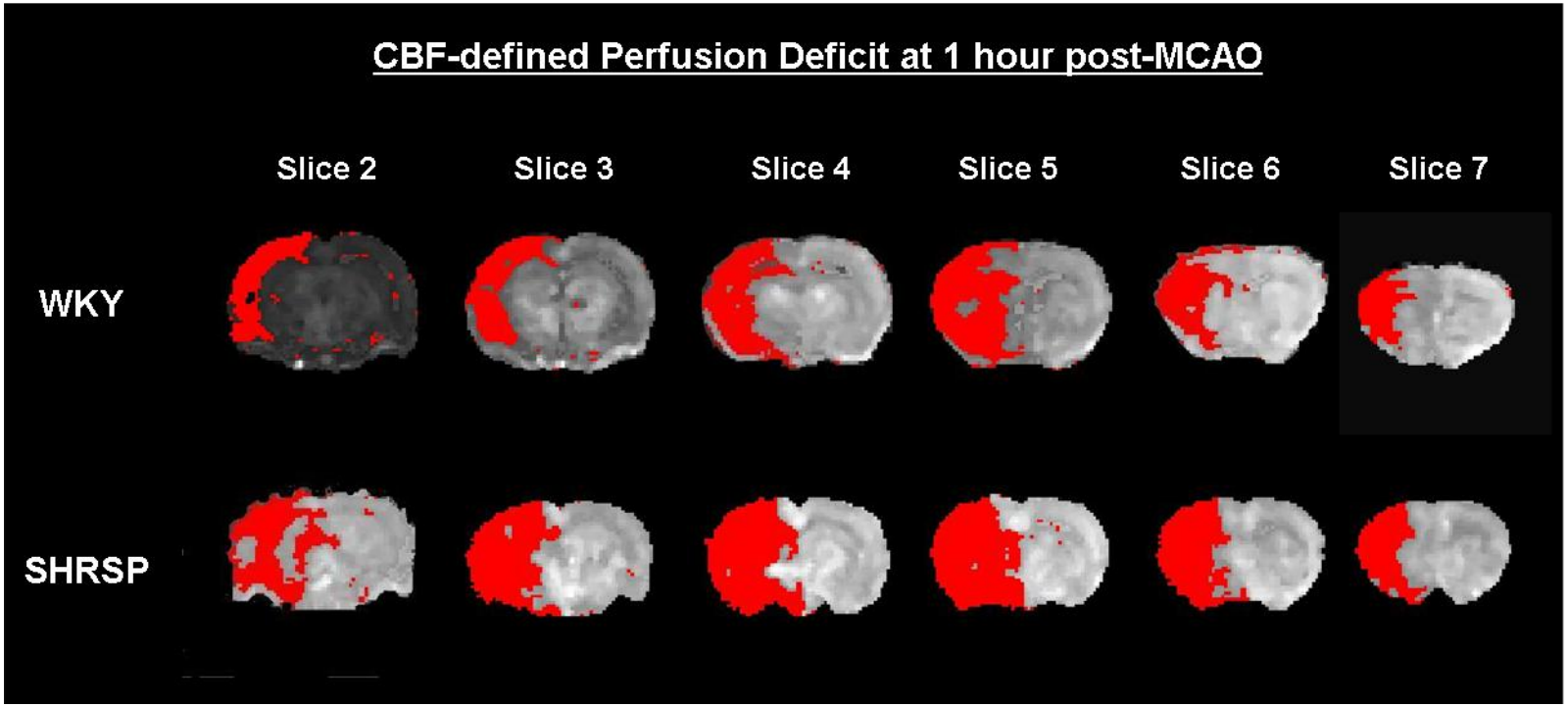

Figure 3-12. The perfusion deficit observed in SHRSP and WKY rats at 1h following permanent MCAO. Strain-specific CBF thresholds were applied to quantitative CBF maps acquired at 1h post-MCAO to assess the spatial distribution of hypoperfused tissue between strains. The perfusion deficit is depicted by red shading on 6 coronal brain slices within the territory of the middle cerebral artery. The data shown are from a representative SHRSP and WKY rat.

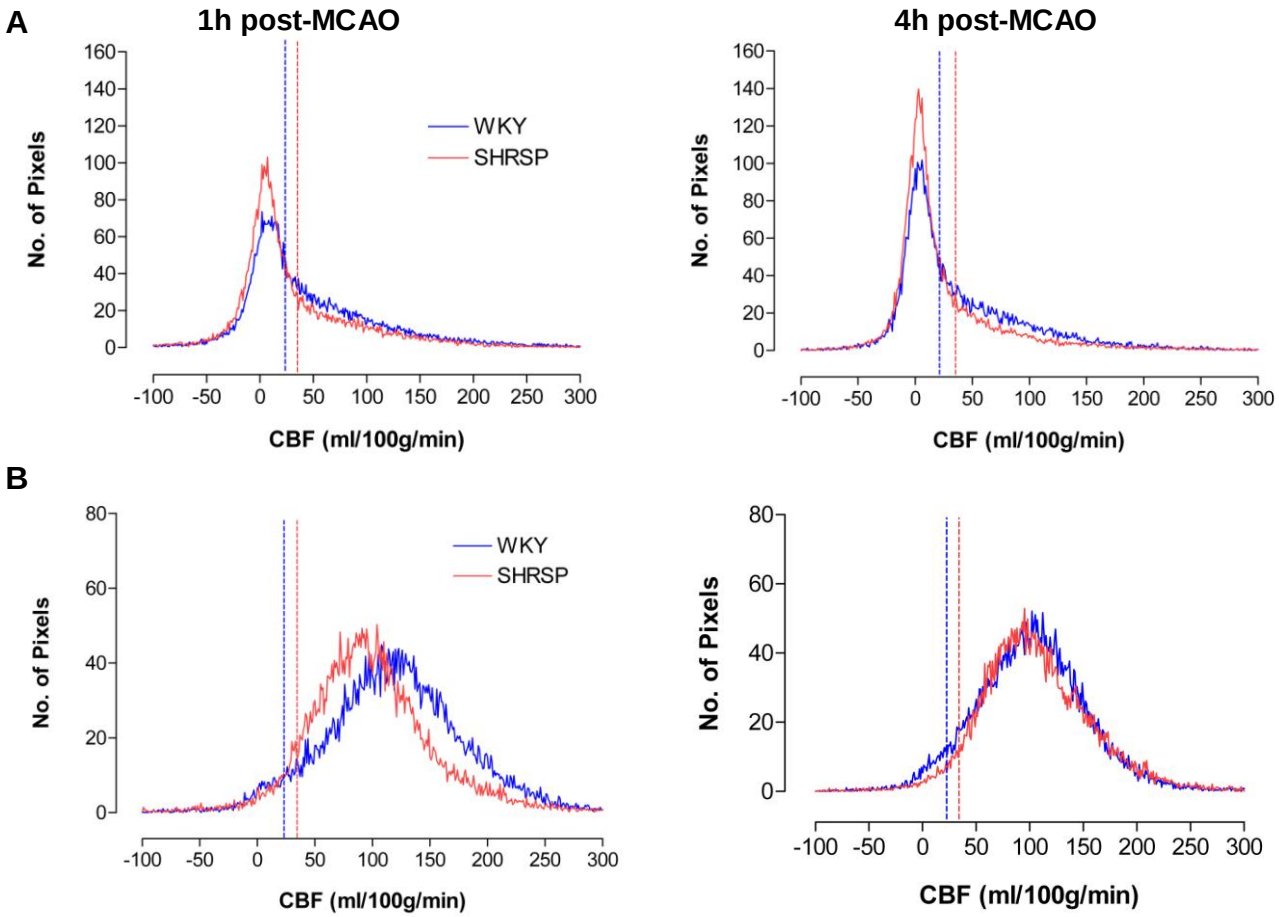

Figure 3-13. Cerebral blood flow profiles of the ipsilateral (A) and contralateral hemisphere (B) in SHRSP and WKY rats from 1-4h post-MCAO.

The figures show the CBF values of each pixel in the ipsilateral and contralateral hemispheres at 1 and 4h post-MCAO. The strain specific CBF thresholds are indicated by the dotted vertical lines. The mean SHRSP threshold (36ml/100g/min) is shown by the red dotted line and the WKY threshold (23ml/100g/min) is shown by the blue dotted line.

deficit between strains over the first 4 hours post-stroke. In SHRSP, the perfusion deficit increased by 43±27mm^3 compared to an increase of 48±20mm^3 in WKY (P=0.65).

These results are also illustrated by the CBF pixel profiles of the ipsilateral hemisphere of WKY and SHRSP, where the hypertensive strain had a greater proportion of pixels with low CBF values. In both strains, the number of pixels which fall below the strain-specific CBF threshold increases over time, as hypoperfused tissue becomes incorporated into the perfusion deficit (Figure 3-13A). The CBF profiles also demonstrate that a greater number of pixels have a low CBF value compared to WKY, irrespective of the application of a ADC threshold to quantify the ADC-derived lesion volume. The CBF profiles of the contralateral hemisphere show that the vast majority of pixels have a CBF value above the strain specific CBF thresholds (Figure 3-13B). In addition, the contralateral CBF profiles are similar between the strains and do not change over time.

3.4 Discussion

This is the first study to define strain-specific thresholds of diffusion and perfusion abnormality in a clinically relevant rodent stroke model with recognised risk factors. In-house ADC and CBF thresholds of abnormality were established for the SHRSP and WKY strain based on final infarct volume at 24 hours post-stroke, defined by T_2-weighted imaging. The mean calculated thresholds were retrospectively applied to MRI diffusion and perfusion data to compare the acute evolution of ADC-derived ischaemic injury and CBF defined perfusion deficit in the SHRSP and the normotensive control strain, WKY.

The calculated ADC thresholds were comparable between the strains, with thresholds associated with a 23% and 21% reduction in ADC for SHRSP and WKY respectively. These thresholds are similar to those reported previously in Wistar rats by examining metabolic failure following MCAO (Hoehn-Berlage et al, 1995; Olah et al, 2001) where an ADC threshold of 77% of control corresponds with the breakdown of energy metabolism. However, the ADC thresholds calculated in the present study, differ from those determined in Sprague-Dawley rats where a 30% reduction in ADC was reported to predict final infarct volume (Shen et al, 2003; Foley et al, 2010). Similarly, an ADC threshold of 30% reduction was reported in male Sprague-Dawley rats within our laboratory, using the same methodology as described in the present study (TA Baskerville, unpublished observations). Furthermore, using a method similar to the one employed in the present study, Shen and colleagues matched the 3 hour lesion volumes with the TTC (2,3,5-triphenyltetrazolium

chloride) defined final infarct at 24 hours post-MCAO in Sprague-Dawley rats and found that a 30% reduction in ADC matched final infarct. Similarly, a 30% reduction in ADC was determined using the empirical rule (by calculating the mean ± 2SD of the mean ADC prior to stroke) in Sprague-Dawley rats (Foley et al, 2010). These studies suggest that the threshold for ischaemic injury may be different between rat strains since ADC thresholds calculated by various study groups using different methods in Sprague-Dawley rats are consistently less severe than those determined in Wistar Kyoto rats.

The perfusion threshold calculated for Wistar Kyoto rats in the present study (23ml/100g/min) is lower than the perfusion threshold calculated previously in Sprague-Dawley rats (30ml/100g/min, Shen et al, 2003). In addition, the present study shows that the mean CBF threshold was significantly different between SHRSP (70% reduction from contalateral CBF) and WKY rats (81% reduction from contralateral CBF). This suggests that SHRSP may have a greater sensitivity to ischaemia than the normotensive control strain. It has been previously reported that *in vitro*, cortical neurons from SHRSP are more vulnerable in hypoxic conditions than those of WKY, with a significantly greater rate of cell death following 36 hours of hypoxia (Tagami et al, 1998). The strain-specific CBF thresholds calculated in the present study from the T_2-defined final infarct at 24 hours differ from those previously determined in Wistar rats (Hoehn-Berlage et al, 1995) where a 40% reduction in ipsilateral CBF was associated with tissue acidosis. Our CBF thresholds also differ from those determined previously in Sprague-Dawley rats (Shen et al, 2003) where a threshold of 57% reduction in CBF was defined. Furthermore, data from our laboratory show that a 63% reduction in CBF predicts final infarct at 24 hours post-MCAO in male Sprague-Dawley rats (TA Baskerville, unpublished observations).

One factor which may influence the calculation of CBF thresholds in the present study is the temporal evolution of the perfusion deficit. The CBF threshold was defined by matching the volume of perfusion deficit to the final infarct but the data show that the perfusion deficit increased from 1-4 hours post-MCAO. It was assumed that the volume of perfusion deficit would be relatively stable over the 4 hour time course in agreement with previous studies where a similar method was used to define perfusion thresholds (Shen et al, 2003; Meng et al, 2004). In the present study it was assumed that there would be no further recruitment of hypoperfused tissue into the perfusion deficit but this may not be the case and the perfusion deficit could expand beyond the 4 hour time point. Further expansion of the perfusion deficit would render the calculated CBF thresholds invalid as in this study the CBF threshold was adjusted until the volume of hypoperfused tissue at 4

hours post-MCAO matched the volume of the final infarct at 24 hours, with the assumption that there is no further expansion of the perfusion deficit at later time points. However, withdrawal of anaesthesia at 4 hours post-MCAO would result in an increase in mean arterial blood pressure in both strains which may support CBF in the ipsilateral hemisphere and prevent further increase in the size of the perfusion deficit.

Many factors can influence the calculation of viability thresholds, including methods used (autoradiography, MRI sequences), rat strain, stroke model and surgical technique. The technique used by Shen et al (2003), where ADC and CBF thresholds were established after 3 hours of permanent MCAO where the volume of ADC abnormality and perfusion deficit matched the volume of the TTC-defined final infarct at 24 hours, has recently been criticised. Foley et al (2010) argue that this technique may create bias in their results as it assumes that the ADC derived lesion has fully evolved to encompass the entire perfusion deficit by 3 hours post-MCAO but later time points were not examined to confirm that there was no further growth beyond this time point. This criticism can also be directed at the present study, although thresholds were matched at the 4 hours time point instead of the 3 hour time point used by Shen et al (2003). It would have been desirable to acquire MRI data for up to 6 hours to assess the evolution of perfusion deficit and ischaemic injury but this would have caused additional problems. Firstly, keeping animals under anaesthetic for that length of time is likely to increase the mortality rate and would have reduced the likelihood of successful recovery to 24 hours post-MCAO. Mortality rate in SHRSP was high when anaesthetic was maintained for 4 hours of MRI scanning, with one in every three rats failing to survive, resulting in unacceptable levels of morbidity and mortality. Secondly, after 4 hours of permanent MCAO, any further increases in the volume of perfusion deficit and ischaemic injury is likely to result from vasogenic oedema, as the integrity of the blood-brain barrier becomes compromised, resulting in a shift of water from the vasculature to the brain (Ayata et al, 2002). Previous work from our study group where the MRI scanning procedure was extended to 6 hours post-MCAO in non-recovery experiments demonstrated that ADC lesion volume is maximal in WKY and SHRSP by 4 hours (McCabe et al, 2009).

The present study demonstrates that final infarct, determined at 24 hours by T_2-weighted imaging, is significantly larger in SHRSP than WKY. This is in agreement with previous studies which have reported an increased sensitivity to experimental stroke in SHRSP (Coyle & Jokelainen, 1983; Jeffs et al, 1997; Carswell et al, 1999; Marks et al, 2001; McGill et al, 2005; McCabe et al, 2009). The present study has also shown that despite

comparable ADC thresholds, ADC-derived ischaemic injury was greater in SHRSP than WKY over the initial 4 hour time course. This confirms earlier reports from our laboratory, where the ADC lesion was significantly greater in SHRSP compared to WKY from 1-6 hours post-MCAO (McCabe et al, 2009). McCabe et al (2009) reported that within the first hour following permanent MCAO, the volume of ADC derived ischaemic injury in SHRSP ($275\pm75mm^3$) was significantly larger than in WKY ($171\pm30mm^3$, $P<0.05$) and increased significantly over time in both strains ($P<0.05$).

The extent of ischaemic injury demonstrated in SHRSP in the present study cannot solely be attributed to the development of severe hypertension in this strain, since an increased sensitivity to experimental stroke is observed in young SHRSP before the onset of hypertension (Coyle & Jokelainen, 1983). These authors demonstrated that SHRSP aged 35-40 days displayed a large cortical lesion following permanent MCAO induced by the method of Tamura et al (1981). In age-matched WKY rats, the lesion was significantly smaller. Other genetic factors which may contribute to increased ischaemic injury in SHRSP include increased levels of oxidative stress, where it has been reported that superoxide dismutase activity is reduced in SHRSP compared to WKY, resulting in increased levels of superoxide anions (Kishi et al, 2004). More recently it has been demonstrated that levels of 20-hydroxyeicosatetraenoic acid (20-HETE) are twice as high in the cerebrovasculature of SHRSP compared to WKY. 20-HETE is a potent vasoconstrictor which contributes to increased stroke sensitivity in SHRSP by mediating endothelial dysfunction and increasing oxidative stress by stimulating superoxide production (Cheng et al, 2008). Inhibition of 20-HETE has been shown to significantly reduce infarct volume in SHRSP (Dunn et al, 2008).

A heightened inflammatory response may also have contributed to the increased infarct volume observed in the present study. Previously, Marks and colleagues reported that the activation of microglia following permanent focal cerebral ischaemia, was significantly higher in SHRSP compared to WKY rats. In the region of the ischaemic core, 183 activated microglia were identified per mm^2, compared to $156/mm^2$ in WKY rats (Marks et al, 2001). Activated microglia can release neurotoxins including oxygen radicals, nitric oxide and glutamate, which can lead to lipid peroxidation, oedema and necrosis.

In addition, dysfunction of the BBB may also have contributed to the larger infarcts observed in SHRSP. It has been demonstrated that there is an alteration in the polarity of endothelial cells of the BBB prior to stroke onset and this may predispose the SHRSP to

stroke-induced breakdown of the BBB (Lippoldt et al, 2000). This may also contribute to the increased brain swelling observed in the hypertensive strain in the present study, where swelling of the ipsilateral hemisphere and compression of the contralateral hemisphere were more apparent in SHRSP than WKY.

The results also show that the CBF-defined perfusion deficit was significantly larger in SHRSP compared to WKY from 1-4 hours following stroke. The larger perfusion deficit exhibited by the hypertensive strain may be attributable to the higher CBF threshold in SHRSP, where a greater volume of tissue will fall below the perfusion threshold, compared to WKY rats. A CBF threshold of 50ml/100g/min has been reported previously in the SHR rat strain, when ischaemia persists for at least 3 hours (Jacewicz et al, 1992). This study highlights that rat strains may have different viability thresholds, particularly those strains which have underlying stroke risk factors, like the SHR and SHRSP. In addition, impaired blood flow through collateral vessels which connect the three major cerebral arteries in each hemisphere is likely to contribute to the increased perfusion deficit in SHRSP. Although the number of collateral vessels is the same between the strains, it has been reported that the internal diameter of anastomoses is reduced in SHRSP, therefore reducing vasodilator capacity following MCAO and contributing to the larger infarct size observed in the hypertensive strain (Coyle & Heistad, 1987).

Furthermore, the results demonstrate that the perfusion deficit significantly increases from 1-4 hours following stroke in both the WKY and SHRSP strains. This has been previously reported in a previous study from our laboratory, where the perfusion deficit in SHRSP significantly increased from 1-6 hours post-MCAO (McCabe et al, 2009). This study, which used published ADC and CBF thresholds, examined the area of perfusion deficit on a single coronal slice within the territory of the MCA and showed that in SHRSP, the perfusion deficit increased from 44±9mm^2 at 1 hour to 49±7mm^2 at 6 hours post-MCAO (P=0.01). However, in WKY, the area of perfusion deficit on the same coronal slice was unchanged from 1-6 hours post-MCAO. This finding differs from those reported in the present study where both the SHRSP and WKY strains display a significant increase in perfusion deficit in the acute phase following permanent MCAO. However, McCabe et al (2009) only examined CBF on a single coronal slice within the MCA territory and therefore would not have detected any increases in perfusion deficit which may have been evident on brain slices located further rostrally and caudally. The increase in perfusion deficit which was observed in both strains in the present study was unlikely to result from global changes in CBF as a result of prolonged anaesthesia as the data shows that

contralateral CBF did not change significantly over the 4 hour time course in either WKY or SHRSP. The temporal increase in perfusion deficit suggests that there is a gradual failure of collateral blood supply over time in SHRSP and WKY rats. This may occur as a result of disruption of the blood-barrier barrier, where water will be drawn from the collateral vessels, thereby reducing blood flow to hypoperfused tissue on the boundary of the perfusion deficit. As blood flow to this region of tissue declines, it will become more severely hypoperfused and will fall below the CBF threshold and consequently become incorporated into the perfusion deficit.

It is particularly interesting that this apparent failure of collateral flow occurs in both SHRSP and WKY. It is unsurprising that the perfusion deficit increases over time in the hypertensive strain as it is well established that the SHRSP exhibits an impaired collateral flow and increased dysfunction of the blood-brain barrier, as previously discussed. Both of these factors would therefore contribute to expansion of the perfusion deficit over time. It has been reported that the severity of blood-brain barrier disruption and brain oedema correspond with the duration and severity of ischaemia (Todd et al, 1986). This may explain why there appears to be evidence of collateral failure in WKY, as despite being normotensive, the WKY strain exhibits larger infarcts following permanent MCAO than other normotensive strains like the Sprague-Dawley rat. Data from our laboratory show that Sprague-Dawley rats, subjected to the same experimental procedure as described in this chapter, demonstrate a final infarct volume of 208±48mm^3, which is significantly lower than that observed in WKY rats in the present study (303±59mm^3, P=0.001). In Sprague-Dawley rats the CBF defined perfusion deficit was relatively stable from 1-4 hours post-MCAO (TA Baskerville, unpublished observations). This suggests that there may be structural or physiological differences between normotensive rat strains which could contribute to the observed differences in the severity of ischaemia between WKY and Sprague-Dawley rats. To date, the potential differences in the structural and physiological characteristics of collateral blood vessels in WKY and Sprague-Dawley rats has yet to be examined. The failure of collateral blood supply in WKY suggested by the data in the present study, conflicts with previous reports where collateral vessels in WKY rats vasodilate to restore flow to levels comparable with the contralateral hemisphere one month after permanent MCAO (Coyle & Heistad, 1987). However, these authors used a different model of MCAO, where the artery was occluded distally by drilling through the skull to expose the middle cerebral artery, which was then tied using a nylon ligature (Coyle, 1982). This model induces the formation of a small cortical lesion and reduced brain swelling as a result of craniectomy and therefore the demands on the collateral

vessels is markedly reduced and collateral blood supply is sufficient to maintain blood supply and prevent infarction.

Summary

In summary, the present study has defined strain-specific MRI perfusion and diffusion thresholds in SHRSP and WKY rats following permanent MCAO. These thresholds were retrospectively applied to acute MRI data to assess and compare the temporal evolution of ischaemic injury and perfusion deficit in both strains. SHRSP rats demonstrated a significantly larger infarct at 24 hours post-MCAO, confirming previous reports of increased sensitivity to experimental stroke in the hypertensive strain. Despite comparable ADC thresholds, the absolute CBF threshold in SHRSP was significantly higher, indicating a greater sensitivity to ischaemia compared to WKY. The volume of ADC-derived ischaemic injury and perfusion deficit was significantly greater in SHRSP from 1-4 hours post-MCAO and increased significantly over time in both strains.

Chapter 4.

A comparison of penumbra calculation methods to identify potentially salvageable tissue in SHRSP and WKY rats

4.1 Introduction

Positron emission tomography (PET) remains the "gold-standard" imaging modality for penumbra detection, identifying penumbral tissue on the basis of specific metabolic parameters (Sobesky et al, 2005) but the radiation exposure, complex logistics and costs of PET limit its wider use. Perfusion-diffusion mismatch is widely used to identify the penumbra, both in clinical and basic stroke research (Heiss, 2010). In acute stroke, MR diffusion weighted imaging (DWI) can identify tissue in which diffusion is restricted as a result of cytotoxic oedema, leading to a reduction in the apparent diffusion coefficient (ADC) value of the tissue. This evidence of brain injury is used within perfusion-diffusion mismatch methodology to represent the irreversibly damaged ischaemic core. Perfusion weighted imaging (PWI) delineates the perfusion deficit, identifying hypoperfused tissue destined to proceed to infarction and the mismatch between the PWI defined perfusion deficit and DWI defined ischaemic core is used to provide an approximation of the ischaemic penumbra: potentially salvageable tissue with a finite lifespan which will proceed to infarction over time.

At present, there is no consensus on which MRI measure of cerebral blood flow to use clinically or what threshold to apply to determine the perfusion deficit. It has been reported that the volume of penumbra quantified by the mismatch technique can vary considerably depending on the perfusion parameter used to define hypoperfused tissue (Kane et al, 2007). In a study of 32 patients, these authors demonstrated that the proportion of those patients presenting with perfusion-diffusion mismatch varied from 9% to 72% using 10 different MRI methods to detect the perfusion deficit in each patient. This will impact on patient management where the volume of potentially salvageable tissue is used to determine suitability for therapy. This report highlights the need for agreement in the method used to identify potentially salvageable tissue in stroke patients in clinical research.

In pre-clinical research there is a notable absence of literature examining the PWI/DWI mismatch methodology and studies investigating the use of PWI and DWI data to define penumbra are urgently required. In addition, there is a lack of pre-clinical data examining the effect of potential neuroprotective strategies on the evolution of the mismatch defined penumbra. In this respect, the perfusion-diffusion mismatch model has been relatively underused and may yet prove to be a useful tool in the development of stroke therapies in experimental animal models.

In experimental stroke models using MRI, mismatch volume is commonly calculated by subtracting the ADC lesion volume from the volume of perfusion deficit without any anatomical co-registration (Meng et al, 2004; Bråtane et al, 2009; Henninger et al, 2009). This method provides no information on the location or spatial distribution of the penumbra and therefore may be of limited use when examining the temporal evolution of potentially salvageable tissue following experimental stroke.

Furthermore, there are limited data examining the lifespan of the penumbra in animal models with genetic stroke risk factors. Legos and colleagues reported that SHR rats demonstrated no evidence of perfusion-diffusion mismatch as early as 1 hour following MCAO. At the same time point, Sprague-Dawley rats exhibited a substantial volume of mismatch tissue (Legos et al, 2008). Similarly, Letourneur and colleagues found that perfusion-diffusion mismatch volume was significantly reduced in SHRs compared to WKY rats from as early as 30 minutes following permanent focal cerebral ischaemia. An alternative model of induced renovascular hypertension in normotensive rats, using a kidney clip procedure was also studied. This group of rats also exhibited a significantly reduced mismatch volume compared to normotensive WKY rats (Letourneur et al, 2011).

At present, only one study group has compared the acute evolution of the ischaemic penumbra in SHRSP and WKY strains but assessment of mismatch was limited to the examination of one coronal slice from within the territory of the middle cerebral artery (McCabe et al, 2009). Multi-slice determination of mismatch volume has not yet been assessed in WKY and SHRSP. However, previous reports suggest that the extent and lifespan of the ischaemic penumbra may be reduced in SHRSP compared to the normotensive control, WKY.

Study Aims

The aims of the study were firstly, to assess and compare three different methods of calculating penumbra volume to evaluate the strengths and limitations of each method. The second aim was to compare the extent and lifespan of the ischaemic penumbra following permanent MCAO in SHRSP and WKY rats.

4.2 Methods

4.2.1 Data Analysis

Determination of Penumbra Volume

The MRI data generated from the study in Chapter 3 were used to assess penumbra in SHRSP (n=15) and WKY (n=12) rats following permanent MCAO. Strain-specific perfusion and diffusion thresholds were applied to quantitative ADC and CBF maps acquired over the first 4 hours post-MCAO. This allowed determination of the volume of ADC-derived ischaemic injury and the volume of CBF-defined perfusion deficit over 6 coronal brain slices for both strains at each time point, as previously described in Chapter 3. Penumbra volume was assessed in 3 ways:

1. By volumetric perfusion-diffusion mismatch, where the volume of ADC-derived ischaemic injury was subtracted from the volume of the perfusion deficit at each time point from 1-4 hours post-MCAO.

2. Spatial assessment of the perfusion-diffusion mismatch was carried out on each of the 6 coronal slices. Using Image J and Matlab® software, the strain specific perfusion and diffusion thresholds were applied to the quantitative CBF map and ADC map, respectively, for each coronal slice. The ADC-derived area of ischaemic injury was overlaid onto the thresholded CBF map and the remaining perfusion deficit was manually delineated and measured as mismatch tissue. The ventricles were excluded when delineating the mismatch area. The mismatch areas on each slice were combined and multiplied by slice thickness (1.5mm) to generate mismatch volume. This was repeated for each time point post-MCAO.

3. Penumbra volume was determined by measuring the growth of the volume of ADC-derived ischaemic injury over time. This was achieved by subtracting the ADC-derived lesion volume at each time point, from 30 minutes to 4 hours post-MCAO, from the final infarct at 24 hours, defined by T_2 weighted imaging. ADC lesion growth was therefore only assessed in rats which survived to 24 hours post-MCAO (WKY: n=10, SHRSP: n=10).

All MRI data analyses were undertaken blind to rat strain. The data from each animal were identified by a numbered code, which gave no indication as to strain identity. The

code was broken on the completion of all data analysis to allow assessment of potential strain differences.

Pixel-by-Pixel Analysis

Pixel-by-pixel analysis was undertaken to evaluate the ADC and CBF values of each pixel of the ipsilateral and contralateral hemispheres across 6 coronal slices using Matlab® software (Mathworks Inc). Quantitative ADC and CBF maps were prepared for pixel-by-pixel analysis using ImageJ software. ROIs of each hemisphere were generated and used to split the ADC and CBF maps for each coronal slice into ipsilateral and contralateral hemispheres. The ADC and CBF maps for each of the 6 coronal slices were put together in a stack for each hemisphere at each time point from 1-4 hours post-MCAO. The ADC and CBF hemispheric stacks for each rat were uploaded into Matlab® and the strain specific ADC and CBF thresholds were inserted into the following command:

ThresholdMRI('ADC_ipsi.tif','CBF_ipsi.tif','ADC_contra.tif','CBF_contra.tif',ADC threshold,CBF threshold)

Matlab® software defined four tissue compartments: (1) a 'normal' compartment, where pixels had a ADC and CBF value above threshold; (2) a 'core' compartment, where pixels had a ADC and CBF value which were below the thresholds; (3) a 'mismatch' compartment, where ADC was above the diffusion threshold but CBF was below the perfusion threshold; and (4) a 'negative-mismatch' compartment, where ADC was below the threshold and CBF was above the threshold.

The number of pixels in each compartment in each hemisphere across 6 slices at each time point was calculated by Matlab®. This allowed the total area of each compartment to be determined by multiplying the total number of pixels by the area of a pixel ($0.0678m^2$). The volume of each compartment was then calculated by multiplying the total pixel area by slice thickness (1.5mm).

The mean CBF of the negative mismatch tissue compartment was also assessed at each time point for both SHRSP and WKY. For each rat, the area of negative mismatch on each slice was selected as a region of interest (ROI). The ROI was then restored onto the quantitative CBF map of the appropriate slice at the same time point using ImageJ and the CBF value of each pixel in the ROI was determined. This was performed for each of the 6 coronal slices and mean CBF was calculated by summing the CBF value for each pixel and dividing by the total number of pixels.

4.2.2 Statistical Analysis

All statistical analyses were undertaken using GraphPad Prism software and all data are presented as mean ± SD. The temporal evolution of mismatch volume and ADC-derived lesion growth for each strain were assessed by Repeated Measures ANOVA, with Bonferroni's multiple comparisons post-test. Temporal comparisons in mismatch volume and ADC-derived lesion expansion between strains were assessed by 2-way ANOVA with Bonferroni's post-test. A comparison of penumbra volume by the 3 different calculation methods for each strain was also assessed by 2-way ANOVA with Bonferroni's post-test. Level of statistical significance was set at $p<0.05$.

4.3 Results

In order to examine the differences between the three different methods of penumbra calculation, it is important to identify the effect of time on the two components which are used to determine penumbra volume; the ADC-derived lesion volume and the perfusion deficit. As previously described in Chapter 3, there is a significant increase in the volume of ADC-derived ischaemic injury and the volume of the perfusion deficit over the first 4 hours post-MCAO in SHRSP and WKY.

4.3.1 Volumetric Perfusion-Diffusion Mismatch

Determination of perfusion-diffusion mismatch volume by the simple subtraction method revealed a limited volume of penumbra in both SHRSP and WKY, even at the earliest time point examined. At 1 hour post-MCAO, mismatch volume was comparable between the strains ($22\pm59mm^3$ and $31\pm50mm^3$ in WKY and SHRSP respectively, $P>0.05$, Figure 4-1A). The volume of perfusion-diffusion mismatch did not change significantly over time in WKY. This is likely to be attributable to the temporal increase in perfusion deficit observed in both strains, as the ADC-derived lesion and the perfusion deficit both expand over time (see Discussion section for greater detail). In WKY, mismatch volume decreased from $22\pm59mm^3$ at 1 hour to $7\pm34mm^3$ at 4 hours post-MCAO ($P=0.24$). However, in SHRSP, mismatch volume decreased significantly from $31\pm50mm^3$ at 1 hour to $1\pm33mm^3$ at 4 hours post-MCAO ($P=0.01$). There was no significant difference in mismatch volume between the strains at any time point ($P=0.63$). The data were highly variable in both strains, as illustrated by the high standard deviations observed in both WKY and SHRSP at all time points post-MCAO (Figure 4-1).

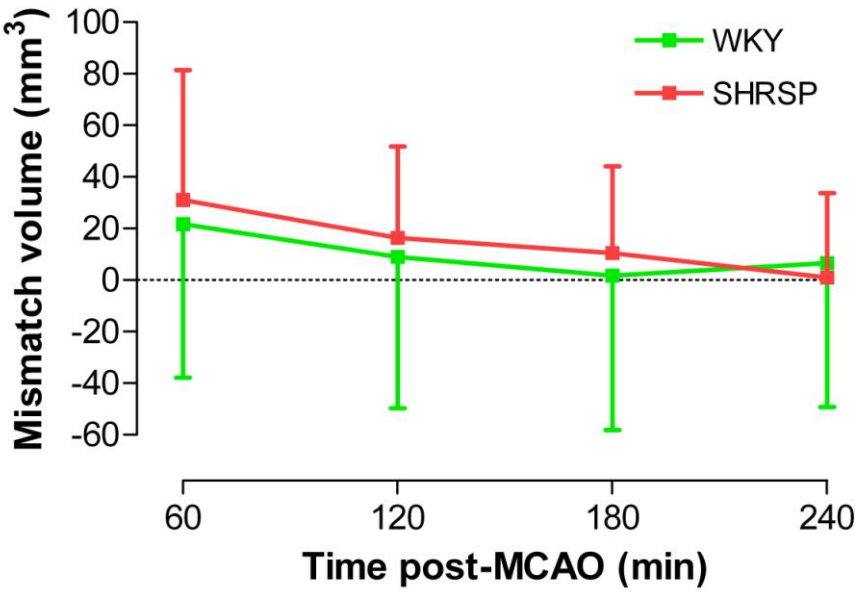

Figure 4-1. Perfusion-diffusion mismatch volume in SHRSP and WKY rats following permanent MCAO. Mismatch volume was calculated by a simple subtraction method, where the volume of ADC-derived ischaemic injury was subtracted from the volume of perfusion deficit. There was no significant difference in mismatch volume between the strains (2-way ANOVA, P=0.63). Data are displayed as mean±SD, WKY; n=12, SHRSP; n=15.

4.3.2 Spatial Assessment of Mismatch Volume

Pixel-by-pixel analysis of quantitative ADC and CBF maps revealed that the core tissue compartment was significantly larger in SHRSP compared to WKY at all time points post-MCAO (Figures 4-2A, 4-3 & 4-4). At 1 hour post-MCAO, core tissue in SHRSP was 284±48mm^3 compared to 193±49mm^3 in WKY ($P<0.001$, Figure 4-2A). The ischaemic core expanded significantly from 1-4 hours post-MCAO in both strains. In WKY, core tissue increased from 193±49mm^3 at 1 hour to 263±41mm^3 at 4 hours post-MCAO ($P<0.001$, Figure 4-2A). Similarly, in SHRSP, the ischaemic core increased from 284±48mm^3 at 1 hour to 354±46mm^3 at 4 hours post-MCAO ($P<0.001$, Figure 4-2A). The differing profiles of the ipsilateral and contralateral hemispheres are illustrated in Figures 4-4 & 4-5. In the ipsilateral hemisphere, the majority of pixels are located in the 'core' quadrant in both WKY and SHRSP. However, as expected in the contralateral hemisphere, the vast majority of pixels are located within the 'normal' quadrant.

Spatial assessment of perfusion-diffusion mismatch produced larger volumes of penumbral tissue in both WKY and SHRSP. At 1 hour post-MCAO, mismatch volume was larger in WKY compared to SHRSP but this was not statistically significant (43±43mm^3 and 36±15mm^3 in WKY and SHRSP respectively, $P>0.05$). The volume of perfusion-diffusion mismatch decreased over time in both WKY and SHRSP. In WKY, mismatch volume decreased from 43±43mm^3 at 1 hour to its lowest value of 27±24mm^3 at 3 hours post-MCAO ($P=0.15$) and mismatch volume at 4 hours was 29±18mm^3. In SHRSP, mismatch volume significantly decreased from 36±15mm^3 at 1 hour to 23±19mm^3 at 4 hours post-MCAO ($P<0.05$). However, there was no significant difference in mismatch volume between the strains at any time point post-MCAO ($P=0.9$, Figure 4-2B).The spatial distribution of mismatch tissue was similar in WKY and SHRSP. In both strains, mismatch tissue was mainly located in the cortex. Perfusion-diffusion mismatch was particularly evident on the rostral and caudal slices, where a larger mismatch area was exhibited on caudal slices 2 and 3 in both WKY and SHRSP. There was also evidence of mismatch on the most rostral slice (slice 7) in both strains. However, there was little evidence of mismatch tissue on coronal slices 4, 5 and 6 and this was particularly evident in SHRSP (Figure 4-3). In both strains, there was evidence of a limited volume of existing perfusion-diffusion mismatch at 4 hours post-MCAO.

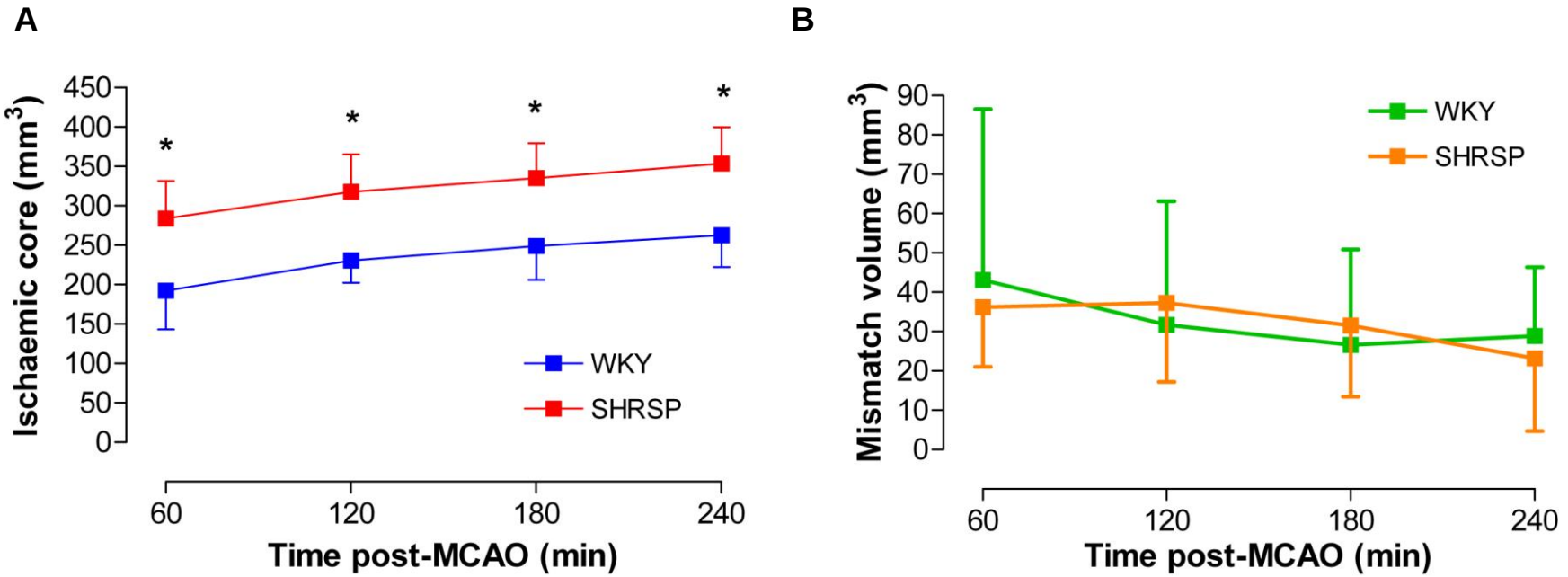

Figure 4-2. Pixel-by-pixel analysis of ADC and CBF values following permanent MCAO in SHRSP & WKY rats. Pixel-by-pixel analysis defined the ischaemic core, where pixels fall below the strain specific ADC and CBF thresholds (A). Mismatch was defined where pixels had an ADC value above threshold but CBF fell below the strain-specific CBF threshold (B). Data are presented as mean±SD, WKY; n=12, SHRSP; n=15. *p<0.0001, 2-way ANOVA with Bonferroni's Multiple comparisons post-test.

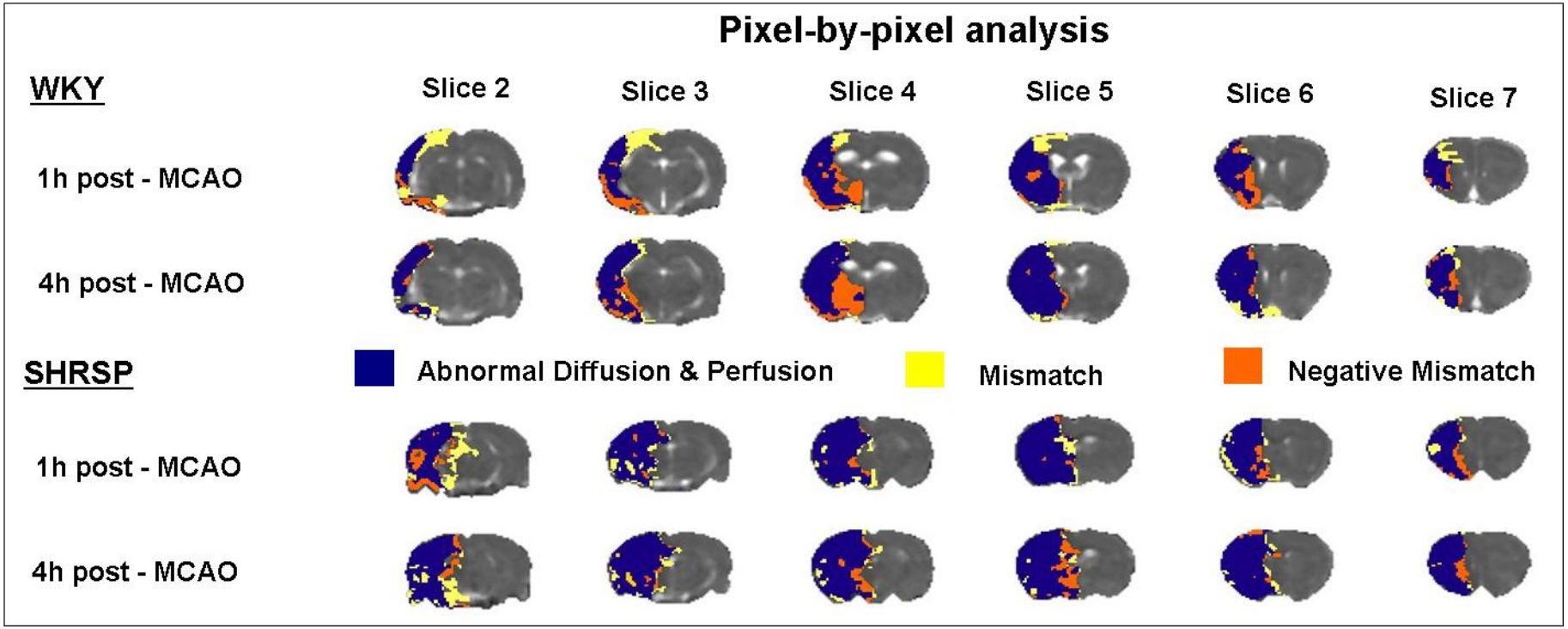

Figure 4-3. Pixel-by-pixel analysis of ADC and CBF values in WKY and SHRSP following permanent MCAO. The data shown are from a representative SHRSP and WKY rat. Pixel-by-pixel analysis identified four tissue compartments: normal tissue, where ADC and CBF values are above threshold; core tissue (blue shading), where ADC and CBF are below threshold; perfusion-diffusion mismatch (yellow shading), where ADC is normal and CBF is below threshold and negative mismatch (orange shading), where CBF is normal and ADC is below threshold. Note the larger ventricles in WKY compared to SHRSP.

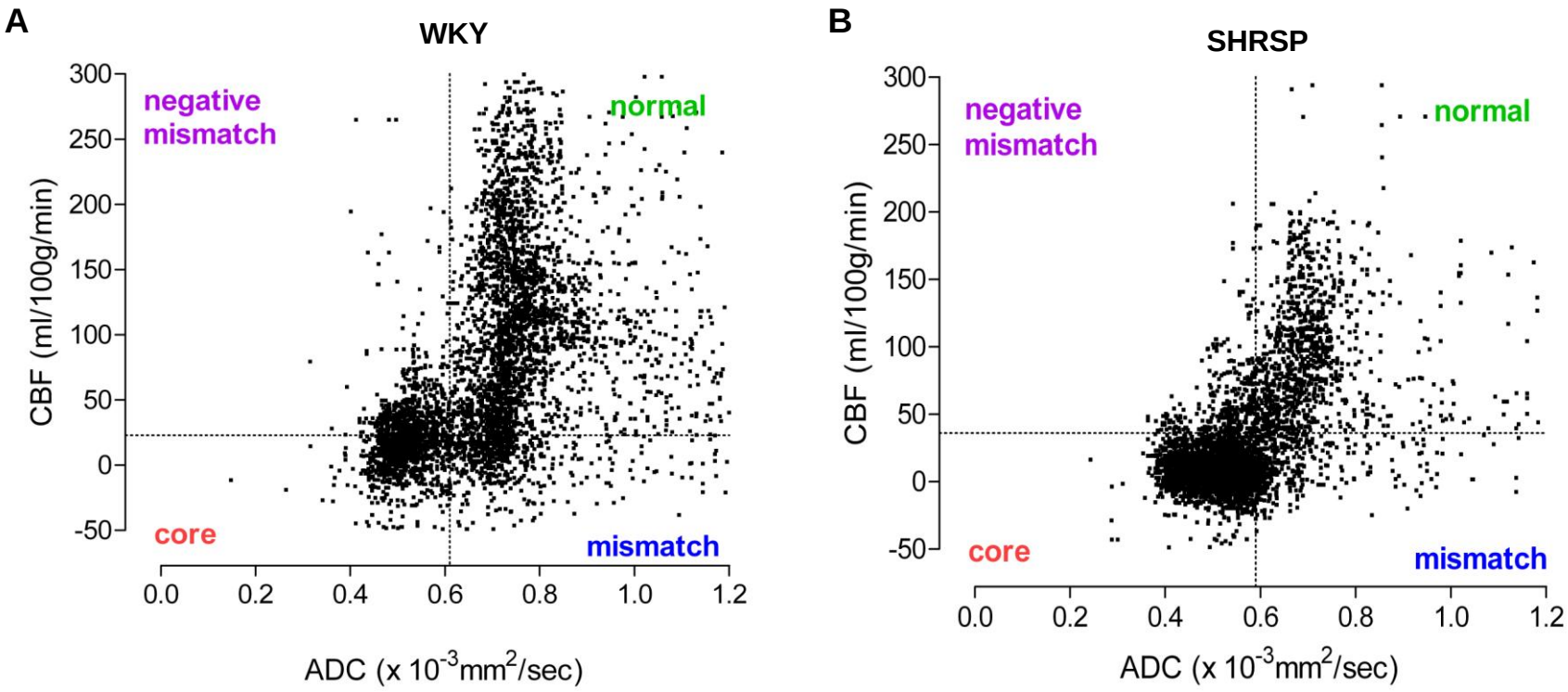

Figure 4-4. Pixel-by-pixel analysis of ADC and CBF values in the ipsilateral hemisphere at 1 hour following permanent MCAO. The data shown are from a representative WKY (A) and SHRSP (B). The mean ADC and CBF thresholds for each strain are shown by the dotted lines. Pixels are assigned to one of four quadrants depending on their ADC and CBF value: normal, core, mismatch or negative mismatch.

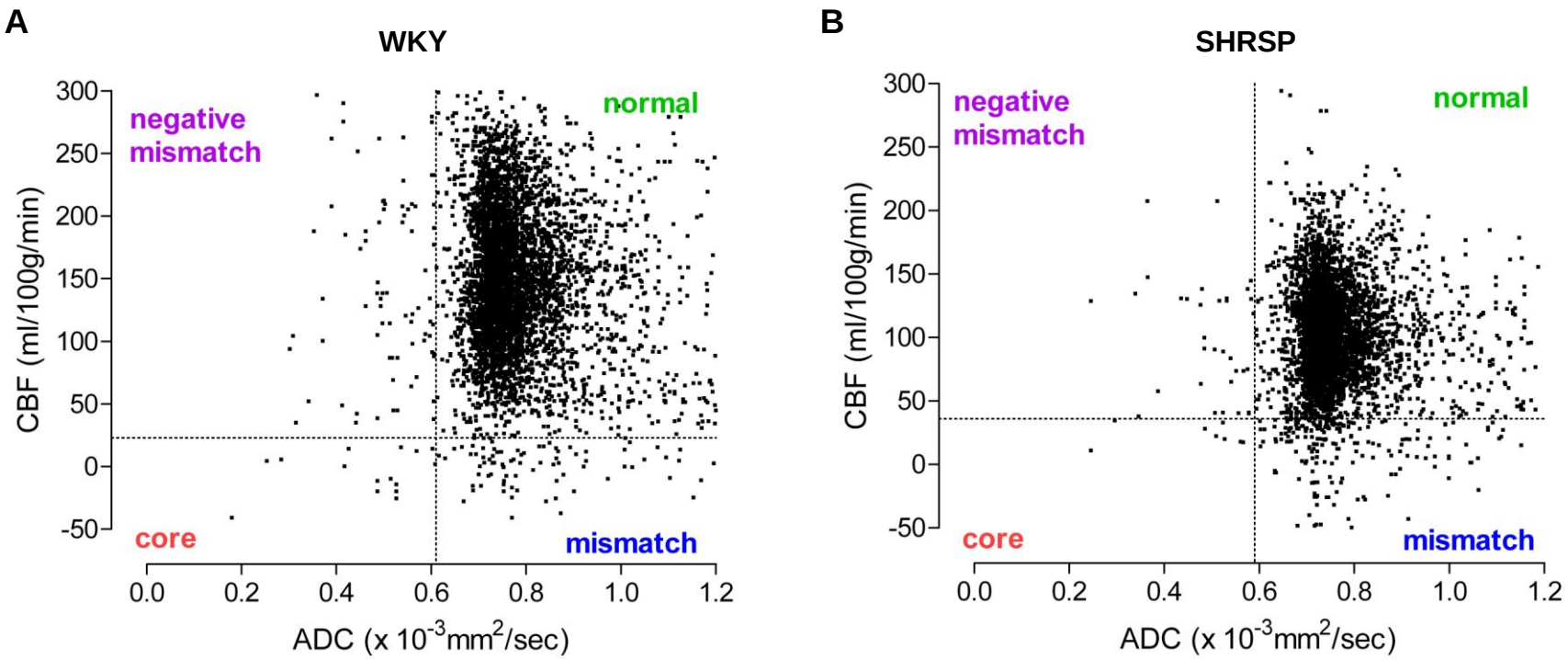

Figure 4-5. Pixel-by-pixel analysis of ADC and CBF values in the contralateral hemisphere at 1 hour following permanent MCAO. The data shown are from a representative WKY (A) and SHRSP (B). The mean ADC and CBF thresholds for each strain are shown by the dotted lines. Pixels are assigned to one of four quadrants depending on their ADC and CBF value: normal, core, mismatch or negative mismatch.

4.3.3 Negative Mismatch

Pixel-by-pixel analysis also revealed evidence of negative mismatch tissue, where the ADC-derived lesion expands outside the boundary of the perfusion deficit, in both WKY and SHRSP (Figures 4-3 & 4-4). Negative mismatch tissue was identified in both strains at all time points following MCAO. Greater negative mismatch volumes were recorded in WKY but differences between the strains were not statistically significant. At 1 hour post-MCAO, negative mismatch volume was 55±17mm^3 in WKY compared to 41±19mm^3 in SHRSP (P>0.05, Figure 4-6). The volume of negative mismatch tissue was persistent and did not change significantly over the 4 hour time course in either strain (P>0.05, Figure 4-6). In WKY, negative mismatch volume was maintained from 55±17mm^3 at 1 hour to 53±20mm^3 at 4 hours post-MCAO (P>0.05). In SHRSP, mismatch volume persisted from 41±19mm^3 at 1 hour to 42±11mm^3 at 4 hours post-MCAO (P>0.05, Figure 4-6). Negative mismatch tissue was identified on all 6 coronal slices and was found sub-cortically at the boundary of the ischaemic core in both strains (Figure 4-3).

Analysis of CBF values revealed negative mismatch tissue was significantly hypoperfused compared to contralateral CBF in both strains but blood flow was significantly higher than the strain specific CBF thresholds (Figure 4-7). In WKY at 1 hour post-MCAO, CBF in negative mismatch tissue was 49±4 ml/100g/min compared to 135±23 ml/100g/min in the contralateral hemisphere (P<0.001), and significantly higher than the strain-specific CBF threshold (23±8 ml/100g/min, P<0.001, Figure 4-7A). Similarly, in SHRSP at the same time point, negative mismatch tissue was 71±9 ml/100g/min compared to a contralateral CBF of 113±22 ml/100g/min (P<0.001), and significantly higher than the SHRSP perfusion threshold (36±13 ml/100g/min, P<0.001, Figure 4-7B).

4.3.4 Penumbra determined from ADC-derived lesion expansion

The volume of the ADC-derived lesion increased over time in both strains as the penumbra became incorporated into the ischaemic core, until it matched the final (oedema-corrected) infarct volume. ADC lesion enlargement can therefore be used to indirectly measure the penumbra. Expansion of the ADC-derived lesion decreased with time and by 3 hours post-stroke, the lesion matched the final (oedema-corrected) infarct volume in both strains. In SHRSP, penumbra volume, derived from ADC lesion volume versus final infarct volume, was 43±45mm^3 at 30 minutes and decreased in size to 0±44mm^3 at 3 hours post-MCAO (P<0.001). In WKY, penumbra volume was 106±73mm^3 at 30 minutes, declining

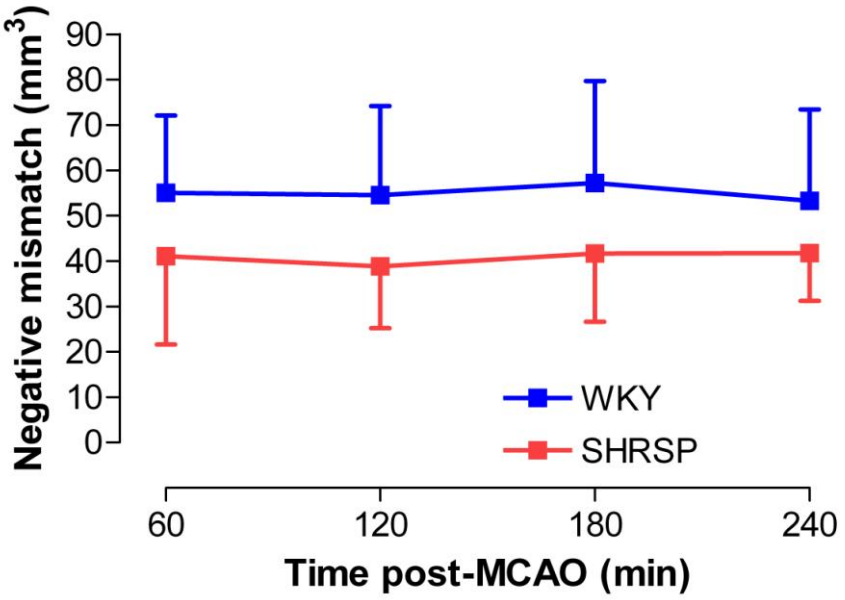

Figure 4-6. The temporal evolution of negative mismatch tissue in SHRSP and WKY rats following permanent MCAO. Negative mismatch represents tissue where CBF is above threshold and ADC is below threshold and identifies expansion of the ADC-derived lesion beyond the boundaries of the perfusion deficit. There was no significant difference in negative mismatch volume between the strains (2-way ANOVA, $p>0.05$). Data are displayed as mean±SD, WKY; n=12, SHRSP; n=15.

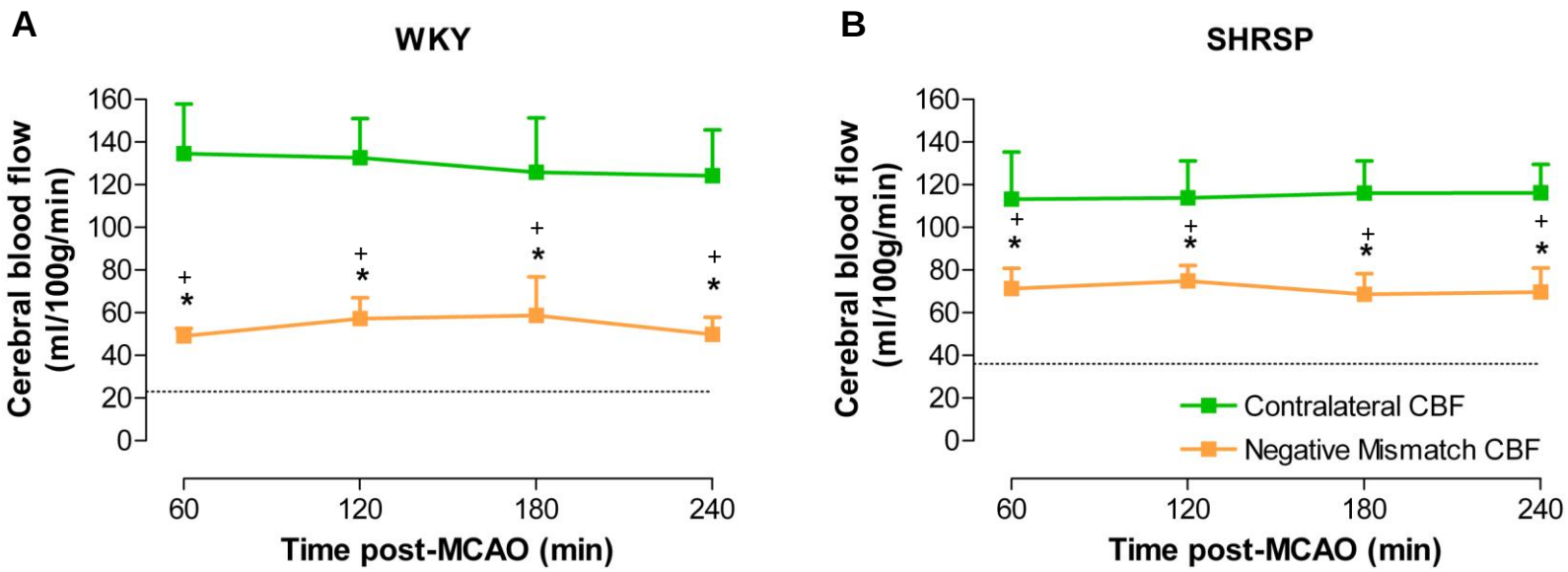

Figure 4-7. Perfusion in the region of negative mismatch compared to the contralateral hemisphere in WKY and SHRSP. The dotted line demarcates the mean CBF threshold for each strain. Negative mismatch CBF vs contralateral CBF *p<0.001, 2-way ANOVA with Bonferroni's post-test. Negative mismatch vs strain-specific CBF threshold +p<0.001, 1-sample t test. Data are presented as mean±SD, WKY; n=12, SHRSP; n=15).

significantly over time to 0±41mm^3 at 3 hours post-MCAO (P<0.001). Penumbra volume was significantly higher in WKY compared to SHRSP at 30 minutes post-MCAO (43±45mm^3 vs 106±73mm^3, for SHRSP and WKY respectively, P<0.05, Figure 4-8) but was not significantly different between the strains at later time points. There was no significant difference in penumbra volume between the strains calculated using ADC expansion from 1-4 hours post-MCAO (P>0.05, Figure 4-9).

The ADC-derived lesion evolves in an annular pattern, whereby the lesion expands relatively uniformly at its boundary and expansion of the ADC lesion is evident across all 6 coronal slices in both WKY and SHRSP. (Figure 4-10). The ADC-derived lesion and perfusion deficit expand in a similar anatomical direction in both strains from 1-4 hours post-MCAO (Figure 4-10).

4.3.5 Comparing penumbra calculation methods

Volumetric analysis generated lower volumes of mismatch tissue compared to spatial assessment in both strains from 1-4 hours post-MCAO (Figure 4-11). However, this difference did not reach the level of statistical significance at any time point. In WKY, mismatch volume defined by spatial assessment was 2 fold larger than mismatch volume determined by the volumetric method at 1 hour post-MCAO (43±43mm^3 vs 22±59mm^3, for spatial and volumetric assessment respectively, P>0.05, Figure 4-11A). However, in SHRSP at the same time point, mismatch volume identified by spatial assessment was comparable to the mismatch volume defined by volumetric assessment (36±15mm^3 vs 31±50mm^3, for spatial and volumetric assessment respectively, P>0.05, Figure 4-11B). In addition, the volumetric data were more variable than the data analysed using the spatial method in both WKY and SHRSP. In WKY, the coefficient of variation for the volumetric method was 268% compared to 100% for the spatial assessment method at 1 hour post-MCAO. Similarly, in SHRSP at the same time point, the coefficient of variation was larger for the volumetric mismatch method compared to the spatial assessment method (161% vs 42% for volumetric and spatial assessment, respectively).

There was no significant difference in penumbra volume calculated by volumetric or spatial perfusion-diffusion mismatch or ADC expansion from 1-4 hours post-MCAO in both strains (P>0.05, Figure 4-11). However, at 1 hour post-MCAO, penumbra volume as measured by ADC growth was higher than mismatch volume in both SHRSP and WKY. In

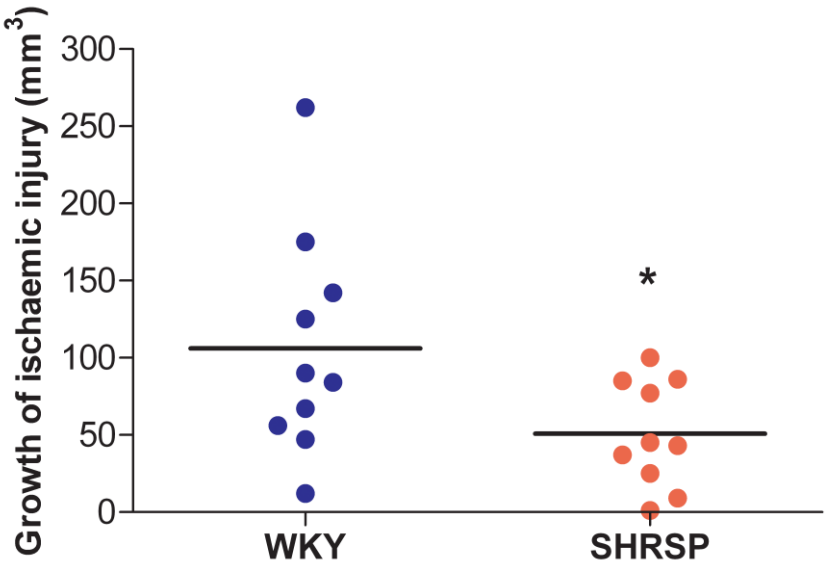

Figure 4-8. Growth of ischaemic injury from 30 minutes to 24 hours post-MCAO in SHRSP and WKY rats. Line denotes the mean. *p<0.05, Student's unpaired t test. WKY; n=10, SHRSP; n=10.

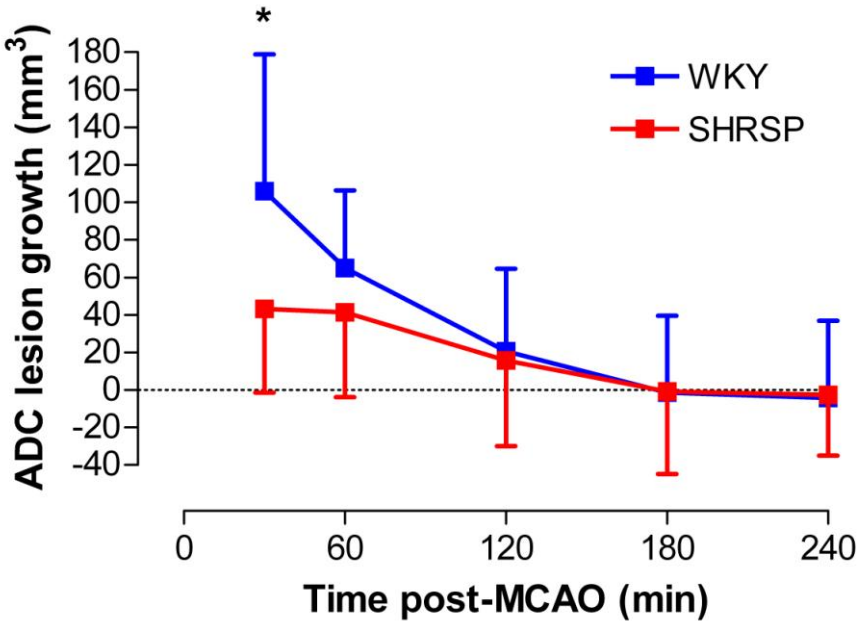

Figure 4-9. Growth of the ADC-derived lesion from 30 minutes to 4 hours post-MCAO. The ADC lesion at each time point was subtracted from final (oedema corrected) infarct volume to calculate the volume of penumbra in WKY (n=10) and SHRSP (n=10) following permanent MCAO. Data are presented as mean±SD. *p<0.05, 2-way ANOVA with Bonferroni's post-test.

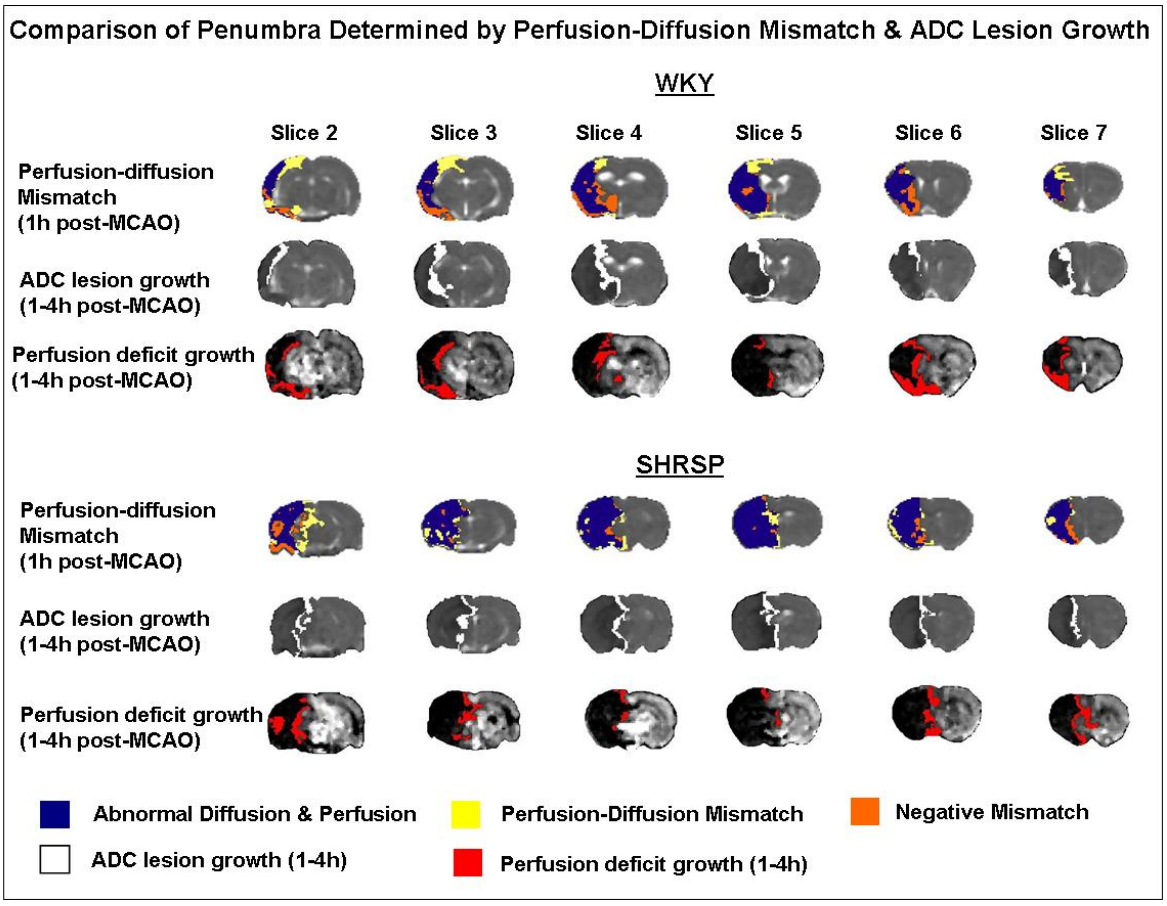

Figure 4-10. Comparison of potentially salvageable penumbra at 1 hour post-MCAO as determined by perfusion-diffusion mismatch (using pixel-by-pixel method) and ADC lesion expansion in a representative SHRSP and WKY rat. Pixel-by-pixel analysis assigns pixels to a tissue compartment according to the ADC and CBF value of each pixel. Penumbra volume was also defined by growth of the ADC-derived lesion, where penumbra at 1 hour post-MCAO can be defined by subtracting the ADC lesion at 1h from the ADC lesion at 4 hours post-MCAO, which matches the final infarct at 24 hours. The spatial distribution of the areas of perfusion deficit growth from 1-4 hours post-MCAO are also shown.

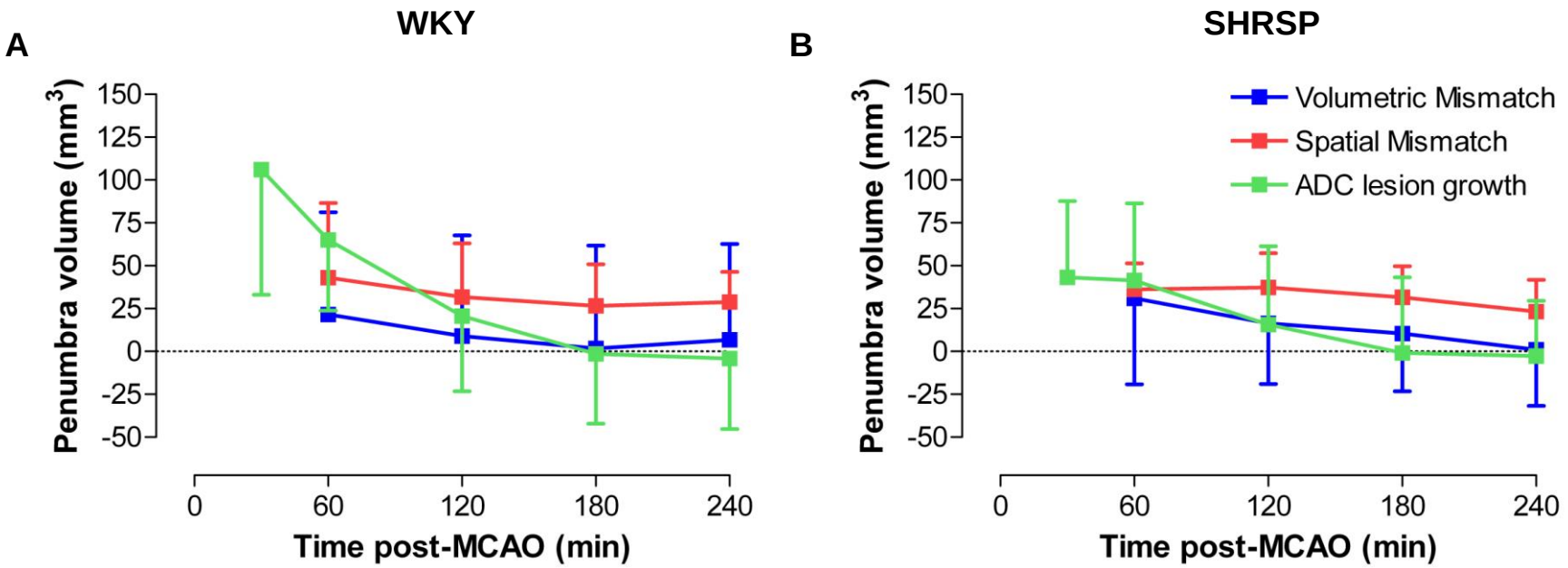

Figure 4-11. Comparison of the 3 methods used to define penumbra in SHRSP and WKY rats following permanent MCAO. Penumbra volume was determined; 1. by volumetric perfusion-diffusion mismatch, where the volume of ADC-derived ischaemic injury is subtracted from the volume of perfusion deficit (blue, WKY: n=12, SHRSP: n=15). 2. spatially, where mismatch area is manually delineated on each of 6 coronal slices to determine total mismatch volume (red, WKY: n=12, SHRSP: n=15). 3. by growth of the ADC-derived lesion, where the ADC lesion at each time point from 30 minutes to 4 hours post-MCAO was subtracted from the final, oedema-corrected infarct volume at 24h (green, WKY: n=10, SHRSP: n=10).

WKY, ADC expansion defined penumbra was 65±41mm^3 compared to 43±43mm^3 and 22±59mm^3 as determined by spatial and volumetric mismatch, respectively, although this was not statistically significant (P>0.05, Figure 4-11A). Similarly, in SHRSP at 1 hour post-MCAO, ADC expansion-defined penumbra was 41±45mm^3 compared to 36±15mm^3 and 31±50mm^3 as determined by spatial and volumetric mismatch, respectively (P>0.05, Figure 4-11B). At later time points, as penumbra volume, defined by ADC lesion growth, declines, penumbra defined by spatial assessment of mismatch volume persists until 4 hours.

The ADC-derived lesion evolves in an annular pattern, whereby the lesion expands relatively uniformly at its boundary (Figure 4-10). The anatomical location of the penumbra defined by this method therefore differs from that identified by perfusion-diffusion mismatch, where the penumbra is found almost exclusively within the cortex (Figure 4-10).

4.4 Discussion

Clinical research has recognised the need for a consensus in the method used to identify potentially salvageable tissue in stroke patients, as well as the need for universally accepted thresholds of tissue abnormality (Bandera et al, 2006). The perfusion-diffusion mismatch method of penumbra determination has yet to be validated in clinical and pre-clinical stroke research. This study is the first to compare different methods to define the ischaemic penumbra in a clinically relevant rodent stroke model with recognised risk factors. Strain-specific diffusion and perfusion thresholds were retrospectively applied to MRI data to define the ADC lesion and perfusion deficit used to calculate mismatch volume (volumetrically or spatially) during the acute phase of stroke in the SHRSP and its normotensive control strain, WKY. In addition to perfusion-diffusion mismatch, the ischaemic penumbra was determined indirectly by assessing expansion of the ADC-derived lesion over time.

Previous studies have reported a reduced volume of penumbral tissue in rat models with stroke risk factors. Following permanent MCAO induced by intraluminal filament, perfusion-diffusion mismatch was assessed over time in spontaneously hypertensive (SHR) and renovascular hypertensive WKY (RH-WKY) and normotensive WKY rats. Mismatch volume was comparable in both hypertensive groups at 30 minutes post-MCAO (66±25mm^3 and 55±17mm^3 in SHR and RH-WKY respectively), however, at the same

time point, normotensive WKY rats exhibited a significantly larger volume of mismatch tissue (117±14mm^3, P<0.01) (Letourneur et al, 2011). The mismatch volumes reported by this study group are comparable to the volume of penumbra reported in the present study at 30 minutes post-MCAO using the ADC lesion expansion method, where penumbra was significantly larger in normotensive WKY compared to the hypertensive SHRSP strain (106±73mm^3 and 43±45mm^3 in WKY and SHRSP respectively). However, Letourneur and colleagues reported that mismatch defined penumbra volume was significantly larger in normotensive WKY compared to SHR and RH-WKY at all time points, from 30 minutes to 4 hours post-MCAO. This differs from the findings of the present study where, penumbra volume was only significantly higher in WKY compared to SHRSP at 30 minutes post-MCAO and at all later time points there was no significant difference between the strains, irrespective of the penumbra calculation method used. This suggests that there may only be an increased potential for tissue salvage in the WKY within the first hour following stroke, compared to SHRSP, where penumbra salvage may be limited at all acute time points following permanent MCAO.

Furthermore, Legos and colleagues found no evidence of perfusion-diffusion mismatch in SHR rats from 1-3 hours following permanent MCAO and the DWI lesion at 1 hour matched the final infarct at 24 hours (Legos et al, 2008). The authors demonstrated a significant mismatch volume in normotensive Sprague-Dawley rats up to 2.5 hours post-MCAO. However, the SHR and Sprague-Dawley groups cannot be directly compared since SHRs underwent distal MCAO by electrocoagulation while Sprague-Dawley rats underwent proximal MCAO by intraluminal filament. Nevertheless, these studies suggest that hypertensive rat strains may have a limited potential for tissue salvage following permanent MCAO.

Previously, only one study has compared penumbra in SHRSP and WKY rat strains. McCabe and colleagues reported that perfusion-diffusion mismatch was significantly reduced in SHRSP compared to WKY at 1 hour following permanent MCAO (McCabe et al, 2009). However, mismatch was only assessed on a single coronal slice within the territory of the MCA and this limitation was recognised by the authors. Mismatch area in SHRSP was 3±6mm^2 compared to 10±4mm^2 in WKY (P<0.05). This differs from the present study, where there was no significant difference in mismatch volume, defined spatially and volumetrically, at 1 hour post-MCAO. The advantage of the present study is that the volume of mismatch (rather than area) was assessed across 6 slices covering the

MCA territory and therefore a more accurate assessment of differences in mismatch tissue was determined.

Mismatch volume has previously been determined in rodent stroke models by volumetric analysis (Meng et al, 2004; Bråtane et al, 2009; Henninger et al, 2009) and by spatial co-registration of MRI perfusion and diffusion images (Letourneur et al, 2011). In the current study, spatial assessment of penumbra gave rise to a small but measurable mismatch volume in SHRSP and WKY and although the SHRSP strain demonstrated a significantly larger perfusion deficit and ADC-derived lesion, mismatch volume was not significantly different between strains from 1-4 hours post-MCAO. However, volumetric analysis revealed a smaller mismatch volume in both strains. It has been reported previously in clinical research, that simple arithmetic subtraction of the DWI lesion from the PWI defined perfusion deficit underestimates penumbral mismatch by 40% compared to mismatch calculated by co-registering DWI and PWI (Ma et al, 2009). In addition, these authors reported that underestimation of mismatch by the simple volumetric method is exacerbated over time, as the ischaemic core expands to encompass the penumbra.

In the present study, pixel-by-pixel analysis revealed the presence of negative mismatch tissue, where the ADC-derived ischaemic lesion expands beyond the boundary of the perfusion deficit. The phenomenon of negative mismatch has been identified previously in rodent stroke models (Foley et al, 2010; Letourneur et al, 2011). Foley and colleagues defined tissue with a low ADC value and CBF above threshold, as a compartment of high-flow infarction. The term high-flow infarction may be misleading as tissue in this compartment may be hypoperfused relative to control CBF but is above the perfusion threshold (as shown in Figure 4-8). In addition, the tissue cannot be classed as infarct since it is being examined in the first 4 hours following stroke. There is both clinical and preclinical evidence that the ADC lesion has the capacity to return to normal ADC values following reperfusion within the first few hours following stroke (Minematsu et al, 1992; Hasegawa et al, 1994; Kidwell et al, 2000). Nevertheless, Foley and colleagues consistently identified tissue which was below their calculated ADC threshold and above their CBF threshold in the acute time period post-MCAO in Sprague-Dawley rats. Similarly, Letourneur and colleagues detected a tissue compartment which they defined as inverse perfusion-diffusion mismatch, where ADC is reduced but perfusion is normal. However, this study group only detected inverse mismatch tissue in hypertensive SHRs and RH-WKYs and did not identify inverse mismatch tissue in the normotensive control strain, WKY (Letourneur et al, 2011). This differs from the results of the present study,

where negative mismatch was identified in SHRSP and in WKY. However, these authors demonstrated evidence of inverse mismatch tissue located subcortically, in a similar anatomical location as reported in the present study.

Despite reports of negative mismatch tissue in the preclinical literature, the physiological basis of this tissue compartment has yet to be discussed. Negative mismatch tissue may potentially occur as a consequence of peri-infarct spreading depolarisations from the ischaemic core, which may increase cellular injury independently of cerebral blood flow, therefore extending the outer boundary of injured tissue beyond the perfusion deficit. High levels of potassium ions and glutamate in the ischaemic core can actively propagate tissue depolarisation, ionic imbalances and glutamate release into adjacent tissue and it has been reported that in rats, peri-infarct depolarisations can originate in the striatum (Hartings et al, 2003). This may explain the location of negative mismatch tissue observed in this study and by others (Foley et al, 2010; Letourneur et al, 2011). Increased levels of potassium ions and glutamate can induce vasodilatation, where glutamate acts via several calcium dependent mechanisms (Drake & Iadecola, 2007). This may increase blood flow in hypoperfused tissues at the boundary of the ischaemic core and contribute to the phenomenon of negative mismatch. Flow independent infarct growth has been reported both in human stroke patients (Heiss et al, 2001) and more recently, in rodent stroke models, where at 12 hours post MCAO, 9% of brain tissue was necrotic but did not demonstrate any flow restrictions (Woitzik et al, 2009). In addition, the extracellular concentration of excitatory amino acids and free radicals produced by severely hypoperfused tissue within the ischaemic core may be increased by cytotoxic oedema, enhancing the spread of detrimental effects to neighbouring tissue, and contributing to expansion of the core (Loubinoux et al, 1997). This illustrates how the influence of toxic mediators is not restricted to their site of origin and can influence tissue which does not fall below the critical blood flow threshold.

It has been previously suggested that the phenomenon of negative mismatch arises from intersubject variations associated with the use of fixed perfusion and diffusion thresholds (Shen et al, 2003). However, the present study demonstrated that although the negative mismatch tissue compartment is hypoperfused relative to the contralateral hemisphere, blood flow is significantly higher than the CBF threshold calculated for each strain. This eliminates the possibility that negative mismatch tissue arises solely as a result of inaccuracy in determining perfusion thresholds and suggests that it is a true phenomenon which can be detected in acute stroke.

In the present study, negative mismatch tissue is consistently identified in the sub cortex, particularly in the region of the caudate putamen and the globus pallidus. This finding is in agreement with previous reports, where negative mismatch tissue was found in a similar anatomical location (Foley et al, 2010; Letourneur et al, 2011). In the present study, negative mismatch tissue was consistently identified across all 6 coronal slices. However, Letourneur and colleagues only detected inverse perfusion-diffusion mismatch on coronal slices located within the core of the MCA territory, equivalent to slices 4, 5 and 6 as defined in the present study.

The volume of negative mismatch tissue was comparable between the strains and did not change over time. This finding is in agreement with Foley et al (2010) who recently reported the persistence of negative mismatch tissue over the first 4 hours following permanent MCAO.

Although the volumetric analysis method can be used to provide a quick and simple measure of penumbra, the inclusion of negative mismatch tissue by this method limits its use, as penumbra volume may be underestimated. Conversely, the volumetric mismatch method may overestimate penumbra as the ventricles are included as a component of the perfusion deficit. Study groups who have used this method have failed to report whether they excluded the ventricles (Meng et al, 2004; Bråtane et al, 2009; Henninger et al, 2009). This may have a major influence on strain comparisons of penumbra volume. This is particularly evident when comparing WKY and SHRSP, since the ventricles are substantially larger in WKY, as observed in the present study. However, this did not appear to influence strain comparisons in this study as mismatch volume was not significantly different in SHRSP and WKY. However, it is still an important point to consider, as failure to exclude the ventricles could potentially contribute to false positive results when comparing perfusion-diffusion mismatch in SHRSP and WKY rat strains.

In addition, the volumetric method provides no information regarding the anatomical location of penumbra or its extent throughout the territory of the middle cerebral artery. Furthermore, there is greater variability in the data analysed using the volumetric method compared to spatial assessment of mismatch. This may arise due to intersubject variation in the volume of negative mismatch tissue which is included when using the volumetric mismatch method. The concept of negative mismatch does not apply with the spatial mismatch method since only regions of perfusion deficit which show no ADC abnormality are included in the calculation of penumbra. Using this method, the volume and anatomical location of the penumbra can be determined throughout the MCA territory and temporal

changes in the evolution of ischaemic injury and the region of hypoperfused tissue can be investigated, making it a much more informative method than simple arithmetic subtraction of the two volumes.

Despite its widespread use as a research tool, the mismatch model has been criticised for the inclusion of benign oligaemic tissue within the perfusion deficit and for the assumption that the diffusion lesion represents irreversibly damaged infarct core, when it has been demonstrated that the DWI lesion can be completely or partially reversed if reperfused within 3 hours of stroke (Minematsu et al, 1992; Hasegawa et al, 1994; Kidwell et al, 2000), although more recent data suggest that only a small component of the DWI lesion is reversible. Chemmanam and colleagues reported that only 6 out of 93 stroke patients demonstrated minor regions of DWI lesion reversal when acute DWI data was compared to subacute DWI or T_2 weighted images acquired at 90 days following stroke onset (Chemmanam et al, 2010). Criticisms of the PWI/DWI mismatch model led to the construction of a revised technique where thresholds are used to distinguish between the perfusion deficit and benign oligaemic tissue and also recognises that a component of the DWI lesion may be salvaged and therefore comprises a component of the penumbra (Kidwell et al, 2003).

In clinical research, DWI lesions provide an approximation of ischaemic injury, whereas more often in experimental stroke research, the ADC-derived lesion is favoured. Calculating growth of the DWI or ADC lesion over time is an alternative indirect method of determining potentially salvageable tissue and this technique has been used in clinical research to examine infarct growth and define penumbra in patients where perfusion imaging was unavailable (Dani et al, 2010). Karonen et al, (2000) reported a significant correlation between DWI lesion growth and the zone of hypoperfused tissue at the boundary of the iachaemic core, which correlated significantly with infarct growth over the following week in 16 stroke patients. Furthermore, these authors reported that infarct growth correlated significantly with clinical outcome. Conversely Butcher et al (2005) failed to identify a significant correlation between mismatch volume and infarct growth. The correlation between DWI lesion growth and mismatch volume may be dependent on the perfusion parameter, as these conflicting studies used different parameters to define the hypoperfused region. Karonen et al, assessed tissue hypoperfusion using SPECT, while Butcher and colleagues used contrast agent bolus tracking to acquire MRI perfusion weighted images.

The DWI lesion growth method provides a retrospective analysis of penumbral volume as the DWI lesion must proceed to infarction to allow salvageable tissue at a particular time point post-stroke to be calculated. Therefore, although a useful research tool, this method is unsuitable for identifying patients suitable for acute stroke therapy. In addition, Dani et al (2010) recognised that this method could potentially overestimate penumbra due to acute tissue swelling. However, in the present study, during the acute phase (within the first 4 hours) there was no evidence of brain swelling, which could influence the calculation of lesion growth, as discussed in the previous chapter.

Penumbra as assessed by ADC lesion growth provides no information regarding temporal alterations in the volume of perfusion deficit and therefore limits the use of this method. Serial imaging in our study revealed an increase in the volume of perfusion deficit over the first 4 hours post-MCAO in both SHRSP and WKY, as described in detail in the previous chapter. Temporal increases in perfusion deficit of a similar magnitude to the growth in ADC lesion will result in a persistence of penumbra volume over time as demonstrated by spatial mismatch analysis, with some existing penumbra being recruited into ischaemic core, as new tissue is incorporated into penumbra. Differences in the anatomical location of the penumbra as defined by the spatial mismatch method and ADC lesion expansion can be explained by the increase in perfusion deficit over time. Growth of the ADC-derived lesion volume at each time point does not take into account the evolving perfusion deficit since it is derived from diffusion data at a later time point or the final infarct volume at 24 hours. In contrast, spatial assessment of mismatch volume uses the perfusion deficit at that each time point and therefore provides a snapshot of hypoperfused tissue capable of responding to reperfusion or neuroprotective intervention.

Summary

The results from this study demonstrate that the hypertensive SHRSP strain may have a reduced potential for penumbra salvage compared to the normotensive control, WKY. However, this is only evident within the first hour following stroke onset. At later time points, from 1-4 hours post-MCAO, neither strain exhibits a significant penumbra volume and there is no significant difference in penumbra volume between the strains, irrespective of the method used to calculate penumbra. The results of this study have also demonstrated that volumetric assessment of mismatch determines a lower volume of mismatch tissue, compared to the spatial assessment method, where a measurable volume of penumbra is detected in both strains. ADC lesion expansion was also examined but this method does not utilise perfusion data and can only be used retrospectively. The method

used to detect penumbra is crucial in pre-clinical MRI research, particularly if assessing potential therapeutic strategies to salvage penumbra, and clinically, where penumbral volume is used as a criterion for identifying those patients who are most likely to benefit from thrombolytic therapy or for recruitment of patients into clinical trials. On the basis of the results of the present study, the spatial assessment method is the most informative method of penumbra determination, as it utilises both perfusion and diffusion data and allows spatial evaluation of mismatch.

Chapter 5.

The effect of NADPH oxidase inhibition with apocynin on stroke outcome following permanent and transient ischaemia

5.1 Introduction

Oxidative stress pathways are a major mediator of irreversible cellular injury following ischaemic stroke. Ischaemia induces the generation of free radical species which overwhelm the endogenous scavenging capacity of cellular antioxidant defences. Free radical species contribute to cellular injury by mediating enzyme inactivation, protein denaturation, lipid peroxidation and damage to DNA and cytoskeletal components (Brouns & De Deyn, 2009). In addition to the reactive oxygen species, superoxide (O_2^-), hydroxyl (OH^-) and the non radical, hydrogen peroxide (H_2O_2), a number of reactive nitrogen species are generated following cerebral ischaemia. These include nitric oxide (NO), which has a protective role by mediating vasodilatation to increase cerebral blood flow. However, increased levels of superoxide under ischaemic conditions reduce the bioavailabity of nitric oxide and therefore limit its vasoprotective action. Superoxide and endothelium derived nitric oxide react to form peroxynitrite ($OONO^-$), which is a highly reactive nitrogen species which also contributes to cellular injury.

Under normal physiological conditions, superoxide is constitutively produced and can act as a cell signalling molecule to influence the tone and proliferation of vascular smooth muscle cells (Miller et al, 2006). However, superoxide has poor membrane permeability due to its negative charge and it has a very short half life which may limit its direct impact on vascular function under normal conditions (Miller et al, 2006). Nevertheless, superoxide can promote vasodilatation of cerebral microvessels although under ischaemic conditions, it generally promotes vasoconstriction by inactivating endothelial nitric oxide synthase (Paravacini et al, 2004).

Until recently, it was widely accepted that under ischaemic conditions, mitochondria were the major source of reactive oxygen species, such as superoxide. However, recent evidence suggests that NADPH oxidase is the principal source of superoxide anions during ischaemia (Brennan et al, 2009). NADPH oxidases are a family of enzyme complexes with the sole function of generating reactive oxygen species. Each isoform of NADPH oxidase is distinguished by the membrane spanning catalytic subunit that it utilises to transfer electrons from NADPH to molecular oxygen to generate superoxide (Selemidis et al,

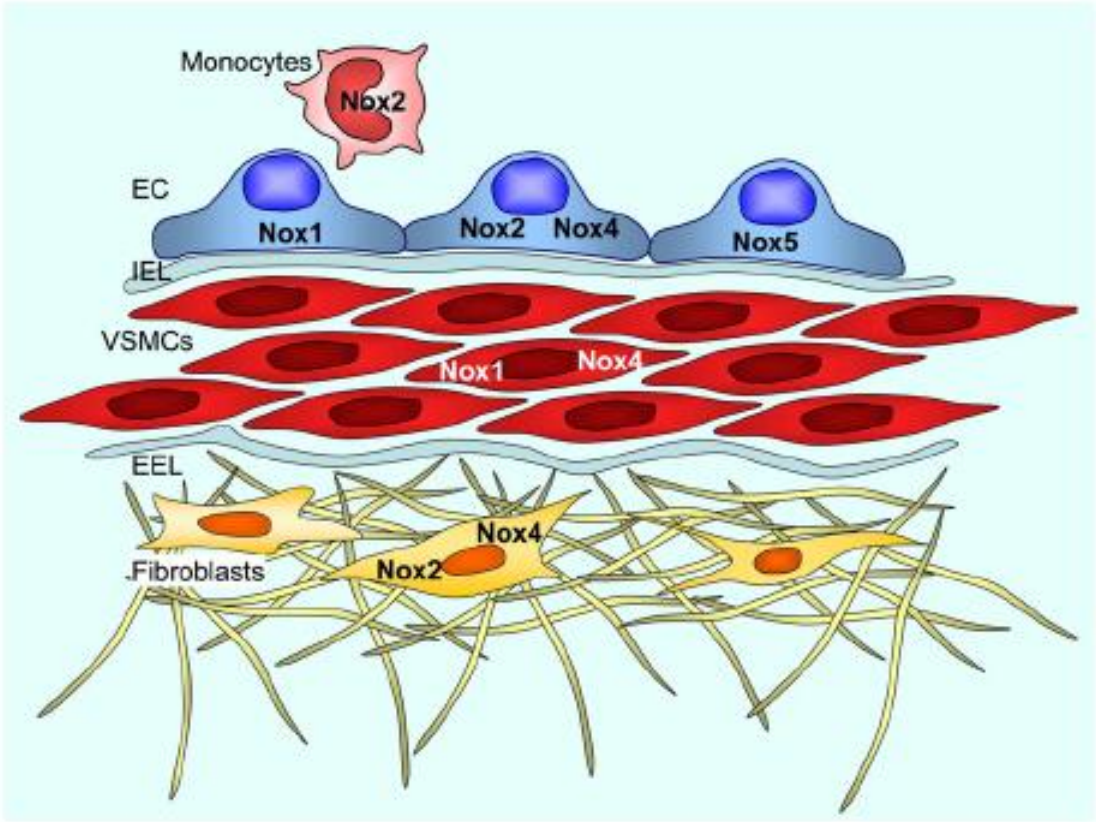

Figure 5-1. The cellular distribution of NADPH oxidase isoforms in the vascular wall. Nox1, Nox2, Nox4 and Nox5 are expressed in endothelial cells (EC). Adventitial fibroblasts express Nox2 and Nox4 and vascular smooth muscle cells (VMSCs) express Nox1 and Nox4. Reproduced from Selemidis et al (2008).

2008). Four isoforms of NADPH oxidase are expressed in the vascular wall (Figure 5-1). Nox1 is expressed in endothelial and vascular smooth muscle cells; Nox2 is expressed in endothelial cells and adventitial fibroblasts; Nox4 is expressed in vascular smooth muscle cells, adventitial fibroblasts and endothelial cells and Nox5 is expressed in endothelial cells only (Selemidis et al, 2008). In addition, the Nox2 isoform is also expressed in neutrophils, macrophages, T cells and platelets. However, the specific role of reactive oxygen species derived from each isoform in stroke is unclear (Miller et al, 2006). Localisation studies have demonstrated that Nox2 and Nox4 are highly localised in the hippocampus and cerebral cortex of mouse brain, with Nox2 upregulation following stroke reported to contribute to oxidative stress-induced neuronal cell death (Serrano et al, 2003; Vallet et al, 2005).

The role of NADPH oxidase in the generation of reactive oxygen species during ischaemia has made it an important target for neuroprotection and there is great interest in developing therapeutic strategies that target NADPH oxidase-derived reactive oxygen species in the treatment of vascular disease. Apocynin (4'-hydroxy-3'-methooxyacetophenone) is a methoxy-substituted catechol which was originally isolated from the roots of Canadian hemp in the late 1800s. It is capable of crossing the blood brain barrier (BBB) and has low toxicity (Tang et al, 2008). It inhibits NADPH oxidase activity by blocking the association of cytosolic components (i.e. the migration of the cytosolic p47phox subunit) with the membrane bound catalytic core (Stolk et al, 1994). However, the mechanism of action of apocynin is not well understood and it is not yet clear whether it inhibits NADPH oxidase directly or by blocking the activity of an upstream element which leads to assembly of the enzyme (Selemidis et al, 2008). Furthermore, there is evidence to suggest that apocynin is a pro-drug and requires activation by cellular myeloperoxidase activity to form metabolically active diapocynin, before it can inhibit NADPH oxidase subunit assembly (Simons et al, 1990; Stolk et al, 1994).

Inhibition of NADPH oxidase by apocynin has been shown to have neuroprotective effects in rodent stroke models. However, to date, all the published studies evaluating the efficacy of apocynin have used transient ischaemia models and there are no reports of the efficacy of apocynin treatment following permanent cerebral ischaemia. Wang and colleagues demonstrated the protective effect of apocynin in a global ischaemia-reperfusion model, where apocynin protected against oxidative stress in the hippocampus of the gerbil (Wang et al, 2006). In a mouse transient focal cerebral ischaemia model, pre-treatment with apocynin reduced brain superoxide levels at 24 hours post-ischaemia (Jackman et al,

2009). Significant improvements in stroke outcome have been reported following apocynin treatment in mouse ischaemia-reperfusion models, where infarct volume has been reduced by up to 50% of control groups at 24 hours post-MCAO (Tang et al, 2008; Chen et al, 2009). Similar results have been observed in rat ischaemia-reperfusion models. Tang and colleagues observed a significant reduction in infarct volume at 24 hours post-MCAO following apocynin administration 1 hour hour after stroke onset in Sprague-Dawley rats. NADPH oxidase activity and superoxide levels were also significantly reduced (Tang et al, 2007). More recently, Genovese and colleagues reported that intraperitoneal administration of 5mg/kg apocynin 5 minutes prior to reperfusion significantly improved behavioural outcome and reduced both cortical and striatal damage compared to vehicle-treated rats (Genovese et al, 2011).

Despite these encouraging reports, there is a lack of pre-clinical studies examining the potential neuroprotective effects on animals with stroke risk factors. To date, only one group has evaluated apocynin in an animal model with a known stroke risk factor, in this case, age. It was reported that apocynin treatment exhibited a neuroprotective effect in young rats, however, when administered to aged rats, apocynin exacerbated ischaemic injury and increased mortality rate (Kelly et al, 2009). Furthermore, NADPH oxidase inhibition with apocynin has yet to be evaluated in rodent stroke models with genetic stroke risk factors, such as hypertension. It is essential that all potential neuroprotective therapies are assessed in animal models with stroke co-morbidities before being considered for clinical trial, to improve the likelihood of a favourable outcome in human stroke patients. The Stroke Therapy Academic Industry Roundtable (STAIR) recommended the use of preclinical models with stroke co-morbidities following the repeated failures of stroke therapies in clinical trials. The predominant use of homogenous animal models with optimised physiological variables is believed to be a factor in the failure of translation from bench to bedside (Saver et al, 2009).

Oxidative stress in the vasculature has been associated with genetic and experimental hypertension. In SHR rats it has been reported that expression of NADPH oxidase subunits is increased, as well as increased activity of the enzyme in the vasculature (Zalba et al, 2000). This leads to increased production of superoxide anions which can reduce the bioavailability of nitric oxide by promoting the formation of peroxynitrite (Figure 5-2) resulting in dysfunction of the endothelium and impaired vasodilatation (Alexander et al, 2000). It has also been demonstrated that NO bioavailability is reduced in aged WKY and SHRSP compared to young rats. An increase in superoxide production in aged WKY and

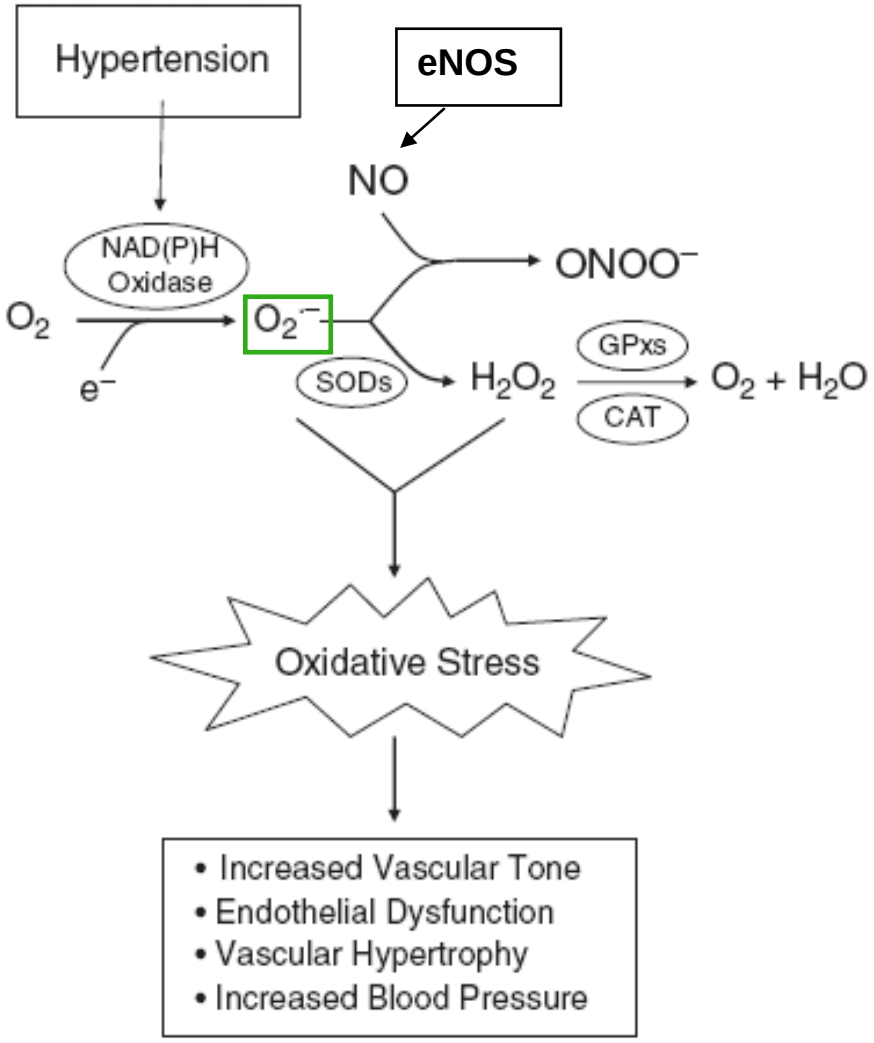

Figure 5-2. The role of oxidative stress in vascular dysfunction. Hypertension induces increased expression and activity of NADPH oxidase leading to enhanced production of superoxide anions (O_2^-) (shown in green) and subsequently, nitric oxide (NO) bioavailabilty is reduced with increased formation of peroxynitrite ($OONO^-$). Increased levels of oxidative stress in hypertension contribute to vascular dysfunction by inhibiting endothelium-mediated vasodilatation and increasing vascular tone, which exacerbates hypertension. Modified from Didion et al (2008).

SHRSP may contribute to the reduced NO bioavailability by scavenging (Hamilton et al, 2001). In addition, SHRSPs demonstrate increased levels of 20-HETE, which is a potent vasoconstrictor which further promotes the generation of superoxide (Cheng et al, 2008; Dunn et al, 2008). Increased levels of superoxide in SHRSP also arise as a result of reduced activity of SOD (Kishi et al, 2004). Furthermore, the activity of endothelial nitric oxide synthase (eNOS) is impaired in SHRSP compared to WKY rats (Yoshitomi et al, 2011). All of these factors contribute to the increased levels of oxidative stress demonstrated by SHRSP and therefore this strain may be particularly amenable to neuroprotection by inhibition of NADPH oxidase with apocynin.

Study Aims

The aims of this study were:

(1) to assess the effects of apocynin treatment on stroke outcome following permanent MCAO
(2) to assess the effects of apocynin treatment on stroke outcome in a model of transient focal ischaemia
(3) to evaluate the influence of apocynin treatment on the acute evolution of penumbral tissue in a rat model displaying known stroke risk factors (SHRSP) using the MRI perfusion-diffusion mismatch model

5.2 Methods

5.2.1 Power Calculations

The sample size in each treatment group was determined prior to the commencement of each study using a priori power analysis calculator (http://www.stat.ubc.ca/~rollin/st/ssize). Based on the reductions in infarct volume with apocynin treatment reported previously (Tang et al, 2007; Genovese et al, 2011), to detect a 35% reduction in infarct volume with a common standard deviation (σ) of 20, would require a sample size of 6 rats in each group, where the type I error rate (α) is 0.05 and the power is 0.80.

5.2.2 Apocynin Dosage

Low (5mg/kg) and high dose (30mg/kg) apocynin treatment was evaluated in this study. These doses were selected due to the disparity in apocynin dosage reported in previous rat studies, where some study groups administered apocynin intraperitoneally at a dose of 50mg/kg (Tang et al, 2007), while other investigators demonstrated neuroprotective efficacy using smaller doses of apocynin, up to 5mg/kg (Kelly et al, 2009; Genovese et al, 2011).

Apocynin was dissolved in 0.1% dimethylsulphoxide (DMSO). The vehicle used was 0.1% DMSO. The rats in all studies discussed in this chapter received 5 mg/kg apocynin, 30mg/kg apocynin or 1.5ml of 0.1% DMSO (vehicle). In the permanent MCAO study (Study 1) rats received treatment by intraperitoneal injection. In the transient MCAO studies (Studies 2 and 3) treatment was administered intravenously.

5.2.3 Randomisation and Blinding

Allocation of rats to treatment group was randomised using a random number generator (http://www.randomization.com). Each rat was given a number and the generator randomly allocated a treatment of vehicle, low dose or high dose apocynin to each number. A copy of this treatment schedule was kept by 3 colleagues within the department. On the day of each experiment, the rat was weighed and the volume of 5mg/kg and 30mg/kg to be administered was calculated and written on the back of an experimental procedures card along with 1.5ml of vehicle. Prior to drug administration, one of the three colleagues with the treatment schedule would prepare the appropriate drug treatment by drawing up the appropriate volume of drug into a 2ml syringe following consultation of the experimental procedures card. Sticky tape was then wrapped around the syringe to conceal the volume of drug. The unused eppendorfs and the flask containing the vehicle were then returned to the freezer and the fridge respectively. These procedures ensured total blinding of the treatment administered to each animal. At the end of the experiments, when all behavioural assessments had been performed and all data analysis pertaining to stroke outcome had been analysed, the treatment administered to each animal was revealed. This prevented any bias when analysing the stroke outcome data.

5.2.4 Permanent Focal Ischaemia (Study 1)

Male WKY rats (n=24) aged 12-16 weeks and weighing 270-330g were used in this study. Rats were randomly allocated to one of the three treatment groups as described previously: 1.5ml vehicle (0.1% DMSO) (n=8), 5mg/kg apocynin (n=8), 30mg/kg apocynin (n=8). On the day prior to surgery, vibrissae evoked forelimb placement was assessed as described in Chapter 2 to ensure that rats showed no limb preference or neurological impairment.

On the day of surgery, rats were initially anaesthetised in an anaesthetic chamber where 5% isoflurane was administered in a 30%/70% mixture of oxygen and nitrous oxide, respectively. Once deeply anaesthetised, rats were immediately transferred to a face mask where surgical anaesthesia was maintained with 2-2.5% isoflurane delivered in a 30%/70% mixture of oxygen and nitrous oxide. The face mask was secured by to the cork surgical board using sticky tape. Body temperature was measured by a rectal thermocouple and maintained at 37±0.5ºC using an angle poise lamp. The neck of the rat was shaved using an electric shaver and permanent focal ischaemia was induced as previously described (Chapter 2.1.2), where a silicon tipped filament (diameter 0.31-0.35mm, length 5-6mm, Doccol) was introduced into the external carotid artery and advanced along the internal carotid artery to block the origin of the middle cerebral artery. The filament was secured in place by electrocoagulation of the incision site located within the external carotid artery stump, using diathermy forceps. The neck was stitched using 4-0 silk suture. Drug treatment was then administered at 5 minutes post-MCAO by intraperitoneal injection.

The rat was then allowed to recover from anaesthesia by delivery of 100% oxygen through the facemask. When the rat started to move, it was transferred to a recovery cage lined with soft absorbent pads and bedding, with a cardboard tube for environmental enrichment. The cage was kept in a small quiet room, where temperature was maintained between 22-24^{o}C. Rats were given a soft diet of baby food mixed with rat chow pellets, with water and solid chow pellets freely available. The general condition of the rat was assessed at least 3 times on the day of surgery and was recorded.

At 24 hours post-MCAO, functional outcome was assessed using the vibrissae-evoked forelimb placement test and the modified Bederson Score, as described in detail in Chapter 2. Following behavioural assessment, the rat was anaesthetised in an anaesthetic chamber (5% isoflurane in 70/30 $N_20/0_2$ mixture) and transferred to the MRI scanner where anaesthesia was maintained via a face mask (2% isoflurane in 70/30 $N_20/0_2$ mixture) and a RARE T_2 weighted sequence was acquired to allow calculation of final infarct volume (Chapter 2.2.3). The rat was then sacrificed by perfusion-fixation (Chapter 2.1.3).

5.2.5 Transient Focal Ischaemia (Study 2)

Male Sprague-Dawley rats (n=24) weighing 300-350g were randomly allocated to one of the three treatment groups: 1.5ml vehicle (0.1% DMSO) (n=9), 5mg/kg apocynin (n=8), 30mg/kg apocynin (n=7). On the day prior to surgery, vibrissae evoked forelimb placement was assessed as described in Chapter 2 to ensure that rats showed no limb preference or neurological impairment.

On the day of surgery, rats were anaesthetised, intubated and artificially ventilated (Chapter 2.1.1). Rats were then given an intraperitoneal injection of 0.4ml of atropine sulphate (600mcg/ml) to limit bronchial secretions The ventral surface of the right hindlimb and the neck were shaved using an electric shaver. The right femoral artery was cannulated to allow continuous monitoring of heart rate and MABP (Biopac) with blood sampling performed 30 minutes prior to MCAO and 30 minutes post-MCAO to ensure blood pH, $PaCO_2$ and PaO_2 (Bayer, Rapidlab 248) were maintained within the physiological range. The right femoral vein was cannulated to allow intravenous administration of drug treatment. It was decided that intravenous administration was preferable to intraperitoneal administration to reduce potential variability in the dose of drug delivered and to speed up the drug reaching a therapeutic concentration in the brain. Body temperature was measured by a rectal thermocouple and maintained at 37±0.5ºC by an angle poise lamp.

Transient focal ischaemia was induced as previously described in detail (Chapter 2.1.2). In brief, a silicon tipped filament was introduced into the common carotid artery and advanced along the internal carotid artery to occlude the proximal origin of the middle cerebral artery. Drug treatment was administered at 5 minutes following the induction of ischaemia by gradually infusing the drug intravenously over a period of 3 minutes. At 1 hour post-MCAO, the intraluminal filament was removed by slowly retracting it using curved edge forceps and the incision point was electrocoagulated using diathermy forceps. The neck was flushed with sterile saline to clean the surgical area and was then stitched, as previously described (Chapter 2.1.2).

At this point, the dose of isoflurane was reduced to 1% to aid the speed of recovery from anaesthesia at the end of surgery. The ligatures around the right femoral artery were cut and the cannula was removed. The vessel was sealed by electrocoagulation using diathermy probes. The same procedure was performed to remove the venous cannula. Care was taken when electrocoagulating the artery and vein to preserve flow within the vessel. This was achieved by only electrocoagulating the incision point. Restoration of flow within the femoral vessels will aid the recovery and minimise post-operative pain. The hindlimb

incision site was then sutured and the rat was allowed to breathe 100% oxygen for a period of 15-20 minutes to aid recovery from anaesthesia before removal of the intubation tube, as described previously (Chapter 3.1.3).

The rat was then placed in a recovery cage with soft bedding and soft diet. General condition was assessed at least 4 times daily and was recorded. Behavioural testing was performed at 24, 48 and 72 hours post-MCAO. The 18-point neurological score assessment was followed by vibrissae-evoked forelimb placement and the modified Bederson score. Animals were also weighed following behavioural assessment as an additional indicator of general condition. At 72 hours post-MCAO, rats were euthanased in an anaesthetic gas chamber and the brain was processed for TTC staining as previously described in detail (Chapter 2.2.2). The TTC defined infarct volume was corrected for swelling of the ipsilateral hemisphere using the following equation (Swanson et al, 1990):

Corrected lesion volume = volume of contralateral hemisphere - (volume of ipsilateral hemisphere – lesion volume)

5.2.6 Effect of Apocynin on the Acute Evolution of Ischaemic Injury in the SHRSP (Study 3)

In the third study examining the potential neuroprotective effects of apocynin, 12 SHRSP rats aged 16-20 weeks, weighing 250-300g, were used. Mean systolic blood pressure was determined in the weeks prior to surgery using tail cuff plethysmography (Chapter 2.4.4). Rats were randomly allocated to the vehicle group (n=6) or the 5mg/kg apocynin group (n=6). Treatment was administered at 5 minutes post-MCAO, which was 55 minutes prior to reperfusion. Only one dose of apocynin treatment was evaluated due to time constraints and the lower dose was selected on the basis of the results from the previous ischaemia-reperfusion study.

Rats were initially anaesthetised in an anaesthetic gas chamber, intubated and artificially ventilated as previously described (Chapter 2.1.1) and then given an intraperitoneal injection of 0.4ml of atropine sulphate (600mcg/ml) to limit bronchial secretions. The right femoral artery and vein were cannulated to allow for continuous monitoring of physiological parameters and drug administration, respectively. Arterial blood sampling every hour ensured blood pH, $PaCO_2$ and PaO_2 (Bayer, Rapidlab 248) were maintained within the physiological range. Transient focal ischaemia was induced (Chapter 2.1.2)

using a silicon tipped filament (diameter 0.31-0.35mm, length 5-6mm, Doccol) which was glued to a 30cm length of 2-0 thread at its distal portion. The ligatures around the common, internal and external carotid arteries were tied securely to hold the filament in place and to prevent blood loss. The neck was sutured and the length of 2-0 thread was allowed to hang freely outside the wound. At 5 minutes post-MCAO, drug treatment was administered intravenously over a 3 minute period.

ECG leads were positioned on the ventral surface of the chest and the left hindlimb and the rat was then immediately transferred to the MRI scanner (Bruker, 7T Pharmascan). The rat was secured in the cradle by tooth and ears bars and a 4-channel phased array rat head surface receiver coil was placed on the head. Body temperature was maintained during the MRI scanning procedure by a heat pad placed over the body and was monitored by a rectal thermocouple.

Once a pilot sequence had been obtained to ensure correct geometry, a 4-shot spin echo planar imaging (EPI) DWI scan (TE=22.5ms, TR=4000.3ms, matrix=96x96, FOV=25x25mm, 3 directions=x, y, z, B-values=0 and 1000s/mm^2, 8 coronal slices; 1.5mm thick) was immediately performed and was repeated at 30 minutes post-MCAO to allow quantitative ADC map production and assessment of ischaemic injured tissue. This was followed by a time of flight (TOF) angiography scan to ensure that the middle cerebral artery had been completely occluded. A DWI scan was acquired just prior to reperfusion, at 1 hour post-MCAO. The filament was then retracted while the rat was in the MRI scanner. This was achieved by pulling the length of 2-0 thread 1.5cm distally, to retract the filament from the origin of the middle cerebral artery to permit reperfusion of the MCA territory. A TOF angiography scan was then performed to confirm that the left middle cerebral artery had reperfused. This was followed by a DWI scan and further DWI scans acquired every 30 minutes following reperfusion until 3 hours post-MCAO.

Perfusion weighted images were acquired using a form of continuous arterial spin labelling (cASL) based on a train of adiabatic inversion pulses (Moffatt et al, 2005). The sequence employs a spin-echo EPI imaging module (TE=20ms, TR=7000ms, matrix=96x96, FOV=25x25mm, slice thickness 1.5mm, 16 averages, 4 shots) preceded by 50 hyperbolic secant inversion pulses in a 3 second train. Inversion pulse frequency offset and gradient strength were set to provide 10mm wide label/control bands centred at ±30mm from the centre of the imaging slice. PWI were acquired for slices 3-6 of the DWI scan, (as time did not permit data acquisition across all 8 slices) and were acquired every hour for 3 hours post-MCAO. For quantification of CBF maps, T_1 maps were also acquired at each hour

post-MCAO, using an EPI inversion recovery sequence (TE=20ms, TR=10000ms, matrix=96x96, FOV=25x25mm, slice thickness 1.5mm, 16 averages, 4 shots, using 16 inversion times).

At 3 hours post-MCAO, the rat was removed from the MRI scanner and transferred back to the operating theatre where surgical anaesthesia was maintained. The sutures in the neck were cut and the ligatures around the internal carotid artery and the upper common carotid artery were loosened to allow the filament to be removed. The incision site was then electrocoagulated and the remaining ties were removed. The neck wound was then re-sutured and the femoral arterial and venous cannulae were removed and the rat was allowed to recover from surgery as previously described (Chapter 5.1.4.). Behavioural testing was performed at 24, 48 and 72 hours post-MCAO. T_2 weighted images were acquired at 24 hours and at 72 hours post-MCAO, animals were then euthanased and the brain was processed for TTC staining (Chapter 5.1.4). However, in this study, the rat brains did not fit into the rat brain matrix due to extensive brain swelling. Therefore, following removal from the skull, brains were rinsed in heparinised saline and put into the freezer at -46^{o}C for 15 minutes. The brains were then cut freehand using a razor blade into coronal sections, approximately 2mm thick and TTC staining was then performed.

5.2.7 Data analysis

In all studies, infarct volume was corrected for brain oedema as previously described (Chapter 2.2.3). In the permanent MCAO study, final infarct volume was assessed at 24 hours post-MCAO by manual delineation of hyperintense areas on T_2 slices, as previously described in detail (Chapter 2.2.3). In the transient MCAO studies, infarct volume at 72 hours post-MCAO was determined by manual delineation of infarcted tissue on TTC stained brain slices using Image J software (Chapter 2.2.2).

The acute serial MRI study data were processed to generate quantitative ADC maps and CBF maps (Chapter 3.1.4). The calculated SHRSP ADC threshold of 0.59 x 10^{-3}mm^2/sec (determined in Chapter 3) was applied to the quantitative ADC maps acquired at each time point to assess the acute evolution of ischaemic injury over the first 3 hours post-MCAO. Similarly, the in-house strain specific CBF threshold of 36ml/100g/min was applied to quantitative CBF maps acquired during ischaemia to determine the volume of perfusion deficit. Perfusion-diffusion mismatch was then measured across coronal slices 3-6 by overlaying the area of ADC derived ischaemic injury at 1 hour post-MCAO onto the

corresponding thresholded CBF map. The remaining perfusion deficit was measured on each slice to calculate mismatch volume, with the exclusion of the ventricles.

5.2.8 Statistical Analysis

In the permanent MCAO study, infarct volume at 24 hours post-MCAO was compared across treatment groups using one-way ANOVA with Bonferroni's post-test. In the transient ischaemia study in Sprague-Dawley rats, infarct volume at 72 hours post-MCAO was also compared across the 3 treatment groups using one-way ANOVA with Bonferroni's post-test. Temporal changes in physiological parameters within treatment groups were assessed by a paired t test. Differences in physiological parameters between treatment groups over time were evaluated using a 2-way ANOVA with Bonferroni's post-test.

In the MRI transient ischaemia study, systolic BP, infarct volume and mismatch volume were compared between groups using an unpaired test. Temporal changes in physiological parameters within treatment groups were assessed by Repeated Measures ANOVA. Physiological parameters were compared between treatment groups over time using a 2-way ANOVA with Bonferroni's post-test. The temporal evolution of ischaemic injury between groups was assessed by 2-way ANOVA with Bonferroni's post-test. Temporal changes in ischaemic injury within each treatment group were evaluated using a Repeated Measures ANOVA.

All data are expressed as mean±SD with the exception of the behavioural data. All behavioural data were expressed as median and interquartile range (IQ) and treatment groups were compared using a non-parametric Mann-Whitney test or Kruskal-Wallis test with Dunn's post-test. Temporal changes in behavioural outcome within each group were assessed by Repeated Measures ANOVA.

5.3 Results

5.3.1 **Study 1**: Apocynin Treatment in a Model of Permanent MCAO

5.3.1.1 Excluded Animals

Rats were excluded from data analysis if they died before 24 hours post-MCAO or if the filament did not advance fully along the internal carotid artery. Two rats from the vehicle treated group were excluded from data analysis. One rat died overnight before 24 hours

post-MCAO and it was suspected that the other rat had an incomplete occlusion of the MCAO. During stroke surgery, there was some difficulty in advancing the filament along the internal carotid artery and as such the filament did not advance the required 22mm. Consequently, the data from this rat was not included in the subsequent data analysis. On T_2 weighted imaging at 24 hours post-MCAO this animal showed evidence of a very small stroke. Consequently, the data from this rat was not included in the subsequent data analysis.

5.3.1.2 Final infarct Volume

MRI T_2 defined infarct volume at 24 hours post-MCAO was not significantly different between treatment groups. Infarct volume in the vehicle treated group was 301±46mm^3 compared to 289±117mm^3 and 240±106mm^3 for the 5mg/kg and 30mg/kg apocynin treated groups, respectively (P=0.47, Figure 5-3A). The data were more variable in the apocynin treated groups compared to the vehicle treated group, as illustrated by the high standard deviations in the apocynin treated groups. In the apocynin treated groups, there was one rat in each group which exhibited a very small infarct. In the 5mg/kg apocynin group, one rat had an infarct measuring 71mm^3 and in the 30mg/kg apocynin treated group, one rat demonstrated a very small infarct of 25mm^3 (Figure 5-3A). It is not known if this was a treatment effect or if the rats had an incomplete occlusion of the MCA.

Infarct was also expressed as percentage of the ipsilateral hemisphere. There was no significant difference between the treatment groups (43±6% vs 41±17% and 35±16% for vehicle, 5mg/kg apocynin and 30mg/kg apocynin treated groups, respectively, P=0.54).
Figure 5-4 illustrates the spatial distribution of infarcted tissue in a representative rat from each treatment group. In all groups, hyperintense infarct tissue is evident across all 16 T_2 slices and is located in the cerebral cortex and sub-cortex. The anatomical extent of the infarct is comparable between the treatment groups.

5.3.1.3 Bederson Score

Functional outcome at 24 hours post-MCAO, as assessed by the modified Bederson scale, was not significantly different between treatment groups (P=0.83, Figure 5-5A). The median score for the vehicle and 5mg/kg apocynin treated groups was 2 (IQ 2, 3) and the median score for the 30mg/kg apocynin group was 3 (IQ 2, 3). The rat in the vehicle group which died before 24 hours post-MCAO, was included in the Bederson scale analysis.

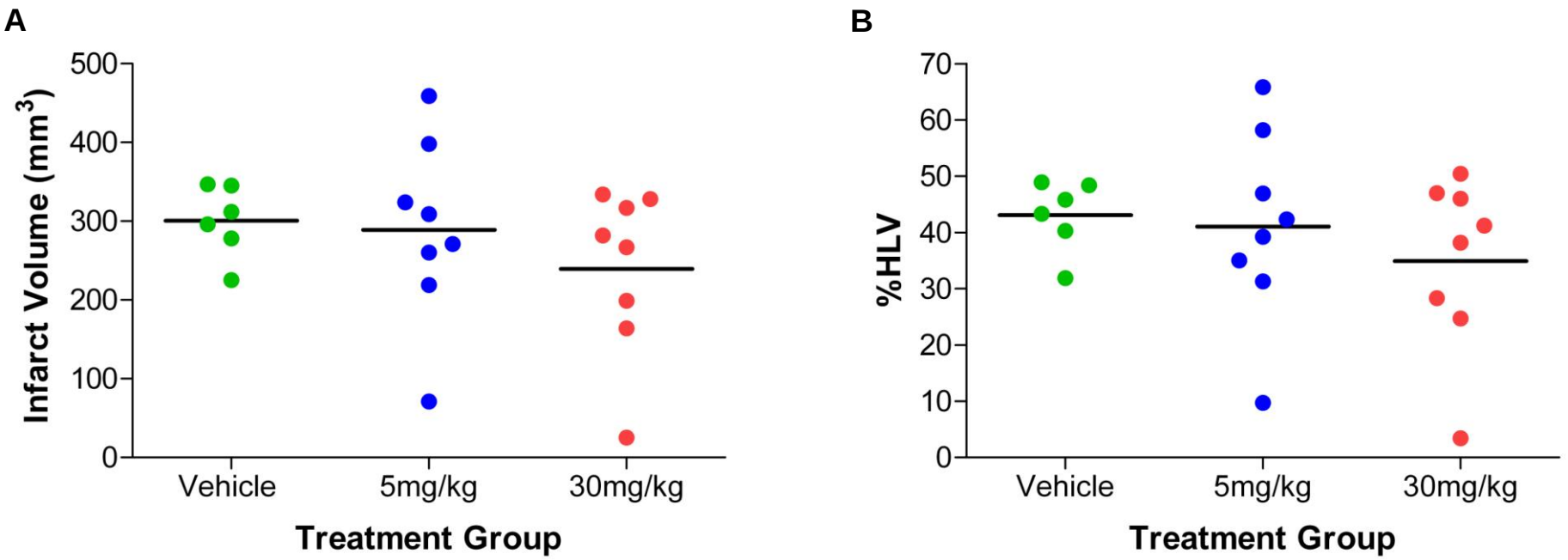

Figure 5-3. Final infarct in vehicle and apocynin treated WKY rats at 24h following permanent MCAO with drug treatment administered at 5 min post-MCAO. Infarct volume defined by T2 weighted imaging (A) was not significantly different between vehicle treated (n=6) and 5mg/kg (n=8) or 30mg/kg apocynin treated rats (n=8) (One-way ANOVA, P=0.47). Infarct expressed as a percentage of the ipsilateral hemisphere was also not significantly different between treatment groups (One-way ANOVA, P=0.54). The horizontal line denotes the mean.

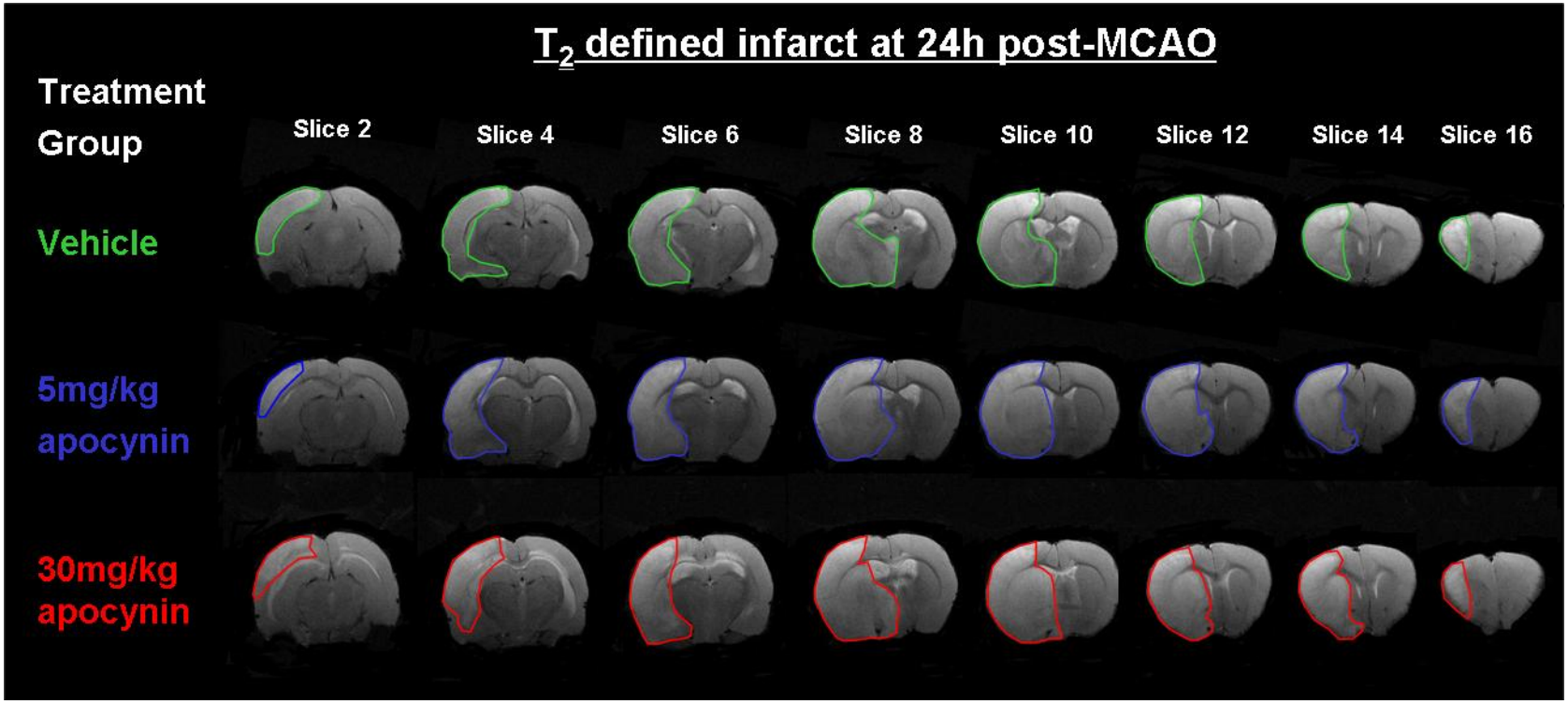

Figure 5-4. The spatial distribution of infarcted tissue in vehicle and apocynin treated rats following permanent MCAO. MRI T_2 weighted images (16 coronal slices) were acquired at 24h post-MCAO and the hyperintense area was manually delineated on each slice to determine infarct volume. Eight of the sixteen T_2 weighted images from the median rat from each treatment group are shown with the hyperintense areas delineated (vehicle-green, 5mg/kg apocynin-blue, 30mg/kg apocynin-red).

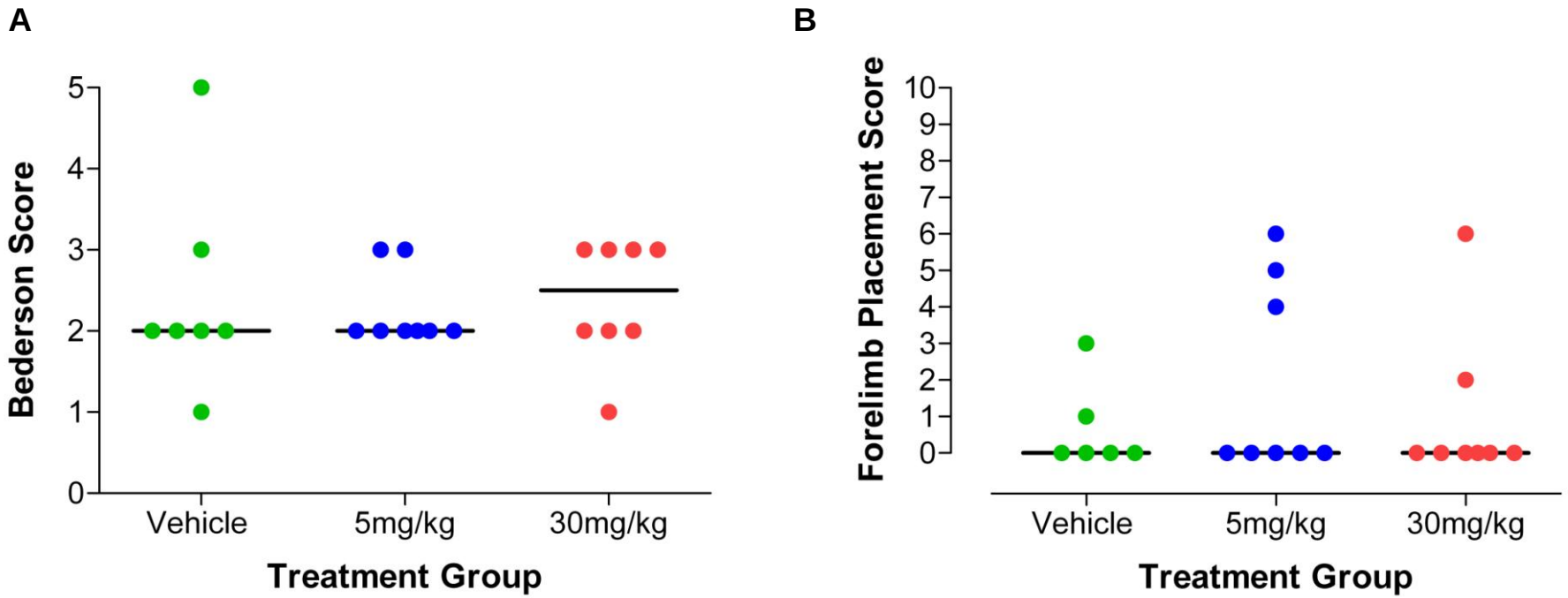

Figure 5-5. Functional outcome scores of WKY rats at 24h post-MCAO following vehicle or apocynin treatment. Functional outcome was assessed by a modified Bederson Score (A): 0=no observable deficit, 1=forelimb flexion, 2=reduced grip strength, 3=circling, 4=no spontaneous activity, 5=dead. Vibrissae-evoked forelimb placement was also used to assess outcome, where the number of successful placements of the contralateral forelimb were scored out of 10 attempts (B). The horizontal line denotes the median score. No statistically significant differences were found between groups for both functional tests, P=0.8 (Kruskal-Wallis test).

5.3.1.4 Vibrissae-evoked Forelimb Placement

Prior to stroke surgery, all rats scored 10 successful placements of the contralateral forelimb out of 10 attempts. Evaluation of functional outcome using the vibrissae-evoked forelimb placement test, revealed that there was no significant difference between the vehicle and apocynin treated groups at 24 hours post-MCAO. (P=0.78, Figure 5-5B). Most rats in all three treatment groups performed poorly and were unable to correctly place the contralateral forelimb in 10 attempts (Figure 5-5B). The median score for all treatment groups was 0, although 3 rats in the low dose apocynin group and one rat in the high dose apocynin group scored at least 4 correct placements out of 10 attempts.

5.3.2 **Study 2:** Apocynin Treatment in a Model of Transient MCAO

5.3.2.1 Mortality

The mortality rate observed in this study following transient ischaemia, was higher than that observed in the previous study following permanent MCAO. Three rats died in the vehicle treated group (3/9, 33% mortality), two rats died following low dose apocynin treatment (2/8, 25% mortality) and one rat died in the high dose apocynin group (1/7, 14% mortality). These 6 rats died between 24 and 48 hours post-MCAO and were excluded from data analysis. All infarct data and behavioural data are from the animals which survived to 72 hours post-MCAO, with the exception of the Bederson scale, where the rats which died are also included.

5.3.2.2 Physiological Parameters

During anaesthesia, all physiological parameters were maintained within physiological range across the three treatment groups, with the exception of arterial PO_2. Arterial PO_2 in all three treatment groups was significantly higher than the physiological range of 80-100mmHg ($P<0.05$, one sample t-test). This is likely to be attributed to the anaesthetic gas mixture, where 30% oxygen is used rather than the 21% oxygen found in air. Within each treatment group, each physiological variable was maintained from 30 minutes before stroke onset to 30 minutes post-ischaemia ($P>0.05$, paired t test). There were no significant differences in any of the physiological variables between treatment groups before or after the onset of ischaemia ($P>0.05$, One-way ANOVA, Table 5-1). No change in mean arterial blood pressure was observed following intravenous administration of vehicle or apocynin.

	30 min pre-MCAO	30 min post-MCAO
Vehicle treated group		
Body Temperature (^oC)	37.2±0.3	37.3±0.2
MABP (mmHg)	101±5	105±7
Heart Rate (bpm)	371±30	365±24
Blood pH	7.42±0.03	7.40±0.03
Arterial PO_2 (mmHg)	161±44	168±49
Arterial PCO_2 (mmHg)	35±3	37±4
5mg/kg apocynin treated group		
Body Temperature (^oC)	37.0±0.3	36.9±0.3
MABP (mmHg)	101±7	108±6
Heart Rate (bpm)	361±19	368±27
Blood pH	7.40±0.06	7.37±0.04
Arterial PO_2 (mmHg)	163±25	171±29
Arterial PCO_2 (mmHg)	37±4	36±4
30mg/kg apocynin treated group		
Body Temperature (^oC)	37.1±0.4	37.2±0.3
MABP (mmHg)	102±6	106±7
Heart Rate (bpm)	372±19	368±22
Blood pH	7.38±0.04	7.40±0.02
Arterial PO_2 (mmHg)	176±32	165±37
Arterial PCO_2 (mmHg)	36±6	37±3

Table 5-1. Physiological parameters in vehicle and apocynin-treated Sprague-Dawley rats before and after the induction of ischaemia by occlusion of the middle cerebral artery. Data presented as mean±SD, n=6 per group. MABP-mean arterial blood pressure, bpm-beats per minute.

5.3.2.3 Final Infarct Volume

TTC defined final infarct volume at 72 hours post-MCAO was significantly lower in low and high dose apocynin treated rats compared to the vehicle treated group. In vehicle treated rats, infarct volume was 112±25mm^3, compared to 40±35mm^3 and 46±31mm^3 in 5mg/kg and 30mg/kg apocynin treated rats, respectively ($P<0.01$, Figure 5-6). This represents a reduction in infarct volume of approximately 60% in the apocynin treated groups. There were 2 apocynin treated rats which did not show a reduction in infarct volume compared to the vehicle treated group. One rat which received 5mg/kg apocynin had an infarct volume of 108mm^3 and one rat which received 30mg/kg apocynin had an infarct volume of 102mm^3 at 72 hours post-MCAO (Figure 5-6). The infarcts exhibited by these rats were comparable to the infarcts observed in the vehicle treated group.

In the vehicle treated group, infarcted tissue was observed in the cerebral cortex and the sub-cortex. The infarct area extended across the territory of the middle cerebral artery. However, in the apocynin treated groups, infarcted tissue was mainly identified sub-cortically and did not extend as far in the rostral caudal plane as observed in the vehicle treated group (Figure 5-7).

5.3.2.4 Bederson Score

The Bederson scores of the animals which survived to 72 hours post-MCAO are shown in Figure 5-8A. There was no significant difference between treatment groups at any time point post-MCAO ($P>0.05$, Kruskal-Wallis test). The low dose apocynin treated group demonstrated less neurological impairment than the high dose apocynin and vehicle treated groups at all time points but did not reach the level of statistical significance (vehicle: 2 (IQ 2, 3), 5mg/kg: 0 (IQ 0, 3), 30mg/kg: 2 (IQ 0, 3) at 24 hours post-MCAO, $P>0.05$).

Furthermore, there was no significant change in score from 24 to 72 hours post-MCAO in any of the treatment groups ($P>0.05$, Repeated Measures ANOVA).

The scores of the animals which died between 24 and 48 hours post-MCAO are shown in Figure 5-8B. The vehicle treated rats which died were more severely neurologically impaired than the apocynin treated rats which died.

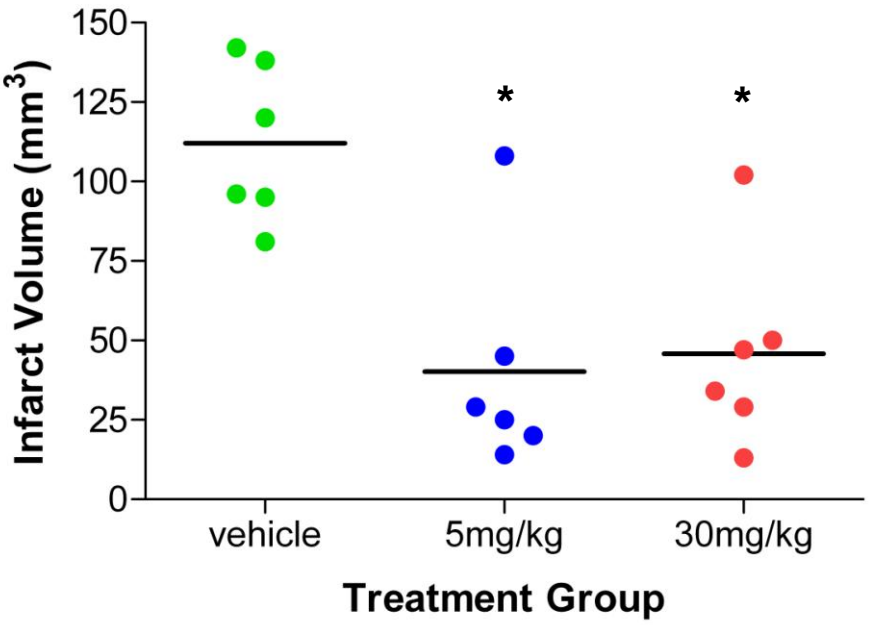

Figure 5-7. TTC defined infarct volume at 72h post-MCAO in vehicle and apocynin treated Sprague-Dawley rats. Drug treatment was administered intravenously 5 min post-MCAO. The intraluminal filament was removed after 1h of ischaemia to allow reperfusion until 72h post-MCAO. Line denotes the mean. *p<0.01, One-way ANOVA with Bonferroni's Multiple Comparisons test.

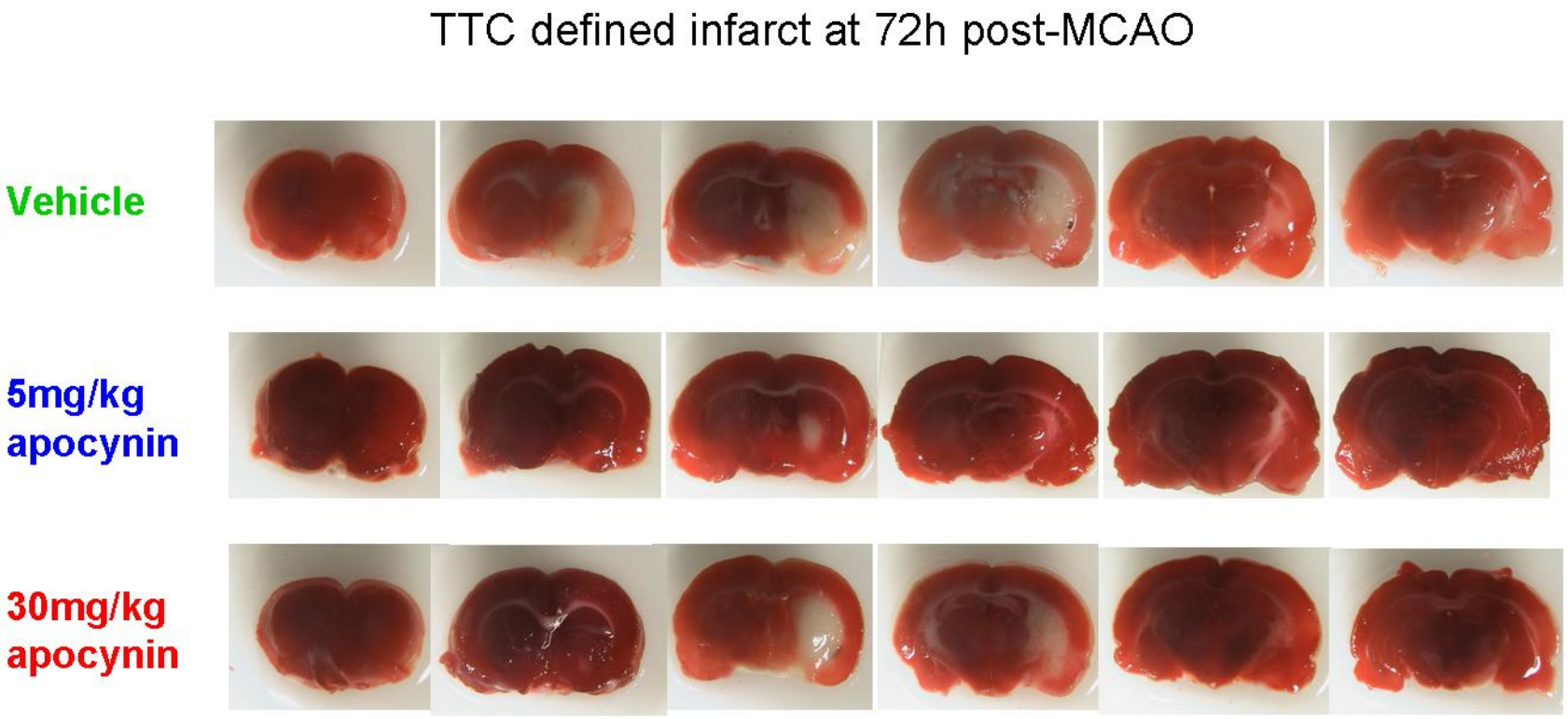

Figure 5-7. Spatial distribution of the TTC defined infarct at 72h post-MCAO in vehicle and apocynin treated Sprague-Dawley rats. Infarcted tissue appears white and unaffected tissue stains deep red with TTC.

5.3.2.5 Vibrissae-evoked Forelimb Placement

Prior to surgery, all rats scored the maximum of 10 successful placements of the contralateral forelimb out of 10 attempts. There was no evidence of neurological impairment or limb preference in any of the rats used in this study.

At all time points post-MCAO, rats which received low dose apocynin treatment performed better than rats in the vehicle and high dose apocynin groups. However, the observed improvement in forelimb placement was not statistically significant at any time point ($P>0.05$, Kruskal-Wallis test, Figure 5-9). The improvement in function was particularly evident at 24 hours post-MCAO (vehicle: 3 (IQ 0, 9), 5mg/kg: 8 (IQ 2, 10), 30mg/kg: 5 (IQ 1, 9), $P>0.05$).

In the vehicle treated group, the contralateral forelimb placement score was maintained at 3 successful placements at 24 and 48 hours post-MCAO. This improved to 4 successful placements out of 10 attempts by 72 hours. However, in the apocynin treated groups, the number of successful placements decreased over time. In the low dose apocynin group, the number of successful placements decreased from 8 at 24 hours to 6 at 72 hours post-MCAO. Similarly, in the high dose apocynin group, the number of successful placements reduced from 5 at 24 hours to 3 at 72 hours post-MCAO. The temporal changes in the number of successful contralateral placements were not significant in any of the treatment groups ($P>0.05$, Repeated Measures ANOVA).

5.3.2.6 18-point Neurological Score

There was no statistically significant improvement in neurological score between treatment groups. However in the low dose apocynin treated animals there was a trend towards an improvement in neurological function at all time points post MCAO ($P>0.05$, Kruskal-Wallis test, Figure 5-10A). At 24 hours post-MCAO, the median score in the 5mg/kg apocynin group was 14 (IQ 11, 17), compared to 12 (IQ 10, 14) in the 30mg/kg apocynin group and 10 in the vehicle treated group (IQ 9, 14), $P>0.05$).

It was also observed that the general condition of rats in the low dose apocynin group was improved compared to rats in the other treatment groups. Rats in the 5mg/kg apocynin group demonstrated more frequent grooming behaviour, were generally more alert and exhibited normal feeding behaviours compared to rats in the vehicle and high dose apocynin groups.

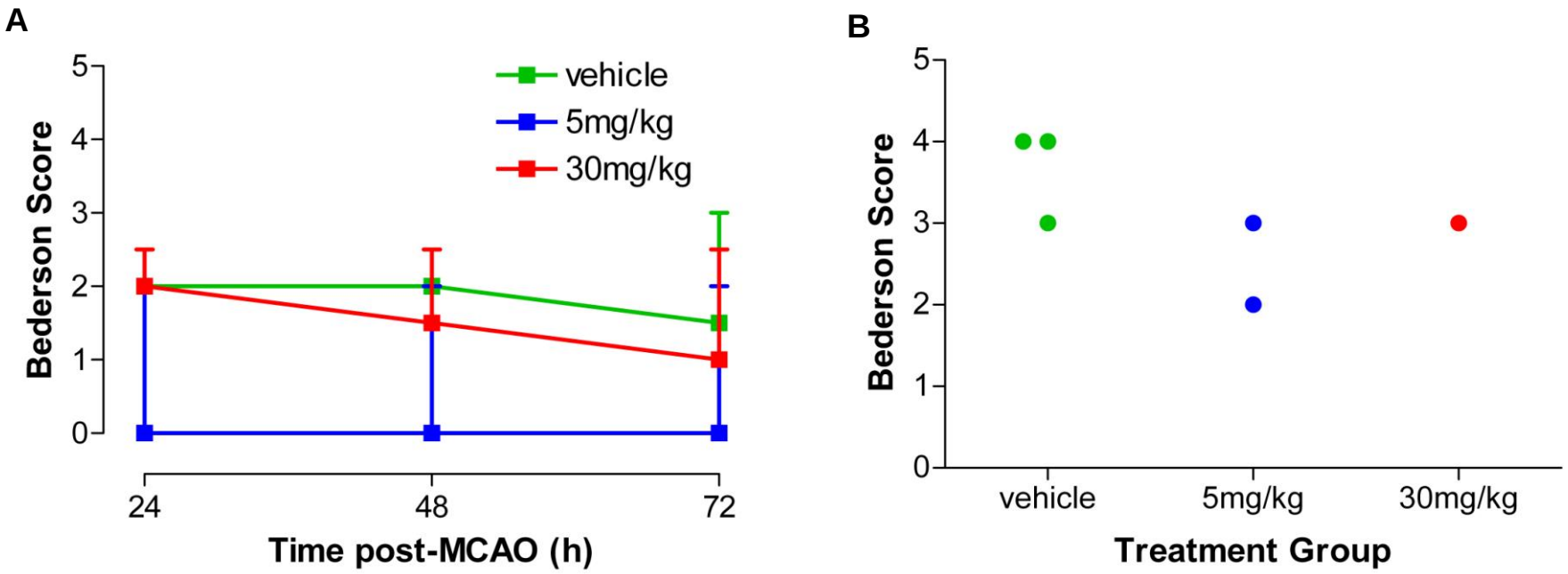

Figure 5-8. Evaluation of neurological function using a modified Bederson Scale following transient ischaemia in vehicle and apocynin treated Sprague-Dawley rats. Rats were tested at 24, 48 and 72h post-MCAO. The median scores and the interquartile range are shown for the animals which survived to 72h post-MCAO (A) ($P>0.05$, Kruskal-Wallis test). The 24 hour scores of the rats which died between 24 and 48h post-MCAO are also shown (B).

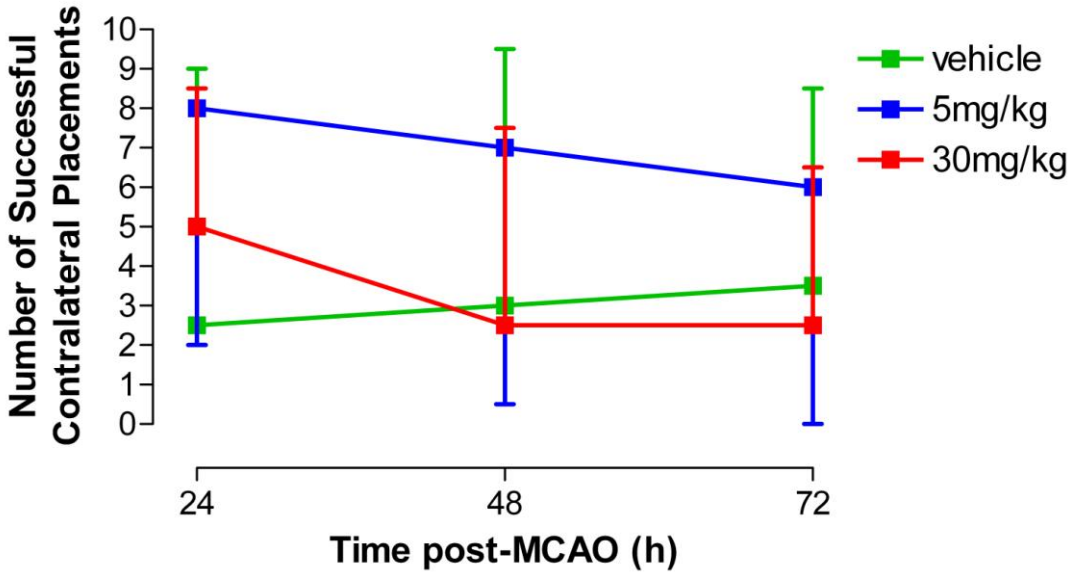

Figure 5-9. Assessment of neurological function following transient ischaemia in Sprague-Dawley rats using the vibrissae-evoked forelimb placement test. Testing was performed at 24, 48 and 72h post-MCAO in rats treated with vehicle, low dose or high dose apocynin treatment following ischaemia. Data presented as median and interquartile range, n=6 per group. P>0.05, Kruskal-Wallis test.

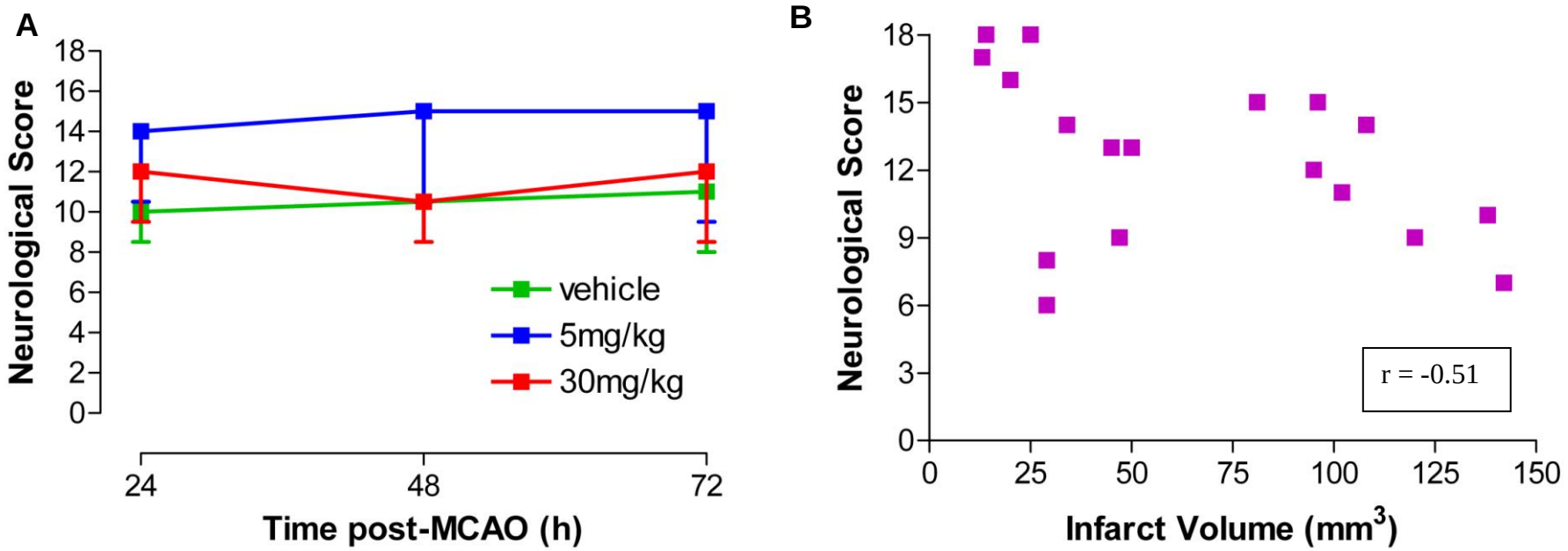

Figure 5-10. Assessment of functional outcome following apocynin treatment using an 18 point composite neurological scoring system. Rats were tested at 24, 48 and 72h post-MCAO (A). A maximum score of 18 is achieved when there is no observable deficit. A score of 3 indicates severe neurological impairment. Data presented as median and interquartile range, n=6 per group. $P>0.05$, Kruskal-Wallis test. A statistically significant inverse correlation was found between final infarct volume at 72h post-MCAO and neurological score at 72h for all rats (B). Spearman's non-parametric correlation, $r=-0.51$, $P<0.05$.

Neurological score at 72 hours post-MCAO correlated significantly with final infarct volume at the same time point ($P<0.05$, Figure 5-10B). Using the non-parametric Spearman's correlation, an r value of -0.51 demonstrates that there is an inverse relationship between infarct volume and neurological score, where as infarct volume decreases, neurological score increases. This shows that neurological function is improved in rats with smaller infarct volumes, compared to rats with larger infarcts, which are more severely functionally impaired.

5.3.3 **Study 3:** MRI Assessment of the Acute Evolution of Ischaemic Injury in an Ischaemia-Reperfusion model in SHRSP rats

5.3.3.1 Systolic Blood Pressure

Tail cuff pleythsmography performed in the weeks prior to surgery revealed that there was no significant difference in the mean systolic pressures of the rats in each treatment group. Prior to stroke surgery, mean systolic blood pressure was not significantly different between groups of rats subsequently randomised to vehicle and apocynin (5mg/kg) treatment (181±25mmHg and 189±17mmHg for vehicle and apocynin treated rats, respectively, P=0.52, Figure 5-11).

5.3.3.2 Mortality

The mortality rate in this study was higher than that observed in the transient ischaemia study using Sprague-Dawley rats. Of the 12 SHRSP rats used in this study, 8 rats died before the 72 hours end point, representing a 67% mortality rate. In both the vehicle and apocynin treated group 4/6 rats died before 72 hours post-MCAO. 5 rats died before 24 hours post-MCAO and 2 rats died between 24 and 48 hours. One vehicle treated rat was euthanased at 48 hours post-MCAO due to poor condition and lack of spontaneous movement. Only 2 rats in each treatment group survived until 72 hours post-MCAO. It was therefore decided that the study would not continue further on ethical grounds. However, the acute MRI data acquired up to 3 hours post-MCAO are presented for all rats in the vehicle treated (n=6) and low dose apocynin treated groups (n=6).

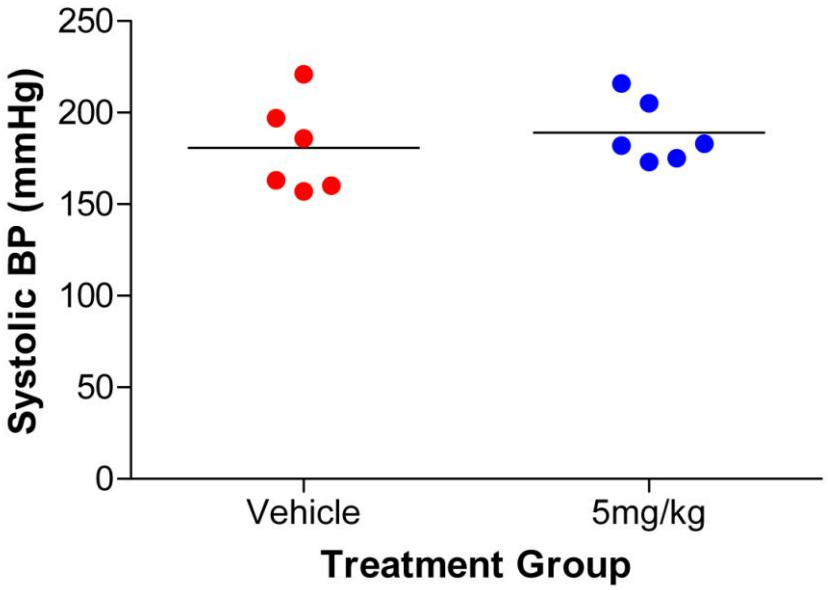

Figure 5-11. Mean Systolic Blood Pressure in SHRSP rats. Tail cuff plethysmography was performed in the weeks prior to stroke surgery. Mean systolic blood pressure was determined in each rat which was then randomly allocated to the vehicle or low dose apocynin treatment group. Horizontal line denotes the mean. P>0.05, unpaired t test.

5.3.3.3 Physiological Parameters

With the exception of arterial PO_2, as previously discussed, all physiological parameters were maintained within physiological range in both treatment groups at all time points post-MCAO. Arterial PO_2 in all three treatment groups was significantly higher than the physiological range of 80-100mmHg ($P<0.05$, one sample t-test). Within each treatment group, each physiological variable was maintained from 30 minutes before stroke onset (baseline) to 3 hours post-MCAO ($P>0.05$, Repeated Measures ANOVA). There were no significant differences in any of the physiological variables between treatment groups before or after the onset of ischaemia ($P>0.05$, Two-way ANOVA, Table 5-2).

5.3.3.4 Assessment of Reperfusion

Immediately following the retraction of the intraluminal filament, MR angiography was acquired and examined in order to confirm successful reperfusion of the left middle cerebral artery. With the exception of one rat in the low dose apocynin treatment group, all rats demonstrated successful reperfusion. In the rat which did not reperfuse at 1 hour post-MCAO, the filament was retracted further following examination of the angiographs at 1 hour 10 minutes post-MCAO. Another angiography scan was then acquired and examined to confirm that the left middle cerebral artery had successfully reperfused. Figure 5-12 illustrates reperfusion of the left middle cerebral artery.

5.3.3.5 Acute Evolution of Ischaemic Injury

DWI was carried out in order to determine if apocynin treatment influences the acute evolution of ischaemic injury following MCAO. There was no significant difference in the volume of ADC defined ischaemic injury at any time point during ischaemia and following reperfusion in the vehicle treated and low dose apocynin groups ($P>0.05$, 2-way ANOVA, Figure 5-13). During the period of ischaemia, the volume of ischaemic injury peaked at $357\pm63mm^3$ and $344\pm92mm^3$ in the vehicle treated and apocynin treated groups, respectively ($P>0.05$). At 1 hour post-MCAO, following retraction of the filament, the volume of ADC derived ischaemic injury sharply declined to less than a third of the volume observed in both groups during ischaemia. Within 30 minutes of reperfusion, the volume of ischaemic injury decreased to $101\pm73mm^3$ and $99\pm82mm^3$ in the vehicle treated and apocynin groups, respectively ($P>0.05$). By 2 hours post-MCAO, the volume of ischaemic injury began to increase in both groups and by 3 hours post-MCAO, it had

	Baseline	***1h***	***2h***	***3h***
Vehicle				
Body Temp (^{o}C)	37.2±0.4	36.8±0.5	36.8±0.3	36.9±0.3
MABP (mmHg)	111±11	111±5	113±10	115±6
HR (bpm)	369±10	378±23	361±10	357±17
Blood pH	7.42±0.05	7.41±0.03	7.37±0.02	7.39±0.04
PaO_2 (mmHg)	131±14	140±21	142±23	136±18
$PaCO_2$ (mmHg)	36±2	39±5	40±4	43±5
5mg/kg apocynin				
Body Temp (^{o}C)	37.1±0.2	36.7±0.3	37.1±0.3	36.9±0.3
MABP (mmHg)	109±12	112±10	110±8	110±9
HR (bpm)	358±17	355±14	355±17	361±9
Blood pH	7.44±0.03	7.38±0.03	7.38±0.03	7.41±0.03
PaO_2 (mmHg)	136±13	152±14	147±18	141±25
$PaCO_2$ (mmHg)	37±1	38±3	41±2	39±3

Table 5-2. Physiological parameters assessed before the induction of ischaemia and at 1, 2 and 3h post-MCAO in SHRSP rats. Data presented as mean±SD. MABP-mean arterial blood pressure, HR-heart rate, PaO_2-arterial PO_2, $PaCO_2$-arterial PCO_2.

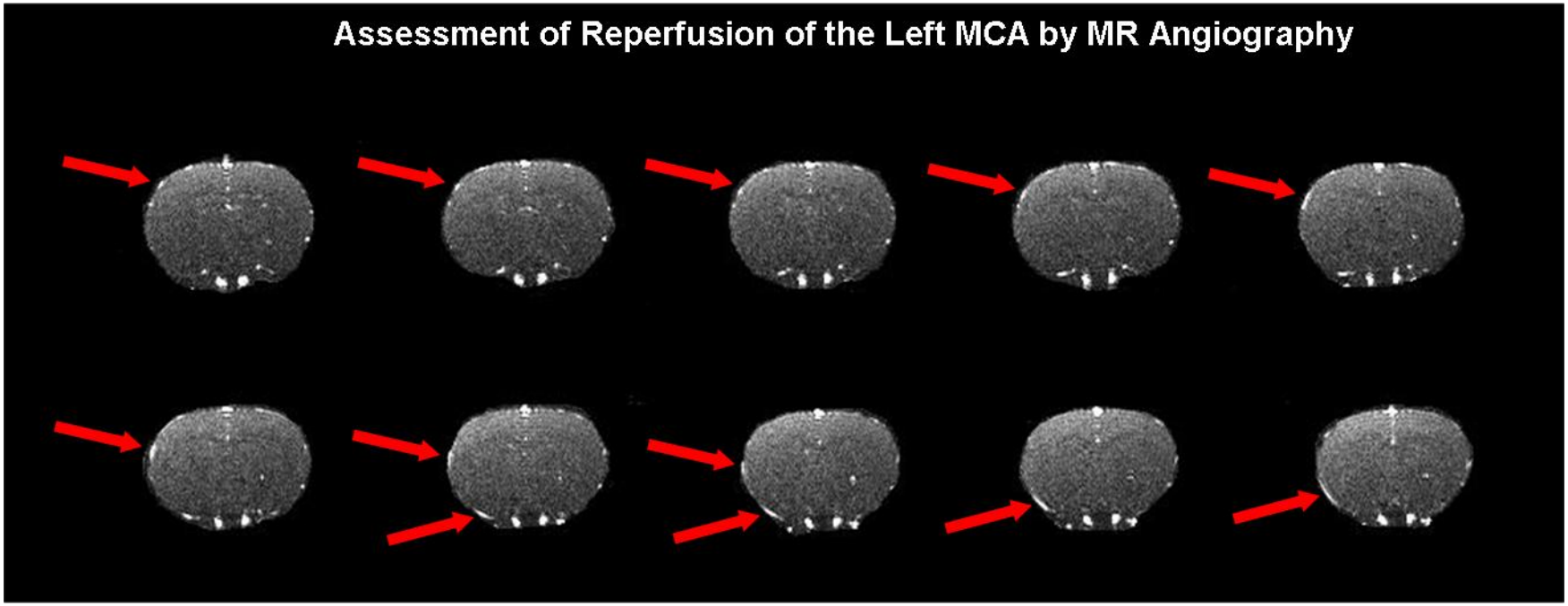

Figure 5-12. Reperfusion of the middle cerebral artery following 1h of ischaemia. MR angiography was performed immediately following withdrawal of the intraluminal filament at 1h post-MCAO. Restoration of flow in the left middle cerebral artery is highlighted by the arrows. Data is from a representative vehicle treated rat.

increased to 149±126mm^3 and 154±121mm^3 in the vehicle and apocynin treated groups, respectively (P>0.05).

The spatial extent of injured tissue was comparable between the treatment groups during ischaemia and following reperfusion. During the 1 hour period of ischaemia, injured tissue was observed across 8 coronal slices within the MCA territory (Figures 5-14A & B). The extent of injury increased between 20 minutes and 1 hour post-MCAO in both groups and this was particularly evident on the coronal slices at the rostral and caudal extremities. Following reperfusion, ischaemic injury decreased but gradually began to rise by 2 hours post-MCAO. Growth of the ADC derived lesion was particularly evident on coronal slices 3, 4 and 5, which are located within the core of the ischaemic MCA territory.

5.3.3.6 Final Infarct Volume

Statistical analysis of the infarct data was not undertaken because only 2 rats in each treatment group survived to the 72 hour end point. In the vehicle treated group, mean infarct volume was 309mm^3, compared to 200mm^3 in the apocynin treated animals. However, the difference in the treatment group means was mainly due to one of the apocynin treated rats which demonstrated a small infarct of 131mm^3 at 72 hours post-MCAO. In addition, TTC staining was performed on the brains of 2 rats which died overnight before 24 hours post-MCAO. Both rats were apocynin treated and displayed large infarcts of 352 and 360mm^3. However, the precise time of death was unknown in these rats and the infarct data were excluded from the analysis of final infarct volume at 72 hours.

Furthermore, infarct volume at 24 and 72 hours was compared to the volume of ADC derived ischaemic injury at 1 hour post-MCAO, just prior to reperfusion (Figure 5-15). In the vehicle treated group, one rat demonstrated an infarct volume of 340mm^3 at 72 hours, which exceeded the volume of ischaemic injury observed during ischaemia (271mm^3). However, the other vehicle treated rat displayed an infarct at 72 hours which was smaller than the volume of ischaemic injury observed following 1 hour of ischaemia (infarct: 278mm^3 vs ADC lesion: 331mm^3, Figure 5-15A). This was also observed in both apocynin treated rats, where the ADC derived lesion during the 1 hour period if ischaemia was larger than the infarct at 72 hours post-MCAO. In one rat, the volume of ischaemic injury 291mm^3 during ischaemia and infarct volume at 72 hours was 268mm^3. The other rat demonstrated an ADC derived lesion volume of 178mm^3 and infarct volume at 72 hours was 131mm^3 (Figure 5-15B).

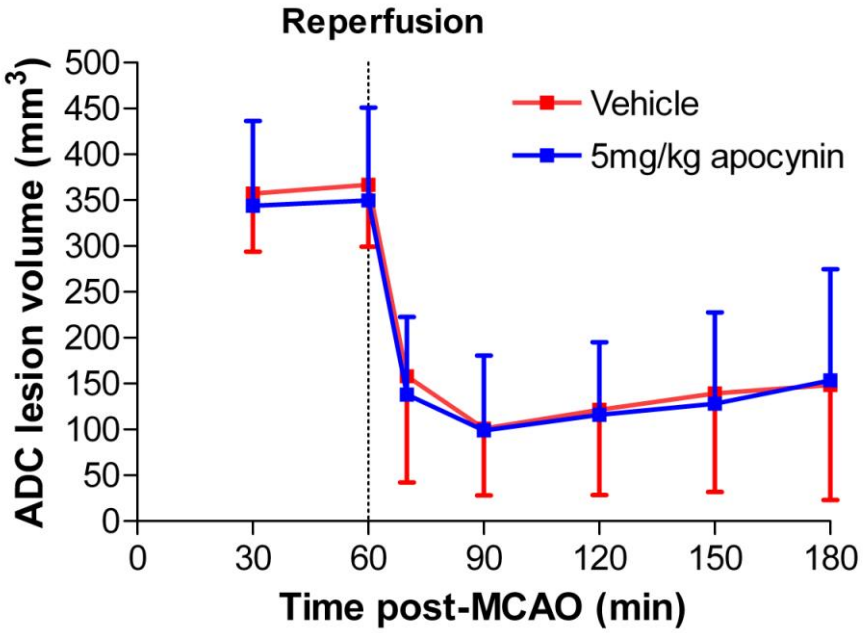

Figure 5-13. The acute evolution of ischaemic injury following reperfusion in vehicle and apocynin treated SHRSP rats. Drug treatment was administered at 5min post-MCAO, which was 55min prior to reperfusion. The strain specific ADC threshold of 0.59 x $10^{-3}$$mm^2$/sec was applied to quantitative ADC maps to assess ischaemic injury during ischaemia and following reperfusion at 60min post-MCAO. Dotted line denotes reperfusion by retraction of the intraluminal filament. Data presented as mean±SD, n=6 per group. P>0.05, 2-way ANOVA.

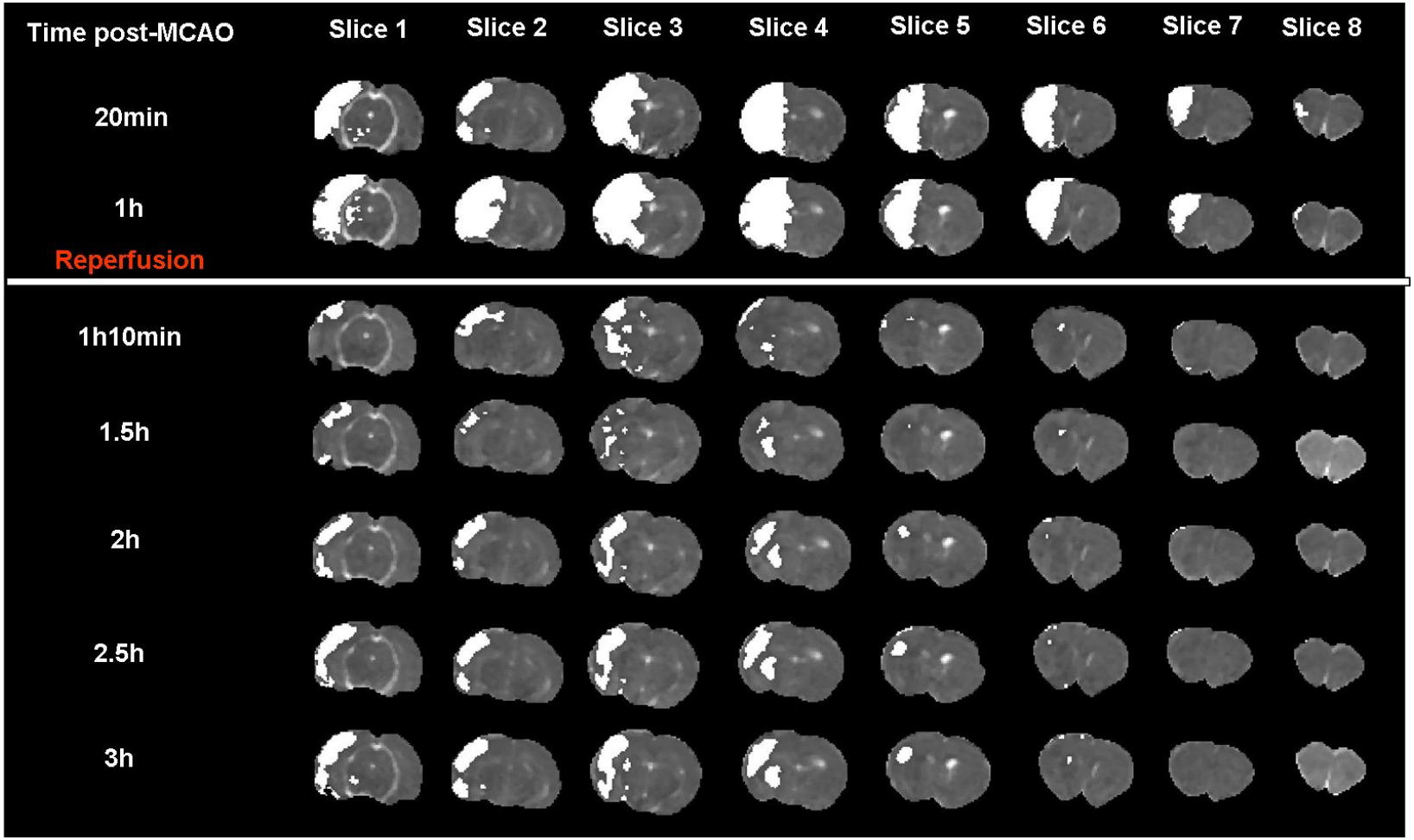

Figure 5-14A. The spatial distribution of acute ischaemic injury during ischaemia and following reperfusion in a vehicle treated SHRSP. The strain specific ADC threshold was applied to quantitative ADC maps to define the extent of injured tissue. Ischaemic injury is shown in white across 8 coronal slices within the territory of the MCA.

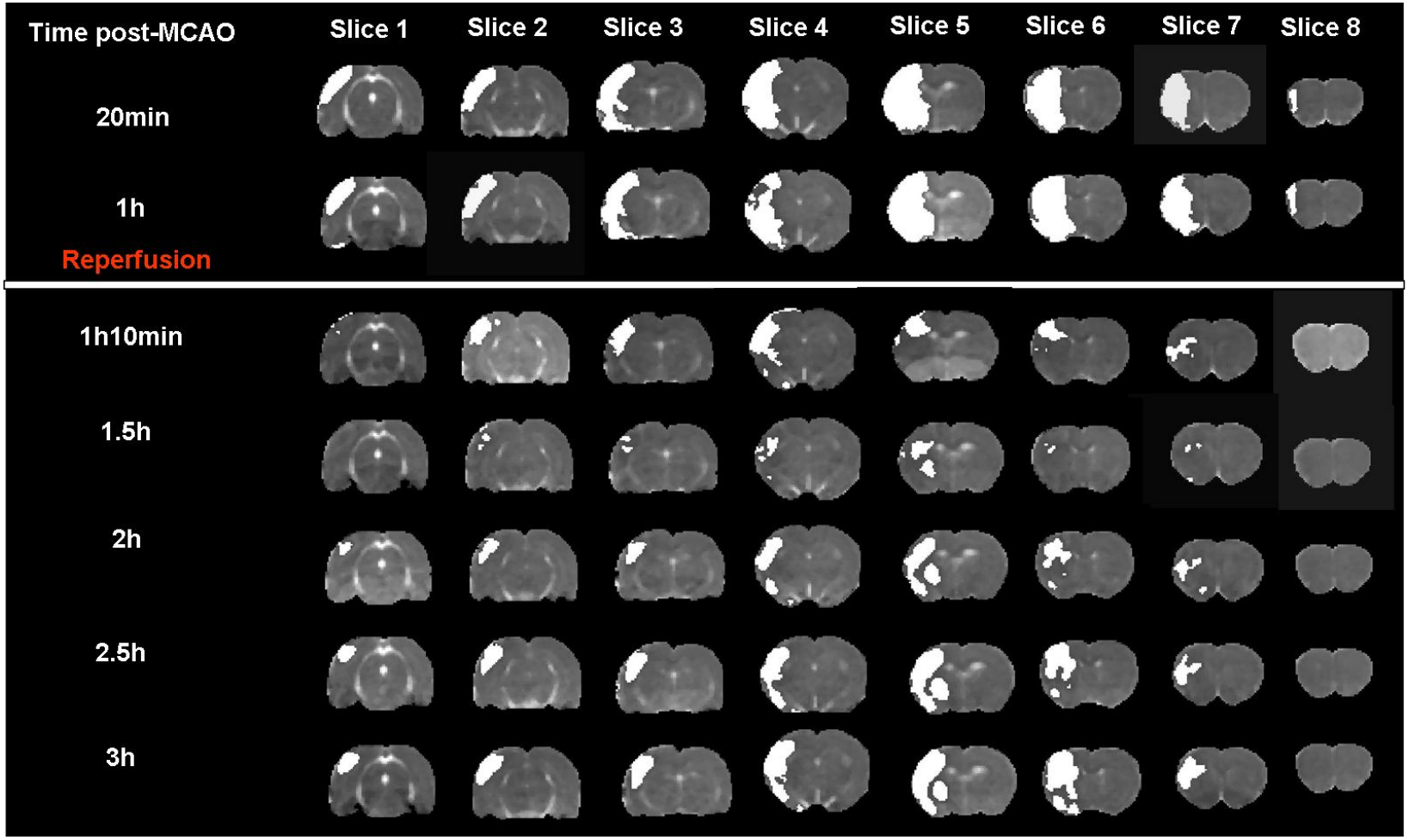

Figure 5-14B. The spatial distribution of ischaemic injury during ischaemia and following reperfusion in a low dose apocynin treated SHRSP. The strain specific ADC threshold was applied to quantitative ADC maps to define the extent of injured tissue. Ischaemic injury is shown in white across 8 coronal slices within the territory of the MCA.

5.3.3.7 Perfusion-Diffusion Mismatch

Mismatch volume prior to reperfusion at 1 hour post-MCAO, was comparable between vehicle treated and apocynin treated rats. In the vehicle treated group, mismatch volume at 1 hour post-MCAO was 32±17mm^3, compared to a mismatch volume of 31±28mm^3 in the apocynin treated group (P=0.91, unpaired t test, Figure 5-16A). The acute MRI data from all 6 vehicle treated rats were used to determine mismatch volume. However, in the apocynin treated group, mismatch data were acquired from 4/6 rats. This was because there were problems with the acquisition of perfusion weighted images on the days when 2/6 animals were being scanned. In one rat, CBF images were only acquired for coronal slices 3, 4 and 5 due to time restrictions and in the other rat, no perfusion data was acquired during ischaemia, as a result of technical difficulties.

Across the 4 coronal slices, mismatch tissue was observed mainly on slice 3 and mismatch area decreased on the rostral slices. Mismatch tissue was identified mainly in the cerebral cortex in both groups, although mismatch was also observed sub-cortically to a lesser extent (Figure 5-16B).

5.3.3.8 Functional Outcome

Figure 5-17A shows the Bederson scores at 24 hours post-MCAO for all rats used in the study. There was no significant difference in score between the groups (P=0.49, Mann-Whitney test). In the vehicle treated group, the median score at 24 hours was 4, which indicates severe impairment and no spontaneous activity. Three rats in the vehicle treated group scored 4 and two of these rats died before 48 hours and the other rat was euthanased at 48 hours due to its poor condition. The 2 rats which survived to 72 hours post-MCAO demonstrated less severe impairment and scored 2 at 24 hours, where reduced grip strength was observed without any circling behaviour. In the apocynin treated group, the median score at 24 hours was 5 as 4 rats out of 6 died before 24 hours post-MCAO. Of the two rats which survived to the 72 hours end point, one rat scored 2 and the other rat scored 0, indicating no observable neurological impairment.

Over the 72 hours time course, the vehicle treated rats did not show any improvement in functional outcome, as assessed by the Bederson scale. One apocynin treated rat showed no evidence of neurological impairment at any time point and the other apocynin treated

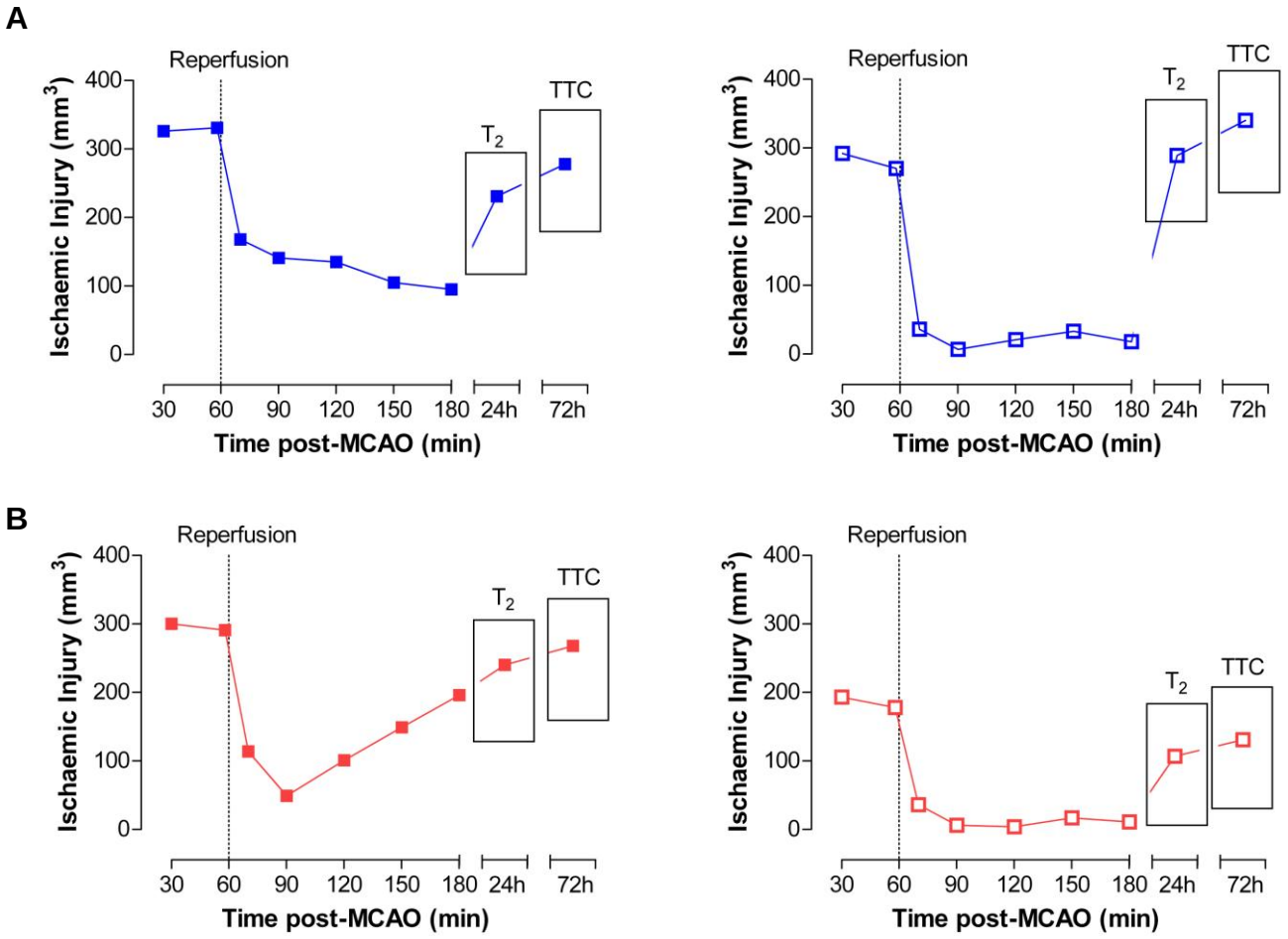

Figure 5-15. Acute evolution of ischaemic injury in the rats which survived to 72h post-MCAO. Row A shows the data from the vehicle treated rats and row B shows the data from the apocynin treated rats. Reperfusion was induced at 1h post-MCAO by withdrawal of the filament (dotted vertical line). Oedema-corrected infarct volume was defined at 24h post-MCAO by T_2 weighted MRI and 72h by TTC staining.

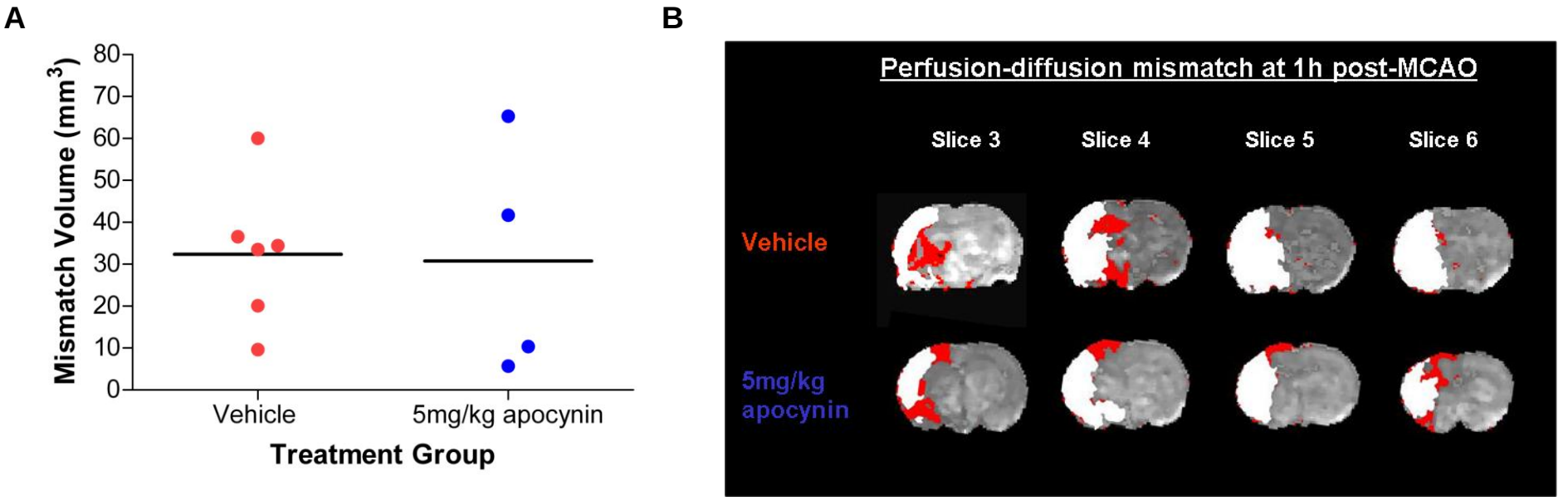

Figure 5-16. Perfusion-diffusion mismatch at 1h post-MCAO in vehicle treated and low dose apocynin treated SHRSP rats. Mismatch area was calculated on 4 coronal slices by superimposing the area of ADC derived ischaemic injury (shown in white) on to the perfusion deficit (shown in red) of the corresponding slice. The remaining perfusion deficit was measured on each slice to calculate mismatch volume. Mismatch volume was determined immediately before reperfusion in vehicle treated (n=6) and low dose apocynin treated (n=4) SHRSP rats (A). The MRI data shown are from a representative vehicle and apocynin treated rat (B).

rat demonstrated an increase in neurological impairment between 24 and 48 hours post-MCAO, as the observed score increased from 2 to 4 (Figure 5-17B).

Functional outcome was also assessed by an 18-point neurological score and by vibrissae-evoked forelimb placement. Prior to surgery, all rats demonstrated successful placement of the right and left forelimbs and there was no evidence of limb preference or neurological impairment. Figure 5-18 presents the data for the rats in each treatment group which survived to 72 hours post-MCAO. In one vehicle treated rat, neurological function improved progressively, where neurological score increased from 11 at 24 hours to 14 at 72 hours post-MCAO. However, the other vehicle treated rat displayed a decrease in neurological score (Figure 5-18A).

In the apocynin treated group, one rat exhibited a decrease in neurological score from 8 at 24 hours to 6 at 48 hours but outcome was improved by 72 hours post-MCAO as the score increased to 9. The other apocynin treated rat demonstrated no neurological impairment at any time point and achieved the maximum score of 18. This rat also showed no impairment in the vibrissae-evoked forelimb placement test and successfully placed the contralateral forelimb at every attempt. This rat demonstrated a smaller infarct than the rest of the rats which survived, where the infarct at 72 hours was 131mm^3 which was less than 50% of infarct volume observed in the other 3 rats which survived to 72 hours post-MCAO. The infarct was located sub-cortically, whereas the other rats demonstrated infarcts which incorporated both the cortex and the sub-cortex. Both of the vehicle treated rats and the apocynin treated rat which demonstrated neurological impairment, showed gradual reduction in the ability to successfully place the contralateral forelimb. This was particularly evident between 24 and 48 hours post-MCAO. These observations conflict with the 18 point neurological score, where the functional outcome of these 3 rats improved over time.

5.4 Discussion

The results of the studies presented in this chapter characterise the effect of apocynin (an NADPH oxidase inhibitor) following both permanent and transient focal cerebral ischaemia and in the presence of stroke co-morbidities. We have provided further evidence that inhibition of NADPH oxidase with apocynin is neuroprotective following transient focal cerebral ischaemia, however no such effect was observed following permanent

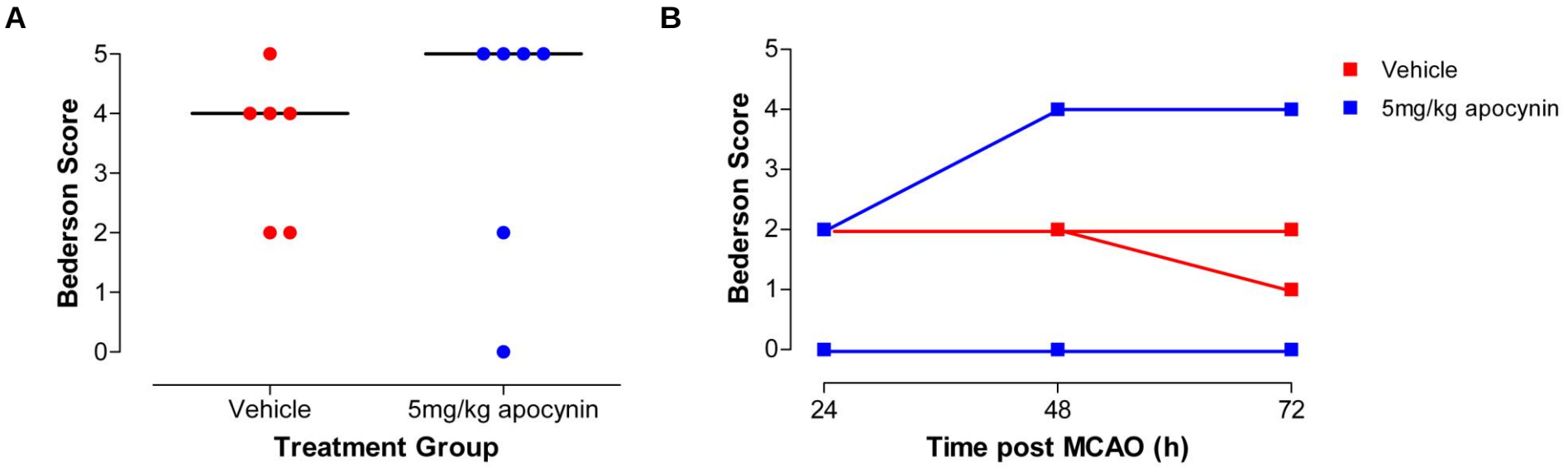

Figure 5-17. Functional outcome in vehicle and apocynin treated rats up to 72h post-MCAO. Functional outcome was assessed by a modified Bederson scale. A score of 0=no observable deficit, 1=forelimb flexion, 2=reduced grip strength, 3=circling, 4=no spontaneous activity, 5=dead. The scores of all vehicle treated (n=6) and apocynin treated rats (n=6) at 24h post-MCAO are shown in figure A. The line denotes the median score. P=0.49, Mann-Whitney Test. Figure B shows the individual scores observed in the 2 rats in each treatment group which survived to 72h post-MCAO.

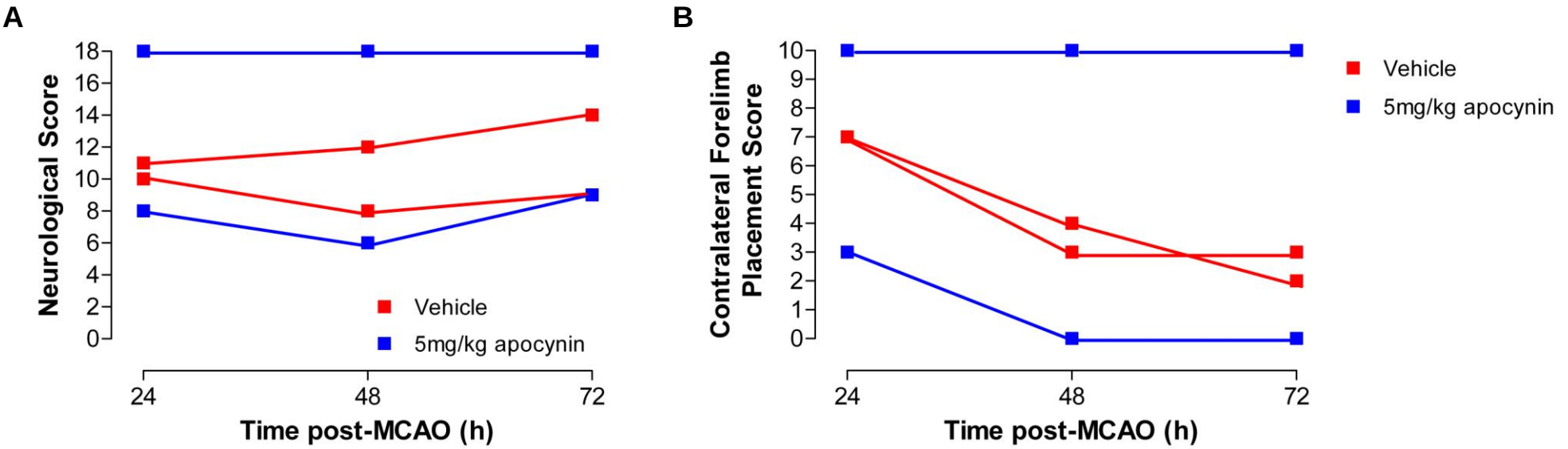

Figure 5-18. Functional outcome in vehicle and apocynin treated rats up to 72h post-MCAO. Functional outcome was assessed by an 18 point neurological score (A) and by the vibrissae-evoked forelimb placement test (B). In the 18 point assessment, a score of 18 indicates no observable deficit and a score of 3 indicates the most severe impairment. The forelimb placement test is scored on the number of successful placements of the contralateral forelimb out of 10 attempts. Therefore, a score of 10 depicts no impairment and a score of 0 indicates failure to place the forelimb. The individual scores of the 2 rats in each treatment group which survived to 72h post-MCAO are shown.

cerebral ischaemia. In addition we have shown that the neuroprotective effect shown following transient cerebral ischaemia is only observed in normotensive rats since no such effect was observed in a rat model exhibiting genetic stroke risk factors (SHRSP).

The precise mechanism involved in the neuroprotective action of apocynin is unclear at present. It has now been widely accepted that apocynin is a pro-drug which requires activation by myeloperoxidase to form diapocynin which is the metabolically active form of the drug (Simons et al, 1990; Ximenes et al, 2007). Since vascular cells do not express myeloperoxidase, it has been proposed that the neuroprotective action of apocynin is mediated by its antioxidant capacity, which may not require dimer formation, and not by the inhibition of vascular NADPH oxidase (Heumüller et al, 2008). These authors demonstrated that apocynin failed to inhibit superoxide generation in HEK293 cells overexpressing NADPH oxidase isoforms (Nox1, Nox2, Nox4). However, when these cells were supplemented with myeloperoxidase, dimerization and activation of apocynin was observed with inhibition of NADPH oxidase activity. Furthermore, apocynin failed to inhibit NADPH oxidase activity and superoxide generation in endothelial and vascular smooth muscle cells which do not express myeloperoxidase. However, apocynin demonstrated antioxidant effects in vascular cells by inhibiting hydrogen peroxide activity and hydroxyl formation. Therefore, apocynin demonstrates free radical scavenging capability and it may be the antioxidant activity of apocynin which leads to the observed neuroprotective effects (Heumüller et al, 2008).

However, the absence of myeloperoxidase in vascular cells may not prevent the oxidation of apocynin into it metabolically active form. Vascular cells may possess other peroxidases which can activate apocynin (Touyz, 2008). It has been previously demonstrated that horseradish peroxidase induces apocynin dimer formation with subsequent inhibition of NADPH oxidase activity (Vejražka et al, 2005). Despite horseradish peroxidase being an exogenous peroxidase, this study provides evidence that other peroxidases can influence apocynin activity.

It has also been proposed that apocynin may inhibit vascular NADPH oxidase even if these cells do not express peroxidases which can activate the drug. It has been demonstrated *in vivo*, that neutrophils secrete myeloperoxidase which can be taken up by endothelial cells by the interaction of cytokeratin 1 on the endothelial cell surface (Astern et al, 2007). The internalised peroxidase can then activate apocynin leading to inhibition of vascular NADPH oxidase (Touyz, 2008, Figure 5-19).

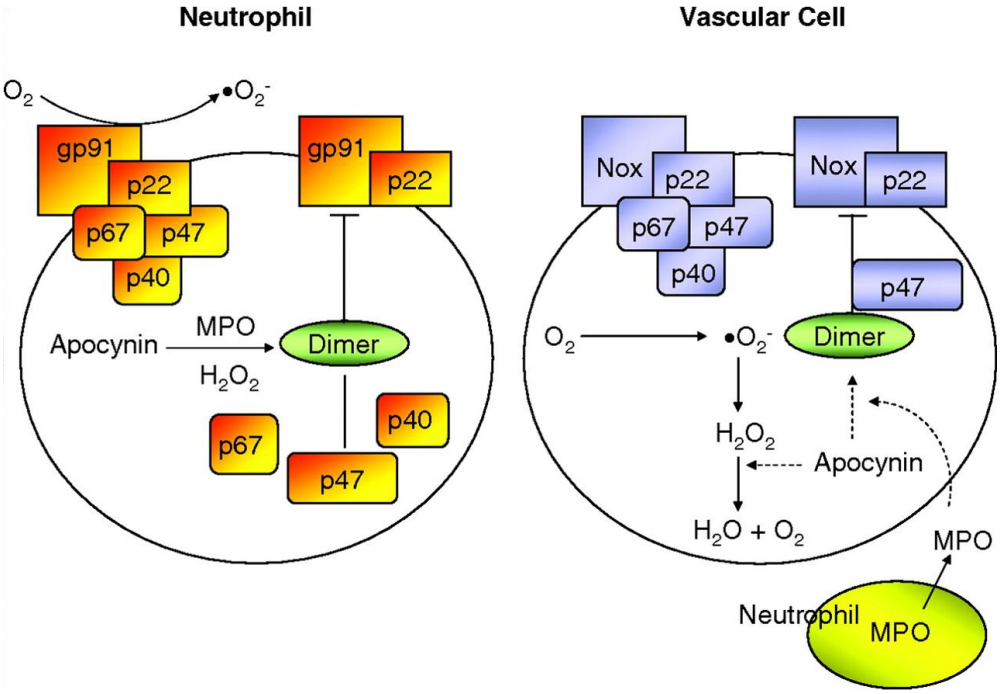

Figure 5-19. The potential effects of apocynin on phagocytic cells (neutrophil) and non-phagocytic cells (vascular cell). In neutrophils, apocynin is oxidised by myeloperoxidase (MPO) to form metabolically active dimers and trimers. NADPH oxidase activity is dependent on the translocation of p47phox/p67phox/p40phox to the cell membrane where the cytosolic complex interacts with gp91phox and p22phox. Apocynin prevents translocation of the p47phox subunit and therefore inhibits superoxide generation mediated by NADPH oxidase. In vascular cells, which do not contain endogenous MPO, apocynin acts as an antioxidant, thereby reducing reactive oxygen species bioavailability, without inhibiting NADPH oxidase. It may be possible that vascular cells possess non-MPO peroxidases that could activate apocynin to dimers and trimers to inhibit vascular NADPH oxidase, which is composed of Nox2 or its homologues (Nox1, Nox4, or Nox5) as the catalytic subunit. In vivo studies suggest that apocynin in vascular cells could also be activated by MPO secreted from neutrophils. Dashed arrows indicate possible effects; →, stimulation; ⊥, inhibition. Reproduced from Touyz (2008).

The reduction in infarct volume observed following apocynin treatment in Sprague-Dawley rats following ischaemia/reperfusion was comparable to that shown in other published studies (Tang et al, 2007). In the present study, infarct volume at 72 hours post-MCAO was reduced by approximately 60% in apocynin treated rats, following 1 hour of ischaemia. Previously, reductions in infarct volume of up to 40% have been observed in normotensive rats following apocynin treatment. Tang and colleagues reported a 37% reduction in infarct volume in Sprague-Dawley rats following apocynin treatment administered at 1 hour post-MCAO (Tang et al, 2007). Similar observations have been reported following apocynin treatment in Wistar rats, where infarct volume was reduced by 40%, when treatment was administered at 2 hours post-MCAO (Genovese et al, 2011). An improved outcome has also been reported with apocynin treatment in mouse transient ischaemia models. Reductions in infarct volume of up to 50% compared to control treated mice have been demonstrated. Chen and colleagues reported a 50% reduction in infarct volume when apocynin treatment was administered following 70 minutes of ischaemia (Chen et al, 2009) and a similar reduction in infarct volume was reported by Jackman et al (2009). However, these authors administered apocynin 30 minutes prior to the induction of ischaemia, which reduces the clinical relevance of these findings.

In the permanent MCAO model, apocynin treatment had no significant effect on infarct volume or behavioural outcome in WKY rats at 24 hours post-MCAO. The vibrissae-evoked forelimb scores observed across the 3 treatment groups were more severe than those previously described following permanent occlusion of the MCA in Sprague-Dawley rats, where 70-80% of contralateral placements were unsuccessful from 24 hours post-MCAO (Schallert et al, 2000). This may be attributable to the larger infarct observed in WKY rats compared to Sprague-Dawley rats, as previously described (Chapter 3). In WKY rats, there is more extensive injury in both the striatum and the cortex and the forelimb placement test is sensitive to both cortical and striatal damage (Schallert et al, 2000).

In the present study, there was a trend (not statistically significant) towards improved functional outcome with low dose apocynin treatment in Sprague-Dawley rats following transient focal ischaemia which was associated with a significantly reduced infarct volume at 72 hours post-MCAO. The functional tests used in this study may not have been sensitive enough to detect subtle improvements in neurological function. The low dose apocynin treated rats exhibited normal feeding and grooming behaviours and their general appearance and condition was improved compared to vehicle and high dose apocynin

treated rats. However, the modified Bederson scale, the forelimb placement test and the 18 point neurological score fail to detect these behaviours. It may therefore be advantageous for the benefit of future studies to develop a composite functional test which assesses feeding and grooming behaviours in addition to tests of general proprioceptive and sensorimotor capabilities.

All previous studies examining the effects of apocynin in ischaemia-reperfusion models have assessed infarct volume at 24 hours post-MCAO. However, at this time point in transient ischaemia models, the infarct is still evolving, as demonstrated in the present study, where infarct volume increased between 24 and 72 hours (Figure 5-15). Neuronal injury following transient cerebral ischaemia is an evolving process which can continue for days following stroke (Williams et al, 2004). It has been previously demonstrated in rat transient ischaemia models that delayed reperfusion injury can contribute to the development of the infarct beyond 24 hours post-MCAO (Du et al, 1996; Li et al, 2000). Therefore, a limitation of the previously published studies with apocynin is that the effect on final infarct volume may have not been assessed accurately due to the use of the 24 hour time point.

In order to increase the likelihood of translation of neuroprotective drugs from bench to bedside, it is necessary to evaluate potential neuroprotective strategies in preclinical models with stroke risk factors, like increasing age and hypertension. The SHRSP is therefore a suitable rat model for assessing the neuroprotective efficacy of apocynin. It has also been demonstrated in this chapter, that apocynin had no protective effect in SHRSP rats following 1 hour of ischaemia. Treatment with 5mg/kg apocynin at 5 minutes post-MCAO did not have any effect on perfusion-diffusion mismatch volume or the evolution of ischaemic injury in SHRSP rats during the critical acute phase following stroke. Mortality rates were high, with 67% of rats dying before the 72 hour end point. This prevented statistical analysis of infarct volume between groups since only 2 rats in each treatment group survived to 72 hours post-MCAO. Previously, it has been reported that apocynin treatment does not improve stroke outcome in aged rats despite an improvement in outcome being observed in young rats. Kelly and colleagues demonstrated that apocynin treatment worsened stroke outcome in aged rats, where the mortality rate was significantly higher in apocynin treated rats (36% mortality) compared to aged vehicle treated rats (14% mortality). Apocynin treatment also failed to improve functional outcome or reduce infarct volume at 24 hours post-MCAO compared to aged vehicle treated rats. Furthermore, oedema formation at 24 hours post-MCAO was significantly higher in aged apocynin

treated rats, where the volume of the ipsilateral hemisphere increased by 20%, compared to a 6% increase in aged vehicle treated rats (Kelly et al, 2009). Aged rats demonstrate reduced levels of SOD, increased generation of reactive oxygen species and reduced antioxidant activity which supports the 'free radical theory of aging' where increased levels of oxidative stress contribute to age-related diseases (Harman, 1994). Increased levels of oxidative stress have been reported in the SHRSP and contribute to the increased infarct volume observed following experimental stroke compared to the normotensive control strain, WKY (Kishi et al, 2004; Cheng et al, 2008; Dunn et al, 2008).

The present studies demonstrate that inhibiting a component of the oxidative stress pathway with apocynin, improves stroke outcome in normotensive Sprague-Dawley rats but has no effect in SHRSP rats. Given the increased oxidative stress response in the SHRSP it was hypothesised that apocynin treatment may improve outcome by inhibiting the production of superoxide through NADPH oxidase inhibition. The fact that we observed no effect in the SHRSP may be attributable to strain specific differences in the expression of NADPH oxidase isoforms. There is some debate regarding the contribution of specific isoforms to the generation of reactive oxygen species during ischaemia. It has been reported that Nox1 and Nox4 account for the generation of reactive oxygen species under physiological conditions (Miller et al, 2005; 2007) and upregulation of Nox2 occurs during ischaemia, making it the predominant source of reactive oxygen species (Kahles et al, 2007). Apocynin is believed to be selective for the Nox1 and Nox2 isoforms by preventing the translocation of p47phox from the cytosol to the Nox1/2 catalytic membrane domain (Stolk et al, 1994). Evidence for the Nox2 selectivity of apocynin was recently provided by Jackman and colleagues. This group of investigators demonstrated a significant neuroprotective effect of apocynin in wild type mice, where stroke outcome was improved and superoxide levels were reduced. However, no protective effect was observed in Nox2-deficient mice. These findings suggest that the neuroprotective effect of apocynin was mediated by inhibition of Nox2 containing NADPH oxidase and provide evidence for the importance of the Nox2 isoform during ischaemia (Jackman et al, 2009).
However, Kleinschnitz and colleagues (Kleinschnitz et al, 2010) proposed that Nox4 is the most relevant source of reactive oxygen species under ischaemic conditions as it is the most abundant vascular isoform in cerebral vessels (Miller et al, 2005) and is upregulated in stroke (McCann et al, 2008). This study group reported that Nox4-deficient mice demonstrated an improved stroke outcome following permanent and transient ischaemia compared to wild-type mice. However, Nox1- and Nox2-deficient mice showed no improvement in stroke outcome (Kleinschnitz et al, 2010).

These findings may explain why apocynin treatment did not improve outcome in a model of permanent MCAO. If Nox4 is the principal isoform under ischaemic conditions, then inhibiting Nox2 with apocynin may not significantly reduce the generation of reactive oxygen species and its contribution to ischaemic injury. In addition, the free radical scavenging capabilities of apocynin may not be sufficient to reduce ischaemic damage. However, this does not explain the clear neuroprotective effects of apocynin demonstrated in transient focal ischaemia models. It may be the case that following reperfusion Nox2 activity becomes the predominant source of reactive oxygen species and that apocynin mediates its neuroprotective actions by inhibiting Nox2 which may be upregulated following restoration of flow. However, this is highly speculative and the possible upregulation of NADPH oxidase isoforms following reperfusion has not yet been examined. It is interesting to note that all studies which report apocynin neuroprotection have employed ischaemia-reperfusion models of focal ischaemia. To date, there are no published reports on the effects of apocynin in stroke models of permanent MCAO. This may be because of negative findings which have not been published due to publication bias towards positive studies.

The lack of a neuroprotective effect of apocynin specifically in SHRSP rats following transient focal ischaemia may be related to strain specific differences in NADPH oxidase isoform expression. It has been reported that SHRs demonstrate higher levels of Nox4 mRNA compared to normotensive WKY rats and this is associated with enhanced cerebrovasodilatation in chronic hypertension (Paravicini et al, 2004). It is therefore not unreasonable to speculate that the SHRSP strain, derived by selective breeding from SHR, may also exhibit increased expression of Nox4. These data suggest that Nox4 may have a protective role in hypertension. However, as previously discussed Nox4 is upregulated during ischaemia and contributes to ischaemic injury (Kleinschnitz et al, 2010). In hypertensive animals, like the SHRSP, Nox4 may continue to be the principal source of reactive oxygen species following reperfusion. Therefore, apocynin treatment would not impact on the extent of ischaemic injury.

Furthermore, apocynin treatment failed to prolong the lifespan of the ischaemic penumbra in SHRSP, as defined by perfusion-diffusion mismatch at 1 hour post-MCAO. This may be attributable, in part, to the small volumes of mismatch tissue detected in this strain. Previously, it has been reported that administration of the selective endothelin antagonist, SB 234551, successfully preserved mismatch defined penumbra in normotensive Sprague-Dawley rats but failed to demonstrate a protective effect in SHR rats, where there was little

evidence of mismatch tissue at 1 hour post-MCAO (Legos et al, 2008). The lack of penumbral tissue in the SHR and SHRSP strains may therefore limit the potential for tissue salvage following stroke in models of genetic hypertension.

It has been reported that increased generation of reactive oxygen species in hypertensive rats contributes to the development of arterial hypertension by inducing endothelial dysfunction (Alexander et al, 2000). Therefore, inhibition of NADPH oxidase with apocynin has been investigated as a potential anti-hypertensive strategy. However, apocynin has no effect on blood pressure in normotensive rats (Li et al, 2003) and there are conflicting reports on the ability of apocynin to lower blood pressure in hypertensive rats. Bäumer and colleagues reported that apocynin treatment lowered systolic blood pressure in SHRs as effectively as the calcium channel blocker, nifedipine. SHRs received daily administration of 33mg/kg apocynin or nifedipine (30mg/kg) for a period of 28 days. Within one week of treatment, apocynin significantly reduced systolic blood pressure from 183±2mmHg to 164±12mmHg ($P<0.05$) and this treatment effect was maintained over the 28 day observation period. The antihypertensive effect of apocynin was comparable to the effect of nifedipine treatment, where systolic BP had reduced to 166±27mmHg by day 2 (Bäumer et al, 2007). The authors also observed that the anti-hypertensive effect of apocynin correlated with reduced vascular ROS levels, increased activity of eNOS and increased NO bioavailability, suggesting that the mechanism of action involves inhibition of vascular NADPH oxidase. However, these findings conflict with a previous study which reported that apocynin treatment over a 3 week period had no significant effect on blood pressure in SHR and WKY rats (Paliege et al, 2006). Similarly, Schlüter and colleagues also reported that apocynin treatment failed to reduce arterial pressure, which was measured via implanted radiotelemetric devices in SHR. Apocynin treatment was administered orally in the drinking water over a period of 5 weeks and arterial pressure continued to be assessed for a further 12 weeks. Apocynin treated SHR demonstrated virtually identical arterial pressures as untreated controls over the entire observation period (Schlüter et al, 2008). Furthermore, these authors assessed the vasodilator capacity of apocynin in vitro and observed that apocynin dilated arterial segments of SHRs in a dose-dependent manner. However, the authors also examined aortic rings from p47phox knockout mice and reported an increased sensitivity to apocynin-induced vasodilatation, which was then prevented by Rho kinase inhibition. These authors therefore suggest that apocynin-mediated vasodilatation is not dependent on NADPH oxidase but involves Rho kinase activity. It has been reported previously that rho kinase activity contributes to

infarct volume following experimental stroke (Shin et al, 2007). These findings further complicate the already complex mechanism of action of apocynin.

The dose of apocynin and the timing of administration appear to be critical to its neuroprotective effects in rodent stroke models. It has been reported that apocynin improves stroke outcome within a narrow dose range. Tang and colleagues reported that intravenous administration of 2.5mg/kg apocynin prior to reperfusion, significantly improved neurological outcome, reduced infarct volume and reduced the incidence of cerebral haemorrhage. However, when apocynin was administered at a dosage of 3.75 or 5mg/kg, no improvement in stroke outcome was observed and there was an increased incidence of cerebral haemorrhage in both the ipsilateral and contralateral hemispheres compared to vehicle treated controls. Furthermore, mice treated with 5mg/kg apocynin demonstrated a higher mortality rate of 38%, compared to vehicle treated mice (25%), whereas mice treated with 2.5mg/kg apocynin had a lower mortality rate (13%).
These findings are supported by other study groups, where mice pre-treated with 5mg/kg apocynin prior to ischaemia demonstrated a significantly higher mortality rate (41%) compared to vehicle treated mice (12%) and those treated with 2.5mg/kg apocynin (0%). Interestingly, mice pre-treated with 5mg/kg apocynin and then subjected to sham MCAO surgery did not die, suggesting that apocynin is only toxic at this dosage when cerebral ischaemia is induced (Jackman et al, 2009). The authors proposed that the higher dose of apocynin may compromise NADPH oxidase dependent cerebral vasodilatation by increased scavenging of H_2O_2. It has been shown previously that H_2O_2 mediates NADPH oxidase dependent vasodilatation in ischaemic brain regions (Paravicini et al, 2004; 2006).

The dosage of apocynin is unlikely to account for the mortality rates observed in the present studies, as in normotensive rats the mortality rate was higher in vehicle treated animals than those treated with apocynin. These results are in conflict with the studies previously discussed. However, those studies examined the effects of apocynin in mice and there may be species differences in the dose of apocynin required to induce toxic effects. The high mortality rate (67%) observed in both vehicle treated and low dose apocynin treated SHRSP rats suggest that drug treatment had no influence on mortality rate. It is more likely that the high mortality rate was attributable to brain swelling following reperfusion. It has been reported that BBB dysfunction may contribute to ischaemic injury and extensive brain oedema in SHRSP rats (Yamagata et al, 1997; Lippoldt et al, 2000; Ishida et al, 2006).

In addition, the timing of administration appears to be important when evaluating the neuroprotective effects of apocynin. Jackman and colleagues reported that administration of apocynin 30 minutes prior to ischaemia had a neuroprotective effect. However, when apocynin treatment was administered 1 hour after reperfusion, following 30 minutes ischaemia, there was no improvement in stroke outcome. These findings therefore suggest that the therapeutic potential of apocynin may be limited. However, other study groups have reported the neuroprotective effect of apocynin when administered up to 2 hours post-MCAO (Genovese et al, 2011), which is a more clinically relevant time point. In the present studies apocynin was administered at 5 minutes post-MCAO, however, the purpose of these experiments was to ascertain if apocynin demonstrated neuroprotective efficacy in a rat model of genetic hypertension and not to evaluate the potential therapeutic window, which would be the next logical step in this series of experiments.

Another limitation of the studies presented in this chapter is that we did not measure oxidative stress levels in the either the vasculature or the brain to assess whether apocynin treatment reduced oxidative stress levels. This could have been achieved by assessing the levels of oxidative stress markers, such as 8-hydroxy-2'-deoxyguanosine (8-OHdG) and 4-hydroxy-2-nonenal (4-HNE), using immunohistochemistry.

Furthermore, apocynin treatment was evaluated in SHRSP rats at a single dose of 5mg/kg. This dose may not have been optimal to confer neuroprotection in this strain despite demonstrating neuroprotective effects in normotensive Sprague-Dawley rats. In future studies, data on dose response should be generated to allow more accurate assessment of the effect of apocynin in SHRSP rats.

When evaluating the effect of apocynin on stroke outcome, care must be taken when deciding on the solvent to dissolve the drug, and its concentration. Apocynin is highly soluble (i.e. to >1mol/L) in non-polar solvents such as dimethylsulphoxide (DMSO), chloroform and alcohols (Selemidis et al, 2008) and DMSO is commonly used as a solvent in studies examining the effects of apocynin on stroke outcome. However, DMSO demonstrates neuroprotective effects at concentrations $\geq$ 10%. For example, when 10% DMSO was used as a vehicle in mouse models of focal cerebral ischaemia, it demonstrated neuroprotective efficacy (Alyson Miller, personal communication, 2010). Furthermore, Bardutzky and colleagues (2005) evaluated the neuroprotective effects of DMSO in a rodent permanent stroke model and reported that administration of 33% DMSO at 60 minutes post-MCAO prolonged the lifespan of the mismatch defined penumbra. This will impact on the findings of Genovese and colleagues, who recently reported an improvement in stroke outcome following apocynin treatment, where 10% DMSO was used as the

treatment vehicle. Therefore, the improvement in stroke outcome reported by this group may be attributable in part to the neuroprotection of DMSO. In the present studies, 0.1% DMSO was used as the vehicle to eliminate the possibility of neuroprotective efficacy. However, it may have been advantageous to include a saline treated control group to compare stroke outcome to the vehicle treated group.

The results of these studies also highlight the need for functional testing in addition to measurement of brain injury, when assessing potential neuroprotective therapy. High dose apocynin treatment significantly reduced infarct volume following 1 hour of ischaemia in Sprague-Dawley rats but there was no improvement in functional outcome. The recovery of neurological function and improvement in quality of life are the outcomes which are important clinically, rather than a reduction in brain injury alone. On this basis, low dose apocynin shows greater potential for clinical efficacy. However, the failure of low dose apocynin treatment to prolong the lifespan of the mismatch defined penumbra in SHRSP rats, suggests that apocynin may be of limited clinical potential. These results highlight the need for studies examining the effects of potential neuroprotective strategies in stroke models with risk factors. The present study demonstrates that apocynin treatment improves stroke outcome in normotensive rats following transient ischaemia but has no effect when administered to rats with genetic hypertension. This finding is likely to explain in part the failure of successful neuroprotectants to translate to clinical trials, since most pre-clinical drug studies use young healthy animals, which have less relevance to the human condition.

Summary

In the present study we have shown that apocynin does not influence infarct volume or functional outcome when administered following permanent focal cerebral ischaemia in normotensive rats. However, following transient cerebral ischaemia, apocynin reduced infarct volume and improve functional outcome when administered post-stroke. In contrast, apocynin, when given at a dose that reduced infarct and improved recovery in normotensive rats, had no significant effect on the acute evolution of ischaemic damage or functional outcome in the hypertensive SHRSP rat.

Chapter 6.
General Discussion

In the crucial first hours of acute ischaemic stroke, identification and salvage of penumbral tissue is the ultimate goal of both clinicians and experimental stroke researchers. Positron emission tomography remains the 'gold-standard' imaging modality for identifying the ischaemic penumbra in stroke research but its use is limited by the complex logistics associated with this technique. Consequently, MRI is now commonly used in clinical research to identify the penumbra as a result of its widespread availability and less complex logistics then PET. However, defining penumbra using the MRI perfusion-diffusion mismatch technique presents its own difficulties. Penumbra may be overestimated by the inclusion of benign oligaemic tissue and may be underestimated by the assumption that the diffusion lesion represents irreversibly injured tissue, which is not necessarily the case as DWI lesion reversal has been demonstrated both in animal models and stroke patients (Minematsu et al, 1992; Hasegawa et al, 1994; Kidwell et al, 2000). In addition, few study groups have determined perfusion and diffusion thresholds to define penumbra and there is a lack of consensus on appropriate thresholds and the parameters used to define hypoperfused tissue.

The findings in this thesis demonstrate that a single perfusion and diffusion threshold may not be appropriate for all rat strains since we have shown different values calculated in a rat model that displays stroke co-morbidities compared with normotensive rats. Strain differences in threshold values may lead to an over- or underestimation of penumbra. This will impact on preclinical drug studies, where salvage of the penumbra is used to evaluate drug efficacy across different rat strains. Therefore, it is important that perfusion and diffusion thresholds are defined in each rat strain used in preclinical stroke research. The calculated diffusion threshold for identifying ischaemically injured tissue was comparable in SHRSP and the normotensive control strain WKY. However, the absolute perfusion threshold was significantly higher in the hypertensive strain, which may indicate that the SHRSP is more sensitive to ischaemia than WKY. Therefore, it would be inappropriate to apply the same perfusion threshold to define the perfusion deficit across different rat strains, particularly those strains which exhibit stroke co-morbidities, like the SHRSP. The perfusion and diffusion thresholds determined in WKY and SHRSP in the present study also differ significantly from those previously defined in Sprague-Dawley rats using a similar method (Shen et al, 2003). In addition, the thresholds calculated in this thesis also differ from those defined in our laboratory in male and female Sprague-Dawley rats using the same method. In both male and female Sprague-Dawley rats a perfusion threshold of 63% reduction from mean contralateral CBF defined the perfusion deficit (TA Baskerville, unpublished observations). These data differ from the perfusion thresholds determined in

SHRSP and WKY rats (70% and 81% reduction from mean contralateral CBF for SHRSP and WKY, respectively). The diffusion thresholds determined in male and female Sprague-Dawley rats were comparable between the sexes, where a 27% and 30% reduction from mean contralateral ADC values defines the volume of ischaemic injury in male and female rats, respectively. However, these thresholds differ from the diffusion thresholds defined in SHRSP and WKY rats (23% and 21% reduction from mean contralateral ADC for SHRSP and WKY, respectively). This suggests that Sprague-Dawley rats may be less sensitive to reductions in ADC values and this may explain, in part, the smaller infarct volumes observed in this strain compared to SHRSP and WKY rats. These data further highlight the need for strain-specific thresholds of perfusion and diffusion abnormality.

The studies presented within this thesis have also highlighted the importance of selecting the method used to define the penumbra using MRI. Despite criticism regarding the inclusion of benign oligaemic tissue and DWI lesion reversal on reperfusion, the MRI perfusion-diffusion mismatch model continues to be a useful tool for approximating the ischaemic penumbra in both clinical and preclinical stroke research. In the present study, the volumetric mismatch method consistently generated lower volumes of perfusion-diffusion mismatch compared to spatially defined mismatch in both SHRSP and WKY rats, although this was not statistically significant. Although it is a simple arithmetic technique, the volumetric method does not provide any information on the extent and location of penumbral tissue, unlike the more precise spatial method, where mismatch tissue was assessed on each coronal slice. These findings are in agreement with previous reports, where volumetric and spatial mismatch methods were employed to define penumbra volume in stroke patients. It was demonstrated that simple arithmetic subtraction of the DWI lesion from the PWI defined perfusion deficit without any anatomical co-registration, consistently underestimated penumbra volume by 40% compared to penumbra defined by co-registration of DWI and PWI (Ma et al, 2009). On the basis of these results and the findings presented in this thesis, it should be recommended that the volumetric method is not used to define the mismatch but rather spatial assessment of perfusion-diffusion mismatch is carried out on each coronal slice.

The studies presented in this thesis also demonstrate that the volumetric and spatial mismatch methods failed to detect any significant difference in mismatch volume between the SHRSP and WKY strains. Mismatch volume was comparable between the strains from 1-4 hours post-MCAO and there was little evidence of mismatch defined penumbra from as early as 1 hours following stroke onset. This suggests that there may be a limited

potential for penumbra salvage in both strains. This is in conflict with previous reports from our laboratory, where mismatch was significantly reduced in SHRSP compared to WKY (McCabe et al, 2009). However, mismatch area was defined only on a single coronal slice within the MCA territory in this study. Other authors have also used the mismatch technique to define penumbra in rat models with stroke co-morbidities. There was no evidence of mismatch as early as 1 hour post-MCAO in SHR rats and administration of a selective ETA antagonist following stroke had no effect on final infarct volume at 24 hours (Legos et al, 2008). Letourneur and colleagues reported that mismatch volume was reduced in the SHR and renovascular hypertensive WKY rats (RH-WKY) compared to normotensive rats up to 4 hours post-MCAO (Letourneur et al, 2011). These results differ from the findings of the present study. It may be that the WKY rats used in the Letourneur study have a different genetic background to the WKY rats used in the studies described in this thesis. This could potentially influence the evolution of ischaemic injury and stroke outcome. Furthermore, the authors used the SHR strain which differs from the SHRSP strain used in the studies presented in this thesis. It has been demonstrated previously that both of the hypertensive strains demonstrate a significantly larger infarct volume than WKY rats following permanent MCAO and in addition, the SHRSP strain exhibits a larger infarct than the SHR strain (Duverger & MacKenzie, 1988). However, to date, there are no published studies in the literature which have compared mismatch volume in the SHR, SHRSP and WKY rat strains.

Criticisms of the perfusion-diffusion mismatch model have led to the development of alternative techniques to define the penumbra in acute ischaemic stroke research. The oxygen challenge is a MRI technique which has recently been developed to overcome the limitations of the mismatch model, using oxygen as a metabolic biotracer in combination with T2* weighted imaging (Santosh et al, 2008). This novel technique should allow a more precise evaluation of penumbra on the basis of its metabolic activity and is based on the differing magnetic properties of deoxyhaemoglobin and oxyhaemoglobin and is currently being validated in preclinical and clinical research. Perfusion CT is another alternative imaging modality to detect the penumbra. This technique involves the intravenous injection of an iodinated contrast agent and the bolus is tracked through the cerebral circulation. However, the radiation dose is a significant issue which needs to be considered as the dose required for perfusion CT is higher than that needed for standard CT. Nevertheless, in clinical research perfusion CT may overtake perfusion-diffusion mismatch due to its cost-effectiveness and the wide availability of CT scanners in the clinical setting (Heiss & Sorensen, 2009).

The acute evolution of the penumbra was also evaluated retrospectively by assessing the growth of the ADC derived lesion. However as previously discussed in Chapter 4, this method is not suitable when examining the lifespan of the penumbra at acute time points as tissue must proceed to infarction to allow retrospective calculation of the penumbra. Nevertheless, this technique has been used in clinical research to provide a retrospective approximation of the penumbra to compare with a new MRI diagnostic technique for penumbra in patients where perfusion data was not available (Dani et al, 2010). However, these authors were aware of the limitations of this method. The findings of the present study demonstrate that ADC lesion growth was significantly larger in WKY compared to SHRSP at 30 minutes post-MCAO. This suggests that there is a reduced potential for penumbra salvage in the SHRSP strain within the first 30 minutes following stroke. However, by 1 hour post-MCAO there is no significant difference in ADC lesion growth between the strains.

The studies presented in this thesis have also shown that the perfusion deficit increased significantly from 1-4 hours post-MCAO in both SHRSP and WKY rats. This is an interesting finding and may be indicative of a failure of collateral blood supply in both strains. Previously, our laboratory has demonstrated that the perfusion deficit increased significantly from 1-6 hours post-MCAO in SHRSP but not in WKY rats (McCabe et al, 2009). One of the limitations of this previous study was that the perfusion deficit was only examined on a single coronal slice within the core territory of the MCA and therefore any changes in CBF within more rostral or caudal regions with different collateral supply will have been missed. It is not surprising that the perfusion deficit increased over time in the hypertensive strain, as it has been demonstrated that collateral flow is impaired in SHRSP rats (Coyle & Heistad, 1987) and this is likely to contribute to the significantly larger perfusion deficit observed in SHRSP compared to WKY in the studies presented in this thesis. However, the temporal increase in perfusion deficit observed in WKY was somewhat unexpected. This is unlikely to be attributable to changes in blood pressure as mean arterial blood pressure and arterial PCO_2 and PO_2 did not change significantly during surgery or the 4 hour MRI scanning period. This finding suggests that the normotensive control strain experiences some impairment of collateral blood supply following stroke. Our laboratory has also demonstrated a small temporal increase in perfusion deficit in Sprague-Dawley rats, although not statistically significant. It would be interesting to compare the collateral blood supply of the WKY to other normotensive rat strains, such as the Sprague-Dawley rat, to assess any potential strain differences. To date,

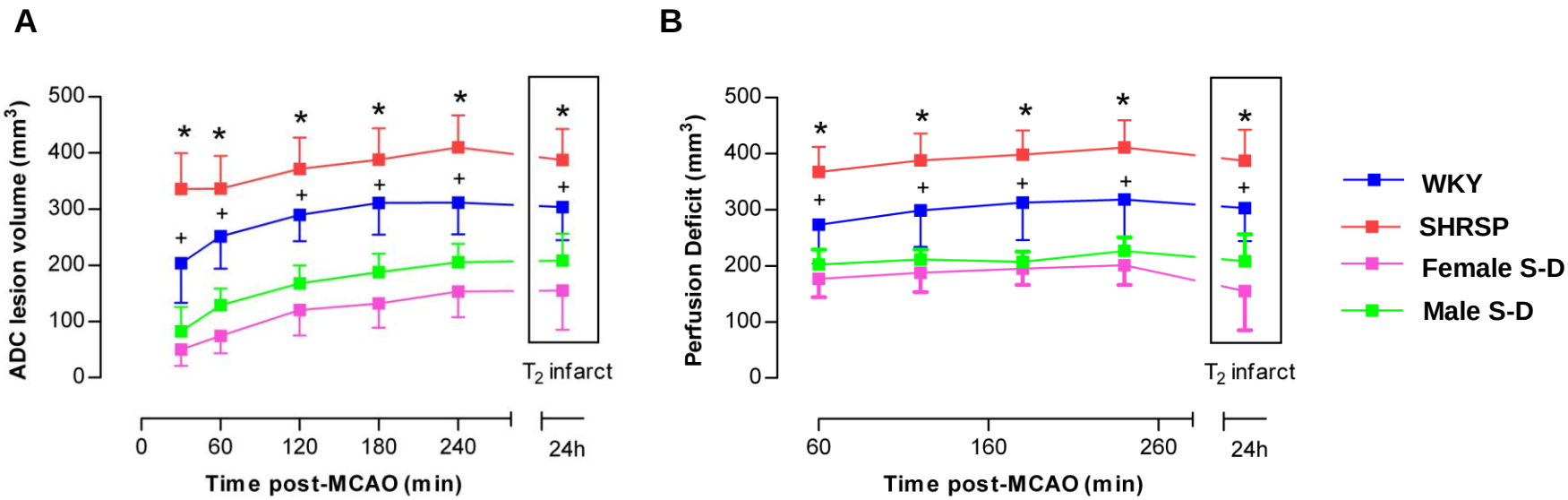

Figure 6-1. Temporal evolution of ischaemic injury and perfusion deficit in SHRSP, WKY and Sprague-Dawley rats. The volume of ischaemic injury is significantly higher in SHRSP and WKY rats compared to male and female Sprague-Dawley rats (S-D) from 30min to 4h post-MCAO (A). The volume of perfusion deficit is significantly higher in SHRSP and WKY rats compared to male and female S-D rats. All data are presented as mean±SD. *p<0.001 (SHRSP vs male and female S-D), +p<0.05 (WKY vs male and female SD), 2-way ANOVA with Bonferroni's post-test. WKY; n=12, SHRSP; n=15, Female S-D; n=10, Male S-D; n=9.

no such study has been undertaken. If indeed, the collateral vessels of the WKY rat differ in number, distribution, diameter or vasoreactivity compared to other normotensive strains, it may help to explain why, when exposed to the same ischaemic insult, the volume of ischaemic injury and perfusion deficit are significantly larger in WKY rats compared to Sprague-Dawley rats, as discussed previously in Chapter 3 (Figure 6-1). The experimental procedures and conditions within our laboratory were identical for the studies of both normotensive rat strains (although the data were produced by two investigators). The results demonstrated a greater extent of injury in WKY compared to Sprague-Dawley rats. The differences observed following focal cerebral ischaemia between normotensive rats strains warrants further investigation and it may be useful for further studies examining the SHRSP strain to also include the Sprague-Dawley rat as an additional control strain, as well as the WKY rat.

Rats are commonly used in animal models of stroke due to similarities to man with respect to their cerebral anatomy and physiology. Furthermore, the use of specific and inbred strains improves homogeneity in outcome measures, the cost of purchasing and maintaining them is relatively low compared to larger mammals and there is a greater level of social acceptance in the use of rodents in preclinical research (Sicard & Fisher, 2009). However, there are disadvantages in using rats to model human neurological diseases. Rats have a small region of subcortical white matter which makes it difficult to study white matter and model lacunar infarction (Carmichael, 2005). In addition, rodents demonstrate rapid behavioural recovery following experimental stroke which is not relevant to the clinical situation and many neurological deficits are difficult to assess (Sicard & Fisher, 2009). Furthermore, rodents possess small lissencephalic brains which are not directly comparable to the large gyrencephalic brains of humans. However, the use of larger species, like dogs, pigs and primates, is more relevant to the clinical situation as these species offer the advantage of having large gyrencephalic brains with proportions of grey and white matter which resemble that observed in humans (Howells et al, 2010, Figure 6-2).

Rodent stroke models have led to a better understanding of the mechanisms involved in the underlying pathophysiology of stroke and the identification of numerous targets for neuroprotective therapy (Mergenthaler et al, 2004). To date, the results of over 7,000 studies examining the neuroprotective effects of over 1,000 therapeutic interventions have been published (O'Collins et al, 2006) but unfortunately there has been a notable failure of

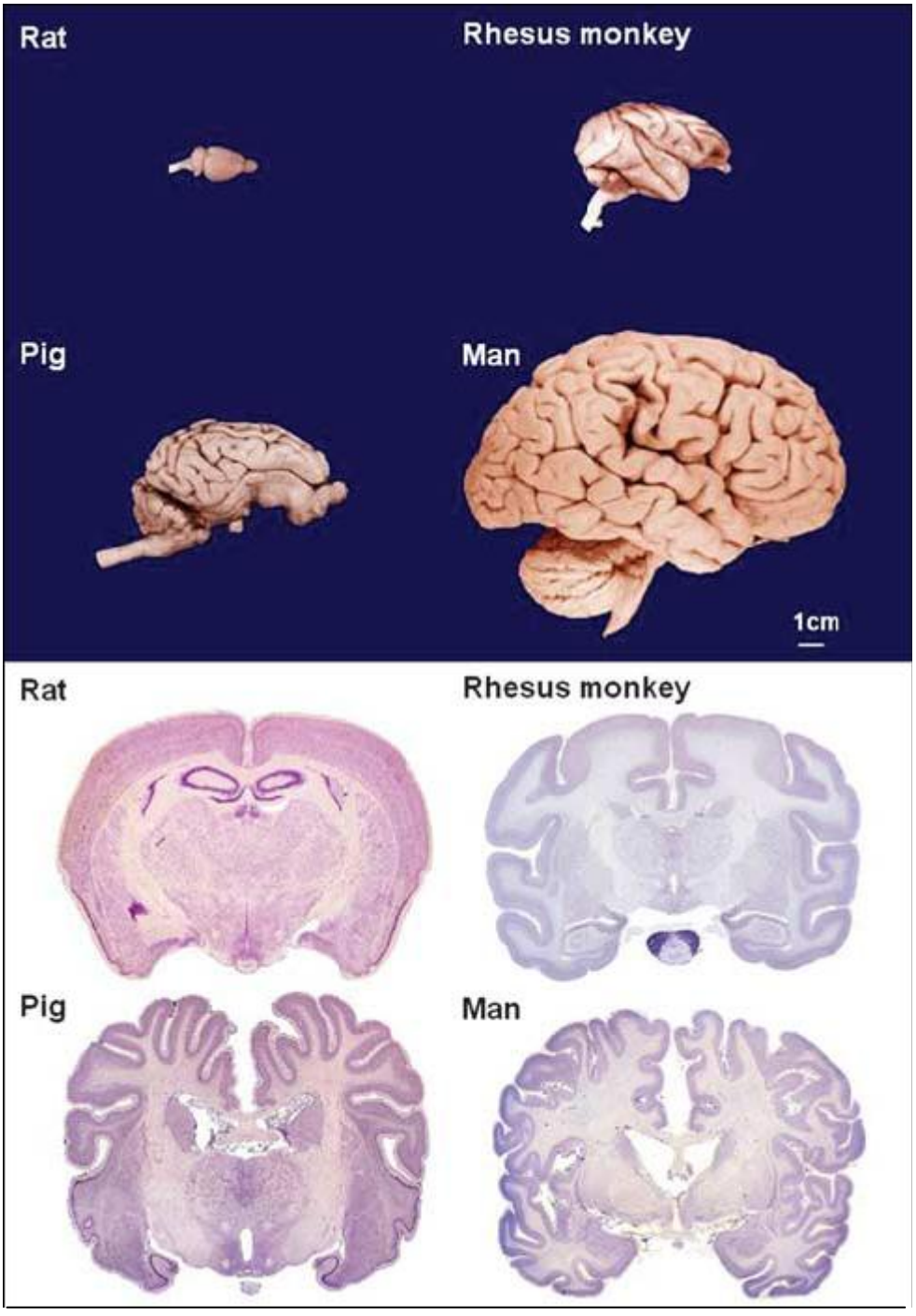

Figure 6-2. Brain size and gyral complexity in mammal species. Reproduced from Howells et al (2010).

translation from bench to bedside and thrombolytic therapy with recombinant tissue plasminogen activator remains the only successful pharmacological treatment in acute ischaemic stroke (NINDS, 1995). There are many factors which may explain why neuroprotective drugs demonstrate efficacy in experimental stroke models but fail to translate to human stroke patients. In some preclinical studies, therapy is administered prior to stroke onset and this does not reflect the clinical situation, where some stroke patients may not be diagnosed until many hours following stroke (Röther, 2008). In the study presented in this thesis, apocynin treatment was administered 5 minutes following stroke, which is not a particularly clinically relevant time point. However, the purpose of the studies was to assess if apocynin demonstrated a neuroprotective effect
and the next logical step in this series of experiments would be to delay administration to determine the therapeutic time window. Unfortunately, time constraints did not permit such a study to be undertaken.

Furthermore, there are significant anatomical, physiological and metabolic differences between humans and small rodents. Small rodents require higher drug doses on a mg/kg body weight basis compared to larger mammals and this means that effectivedoses cannot simply be translated from preclinical studies to clinical trial (Braeuninger & Kleinschnitz, 2009). In addition, the ischaemic lesion induced in experimental models is highly reproducible but a heterogenous population of stroke patients with a wide range of stroke severity and etiology is included in clinical trials.

Selecting the most appropriate stroke model is also important. Models which require a craniectomy, like the electrocoagulation method of distal middle cerebral artery occlusion (Tamura et al, 1981), are traumatic and do not mimic the clinical situation. Therefore, embolic and intraluminal thread models of middle cerebral artery occlusion may be more relevant to human stroke and also offer the significant advantage of permitting reperfusion (Braueninger & Kleinschnitz, 2009). However, the infarct produced by the intraluminal filament and the embolic model may be variable due to incomplete occlusion. In particular, infarcts produced by embolic models are generally less reproducible than those produced by the intraluminal filament and electrocoagulation models of MCAO due to variations in clot stability and the final lodgement of the embolus (DiNapoli et al, 2006).

Poor study design may also contribute to the failure of translation of neuroprotective strategies from preclinical research to clinical trial. Only a minority of published studies reporting neuroprotection have reported randomised treatment allocation and blinding of

investigators (Worp et al, 2005). A previous meta-epidemiological study examined 13 meta-analyses of experimental stroke studies and reported that those studies where induction of ischaemia was unblinded reported greater treatment effects than those studies which were blinded (Crossley et al, 2008). This demonstrates evidence of bias in preclinical stroke research when evaluating potential therapeutic strategies. In the studies presented in this thesis evaluating the potential neuroprotective effect of apocynin, the allocation of rats to treatment groups was carried out in a randomised manner using a random number generator, with the investigator performing the stroke surgery, drug administration and behavioural assessment (Emma Reid) completely blind to treatment group until completion of the experiments and data analysis. This limited any bias from the results presented in this thesis. Therefore, the improvements observed in stroke outcome following apocynin treatment in Sprague-Dawley rats following 1 hour of focal ischaemia, are likely to be true treatment effects. However, one source of bias in the studies presented in this thesis could not be removed. Although identical in general appearance, WKY rats are larger than age-matched SHRSP rats and this is a limitation which could not be controlled. Therefore the bias of knowing the strain of rat during stroke surgery could not be removed.

The recommendations of the Stroke Therapy Academic Industry Roundtable (STAIR, 1999) were taken into account when designing the studies to evaluate the neuroprotective efficacy of apocynin. Power calculations were performed to determine the group sizes necessary to detect a treatment effect. Apocynin efficacy was assessed following both permanent and transient ischaemia and rats with stroke co-morbidities (SHRSP) were used. In addition, treatment allocation was randomised and the investigator administering the drug and performing behavioural assessment was blind to treatment group. Furthermore, perfusion-diffusion mismatch was used as an outcome measure when evaluating the efficacy of apocynin in SHRSP rats.

The results of Chapter 5 demonstrated that apocynin treatment had no effect on stroke outcome following permanent MCAO in WKY rats. However, both low and high dose apocynin treatment significantly reduced infarct volume by 60% in Sprague-Dawley rats following transient ischaemia of 1 hour duration. These findings are in agreement with previous reports of the neuroprotective effect of apocynin treatment in rat transient ischaemia models, where reductions in infarct volume of up to 40% have been demonstrated (Tang et al, 2007; Genovese et al, 2011). Furthermore, there was a trend towards improved functional outcome with low dose apocynin treatment, although this

improvement did not reach the level of statistical significance. However, the general condition of low dose apocynin treated rats was observed to be markedly improved compared to vehicle and high dose treated rats. Therefore, in future studies, it may be advantageous to develop a test of functional outcome which incorporates feeding and grooming behaviours, in addition to the standard tests of sensorimotor function.

Interestingly, when low dose apocynin treatment was evaluated in the SHRSP strain, it failed to confer neuroprotection and a mortality rate of over 60% was observed in both the vehicle treated and apocynin treated rats. This demonstrates that although apocynin improved stroke outcome in normotensive rats following 1 hour of focal ischaemia, it failed to confer neuroprotection under the same conditions in a rat model with genetic stroke risk factors. The STAIR guidelines recommend the use of perfusion-diffusion mismatch as an imaging biomarker to evaluate the efficacy of potential therapeutic strategies to improve the translation from preclinical to clinical trials (Fisher et al, 2009). The use of the mismatch model allowed the effect of apocynin on the acute evolution of ischaemic injury in SHRSP to be assessed. The failure of apocynin to confer neuroprotection in SHRSP rats may be attributable to the possibility that Nox4 is the predominant isoform of NADPH oxidase during ischaemia and reperfusion, rather than Nox2, which is inhibited by apocynin. Furthermore, the lack of neuroprotective efficacy may also be attributable in part to the small volumes of mismatch tissue observed in the hypertensive strain. Therefore, there may be a limited potential for penumbra salvage in the SHRSP strain. The efficacy of potential therapeutic strategies may therefore be limited in preclinical models with stroke co-morbidities. Kelly and colleagues previously demonstrated that apocynin worsened stroke outcome in aged rats, compared to vehicle treated controls, where mortality rate was increased from 14% to 36% (Kelly et al, 2009). It may be that in aged rats, apocynin is not activated to the active dimer form as it has been reported that unactivated apocynin has pro-oxidant effects (Riganti et al, 2006) and this may have exacerbated ischaemic injury. The findings of Kelly and colleagues and the results reported in this may help to explain the failure of neuroprotective agents to translate to clinical trial. One of the major failings of preclinical research is the use of young healthy animals to assess the potential efficacy of therapeutic interventions. The majority of stroke patients recruited into clinical trials are elderly and may suffer from stroke co-morbidities such as hypertension, diabetes and atherosclerosis (Braeuninger & Kleinschnitz, 2009). It is therefore essential, that when evaluating the therapeutic strategies in preclinical research, that there should be increasing focus on aged animals and animals with stroke co-morbidities, like the SHRSP strain. However, there are additional problems of increased

mortality when using aged animals and animals with stroke-comorbidities. Furthermore, there is an increased cost of housing, feeding and maintenance when using aged animals.

Furthermore, preclinical studies to evaluate potential therapeutic strategies should routinely assess stroke outcome by functional testing, in addition to infarct volume. This step is vital for translation to clinical trial as a desirable outcome in human stroke patients is determined by the degree of disability and the improvement in quality of life, not solely by a reduction in brain injury, as this will not necessarily equate to an improved outcome for the patient. The need for combined assessment of brain injury and functional outcome is highlighted by the studies reported in this thesis, where low dose apocynin treatment significantly reduced infarct volume and improved functional outcome in Sprague-Dawley rats following 1 hour of ischaemia. However, high dose apocynin treatment failed to improve functional outcome despite reducing infarct volume by 60% compared to the vehicle treated group, although this may be related to the sensitivity of the behavioural tests. Furthermore, the design of the study could have been improved by increasing the number of rats in each group to increase the the likelihood of detecting differences in behavioural outcome between groups. However, on the basis of the results presented in this thesis, low dose apocynin treatment improves stroke outcome in terms of functionality and should be used in future studies rather than the higher dose of apocynin.

In terms of future strategies to salvage brain tissue following stroke, combination therapy may be the way forward. The pathophysiological mechanisms are so highly complex that targeting a single component of the ischaemic cascade may have a limited effect on stroke outcome. There is an increasing focus on evaluating the combined effects of neuroprotective strategies and thrombolysis with rtPA (Fujiwara et al, 2009, Figure 6-3). Any new neuroprotective drug under test should be given in combination with rtPA or tested only in those patients not receiving treatment as it would be unethical to not to give eligible patients rtPA.

An alternative example of a potential combination therapy is magnesium treatment and hypothermia. The neuroprotective effects of hypothermia are well established and it is used clinically to limit brain ischaemia in comatose cardiac arrest patients (Hypothermia After Cardiac arrest Study Group, 2002). Magnesium therapy has also been demonstrated to be neuroprotective in animal models of cerebral ischaemia but failed to translate to clinical trial, with some evidence that magnesium may be beneficial in lacunar strokes (IMAGES Study Group, 2004).

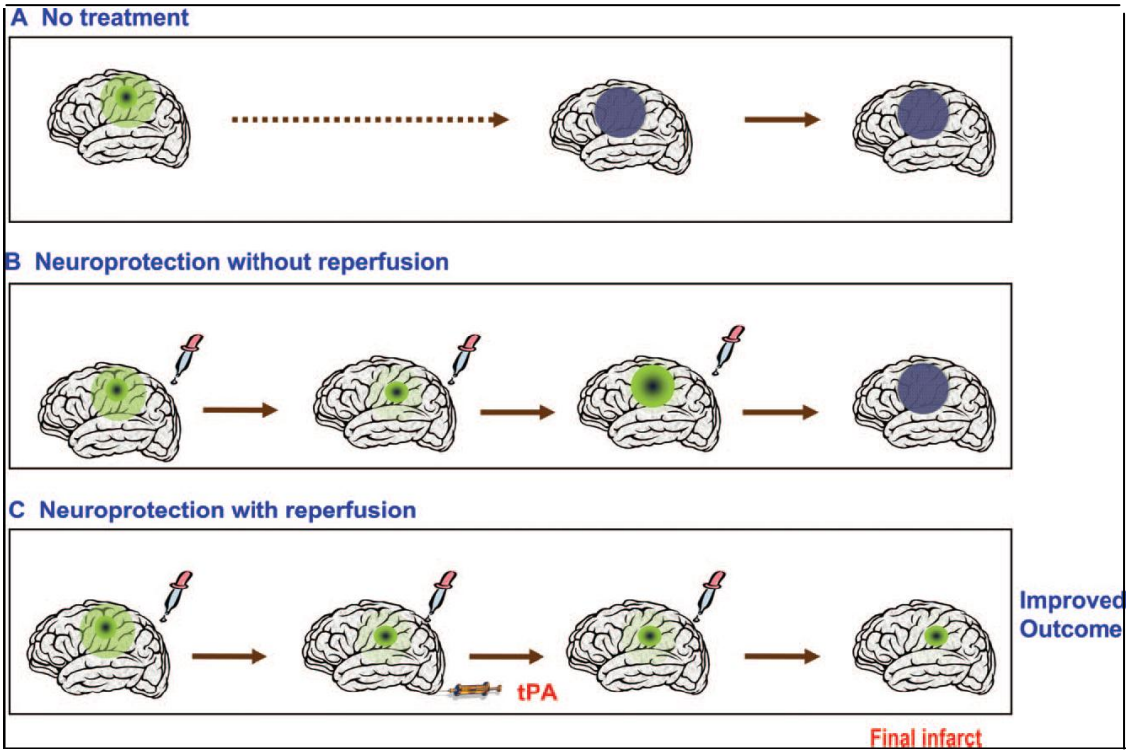

Figure 6-3. Hypothetical scenarios for the progression of brain injury following ischaemic stroke. In the absence of any treatment the infarct will rapidly evolve leading to permanent injury (A). If a neuroprotective drug is administered but it does not alter the ischaemic environment then the infarct will progressively expand to reach its maximum volume although growth may be delayed by the action of the drug (B). The progression of infarction could be reduced by interventions which improve collateral blood flow to the penumbra or recanalise the ischaemic territory (C). Neuroprotective drugs may be useful in prolonging the time window for thrombolysis. Reproduced from Chavez et al (2009).

However, the mechanisms involved in the neuroprotective effects of hypothermia and magnesium therapy are poorly understood. It has been proposed that the neuroprotective action of magnesium is 'unmasked' at low temperatures. Campbell and colleagues demonstrated that mild hypothermia and magnesium treatment had no significant effect on infarct volume following permanent focal cerebral ischaemia in rats but in combination a significant reduction in infarct volume of over 50% compared to vehicle treated groups (Campbell et al, 2008). This apparent synergistic effect of combination therapy may explain, in part, the failure of magnesium therapy to translate to clinical trial since patient management in the IMAGES trial did not involve the active induction of hypothermia (Meloni et al, 2009). In addition, in the majority of the preclinical studies reporting the neuroprotective effect of magnesium therapy, post-ischaemic body temperature was not reported. Therefore, it may be possible that spontaneous hypothermia induced the observed treatment effects (Meloni et al, 2009). In addition, magnesium and mild hypothermia treatment could potentially be administered in combination with thrombolytic therapy to extend the therapeutic time window in acute ischaemic stroke as magnesium and hypothermia treatment do not alter the enzymatic activity of tPA (Meloni et al, 2009).

An alternative therapy could involve the combination of rtPA with hypothermia and apocynin. The results presented in this thesis demonstrated that apocynin improved stroke outcome in normotensive rats in combination with reperfusion. Hypothermia may further improve stroke outcome. However, it would first have to be determined if apocynin has any detrimental effect on the enzymatic activity of rtPA before combining these treatments. Apocynin treatment could be administered simultaneously with rtPA and hypothermia could be induced concurrently by surface cooling.

To conclude, perfusion-diffusion weighted MRI is an important imaging biomarker for identifying potentially salvageable penumbra in clinical and preclinical stroke research and in assessing the effect of potential neuroprotective strategies. However, the findings reported in this thesis demonstrate that care should be taken when applying thresholds to define hypoperfused and injured tissue, as the present study has shown variability between rat strains with and without stroke-comorbidities. The method used to determine penumbra should also be taken into consideration and on the basis of the results presented within this thesis, spatial co-registration of perfusion and diffusion lesions appears to be the most informative and precise method to define perfusion-diffusion mismatch. In addition, the work contained within this thesis has also reported that neuroprotective therapies may demonstrate efficacy in young, healthy rodent models of stroke but fail to confer neuroprotection in models with genetic stroke risk factors, like hypertension. These

findings highlight the need to evaluate potential therapeutic strategies in a range of animal models with stroke risk factors to improve the chance of successful translation to human stroke patients.

References

Abe O, Aoki S, Shirouzu I, Kunimatsu A, Hayashi N, Matsumoto T, Mori H, Yamada H, Watanabe M, Masutani Y, Ohtomo K. MR imaging of ischemic penumbra. *Eur J Radiol* 2003;46:67-78.

Ackerman RH, Correia JA, Alpert NM, Baron JC, Gouliamos A, Grotta JC, Brownell GL, Taveras JM. Positron imaging in ischemic stroke disease using compounds labeled with oxygen 15. Initial results of clinicophysiologic correlations. *Arch Neurol* 1981;38:537-543.

Adibhatla AY & Hatcher JF. Lipid oxidation and peroxidation in CNS health and disease: from molecular mechanisms to therapeutic opportunities. *Antioxid Redox Signal* 2010;12:125-169.

Albers GW, Thijs VN, Wechsler L, Kemp S, Schlaug G, Skalabrin E, Bammer R, Kakuda W, Lansberg MG, Shuaib A, Coplin W, Hamilton S, Moseley M, Marks MP. Magnetic resonance imaging profiles predict clinical response to early reperfusion: The diffusion and perfusion imaging evaluation for understanding stroke evolution (DEFUSE) study. *Ann Neurol* 2006;60:508-517.

Alexander MY, Brosnan MJ, Hamilton CA, Fennell JP, Beattie EC, Jardine E, Heistad DD, Dominiczak AF. Gene transfer of endothelial nitric oxide synthase but not Cu/Zn superoxide dismutase restores nitric oxide availability in the SHRSP. *Cardiovasc Res* 2000;47:609-617.

Allan SM & Rothwell NJ. Cytokines and acute neurodegeneration. *Nature Rev Neurosci* 2001;2:734-744.

Almekhlafi MA, Wilton SB, Rabi DM, Ghali WA, Lorenzetti DA, Hill MD. Recurrent cerebral ischemia in medically treated patent foramen ovale. *Neurology* 2009;73:89-97.

Ariesen MJ, Claus SP, Rinkel GJE, Algra A. Risk factors for intracerebral hemorrhage in the general population: a systematic review. *Stroke* 2003;34:2060-2065.

Astern JM, Pendergraft WF, Falk RJ, Jennette JC, Schmaier AH, Mahdi F, Preston GA. Myeloperoxidase interacts with endothelial cell-surface cytokeratin 1 and modulates bradykinin production by the plasma kallikrein-kinin system. *Am J Pathol* 2007;171:349-360.

Astrup J, Symon L, Branston NM, Lassen NA. Cortical evoked potential and extracellular K^+ and H^+ at critical levels of brain ischemia. *Stroke* 1977;8:51-57.

Astrup J, Siesjö BK, Symon L. Thresholds in cerebral ischemia – the ischemic penumbra. *Stroke* 1981;12:723–725.

Ayata C, Ropper A. Ischaemic brain oedema. *J Clin Neurosci*. 2002;9(2):113-124.

Baird AE, Benfield A, Schlaug G, Siewert B, Lovblad K, Edelman RR, Warach S. Enlargement of human cerebral ischemic lesion volumes measured by diffusion-weighted magnetic resonance imaging. *Ann Neurol* 1997;41:581−589.

Baird AE, Warach S. Magnetic resonance imaging of acute stroke. *J CerebBlood Flow Metab* 1998;18:583-609.

Bandera E, Botteri M, Minelli C, Sutton A, Abrams KR, Latronico N. Cerebral blood flow threshold of ischaemic penumbra and infarct core in acute ischemic stroke: a systematic review. *Stroke* 2006;37:1334-1339.

Bardutzky J, Shen Q, Henninger N, Bouley J, Duong TQ, Fisher M. Differences in ischemic lesion evolution in different rat strains using diffusion and perfusion imaging. *Stroke* 2005a;36:2000-2005.

Bardutzky J, Meng X, Bouley J, Duong TQ, Ratan R, Fisher M. Effects of IV dimethyl sulfoxide on ischemia evolution in permanently occluded rats. *J Cereb Blood Flow Metab* 2005b;25:968-977.

Baron JC, Bousser MG, Rey A, Guillard A, Comar D, Castaigne P. Reversal of focal "misery-perfusion syndrome" by extra-intracranial arterial bypass in hemodynamic cerebral ischemia. A case study with 15O positron emission tomography. *Stroke* 1981;12:454-459.

Barone FC, Clark RK, Feuerstein G, Lenkinski RE, Sarkar SK. Quantitative comparison of magnetic resonance imaging (MRI) and histologic analyses of focal ischemic damage in the rat. *Brain Res Bull* 1991;26:285-291.

Barone FC, Arvin B, White RF, Miller A, Webb CL, Willette RN, Lysko PG, Feuerstein GZ. Tumour necrosis factor α: a mediator of focal ischemic brain injury. *Stroke* 1997;28:1233-1244.

Bäumer AT, Krüger CA, Falkenberg J, Ten Freyhaus H, Rösen R, Fink K, Rosenkranz S. The NAD(P)H oxidase inhibitor apocynin improves endothelial NO/superoxide balance and lowers effectively blood pressure in spontaneously hypertensive rats: comparison to calcium channel blockade. *Clinical & Exp Hypertens* 2007;29:287-299.

Beaulieu C, de Crespigny A, Tong DC, Moseley ME, Albers GW. Longitudinal magnetic resonance imaging study of perfusion and diffusion in stroke: Evolution of lesion volume and correlation with clinical outcome. *Ann Neurol* 1999;46:568-578.

Beckman JS, Koppenol WH. Nitric oxide, superoxide and peroxynitrite: the good, the bad, and ugly. *Am J Physiol* 1996;271:C1424-C1437.

Bederson JB, Pitts LH, Germano SM, Nishimura MC, Davis RL, Bartowski HM. Evaluation of 2,3,5-triphenyltetrazolium chloride as a stain for detection and quantification of experimental cerebral infarction in rats. *Stroke* 1986a;17:1304-1308.

Bederson JB, Pitts LH, Tsuji M, Nishimura MC, Davis RL, Bartkowski H. Rat middle cerebral artery occlusion: Evaluation of the model and development of a neurologic examination. *Stroke* 1986b;17:472-476.

Belayev L, Alonso OF, Busto R, Zhao W, Ginsberg MD. Middle cerebral artery occlusion in the rat by intraluminal suture. Neurological and pathological evaluation of an improved model. *Stroke* 1996;27:1616-1622.

Belliveau JW, Rosen BR, Kantor HL, Rzedzian RR, Kennedy DN, McKinstry RC, Vevea JM, Cohen MS, Pykett IL, Brady TJ. Functional cerebral imaging by susceptibility-contrast NMR. *Magn Reson Med* 1990;14:538−546.

Besancon E, Guo S, Lok J, Tymianski M, Lo EH. Beyond NMDA and AMPA glutamate receptors: emerging mechanisms for ionic imbalance and cell death in stroke. *Trends Pharmac Sci* 2008;29:268-275.

Branston NM, Symon L, Crockard HA, Pasztor E. Relationship between the cortical evoked potential and local cortical blood flow following acute middle cerebral artery occlusion in the baboon. *Exp Neurol* 1974;45(2):195-208.

Branston NM, Strong AJ, Symon L. Extracellular potassium activity, evoked potential and tissue blood flow. Relationships during progressive ischemia in baboon cerebral cortex. *J Neurol Sci* 1977;32(3):305-321.

Braueninger S, Kleinschnitz C. Rodent models of focal cerebral ischemia: procedural pitfalls and translational problems. *Exp Trans Stroke Med* 2009;1:8

Braeuninger S, Kleinschnitz C, Stoll G. Interleukin-18 does not influence infarct volume or functional outcome in the early stage after transient focal ischaemia in mice. *Exp Trans Stroke Med* 2010;2:1-5.

Bråtane BT, Bouley J, Schneider A, Bastan B, Henninger N, Fisher M. Granulocyte-colony stimulating factor delays PWI/DWI mismatch evolution and reduces final infarct volume in permanent-suture and embolic focal cerebral ischemia models in the rat. *Stroke* 2009;40:3102-3106.

Brennan AM, Suh SW, Won SJ, Narasimhan P, Kauppinen TM, Lee H, Edling Y, Chan PH, Swanson RA. NADPH oxidase is the primary source of superoxide induced by NMDA receptor activation. *Nat Neurosci* 2009;12:857-863.

Brosnan MJ, Clark JS, Jeffs B, Negrin CD, Van Vooren P, Arribas SM, Carswell H, Aitman TJ, Szpirer C, Macrae IM, Dominiczak. Genes encoding atrial and brain natriuretic peptides as candidates for sensitivity to brain ischemia in stroke-prone hypertensive rats. *Hypertension* 1999;33:290-297.

Brouns R & De Deyn PP. The complexity of neurobiological processes in acute ischemic stroke. *Clin Neurol Neurosurg* 2009;111:483-495.

Butcher KS, Parsons M, MacGregor L, Barber PA, Chalk J, Bladin C, Levi C, Kimber T, Schultz D, Fink J, Tress B, Donnan G, Davis S. Refining the perfusion-diffusion mismatch hypothesis. *Stroke* 2005;36:1153-1159.

Campbell K, Meloni BP, Knuckey NV. Combined magnesium and mild hypothermia (35^{o}C) treatment reduces infarct volumes after permanent middle cerebral artery occlusion in the rat at 2 and 4, but not 6 h. *Brain Res* 2008;1230:258-264.

Carmichael ST. Rodent models of focal stroke: size, mechanism and purpose. *NeuroRx* 2005;2:396-409.

Carswell HVO, Anderson NH, Clark JS, Graham D, Jeffs B, Dominiczak AF, Macrae IM. Genetic and gender influences on sensitivity to focal cerebral ischemia in the stroke-prone spontaneously hypertensive rat. *Stroke* 1999;33:681-685.

Chavez JC, Hurko O, Barone FC, Feuerstein GZ. Pharmacologic interventions for stroke. Looking beyond the thrombolysis time window into the penumbra with biomarkers, not a stopwatch. *Stroke* 2009;40:e558-e563.

Chemmanam T, Campbell BC, Christensen S, Nagakane Y, Desmond PM, Bladin CF, Parsons MW, Levi CR, Barber PA, Donnan GA, Davis SM. Ischemic diffusion lesion reversal is uncommon and rarely alters perfusion-diffusion mismatch. *Neurology* 2010;75:1040-1047.

Chen H, Song YS, Chan PH. Inhibition of NADPH oxidase is neuroprotective after ischemia-reperfusion. *J Cereb Blood Flow Metab* 2009;29:1262-1272.

Cheng J, Ou JS, Singh H, Falck JR, Narsimhaswamy D, Pritchard KA, Schwartzman ML. 20-Hydroxyeicosatetraenoic acid causes endothelial dysfunction via eNOS uncoupling. *Am J Physiol* 2008;294:H1018-H1026.

Chopp M, Li Y, Jiang N, Zhang RL, Prostak J. Antibodies against adhesion molecules reduce apoptosis after transient middle cerebral artery occlusion in rat brain. *J Cereb Blood Flow Metab* 1996;16:578-584.

Coyle P. Middle cerebral artery occlusion in the young rat. *Stroke* 1982;13:855-859.

Coyle P. Dorsal cerebral collaterals of stroke-prone spontaneously hypertensive rats (SHRSP) and Wistar Kyoto rats (WKY). *Anat Rec* 1987;218:40-44.

Coyle P, Heistad DD. Blood flow through cerebral collateral vessels one month after middle cerebral artery occlusion. *Stroke* 1987;18:407-411.

Coyle P, Jokelainen PT. Differential outcome to middle cerebral artery occlusion in hypertensive stroke-prone rats (SHRSP) and Wistar Kyoto (WKY) rats. *Stroke* 1983;14:605-611.

Crossley NA, Senna E, Gohler J, Horn J, van der Worp B, Bath PMW, Macleod M, Dirnagl U. Empirical evidence of bias in the design of experimental stroke studies. *Stroke* 2008;39:929-934.

Dani KA, Santosh C, Brennan D, McCabe C, Holmes WM, Condon B, Hadley DM, Macrae IM, Shaw M, Muir KW. T2*-weighted magnetic resonance imaging with hyperoxia in acute ischemic stroke. *Ann Neurol* 2010;68:37-47.

Darby DG, Barber PA, Gerraty RP, Desmond PM, Yang Q, Parsons M, Li T, Tress BM, Davis SM. Pathophysiological topography of acute ischemia by combined diffusion-weighted and perfusion MRI. *Stroke* 1999;30:2043-2052.

Dardzinski BJ, Sotak CH, Fisher M, Hasegawa Y, Li L, Minematsu K. Apparent diffusion coefficient mapping of experimental focal cerebral focal ischemia using diffusion-weighted echo-planar imaging. *Magn Reson Med* 1993;30:318-325.

Davidson AO, Schork N, Jaques BC, Kelman AW, Sutcliffe RG, Reid JL, Dominiczak AF. Blood pressure in genetically hypertensive rats: Influence of the Y chromosome. *Hypertension* 1995;26:452-459.

Davis SM, Donnan GA. Advances in penumbra imaging with MR. *Cerebrovasc Dis* 2004;17(suppl 3):23-27.

Davis S, Donnan GA, Parsons MW, Levi C, Butcher KS, Peeters A, Barber PA, Bladin C, De Silva DA, Byrnes G, Chalk JB, Fink JN, Kimber TE, Schultz D, Hand PJ, Frayne J, Hankey G, Muir K, Gerraty R, Tress BM, Desmond PM, EPITHET investigators. Effects of alteplase beyond 3 h after stroke in the Echoplanar Imaging Thrombolytic Evaluation Trial (EPITHET): a placebo-controlled randomised trial. *Lancet Neurol* 2008;7:299-309.

Deb P, Sharma S, Hassan KM. Pathologic mechanisms of acute ischemic stroke: An overview with emphasis on therapeutic significance beyond thrombolysis. *Pathophysiology* 2010;17(3):197-218.

del Zoppo GJ, Schmid-Schonbein GW, Mori E, Copeland BR, Chang CM. Polymorphonuclear leukocytes occlude capillaries following middle cerebral artery occlusion and reperfusion in baboons. *Stroke* 1991;22:1276-1283.

del Zoppo GJ, Sharp FR, Heiss W-D, Albers GW. Heterogeneity in the penumbra. *J Cereb Blood Flow Metab* (advance online publication 6 July 2011: 1-16).

Didion SP, Chrissobolis S, Faraci FM (2008) Oxidative stress in hypertension. In: Miwa S, Beckman KB, Muller FL. Oxidative stress in aging: From model systems to human diseases. New Jersey: Humana Press.

Di Napoli VA, Rosen CL, Nagamine T, Crocco T. Selective MCA occlusion: a precise embolic stroke model. *J Neurosci Methods* 2006;154:233-238.

Dirnagl U, Iadecola C, Moskowitz MA. Pathobiology of ischaemic stroke: an integrated view. *Trends Neurosci* 1999;22:391-397.

Dohmen C, Sakowitz OW, Fabricus M, Bosche B, Reithmeier T, Ernestus R-I, Brinker G, Dreier JP, Woitzik J, Strong AJ, Graf R. Spreading depolarizations occur in human ischemic stroke with high incidence. *Ann Neurol* 2008;63:720-728.

Donnan GA, Baron JC, Davis SM, Sharp FR (2007) The Ischemic Penumbra. New York: Informa Healthcare.

Donnan GA, Fisher M, Macleod M, Davis SM. Stroke. *Lancet* 2008;371:1612-1623.

Drake CT, Iadecola C. The role of neuronal signalling in controlling cerebral blood flow. *Brain Lang* 2007;102:141-152.

Dreier JP, Woitzik J, Fabricus M, Bhatia R, Major S, Drenckhahn C, Lehmann T-N, Sarrafzadeh A, Willumsen L, Hartings JA, Sakowitz OW, Seemann JH, Thieme A, Lauritzen M, Strong AJ. Delayed ischaemic neurological deficits after subarachnoid haemorrhage are asscociated with clusters of spreading depolarizations. *Brain* 2006;129:3224-3237.

Du C, Hu R, Csernansky CA, Hsu CY, Choi DW. Very delayed infarction after mild focal cerebral ischaemia: a role for apoptosis? *J Cereb Blood Flow Metab* 1996;16:195-201.

Dugan LL, Choi DW. Excitotoxicity, free radicals and cell membrane changes. *Ann Neurol* 1994;35:S17-S21.

Dunn KM, Renic M, Flasch AK, Harder DR, Falck J, Roman RJ. Elevated production of 20-HETE in the cerebral vasculature contributes to the severity of ischemic stroke and oxidative stress in spontaneously hypertensive rats. *Am J Physiol* 2008;295:2455-2465.

Duong TQ, Fisher M in Donnan GA, Baron JC, Davis SM, Sharp FR (2007) The Ischemic Penumbra. New York: Informa Healthcare.

Durukan A, Tatlismak T. Acute ischaemic stroke: Overview of major experimental rodent models, pathophysiology, and therapy of focal cerebral ischaemia. *Pharmacol Biochem Behav* 2007;87:179-197.

Duverger D & MacKenzie ET. The quantification of cerebral infarction following focal ischemia in the rat: influence of strain, arterial pressure, blood glucose concentration, and age. *J Cereb Blood Flow Metab* 1988;8:449-461.

Ebinger M, De Silva DA, Christensen S, Parsons MW, Markus R, Donnan GA, Davis SM. Imaging the penumbra – strategies to detect tissue at risk after ischemic stroke. *J Clin Neurosci* 2009;16:178-187.

Edelman RR, Mattle HP, Atkinson G, Hill T, Finn JJ, Mayman C, Ronthal M, Hoogewoud HM, Kleefield J. Cerebral blood flow: assessment with dynamic contrast-enhanced T2*-weighted imaging at 1.5 T. *Radiology* 1990;176:211−220.

Endres M, Namura S, Shimizu-Sasamata S, Waeber C, Zhang L, Gómez-Isla T, Hyman BT, Moskowitz MA. Attenuation of delayed neuronal death after mild focal ischemia in mice by inhibition of the caspase family. *J Cereb Blood Flow Metab* 1998;18:238-247.

Evans AL, Brown W, Kenyon CJ, Maxted KJ, Smith DC. Improved system for measuring systolic blood pressure in the conscious rat. *Med & Biol Eng & Comput* 1994;32:101-102.

Feigin V, Rinkel G, Lawes C, Algra A, Bennett D, van Gijn J, Anderson CS. Risk factors for subarachnoid hemorrhage: an updated systematic review of epidemiological studies. *Stroke* 2005;36:2773-2780.

Feng M, Whiteshall S, Zhang Y, Beibel M, D'Alecy L, DiPetrillo K. Validation of volume-pressure recording tail-cuff blood pressure measurements. *Am J Hypertens* 2008;21:1288-1291.

Fisher M, Prichard J, Warach S. New magnetic resonance techniques for acute ischemic stroke. *JAMA* 1995;274:908-911.

Fisher M, Feuerstein G, Howells DW, Hurn PD, Kent TA, Savitz SI, Lo EH for the Stroke Therapy Academic Industry Roundtable (STAIR) Group. Update of the Stroke Therapy Academic Industry Roundtable preclinical recommendations. *Stroke* 2009;40: 2244-2250.

Foley LM, Hitchens TK, Barbe B, Zhang F, Ho C, Rao GR, Nemoto ER. Quantitative temporal profiles of penumbra and infarction during permanent middle cerebral artery occlusion in rats. *Transl Stroke Res* 2010;1:220-229.

Frost SB, Barbay S, Mumert ML, Stowe AM, Nudo RJ. An animal model of capsular infarct: endothelin-1 injections in the rat. *Behav Brain Res* 2006;169:206-211.

Fujimura M, Morita-Fujimura Y, Kawase M, Copin JC, Calagui B, Epstein CJ et al. Manganese superoxide dismutase mediates the early release of mitochondrial cytochrome c and subsequent DNA fragmentation after permanent focal cerebral ischemia in mice. *J Neurosci* 1999;19:3414-3422.

Fujiwara N, Murata Y, Arai K, Egi Y, Lu J, Wu O, Singhal AB, Lo EH. Combination therapy with normobaric oxygen (NBO) plus thrombolysis in experimental ischemic stroke. *BMC Neurosci* 2009;10:79.

Garcia JH, Wagner S, Liu K-F, Hu X-J. Neurological deficit and extent of neuronal necrosis attributable to middle cerebral artery occlusion in rats. *Stroke* 1995;26(4):627-635.

Gebel JM, Broderick JP. Intracerebral hemorrhage. *Neurol Clin* 2000;18:419-438.

Gemba T, Matsunaga K, Ueda M. Changes in extracellular concentration of amino acids in the hippocampus during cerebral ischemia in stroke-prone SHR, stroke-resistant SHR and normotensive rats. *Neurosci Lett* 1992;135:184-188.

Genovese T, Mazzon E, Paterniti I, Esposito E, Bramanti P, Cuzzocrea S. Modulation of NADPH oxidase activation in cerebral ischemia/reperfusion injury in rats. *Brain Res* 2011;1372:92-102.

Gerriets T, Stolz E, Walberer M, Müller C, Kluge A, Bachmann A, Fisher M, Kaps M, Bachmann G. Noninvasive quantification of brain edema and the space-occupying effect in rat stroke models using magnetic resonance imaging. *Stroke* 2004;35:566-571.

Gill R, Sibson NR, Hatfield RH, Burdett NG, Carpenter TA, Hall LD, Pickard JD. A comparison of the early development of ischaemic damage following permanent middle cerebral artery occlusion in rats as assessed using magnetic resonance imaging and histology. *J Cereb Blood Flow Metab* 1995;15:1-11.

Go AS. The ACTIVE pursuit of stroke prevention in patients with atrial fibrillation. *N Eng J Med* 2009;360:2127-2129.

Gratton JA, Sauter A, Rudin M, Lees KR, McColl J, Reid JL, Dominiczak AF, Macrae IM, Bohr DF. Susceptibility to cerebral infarction in the stroke-prone spontaneously hypertensive rat is inherited as a dominant trait. *Stroke* 1998;29:690-694.

Hacke W, Kaste M, Fiesche C, Toni D, Lesaffre E, von Kummer R, Boysen G, Bluhmki E, Hoxter G, Mahagne M-H, Hennerici M. Intravenous thrombolysis with recombinant tissue plasminogen activator for acute hemispheric stroke: the European Cooperative Acute Stroke Study (ECASS) *JAMA* 1995;274:1017-1025.

Hacke W, Kaste M, Fiesche C, von Kummer R, Davalos A, Meier D, Larrue V, Bluhmki E, Davis S, Donnan G, Schneider D, Diez-Tejedor T, Trouillas P. Randomised double-blind placebo-controlled trial of thrombolytic therapy with intravenous alteplase in acute ischaemic stroke (ECASS II) *Lancet* 1998;352:1245-1251.

Hacke W, Albers G, Al-Rawi Y, Bogousslavsky J, Davalos A, Eliasziw M, Fischer M, Furlan A, Kaste M, Lees KR, Soenhegn M, Warach S. The desmoteplase in acute stroke trial (DIAS): a phase II MRI-based 9-hour window acute stroke thrombolysis trial with intravenous desmoteplase. *Stroke* 2005;36:66-73.

Hacke W, Kaste M, Bluhmki E, Brozman M, Davalos A, Giudetti D, Larrue V, Lees KR, Medeghri Z, Machnig T, Schneider D, von Kummer R, Wahlgren N, Toni D. Thrombolysis with alteplase 3 to 4.5 hours after acute ischaemic stroke. *N Eng J Med* 2008;359:1317-1329.

Hacke W, Furlan A, Al-Rawi Y, Davalos A, Fiebach JB, Gruber F, Kaste M, Linka LJ. Pedraza S, Ringleb PA, Rowley HA, Schneider D, Schwamm LH, Leal JS, Soenhegn M, Teal PA, Willhelm-Ogunbiyi K, Wintermark M, Warach S. Intravenous desmoteplase in patients with acute ischemic stroke selected by MRI perfusion-diffusion weighted imaging or perfusion CT (DIAS-2): a prospective, randomised, double-blind, placebo-controlled study. *Lancet Neurol* 2009;8:141-150.

Hallenbeck JM, Dutka AJ, Vogel SN, Heldman E, Doron DA, Feuerstein G. Lipopolysaccharide-induced production of tumor necrosis factor activity in rats with and without risk factors for stroke. *Brain Res* 1991;541:115-120.

Hamilton CA, Brosnan MJ, McIntyre M, Graham D, Dominiczak AF. Superoxide excess in hypertension and aging: a common cause of endothelial dysfunction. *Hypertension* 2001;37:529-534.

Harman D. Free-radical theory of aging. Increasing the functional life span. *Ann NY Acad Sci* 1994;717:1-15.

Hartings JA, Rolli ML, Lu X-CM, Tortella FC. Delayed secondary phase of peri-infarct depolarisations after focal cerebral ischaemia: relation to infarct growth and neuroprotection. *J Neurosci* 2003;23(37):11602-11610.

Hasegawa Y, Fisher M, Latour LL, Dardzinski BJ, Sotak CH. MRI diffusion mapping of reversible and irreversible ischemic injury in focal brain ischemia. *Neurology* 1994;44:1484–1490.

Heiss WD. Ischemic penumbra: evidence from functional imaging in man. *J Cereb Blood Flow Metab* 2000;20:1276-1293.

Heiss WD. Best measure of ischemic penumbra: Positron emission tomography. *Stroke* 2003;34:2534-2535.

Heiss, WD. The concept of the penumbra: can it be translated to stroke management? *Int J Stroke* 2010;5:290-5.

Heiss WD, Graf R, Wienhard K, Lottgen J, Saito R, Fujita T, Rosner G, Wagner R. Dynamic penumbra demonstrated by sequential multitracer PET after middle cerebral artery occlusion in cats. *J Cereb Blood Flow Metab* 1994;14(6):892-902.

Heiss WD, Kracht LW, Thiel A, Grond M, Pawlik. Penumbral probability thresholds of cortical flumazenil binding and blood flow predicting tissue outcome in patients with cerebral ischaemia. *Brain* 2001;124:20-29.

Heiss WD, Sorensen AG. Advances in imaging. *Stroke* 2009;40:e313-e314.

Henninger N, Bratane BT, Bastan B, Bouley J, Fisher M. Normobaric hyperoxia and delayed tPA treatment in a rat embolic stroke model. *J Cereb Blood Flow Metab* 2009;29(1):119-129.

Heumüller S, Wind S, Barbosa-Sicard E, Schmidt HHHW, Busse R, Schröder K, Brandes RP. Apocynin is not an inhibitor of vascular NADPH oxidases but an antioxidant. *Hypertension* 2008;51:211-217.

Hoehn-Berlage M, Norris DG, Kohno K, Mies G, Liebfritz D, Hossman KA. Evolution of regional changes in apparent diffusion coefficient during focal ischaemia of rat brain: the relationship of quantitative diffusion NMR imaging toreduction in cerebral blood flow and metabolic disturbances. *J Cereb Blood Flow Metab* 1995;15:1002-1011.

Hohfeld J, Cyr DM, Patterson C. From the cradle to the grave: molecular chaperones that may choose between folding and degradation. *EMBO Rep* 2001;2:885-890.

Hossman KA. Viability thresholds and the penumbra of focal ischemia. *Ann Neurol* 1994;36:557-565.

Howells DW, Porritt MJ, Rewell SSJ, O'Collins V, Sena ES, van der Worp HB, Traystman SJ, Macleod MR. Different strokes for different folks: the rich diversity of animal models of stroke. *J Cereb Blood Flow Metab* 2010;30:1412-1431..

Hunter AJ, Green AR, Cross AJ. Animal models of acute ischaemic stroke: can they predict clinically successful neuroprotective drugs? *Trends Pharmacol Sci* 1995;16:123-128.

Hypothermia After Cardiac Arrest Study Group. Mild therapeutic hypothermia to improve the neurologic outcome after cardiac arrest. *N Eng J Med* 2002;346:549-556.

Iadecola C. Bright and dark sides of nitric oxide in ischaemic brain injury. *Trends Neurosci* 1997;20:132-139.

Ibrahim J, McGee A, Graham D, McGrath JC, Dominiczak AF. Sex-specific differences in cerebral arterial myogenic tone in hypertensive and normotensive rats. *Am J Physiol* 2006;290:H1081-H1089.

Intravenous Magnesium Efficacy in Stroke (IMAGES) Study Investigators. Magnesium for acute stroke (Intravenous Magnesium Efficacy in Stroke trial): randomised controlled trial. *Lancet* 2004;363:439-445.

Ishida H, Takemori K, Dote K, Ito H. Expression of Glucose Transporter-1 and Aquaporin -4 in the cerebral cortex of stroke-prone spontaneously hypertensive rats in relation to the blood-brain barrier function. *Am J Hypertens* 2006;19:33-39.

Izzard AS, Graham D, Burnham MP, Heerkens EH Dominiczak AF, Heagerty AM. Myogenic and structural properties of cerebral arteries from the stroke-prone spontaneously hypertensive rat. *Am J Physiol* 2003;285:H1489-H1494.

Jacewicz M, Tanabe J, Pulsinelli WA. The CBF threshold and dynamics for focal cerebral infarction in spontaneously hypertensive rats. *J Cereb Blood Flow Metab* 1992;12:359-70.

Jackman KA, Miller AA, De Silva TM, Crack PJ, Drummond GR, Sobey CG. Reduction of cerebral infarct volume by apocynin requires pretreatment and is absent in Nox2-deficient mice. *Br J Pharmacol* 2009;156:680-688.

Jeffs B, Clark JS, Anderson NH, Gratton J, Brosnan MJ, Gauguier D, Reid JL, Macrae IM, Dominiczak AF. Sensitivity to cerebral ischaemic insult in a rat model of stroke is determined by a single genetic locus. *Nat Gen* 1997;16:364-367.

Johnston SC, Selvin S, Gress DR (1998) The burden, trends, and demographics of mortality from subarachnoid hemorrhage. *Neurology* 1998;50:1413-1418.

Kahles T, Luedike P, Endres M, Galla HJ, Steinmetz H, Busse R, Neumann-Haefelin T, Brandes RP. NADPH oxidase plays a central role in blood-brain barrier damage in experimental stroke. *Stroke* 2007;38:3000-3006.

Kane I, Carpenter T, Chappell F, Rivers C, Armitage P, Sandercock P, Wardlaw J. Comparison of 10 different magnetic resonance perfusion imaging processing methods in acute ischemic stroke: effect on lesion size, proportion of patients with diffusion/perfusion mismatch, clinical scores, and radiologic outcomes. *Stroke* 2007;38: 3158-3164.

Karlsen OT, Verhagen R, Bovée WM. Parameter estimation from Rician-distributed data sets using a maximum likelihood estimator: application to T1 and perfusion measurements. *Magn Reson Med* 1999;41(3):614-623.

Karonen JO, Nuutinen J, Kuikka JT, Vanninen EJ, Vanninen RL, Partanen PLK, Vainio PA, Roivainen R, Sivenius J, Aronen HJ. Combined SPECT and diffusion-weighted MRI as a predictor of infarct growth in acute ischemic stroke. *J Nucl Med* 2000;41:788-794.

Kaufmann AM, Firlik AD, Fukui MB, Wechsler LR, Jungries CA, Yonas H. Ischemic core and penumbra in human stroke. *Stroke* 1999;30:93-99.

Kazemi M, Silva MD, Li F, Fisher M, Sotak CH. Investigation of techniques to quantify in vivo lesion volume based on comparison of apparent diffusion coefficient (ADC) maps with histology in focal cerebral ischemia of rats. *Magn Reson Imaging* 2004;22:653-659.

Kelly KA, Li X, Tan Z, vanGilder RL, Rosen CL, Huber JD. Nox2 inhibition with apocynin worsens stroke outcome in aged rats. *Brain Res* 2009;1292:165-172.

Kerr S, Brosman J, McIntyre M, Reid JL, Dominiczak AF, Hamilton CA. Superoxide anion production is increased in a model of genetic hypertension. *Hypertension* 1999;33:1353-1358.

Kidwell CS, Saver JL, Mattiello J, Starkman S, Vinuela F, Duckwiler G, Gobin YP, Jahan R, Vespa P, Kalafut M, Alger JR. Thrombolytic reversal of acute human cerebral ischemic injury shown by diffusion/perfusion magnetic resonance imaging. *Ann Neurol* 2000;47:462-469.

Kidwell CS, Saver JL, Starkman S, Duckwiler G, Jahan R, Vespa P, Villablanca JP, Liebeskind DS, Gobin YP, Vinuela F, Alger JR. Late secondary ischemic injury in patients receiving intraarterial thrombolysis. *Ann Neurol* 2002;52:698-703.

Kidwell CS, Alger JR, Saver JL. Beyond mismatch: Evolving paradigms in imaging the ischemic penumbra with multimodal magnetic resonance imaging. *Stroke* 2003;34:2729-2735.

Kim HY, Singhal AB, Lo EH. Normobaric hyperoxia extends the reperfusion window in focal cerebral ischemia. *Ann Neurol* 2005;57:571-575.

Kim-Mitsuyama S, Yamamoto E, Tanaka T, Zhan Y, Izumi Y, Izumiya Y, Ioroi T, Wanibuchi H, Iwao H. Critical role of angiotensin II in excess salt-induced brain oxidative stress of stroke-prone spontaneously hypertensive rats. *Stroke* 2005;36: 1077-1082.

Kinouchi H, Sharp FR, Koistinaho J, Hicks K, Kamii H, Chan PH. Induction of 70-kDa heat shock protein and hsp70 mRNA following transient focal cerebral ischemia in the rat. *J Cereb Blood Flow Metab* 1993;13:105-115.

Kishi T, Hirooka Y, Kimura Y, Ito K, Shimokawa H, Takeshita A. Increased reactive oxygen species in rostral ventrolateral medulla contribute to neural mechanisms of hypertension in stroke-prone spontaneously hypertensive rats. *Circulation* 2004;109:2357-2362.

Kissela BM, Sauerbeck L, Woo D, Khoury J, Carrozzella, Pancioli A, Jauch E, Moomaw CJ, Shukla R, Gebel J, Fontaine R, Broderick J. Subarachnoid Hemorrhage: A preventable disease with a heritable component. *Stroke* 2002;33:1321-1326.

Kleinschnitz C, Grund H, Wingler K, Armitage ME, Jones E, Mittal M, Barit D, Schwarz T, Geis C, Kraft P, Barthel K, Schuhmann MK, Herrmann AM, Meuth SG, Stoll G, Meurer S, Schrewe A, Becker L, Gailus-Durner V, Fuchs H, Klopstock T, Hrabé de Angelis M, Jandeleit-Dahm K, Sham AM, Weissmann N, Schmidt HHHW. Post-stroke inhibition of induced NADPH oxidase type 4 prevents oxidative stress and neurodegeneration. *PLoS Biology* 2010;8(9):1-13.

Kohno K, Hoehn-Berlage M, Mies G, Back T, Hossman K-A. Relationship between diffusion-weighted MR images, cerebral blood flow and energy state in experimental brain infarction. *Mag Res Imag* 1995;13:73-80.

Koizumi J, Yoshida Y, Nakazawa T, Ooneda G. Experimental studies of brain edema, I. A new experimental model of cerebral embolism in which recirculation can be introduced into the ischemic area. *Jpn J Stroke* 1986;8:1-8.

Kristian T, Siesjo BK. Calcium in ischemic cell death. *Stroke* 1998;29:705-718.

Kurtz TW, Griffin KA, Bidani AK, Davisson RL, Hall JE. Recommendations for blood pressure measurement in humans and experimental animals. Part 2: Blood pressure measurement in experimental animals. *Hypertension* 2005;45:299-310.

Lansberg MG, O'Brien MW, Tong DC, Moseley ME, Albers GW. Evolution of cerebral infarct volume assessed by diffusion-weighted magnetic resonance imaging. *Arch Neurol* 2001;58(4):613-617.

Leist M, Nicotera P. Apoptosis, excitotoxicity and neuropathology. *Exp Cell Res* 1998;239:183-201.

Legos JJ, Lenhard SC, Haimbach RE, Schaeffer TR, Bentley RG, McVey MJ, Chandra S, Irving EA, Parsons AA, Barone FC. SB 234551 selective ET_A receptor antagonism: Perfusion/diffusion MRI used to define treatable stroke model, time to treat and mechanism of protection. *Exp Neurol* 2008;212:53-62.

Letourneur A, Roussel, Toutain J, Bernaudin M, Touzani O. Impact of genetic and renovascular chronic arterial hypertension on the acute spatiotemporal evolution of the ischemic penumbra: a sequential study with MRI in the rat. *J Cereb Blood Flow Metab* 2011;31:504-513.

Li F, Carano RAD, Irie K, Sotak CH, Fisher M. Temporal evolution of average apparent diffusion coefficient threshold to define ischemic abnormalities in a rat permanent occlusion model. *J Stroke Cerebrovasc Dis* 2000;9:1-7.

Li L, Watts SW, Banes AK, Galligan JJ, Fink GD, Chen AF. NADPH oxidase-derived superoxide augments endothelin-1-induced venoconstriction in mineralocorticoid hypertension. *Hypertension* 2003;42:316-321.

Li L, Lundkvist A, Andersson D, Wilhelmsson U, Nagai N, Pardo AC, Nodin C, Stahlberg A, Aprico K, Larsson K, Yabe T, Moons L, Fotheringham A, Davies I, Carmeliet P, Schwartz JP, Pekna M, Kubista M, Blomstrand F, Maragakis N, Nilsson M, Pekny M. Protective role of reactive astrocytes in brain ischemia. *J Cereb Blood Flow Metab* 2008;28:468-481.

Lippoldt A, Kniesel U, Liebner S, Kalbacher H, Kirsch T, Wolburg H, Haller H. Structural alterations of tight junctions are associated with loss of polarity in stroke-prone spontaneously hypertensive rat blood-brain barrier endothelial cells. *Brain Res* 2000;885:251-261.

Lipton P. Ischemic cell death in brain neurons. *Physiol Rev* 1999;79:1431-1567.

Liu X, Rinkel GJE. Aneurysmal and clinical characteristics as risk factors for intracerebral haematoma from aneurysmal rupture. *J Neurol* 2011;258:862-865.

Lloyd-Jones D, Adams RJ, Brown TM, Carnethon M, Dai S, De Simone G, Ferguson TB, Ford E, Furie K, Gillespie C, Go A, Greenlund K, Haase N, Hailpern S, Ho PM, Howard V, Kissela B, Kittner S, Lackland D, Lisabeth L, Marelli A, McDermott MM, Meigs J, Mozaffarian D, Mussolino M, Nichol G, Roger VL, Rosamond W, Sacco R, Sorlie P, Stafford R, Thom T, Wassertgiel-Smoller S, Wong ND, Wylie-Rosett J. Heart disease and stroke statistics-2010 update: A report from the American Heart Asscociation. *Circulation* 2010;121:e46-e215.

Lo EH, Dalkara T, Moskowitz MA. Mechanisms, challenges and opportunities in stroke. *Nat Rev Neurosci* 2003;4:399-415.

Longa EZ, Weinstein PR, Carlson S, Cummins R. Reversible middle cerebral artery occlusion without craniectomy in rats. *Stroke* 1989;20:84-91.

Loubinoux I, Volk A, Borredon J, Guirimand S, Tiffon B, Seylaz J, Meric P. Spreading of vasogenic edema and cytotoxic edema assessed by quantitative diffusion and T2 magnetic resonance imaging. *Stroke* 1997;28:419-427.

Ma H, Zavala JA, Teoh H, Churilov L, Gunawan M, Ly J, Wright P, Phan T, Arakawa S, Davis SM, Donnan GA. Penumbral mismatch is underestimated using standard volumetric methods and this is exacerbated with time. *J Neurol Neurosurg Psychiatry* 2009;60:991-997.

Macrae IM. New models of focal cerebral ischaemia. *Br J Clin Pharmac* 1992 ;34:302-308.

Magistretti PJ, Pellerin L. Cellular mechanisms of brain energy metabolism: relevance to functional brain imaging and to neurodegenerative disorders. *Ann N Y Acad Sci* 1996;777:380-387.

Maguire S, Strittmatter R, Chandra S, Barone FC. Stroke-prone rats exhibit prolonged behavioral deficits without increased brain injury: an indication of disrupted post-stroke brain recovery of function. *Neurosci Lett* 2004;354:229-233.

Mancuso A, Karibe H, Rooney WD, Zarow GJ, Graham SH, Weiner MW, Weinstein PR. Correlation of early reduction in the apparent diffusion coefficient of water with blood flow reduction during middle cerebral artery occlusion in rats. *Magn Reson Med* 1995;34:368-377.

Marks L, Carswell HVO, Peters EE, Graham DI, Patterson J, Dominiczak AF, Macrae IM. Characterization of the microglial response to cerebral ischemia in the stroke-prone spontaneously hypertensive rat. *Hypertension* 2001;38:116-122.

Mas JL. Patent foramen ovale and stroke. *Pract Neurol* 2003;3:4-11.

Mashimo T, Nabika T, Matsumoto C, Tamada T, Ueno K, Sawamura M, Ikeda K, Kato N, Nara Y, Yamori Y. Aging and salt-loading modulate blood pressure QTLs in rats. *Am J Hypertens* 1999;12:1098-1104.

McCabe C, Gallagher L, Gsell W, Graham D, Dominiczak AF, Macrae IM. Differences in the evolution of the ischemic penumbra in stroke-prone spontaneously hypertensive and Wistar-Kyoto rats. *Stroke* 2009;40:3864-3868.

McCann SK, Dusting GJ, Roulston CL. Early increase of Nox4 NADPH oxidase and superoxide generation following endothelin-1-induced stroke in conscious rats. *J Neurosci Res* 2008;86:2524-2534.

McGill JK, Gallagher L, Carswell HVO, Irving EA, Dominiczak AF, Macrae IM. Impaired functional recovery after stroke in the stroke-prone spontaneously hypertensive rat. *Stroke* 2005;36:135-141.

Meloni BP, Campbell K, Zhu H, Knuckey NW. In search of clinical neuroprotection after brain ischemia. The case for mild hypothermia (35^{o}C) and magnesium. *Stroke* 2009;40:2236-2240.

Meng X, Fisher M, Shen Q, Sotak CH, Duong TQ. Characterizing the diffusion/perfusion mismatch in experimental focal cerebral ischemia. *Ann Neurol* 2004;55:207-212.

Mergenthaler P, Dirnagl U, Meisel A. Pathophysiology of stroke: lessons from animal models. *Metab Brain Dis* 2004;19:151-167.

Mies G, Iijima T, Hossman KA. Correlation between periinfarct DC shifts and ischaemic neuronal damage in rat. *Neuroreport* 1993;4:709-711.

Miller AA, Drummond GR, Schmidt HH, Sobey CG. NADPH oxidase activity and function are profoundly greater in cerebral versus systemic arteries. *Circ Res* 2005;97: 1055-1062.

Miller AA, Drummond GR, Sobey CG. Novel isoforms of NADPH-oxidase in cerebral vascular control. *Pharmacology & Therapeutics* 2006;111:928-948.

Miller AA, Drummond GR, Mast AE, Schmidt HH, Sobey CG. Effect of gender on NADPH-oxidase activity, expression, and function in the cerebral circulation: role of estrogen. *Stroke* 2007;38:2142-2149.

Minematsu K, Li L, Sotak CH, Davis MA, Fisher M. Reversible focal ischemic injury demonstrated by diffusion-weighted magnetic resonance imaging in rats. *Stroke* 1992;23:1304-1310.

Moffat BA, Chenevert TL, Hall DE, Rehemtulla A, Ross BD. Continuous arterial spin labeling using a train of adiabatic inversion pulses. *J Magn Reson Imaging* 2005;21:290-6.

Mohr JP, Gautier JC, Hier D, Stein RW (1986) Middle cerebral artery. In Stroke, Vol 1: Pathophysiology, Diagnosis and Management, eds Barnett HJM, Stein BM, Mohr JP, Yatsu FM. pp 377-450. New York: Churchill Livingstone.

Moseley ME, Cohen Y, Mintorovitch J Chileuitt L, Shimizu H, Kucharczyk J, Wendland MF, Weinstein PR. Early detection of regional cerebral ischemia in cats: comparison of diffusion- and T2-weighted MRI and spectroscopy. *Magn Reson Med* 1990a;14:330-346.

Moseley ME, Kucharczyk J, Mintorovitch J, Cohen Y, Kurhanewicz J, Derugin N, Asgari H, Norman D. Diffusion-weighted MR imaging of acute stroke: correlation with T2-weighted and magnetic susceptibility-enhanced MR imaging in cats. *Am J Neuroradiol* 1990b;11(3):423-429.

Nabika T, Cui ZH, Masuda J. The stroke-prone spontaneously hypertensive rat: how good is it as a model for cerebrovascular diseases? *Cell Mol Neurobiol* 2004;24: 639-646.

Neumann-Haefelin T, Wittsack HJ, Wenserski F, Siebler M, Seitz RJ, Modder U, Freund HJ. Diffusion- and perfusion-weighted MRI: the DWI/PWI mismatch region in acute stroke. *Stroke* 1999;30:1591-1597.

O' Collins VE, Macleod MR, Donnan GA, Horky LL, van der Worp BH, Howells DW. 1,026 experimental treatments in acute stroke. *Ann Neurol* 2006;59:467-477.

Ogata J, Fujishima M, Tamaki K, Nakatomi Y, Ishitsuka T, Omae T. Stroke-prone hypertensive rats as an experimental model of malignant hypertension I. A light and electron-microscopic stud of the brain. *Acta Neuropathol* 1980;51:179-184.

Ogata J, Fujishima M, Tamaki K, Nakatomi Y, Ishitsuka T, Omae T. Stroke- prone hypertensive rats as an experimental model of malignant hypertension: A pathological study. *Virchows Arch A Pathol Anat Histol* 1982;394:185-194.

Ogata J, Yamanishi H, Ishibashi-Ueda H. Role of cerebral vessels in ischaemic injury of the brain. *Neuropathol Appl Neurobiol* 2011;37:40-55.

Okamoto K, Aoki K. Development of a strain of spontaneously hypertensive rats. *Jap Circ J* 1963;27: 282-293.

Okamoto K, Yamori Y, Nagaoka A. Establishment of the stroke-prone spontaneously hypertensive rat (SHR). *Circ Res* 1974;34/35 (Suppl. I):143-153.

Olah L, Wecker S, Hoehn M. Relation of apparent diffusion coefficient changes and metabolic disturbances after 1 hour of focal cerebral ischemia and at different reperfusion phases in rats. *J Cereb Blood Flow Metab* 2001;21:430-439.

Olivot JM, Mlynash M, Thijs VN, Kemp S, Lansberg MG, Wechsler L, Bammer R, Marks MP, Albers GW. Optimal Tmax threshold for predicting penumbral tissue in acute stroke. *Stroke* 2009;40:469-475.

Osborne KA, Shigeno T, Balarsky AM, Ford I, McCulloch J, Teasdale GM, Graham DI. Quantitative assessment of early brain damage in a rat model of focal cerebral ischaemia. *J Neurol Neurosurg Psych* 1987;50:402-410.

Ostergaard JR. Risk factors in intracranial saccular aneurysms: aspects on the formation and rupture of aneurysms, and development of cerebral vasospasm. *Acta Neurol Scand* 1989;80:81-98.

Pacher P, Beckman JS, Llaudet L. Nitric oxide and peroxynitrite in health and disease. *Physiol Rev* 2007;87:315-424.

Paliege A, Parsumathy A, Mizel D, Yang T, Schnermann J, Bachmann S. Effect of apocynin treatment on renal expression of COX-2, NOS1 and renin in Wistar-Kyoto and spontaneously hypertensive rats. *Am J Physiol Regul Integr Comp Physiol* 2006;290: R694-R700.

Paravacini TM, Chrissobolis S, Drummond GR, Sobey CG. Increased NADPH-oxidase activity and Nox4 expression during chronic hypertension is associated with enhanced cerebral vasodilatation to NADPH in vivo. *Stroke* 2004;35(2):584-589.

Paravacini TM, Miller AA, Drummond GR, Sobey CG. Flow-induced cerebral vasodilatation in vivo involves activation of phosphatidylinositol 3-kinase (PI3-K), NADPH-oxidase, and nitric oxide synthase. *J Cereb Blood Flow Metab* 2006;26:836-845.

Pastor MD, Garcia-Yébenes I, Fradejas N, Pérez-Ortiz JM, Mora-Lee S, Tranque P, Angeles Moro M, Pende M, Calvo S. mTOR/S6 kinase pathway contributes to astrocyte survival during ischemia. *J Biol Chem* 2009;284 (33):22067-22078.

Paxinos G, Watson C (1998) The rat brain in stereotaxic coordinates (Fourth Edition) London: Academic Press.

Reith W, Hasegawa Y, Latour LL, Dardzinski BJ, Sotak CH, Fisher M. Multislice diffusion mapping for 3-D evolution of cerebral ischemia in a rat stroke model. *Neurology* 1995;45:172-177.

Ridet JL, Malhotra SA, Privat A, Gage FH. Reactive astrocytes: cellular and molecular cues to biological function. *Trends Neurosci* 1997;20:570-577.

Riganti C, Costamagna C, Bosia A, Ghigo D. The NADPH oxidase inhibitor apocynin (acetovanillone) induces oxidative stress. *Toxicol Appl Pharmacol* 2006;212: 179-187.

Röther J. Neuroprotection does not work! *Stroke* 2008;39:523-524.

Rubattu S, Lee-Kirsch MA, DePaolis P, Giliberti R, Gigante B, Lombardi A, Volpe M, Lindpaintner K. Altered structure, regulation, and function of the gene encoding the atrial natriuretic peptide in the stroke-prone spontaneously hypertensive rat. *Circ Res* 1999;85:900-905.

Saver JL, Albers GW, Dunn B, Johnston KC, Fisher M and for the STAIR VI Consortium Stroke Therapy Academic Industry Roundatable (STAIR) recommendations for extended window acute stroke therapy trials. *Stroke* 2009;40:2594-2600.

Schaefer PW, Barak ER, Kamalian S, Gharai LR, Schwamm L, Gonzalez RG, Lev MH. Quantitative assessment of core/penumbra mismatch in acute stroke: CT and MR perfusion imaging are strongly correlated when sufficient brain volume is imaged. *Stroke* 2008;39:2986-2992.

Schallert T, Fleming SM, Leasure JL, Tillerson JL, Bland ST. CNS plasticity and assessment of sensorimotor outcome in unilateral rat models of stroke, cortical ablation, parkinsonism and spinal cord injury. *Neuropharmacology* 2000;39:777-787.

Schlaug G, Benfield A, Baird AE, Siewert B, Lövblad KO, Parker RA, Edelman RR, Warach S. The ischemic penumbra: operationally defined by diffusion and perfusion MRI. *Neurology* 1999;53:1528-1537.

Schlüter T, Steinbach AC, Steffen A, Rettig R, Grisk O. Apocynin-induced vasodilation involves Rho kinase inhibition but not NADPH oxidase inhibition. *Cardiovascular Res* 2008;80:271-279.

Schmid Elsaesser R, Zausinger S, Hungerhuber E, Baethmann A, Reulen HJ. A critical reevaluation of the intraluminal thread model of focal cerebral ischemia: evidence of inadvertent premature reperfusion and subarachnoid haemorrhage in rats by laser-Doppler flowmetry. *Stroke* 1998;29:2162-2170.

Selemidis S, Sobey CG, Wingler K, Schmidt HHHW, Drummond GR. NADPH oxidases in the vasculature: Molecular features, roles in disease and pharmacological inhibition. *Pharmacology & Therapeutics* 2008;120:254-291.

Serrano F, Kolluri NS, Wientjes FB, Card JP, Klann E. NADPH oxidase immunoreactivity in the mouse brain. *Brain Res* 2003;988:193–198.

Sharkey J, Ritchie IM, Kelly PAT. Perivascular microapplication of endothelin-1: a new model of focal cerebral ischaemia in the rat. *J Cereb Blood Flow Metab* 1993;13: 865-871.

Shen Q, Meng X, Sotak CH, Fisher M, Duong TQ. Pixel-by-pixel spatiotemporal progression of focal ischemia derived using quantitative perfusion and diffusion imaging. *J Cereb Blood Flow Metab* 2003;23:1479-88.

Shih LC, Saver JL, Alger JR, Starkman S, Leary MC, Vinuela F, Duckwiler G, Gobin YP, Jahan R, Villablanca JP, Vespa PM, Kidwell CS. Perfusion-weighted magnetic resonance imaging thresholds identifying core, irreversibly infarcted tissue. *Stroke* 2003;34:1425-1430.

Sicard KM, Fisher M. Animal models of focal brain ischemia. *Exp Trans Stroke Med* 2009;1:7.

Simons JM, 'T Hart BA, Theo RAM, Ching IV, Duk HV, Labadie RP. Metabolic activation of natural phenols into selective oxidative burst agonists by activated human neutrophils. *Free Rad Biol & Med* 1990;8:251-258.

Sobesky J, Weber OZ, Lehnhardt FG, Hesselmann V, Neveling M, Jacobs A, Heiss WD Does the mismatch match the penumbra? Magnetic resonance imaging and positron emission tomography in early ischemic stroke. *Stroke* 2005;36:980-985.

Stroke Therapy Academic Industry Roundtable (STAIR). Recommendations for standards regarding preclinical neuroprotective and restorative drug development. *Stroke* 1999;30:2752-2758.

Strahorn P, Graham D, Charchar FJ, Sattar N, McBride MW, Dominiczak AF. Genetic determinants of metabolic syndrome components in the stroke-prone spontaneously hypertensive rat. *J Hypertens* 2005;23:2179-2186.

Stolk J, Hiltermann TJ, Dijkman JH, Verhoeven AJ. Characteristics of the inhibition of NADPH oxidase activation in neutrophils by apocynin, a methoxy-substituted catechol. *Am J Respir Cell Mol Biol* 1994;11(1):95-102.

Strandgaard S, Paulson OB. Pathophysiology of stroke. *J Cardiovasc Pharmacol* 1990;15: S38-S42.

Sudlow CLM, Warlow CP. Comparable studies of the incidence of stroke and its pathological types: results from an international collaboration. *Stroke* 1997;28:491-499.

Suzuki H, Swei A, Zweifach BW, Schmid- Schönbien GW. In vivo evidence for microvascular oxidative stress in spontaneously hypertensive rats: hydroethidine microfluorography. *Hypertension* 1995;25:1083-1089.

Suzuki Y, Chen F, Ni Y, Marchal G, Collen D, Nagai N. Microplasmin reduces ischemic brain damage and improves neurological function in a rat stroke model monitored with MRI. *Stroke* 2004;35:2402-2406.

Swanson RA, Morton MT, Tsao-Wu G, Savalos RA, Davidson C, Sharp FR. A semiautomated method for measuring brain infarct volume. *J Cereb Blood Flow Metab* 1990;10:290-293.

Symon L, Branston NM, Strong AJ, Hope TD. The concepts of thresholds of ischaemia in relation to brain structure and function. *J Clin Pathol* 1977;S3-S11:149-154.

Tagami M, Ikeda K, Nara Y, Fujino H, Kubota A, Numano F, Yamori Y. Insulin-like growth factor-1 attenuates apoptosis in hippocampal neurons caused by cerebral ischaemia and reperfusion in stroke-prone spontaneously hypertensive rats. *Lab Invest* 1997;76:603-612.

Tagami M, Yamagata K, Ikeda K, Nara Y, Fujino H, Kubota A, Numano F, Yamori Y. Vitamin E prevents apoptosis in cortical neurons during hypoxia and oxygen reperfusion. *Lab Invest* 1998;78:1415-1429.

Tamura A, Graham DI, McCulloch J, Teasdale GM. Focal cerebral ischaemia in the rat: description of technique and early neuropathological consequences following middle cerebral artery occlusion. *J Cereb Blood Flow Metab* 1981;1:53-60.

Tang LL, Ye K, Yang XF, Zheng JS. Apocynin attenuates cerebral infarction after transient focal ischaemia in rats. *J Int Med Res* 2007;35:517-522.

Tang XN, Cairns B, Cairns N, Yenari MA. Apocynin improves outcome in experimental stroke in a narrow dose range. *Neuroscience* 2008;154:556-562.

Tawasaka M, Jones PS, Guadagno JV, Christensen S, Fryer TD, Harding S, Gillard JH, Willliams GB, Aigbirhio FI, Warburton EA, Ostergaard L, Baron JC. How reliable is perfusion MR in acute stroke? : Validation and determination of the penumbra threshold against quantitative PET. *Stroke* 2008;39:870-877.

The National Institute of Neurological Disorders and Stroke rt-PA Stroke Study Group. Tissue plasminogen activator for acute ischemic stroke. *N Eng J Med* 1995;333: 1581-1587.

Thomalla GJ, Kucinski T, Schoder V, Fiehler J, Knab R, Zeumer H, Weiller C, Rother J. Prediction of malignant middle cerebral artery infarction by early perfusion- and diffusion- weighted magnetic resonance imaging. *Stroke* 2003;34:1892-189.

Todd NV, Picozzi P, Crockard A, Russell RW. Duration of ischemia influences the development and resolution of ischemic brain edema. *Stroke* 1986;17:466-471.

Touyz RM. Apocynin, NADPH oxidase, and vascular cells: a complex matter. *Hypertension* 2008;51:172-174.

Touzani O, Young AR, Derlon JM, Beaudouin V, Marchal G, Rioux P, Mezenge F, Baron JC, MacKenzie ET. Sequential studies of severely hypometabolic tissue volumes after permanent middle cerebral artery occlusion. A positron emission tomographic investigation in anesthetized baboons. *Stroke* 1995;26:2112-2119.

Tyson GW, Teasdale GM,Graham DI, McCulloch J. Cerebrovascular permeability following MCA occlusion in the rat. The effect of halothane-induced hypotension. *J Neurosurg* 1982;57:186–196.

Vallet P, Charnay Y, Steger K, Ogier-Denis E, Kovari E, Herrmann F, Michel J-P, Szanto I. Neuronal expression of the NADPH oxidase NOX4, and its regulation in mouse experimental brain ischemia. *Neuroscience* 2005;132:233–238.

van Gijn J, Kerr RS, Rinkel GJ. Subarachnoid haemorrhage. *Lancet* 2007;369:306-318.

van der Worp HB, de Haan P, Morrema E, Kalkman CJ. Methodological quality of animal studies on neuroprotection in focal cerebral ischaemia. *J Neurol* 2005;252: 1108-1114.

Vejražka M, Míček R, Štípek S. Apocynin inhibits NADPH oxidase in phagocytes but stimulates ROS production in non-phagocytic cells. *Biochim Biophys Acta* 2005;1722:143-147.

Volpe M, Iaccarino G, Vecchione C, Rizzoni D, Russo R, Rubattu S, Condorelli G, Ganten U, Ganten D, Trimarco B, Lindpaintner K. Association and cosegregation of stroke with impaired endothelium-dependent vasorelaxation in stroke prone spontaneously hypertensive rats. *J Clin Invest* 1996;98:256-261.

Wang Q, Tompkins KD, Simonyi A, Korthuis RJ, Sun AY, Sun GY. Apocynin protects against global cerebral ischemia-reperfusion-induced oxidative stress and injury in the gerbil hippocampus. *Brain Res* 2006;1090:182-189.

Warach S, Gaa J, Siewert B, Wielpolski P, Edelman RR. Acute human stroke studied by whole brain echo planar diffusion weighted MRI. *Ann Neurol* 1995;37: 231−241.

Warlow C, Sudlow C, Dennis M, Wardlaw J, Sandercock P. Stroke. *Lancet* 2003; 362: 1211-1224.

Weinberger JM. Evolving therapeutic approaches to treating acute ischemic stroke. *J Neurol Sci* 2006;249:101-109.

Weishaupt D, Köchli VD, Marincek B (2006) How does MRI work? An introduction to the physics and function of magnetic resonance imaging. Second Edition. Berlin: Springer.

Williams DS, Detre JA, Leigh JS, Koretsky, AP. Magnetic resonance imaging of perfusion using spin inversion of arterial water. *Proc Natl Acad Sci U S A* 1992;89:212-216.

Williams AJ, Berti R, Dave JR, Elliot PJ, Adams J, Tortella FC. Delayed treatment of ischemia/reperfusion brain injury: extended therapeutic time window with the proteasome inhibitor MLN519. *Stroke* 2004;35:1186-1191.

Wintermark M, Flanders AE, Velthuis B, Meuli R, van Leeuwen M, Goldsher D, Pineda C, Serena J, van der Schaaf I, Waaijer A, Anderson J, Nesbit G, Gabriely I, Medina V, Quiles A, Pohlman S, Quist M, Schnyder P, Bogousslavsky J, Dillon WP, Pedraza S. Perfusion-CT assessment of infarct core and penumbra: receiver operating characteristic curve analysis in 130 patients suspected of acute hemispheric stroke. *Stroke* 2006;37:979-985.

Woitzik J, Lassel E, Hecht N, Schneider UC, Schroeck H, Vajkoczy P, Graf R. Ischemia independent lesion evolution during focal stroke in rats. *Exp Neurol* 2009;218: 41-46.

Ximenes VF, Kanegae MP, Rissato SR, Galhiane MS. The oxidation of apocynin catalyzed by myleoperoxidase: proposal for NADPH oxidase inhibition. *Arch Biochem Biophys* 2007; 457:134-141.

Yamagata K, Tagami M, Nara Y, Fujino H, Kubota A, Numano F, Kato T, Yamori Y. Faulty induction of blood-brain barrier functions by astrocytes isolated from stroke-prone spontaneously hypertensive rats. *Clin Exp Pharmacol Physiol* 1997;24: 686-691.

Yamori Y, Igawa T, Kanbe T, Nara Y, Tagami M. Enhanced growth rate of cultured smooth muscle cells from spontaneously hypertensive rats. *Heart Vessels* 1988;4:94-99.

Yoneda Y, Tokui K, Hanihara T, Kitagaki H, Tabuchi M, Mori E. Diffusion-weighted magnetic resonance imaging: detection of ischemic injury 39 minutes after onset in a stroke patient. *Ann Neurol* 1999;45:794-797.

Yoshitomi H, Xu Q, Gao M, Yamori Y. Phosphorylated endothelial NOS Ser1177 via the PI3K/Akt pathway is depressed in the brain stroke-prone spontaneously hypertensive rat. *J Stroke Cerebrovasc Dis* 2011;20(5):406-412.

Zalba G, Beaumont FJ, San Jose G, Fortuno A, Fortuno MA, Etayo JC, Diez J. Vascular NADH/NADPH oxidase is involved in enhanced superoxide production in spontaneously hypertensive rats. *Hypertension* 2000;35(5):1055-1061.

Zaro-Weber O, Moeller-Hartmann W, Heiss WD, Sobesky J. The performance of MRI-based cerebral blood flow measurements in acute and subacute stroke compared with 15O-water positron emission tomography. *Stroke* 2009;40:2413-2421.

Zeng J, Zhang Y, Mo J, Su Z, Huang R. Two-kidney, two clip renovascular hypertensive rats can be used as stroke-prone rats. *Stroke* 1998;29:1708-1714.

Zhu H, Fan X, Yu Z, Liu J, Murata Y, Lu J, Zhao S, Hajjar KA, Lo EH, Wang X. Annexin A2 combined with low-dose tPA improves thrombolytic therapy in a rat model of focal embolic stroke. *J Cereb Blood Flow Metab* 2010;30(6):1137-1146.

Zia E, Hedblad B, Pessah-Rasmussen H, Berglund G, Janzon L, Engstrom G. Blood pressure in relation to the incidence of cerebral infarction and intracerebral hemorrhage: hypertensive hemorrhage: debated nomenclature is still relevant. *Stroke* 2007;38:2681-2685.